ULTRASONIC STUDIES OF FOODS CONTAINING AIR

Peter Fairley

Submitted in accordance with the requirements
for the degree of Doctor of Philosophy

The University of Leeds

Procter Department of Food Science

July 1992

The candidate confirms that the work submitted is
his own and that appropriate credit has been given
where reference has been made to the work of others

ACKNOWLEDGEMENTS

Thanks are due to my academic supervisor, Dr Malcolm Povey for his advice and encouragement throughout this project. Thanks are also due to my industrial supervisor, Dr Rodney Bee of Unilever Research Ltd, Colworth, for his advice and for making my visits to Colworth pleasant ones.

Special thanks are due to Dr Julian McClements, for his invaluable advice, encouragement and support.

I am grateful to Dr Olga Flint for her advice and assistance with the light microscopy used in this project. I would also like to thank all the technical staff at the Department of Food Science and at Colworth, and in particular Mr Philip Nelson of the Workshop at the Department of Food Science.

This project was financed through the CASE (Co-operative Awards in Science and Engineering) scheme. Thanks are therefore due to the Agricultural and Food Research Council and especially to Unilever plc, for their generous financial support.

SUMMARY

Aerated foods are an important sector of the processed food market, but they are poorly characterised by the available techniques. Ultrasound has a complex interaction with bubbly liquids, which has the potential to be used as a means of non-destructively characterising bubbly food liquids. The ultrasonic velocity, attenuation coefficient and reflection coefficient can be related to the volume fraction of gas and bubble size distribution using theories which are known to work at low volume fraction. Ultrasonic equipment has been described which can measure the ultrasonic velocity and attenuation coefficient very accurately, and which can make reflection measurements on systems which defy transmission measurements. A dilute model bubbly system, a concentrated model bubbly system, yogurt, cream, bread dough and beer foam have been characterised ultrasonically, and by densitometry, light microscopy, electron microscopy and light scattering. The model system has been shown to be stabilised by an unusual and novel structured surfactant layer at the interface.

Conventional measurements on the dilute model system did not agree with ultrasonic transmission measurements. The ultrasonic technique was able to measure volume fractions as low as 10^{-7}, but it could not measure the bubble size. Reflection measurements on the concentrated bubbly liquid demonstrated that the theory fails at high volume fractions of air. The ultrasonic technique has been shown to be able to measure the bubble size in whipped yogurt. The presence of an agglomerated fat globule network has been shown to have a dramatic effect on the ultrasonic properties of whipped cream. The ultrasonic technique was able to discriminate between conventional whipped cream and spray cream, and the technique has been shown to be sensitive to the time-dependent properties of spray cream. The small volume fraction of air present in unfermented dough was detected by the ultrasonic reflection technique. Fermented dough could not be characterised ultrasonically. Marked inter sample variability was demonstrated in measurements on beer. The ultrasonic technique was of limited use for characterising beer foam.

Realisation of the full potential of ultrasound for characterising real aerated foods will not be possible without an improved theory for concentrated systems.

PREFACE

Huge quantities of foods containing air are prepared and consumed everyday. Many of these aerated foods are surprisingly difficult to characterise by conventional methods. Ultrasound has considerable potential as a non-destructive technique for the characterisation of foods. The objective of the work reported here was to evaluate the potential of ultrasound for the characterisation of aerated foods.

Aerated foods vary widely in character, from carbonated drinks to bread to fruit and vegetables. In Chapter One the different types of aerated foods are discussed. Everyday experience tells us that bubbly liquids are not stable with respect to time. The mechanisms underlying this instability are examined in detail. The important physical characteristics of bubbly foods are the volume fraction of dispersed gas and the bubble size distribution. The chapter concludes with a description of the techniques which can be used to determine these parameters.

Ultrasound has a complex interaction with bubbles in liquids, leading to a rich variety of behaviour, which is considered on a theoretical basis in Chapter Two. The description starts with the simplest case, a single bubble resonating freely in a liquid, and proceeds to a consideration of the velocity and attenuation coefficient of ultrasound in a bubbly liquid. Finally the unusual behaviour associated with bubbles subjected to high-power ultrasound is described.

In the course of this investigation a range of bubbly foods were examined using a variety of techniques. A description of these foods, and the methods used to prepare them, make up the first half of Chapter Three. The second half is given over to a detailed description of the ultrasonic and light-scattering equipment which was used.

Chapter Four compares the ultrasonic measurements made on model and real foods with the predictions from theory. The results are presented as graphs wherever possible, and the discussion aims to evaluate the sources of the marked discrepancies which are found between theory and experiment.

Conclusions about the usefulness of ultrasonic and conventional techniques are drawn in Chapter Five, and suggestions for further work conclude the body of the thesis.

Finally, a series of appendices are included in order to provide some reference material. Appendix I describes the approach which has been adopted in order to account for the effects of diffraction. Appendix II describes in detail how the raw ultrasonic data were converted into values of velocity and attenuation. Appendix III lists the presentations and publications which have resulted from the work described in this thesis. Appendix IV is a glossary of terms, which are not defined in the text because they are in common usage in ultrasonics and colloid science.

CONTENTS

CHAPTER ONE

Bubbly foods and bubbly liquids

1.1 Introduction

In this introductory chapter, the different sorts of foods which contain air are discussed. After a brief examination of ultrasonics, the stability of bubbly liquids is addressed. Finally, the characterisation and manufacture of bubbly liquids are reviewed.

1.2 Foods containing air

Foods containing gas as a dispersed phase are familiar to everyone, and are commonly referred to as aerated products. In nearly all cases the dispersed gas is air, but there are a few notable exceptions. Carbon dioxide provides the dispersed gas in carbonated drinks and fermented beverages. Carbon dioxide also leavens products such as bread and buns, but it diffuses out during baking, to be replaced by air. Nitrous oxide is used in 'spray' dairy products such as whipped cream and chocolate mousse. Nitrogen is used in some canned beers in order to provide a good 'head' when the beer is poured. Nitrogen forms smaller bubbles than carbon dioxide, giving a creamier, longer lasting head.

Aside from plant tissues, which frequently contain gas in the spaces between cells, the dispersed gas in foods is introduced deliberately. The gas may be produced *in situ* or by whipping (both of which will be discussed in more detail later on). Examples of *in situ* production are:

- the leavening of bread and cakes, through the action of yeast or baking powder,
- the fermentation of beers and wines,
- the microbial action in the production of some types of cheese.

Much more commonly, the gas is introduced by beating or whipping. This gives rise to a variety of products, which can be classified according to the way in which the product is stabilised:

- whipped cream, whipped toppings and desserts (structured liquid phase),
- mousse, marshmallow (gelled liquid phase)
- meringue, nougat (liquid phase converted to semi-solid),
- ice cream, sorbet, aerated chocolate and a variety of items of confectionery such

as ‘Maltesers’ and ‘Crunchie’ (liquid phase converted to solid).

In commercial production, aeration is an extremely cost efficient method of adding value. Gas dispersions in food are poorly characterised as a rule, because the existing techniques for characterising bubbly systems are inadequate. Ultrasound is a versatile technique for the non-destructive evaluation of a wide variety of materials. The objective of this thesis is to evaluate the potential of ultrasound as a means of characterising foods containing air.

1.3 What is ultrasound?

Sound which has a frequency above the upper limit audible to humans is described as *ultrasound*. The highest frequency which most people can hear is typically 16 to 20 kHz. The study and application of ultrasound, known broadly as *ultrasonics*, has developed rapidly from the first efforts to establish the upper frequency limit for humans, to today’s diverse and sophisticated discipline (Graf, 1981). In fact, the human ear is sensitive to only a very small part of the acoustic spectrum. It is possible to generate and detect ultrasound at frequencies in excess of 10^9 Hz, and to routinely make ultrasonic measurements with accuracies of ten parts per million. The basic principles of the generation, detection and theory of propagation of ultrasound are widely accessible (see for example the textbooks by Wood (1964), Blitz (1963), Morse & Ingard (1968), Blitz (1971) and Cracknell (1980)). In the discussions which follow, the reader will be assumed to be familiar with the basic principles of ultrasound. In the meantime, a brief discussion of the applications of ultrasound will demonstrate why it is thought that ultrasound might be useful in the study of aerated foods. Since much of the terminology used in this thesis is specific to ultrasonics and to colloid science, a glossary of terms can be found at the back of the thesis.

1.4 High and low power ultrasound

Ultrasound has proved useful in a wide variety of applications, which can be broadly divided into two areas: high power (1 W cm^{-2} upwards) and low power (< 100 mW cm^{-2}). In high power applications, the aim is to use ultrasound in order to cause a permanent physical or chemical change in the system through which the ultrasound propagates. In low power applications, the aim is to use ultrasound to provide some information about the system through which the ultrasound propagates. Some general applications of ultrasound are listed below (*Table 1.1*)

In the food industry, high power applications, such as homogenisation and cleaning, are well established (Bjϕrnϕ, 1991). More recently, the potential of low power ultrasound for characterising foods has come to be recognised (McCann, 1986, Javanaud, 1988, Povey & McClements, 1988, McClements and Povey, 1989, Povey, 1989, Bjϕrnϕ, 1991). Some applications of ultrasound to the manufacture and study of foods are listed briefly below (*Table 1.2*). Ultrasound has been particularly successfully applied to the characterisation of emulsions and particulate suspensions. The interaction between low power ultrasound and most colloidal systems is well understood (see for example Kol'tsova & Mikhailov, 1976, Harker & Temple, 1988, Harker & Ogilvy, 1991, Schwarz & Margulies, 1991) and the literature is extensive. A useful overview can be found in the review article by McClements (1991).

The interaction between ultrasound and bubbles is well understood at low volume fractions of dispersed air. Bubbly systems have not, however, received as much attention as emulsions, not least because of the practical difficulties associated with bubbles, such as high attenuation and poor repeatability. Indeed, the presence of dispersed air is usually seen as a problem in ultrasonic measurements, because small amounts of air can be sufficient to completely attenuate the ultra-

Table 1.1 *Some applications of ultrasound*

Category	*Applications*
High power ultrasound	
Cleaning	*ultrasonic baths, cleaning-in-place*
Sonochemistry	*increased reaction rates*
Medicine	*lithotrypsy, physiotherapy*
Low power ultrasound	
Non-destructive testing	*flaw detection*
Medicine	*foetal imaging, echocardiography*
Ranging	*camera focussing, liquid level sensing, sonar, ultrasonic measuring tapes*
Presence/absence indication	*car alarms, hand driers*

sonic signal. Nevertheless, ultrasonic measurements can, in principle, be related to physical parameters such as the volume fraction of air and the bubble size distribution. Ultrasound is attractive as a potential technique for characterising bubbly systems because it can cope with systems which are opaque and non-conducting. The technique is non-invasive, non-destructive and robust. It is relatively low-cost, it can be made fully hygienic, and it can be automated for use in-line in food processing plant. It thus has considerable potential as a technique for characterising bubbly systems.

1.5 Bubbly solids

Some foods which contain air are solids or are solid-like. The propagation of ultrasound in solids is more complex than propagation of ultrasound in liquids. Solids can support shear waves, and a variety of structural relaxations can contribute to the attenuation of ultrasound. A wide variety of theories are available which attempt to describe ultrasonic propagation in inhomogeneous solids (Biot, 1962, Anderson & Hampton, 1980, Berryman, 1980(a,b), Brill *et al*, 1980, Lefebvre *et al*, 1980, Sayers, 1981, Sayers & Smith, 1982, Gaunaurd & Uberall, 1982, Teunissen, 1982, Gaunaurd & Uberall, 1983(a,b), Gaunaurd & Barlow, 1984, Brauner & Beltzer, 1985, Adler *et al*, 1986, Gaunaurd & Wertman, 1988, Nair *et al*, 1989) and in fruits and vegetables which contain air (Miller, 1979). The propagation of ultrasound in liquids is simpler, and in food systems there is a greater likelihood of

Table 1.2 *Some applications of ultrasound in the food industry*

High power ultrasound (Bjϕrnϕ, 1991, Hafsteinsson *et al*, 1992)

Enhanced cleaning-in-place
Formation of suspensions, emulsions and aerosols
Improved rates of filtration, drying, extraction and heat transfer in food processing
Degassing and defoaming of solutions
Enhanced sterilisation

Low power ultrasound (Javanaud, 1988, Povey & McClements, 1988, Povey, 1989)

Back fat thickness measurement in live animals and carcasses
Solid fat content determination
Characterisation of emulsions and suspensions
Concentration measurements
Level detection and flow rate measurement

---

agreement between measurement and theory. This work has therefore concentrated on bubbly liquids. The vast majority of bubbly foods are liquid at some point in their manufacture, which would make them more amenable to ultrasonic characterisation.

1.6 Nomenclature

A dispersion of gas bubbles in a liquid may be termed a bubbly liquid or a foam. In this work, a system where all the bubbles are spherical is described as a *bubbly liquid*, even if the volume fraction of air is quite high. The term *foam* is reserved for a system which contains polyhedral air cells which are separated by lamellae which have colloidal dimensions. In some of the older literature, bubbles which are too small to be seen with the naked eye (which therefore have radii of 15 μm or less) are described as *microbubbles*. No distinction is drawn here between visible bubbles and their smaller colleagues. A bubble is described as *dirty* if there is any adsorbed material present at the gas/liquid interface, such as surfactant molecules, particulate matter or a fatty film.

1.7 The stability of bubbly liquids and foams

A pure liquid cannot support a stable dispersion of gas. As soon as the supply of gas is discontinued the bubbles rise to the surface and burst, and any foam which has formed rapidly collapses. Gas dispersions are destabilised by three very effective mechanisms: creaming, coalescence and disproportionation. Creaming is the tendency of the bubbles to rise to the surface of the bubbly liquid. Coalescence is the process whereby two bubbles or gas cells merge into one. Disproportionation is the process whereby small bubbles dissolve under the influence of the excess pressure within the bubbles. In polydisperse bubbly systems, the dissolved gas diffuses through the liquid into larger bubbles, causing them to grow at the expense of the small bubbles.

1.7.1 Creaming

A gas bubble is much less dense than the liquid which surrounds it, so it experiences a buoyant force which makes it rise or, in the terminology of emulsions, *cream*. As the bubble rises, its motion is retarded by a frictional force due to the viscosity of the liquid. A bubble which starts from rest quickly reaches a terminal rise velocity, v, when the buoyant force is balanced by the frictional force. An expression for v is easily found by selecting an appropriate expression for the frictional force. A common assumption is that the bubble can be treated as a rigid sphere, and that there is laminar flow of the liquid over the bubble as it rises. This assumption leads to the familiar Stokes' equation

$$v = \frac{2gr_0^2}{9\eta_l} |\rho_l - \rho_g| \qquad [1.1]$$

where g is the acceleration due to gravity, r_0 is the radius of the bubble, η is viscosity, ρ is density, and the subscripts g and l refer to the gas and the liquid respectively. Small bubbles ($r_0 < 500\ \mu$m) do not deform easily, because of the effect of surface tension. Foreign material effectively 'freezes' the surface of dirty bubbles, promoting a non-slip boundary condition for the flow around the bubble. Larger bubbles, however, can deform as they rise, and there may be internal circulation of the gas due to the drag at the bubble surface. An alternative formula for the rise velocity is due to Rybczynski (Epstein & Plesset, 1950)

$$v = \frac{2gr_0^2}{9\eta_l} |\rho_l - \rho_g| \times \frac{3\eta_l + 3\eta_g}{2\eta_l + 3\eta_g} \qquad [1.2]$$

Measurements of the rise velocity of bubbles with radii in the range 10 μm to 500 μm in reagent grade water and sea water have shown that the true rise velocity lies somewhere between the values predicted by these two equations. Stokes' equation generally gives the best estimate (Detsch, 1991).

Three factors which affect the accuracy of Stokes' equation are distortions in the bubble shape, the effects of pressure and the effects of disproportionation. As the bubble rises, the drag changes the shape from a sphere to an inverted teardrop, and when the bubble is very large ($r_0 >$ 3-4 mm) it can stretch and undergo chaotic oscillations. Thus Stokes' equation is of limited use for larger bubbles. As the bubble rises, the hydrostatic pressure becomes lower and the bubble expands, which causes the rise velocity to increase. This is a small effect in waters which are no deeper than a few metres, as the hydrostatic pressure is governed chiefly by the atmospheric pressure. This tendency for the bubble to expand is countered by the diffusion of gas out of the bubble. The rate of diffusion is increased by the flow of liquid over the bubble as it rises. The effect of disproportionation on the bubble radius and hence the rise velocity can be quite marked, and will be discussed more fully in Section 1.7.3.

Despite its imperfections, Stokes' equation is very widely used to relate the rise velocity of a bubble to its radius. For air bubbles in pure water, v is around $2 \times 10^6 \times r_0^2$ m s^{-1},† so any bubble of millimetre dimensions which is free to move will rapidly rise the top of the liquid. In order to be stable to creaming, the bubble must be so small that its rise velocity is negligible compared to Brownian motion. This requires a rise velocity of about 1 mm per day (Dickinson, 1992), which implies a bubble radius of around 80 nm. In practice it is not possible to make such small bubbles, and so aerated pure water would be unstable even in the absence of other destabilising mechanisms. In order to stabilise a bubbly liquid with respect to creaming, it is necessary to increase the viscosity of the liquid. In food systems this can be achieved by adding a thickening agent which imparts a yield stress to the liquid. Alternatively, an increase in the volume fraction can result in the presence of so many bubbles that any individual bubble is prevented from rising by the presence of so many near neighbours.

1.7.2 Coalescence

Coalescence occurs when two bubbles approach each other very closely. This can happen when a bubbly system is violently agitated, or when the volume fraction is very high and a foam is formed (*Fig 1.1*). The films between the gas cells are of colloidal dimensions, and are often referred to as lamellae. The junctions between lamellae are referred to as Plateau borders. The liquid from the films tends to drain into the Plateau borders, and the lamellae become thinner and thinner. A critical thickness is eventually reached, when any small perturbation such as a draught or thermal disturbance can cause the film to rupture. Coalescence can be thus be thought of as a two stage process, consisting of film drainage followed by film rupture, where the drainage is the rate limiting step.

The liquid drains from the lamellae into the Plateau borders because of a pressure difference, ΔP ($= P_c - P_d$), between the two volumes. P_c is an overall capillary

---

†: where r_0 is measured in metres.

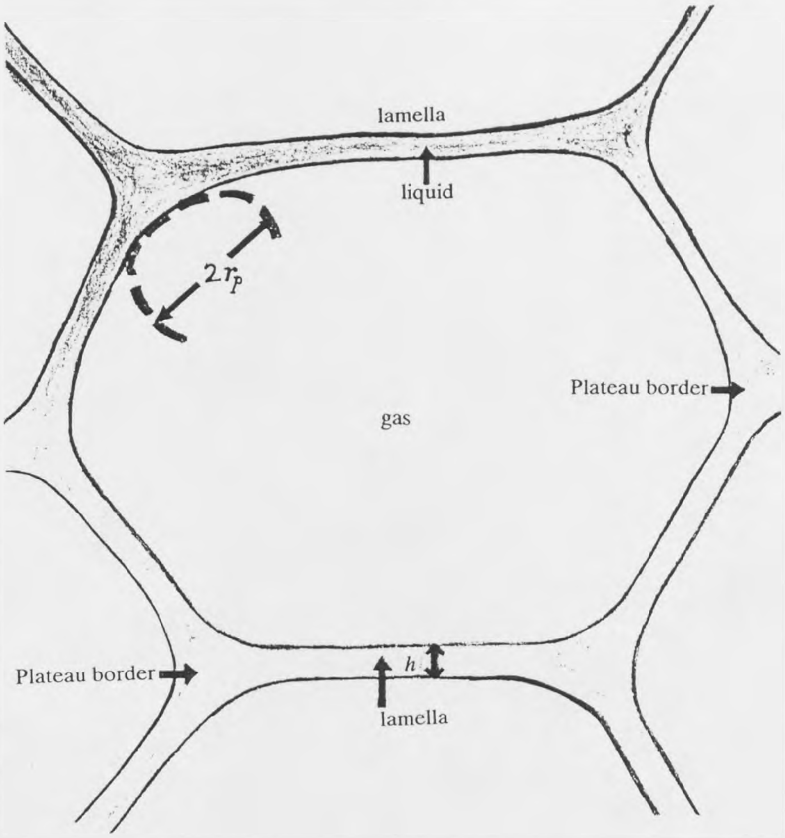

Figure 1.1 The structure of a foam, showing the thin films separating the bubbles (lamellae) and the junctions between the films (Plateau borders).

pressure which is principally due to a suction in the Plateau borders which is given by σ / r_p, where σ is the surface tension and r_p is the radius of the Plateau border (see *Fig. 1.1*). P_d is a disjoining pressure which represents the balance between the forces acting on the surfaces on each side of the lamellae. The gas cells are attracted to one another through van der Waals forces. These make a negative contribution to P_d, bringing the surfaces closer together. The close approach of the two surfaces is resisted by charge repulsion if there is any charged material at the surface, so electrostatic forces make a positive contribution to P_d.

The rate at which the film thins can be predicted by treating the two surfaces of the film as rigid disks of radius R, which are separated by a liquid of viscosity η_l at a distance h. The disks move closer to one another at a rate v_{Re}, driven by the pressure difference ΔP. This model is due to Reynolds (1886), and gives the following equation for v_{Re}:

$$v_{Re} = - \frac{h^3}{3\eta_l R^2} \Delta P \approx - \frac{h^3 \sigma}{3\eta_l R^2 r_p} \quad [1.3]$$

This implies that the drainage time is proportional to R^{-2}, but experimental measurements (Malhotra & Wasan, 1987) have shown that drainage time is proportional to $R^{-0.8}$. There are many factors which affect the drainage time which are not accounted for by the Reynolds model, such as surface tension gradient, surface viscosity, gas viscosity, surface mobility, surfactant transfer onto the interface, surfactant adsorption-desorption kinetics, dispersion forces, interfacial curvature and dimple formation (Malhotra & Wasan, 1987). A more sophisticated hydrodynamic analysis of the thinning rate, taking into account some of these factors, requires a knowledge of the effective Hamaker's constant for the system and the geometry of the Plateau borders. The rate of thinning is found by a numerical solution of the equations of flow in the lamellae and in the Plateau borders (Malhotra & Wasan, 1987). There is good agreement between the predicted rate of thinning and the observed rate of foam drainage.

The presence of surfactant has a significant effect on the rate of drainage, by lowering the surface tension and hence reducing P_c. A secondary stabilising effect is due to the Gibbs-Marangoni effect, which resists local film thinning. The presence of surfactant at the surface increases the surface viscosity and elasticity, which makes the film more resistant to rupture. The drainage of surfactant stabilised foams is not fully understood (Kim & Lee, 1988). Surfactants which adsorb rapidly at the surface are most effective at retarding drainage (Gryzhina & Trapeznikov, 1988), and higher volume fractions of incorporated gas can be achieved using a surfactant, because very thin lamellae can form (Sita Ram Sarma & Khilar, 1988). The drainage rate is proportional to the third power of h, so the thinner the film, the more slowly it drains (in the absence of surface waves). Macromolecular surfactants, which are nearly always proteins or polypeptides in food systems, can exert a stabilising effect through so-called steric stabilisation (Tabor, 1991, Dickinson, 1992). Protein molecules, which are usually highly structured, have a tendency to unfold at the surface of the bubble. The affinity of the molecule for the surface varies along the length of the molecule, resulting in a configuration made up of 'loops' and 'trains' (*Figure 1.2*). As the surfaces of the film approach one another the loops start to interact with each other. The configurational entropy of the loops is reduced as the loops come closer together, and the close approach of the interfaces is energetically resisted.

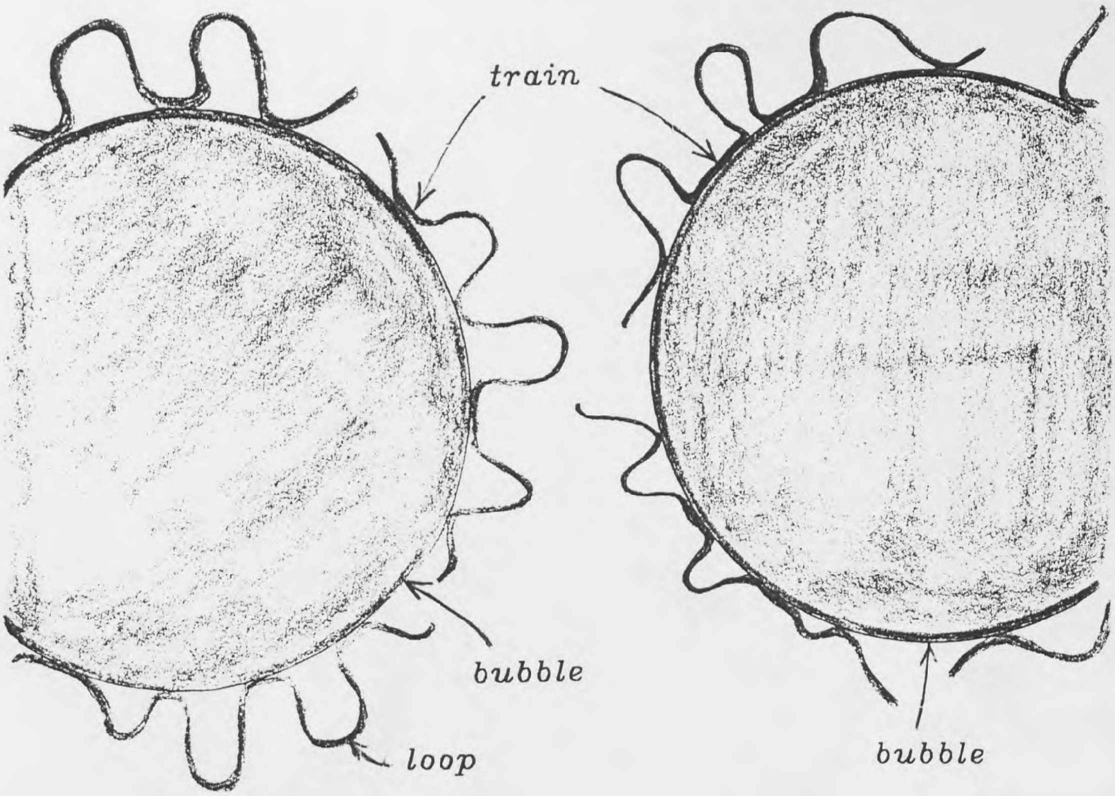

Figure 1.2 Macromolecules adsorbed at the bubble surface. 'Loop' sections of the molecule protrude into the liquid, whilst 'train' sections are located at the interface.

In addition to this entropic effect, there may also be an osmotic entropic effect. The liquid, which in foods is usually aqueous, is nearly always a good solvent for the loops. As the loops become more closely packed, the local concentration of solvent is reduced. This gives rise to an osmotic pressure gradient, which opposes the close approach of the loop sections. In the rare case where the loops are poorly solvated by the liquid, close association will be entropically preferred, and the presence of adsorbed macromolecule will be a destabilising influence. In general, steric stabilisation makes a positive contribution to the disjoining pressure, leading to a lower rate of drainage. The partial denaturation and cross-linking of protein at the surface also increase the structural strength, so that the film is more resistant to rupture.

Film drainage is particularly enhanced when the liquid also contains a dispersed liquid such as lipid. When a droplet of the dispersed liquid adsorbs at the surface, it spreads out, and as it spreads it pushes liquid from the lamellae into the Plateau borders. Lipids adsorb very strongly at the gas-liquid interface in foods, and displace nearly all surfactants as they spread out. Thus foams are strongly destabilised by lipids which are liquid at room temperature.

Sharma and Ruckenstein (1987, 1989) have demonstrated that surface waves propagate along the lamellae, which have their origin at the thinnest point of the film (usually the centre) and propagate outwards. They claim that a pumping action associated with the passage of the wave is responsible for film thinning in large films ($R > 100\,\mu m$) and in all films which are nearing the critical thickness for film rupture. Nevertheless, their theoretical calculations of foam drainage time show a $R^{-0.8}$ dependence (cf Malhotra & Wasan, 1987), and are thus also in good agreement with experimental observations. The presence of particles in the lamellae which span the film will retard film drainage (provided that they are wetted by the liquid), because such particles disperse the surface waves, and greatly reduce the pumping effect (Hudales & Stein, 1990). On the other hand, particles which are smaller than h have a destabilising effect, by reducing the local surfactant concentration at the surface, due to preferential adsorption of the surfactant onto the particle. Particles which are not wetted by the liquid can cause local thinning, and promote film rupture (Prins, 1988).

Film drainage can be retarded by increasing the viscosity of the liquid in the lamellae. This is particularly useful in coarse foams, where the effects of gravity on drainage can be significant (Dickinson, 1992). Thickening agents such as sodium carboxymethylcellulose and guar gum have been shown to significantly reduce drainage rates in foams made with the surfactant sodium lauryl sulphate (Pradhan *et al*, 1990). It was noted that thickening agents which can form a film at the surface are particularly effective in retarding film drainage.

1.7.3 Disproportionation

Disproportionation in gas dispersions is analogous to Ostwald ripening in emulsions, but it occurs over a much shorter timescale, and is a powerful destabilising force. The driving force for diffusion of gas out of the bubble is the pressure within the bubble, P, which is related to the ambient pressure in the liquid, P_0, the surface tension, σ, and the bubble radius, r_0, by the well-known Laplace equation:

$$P = P_0 + \frac{2\sigma}{r_0} \qquad [1.4]$$

If the radius of the bubble is of the order of a micrometre, then the excess pressure within the bubble is of the order of atmospheric pressure. The gas exchange between bubble and liquid depends on P, on the solubility of the gas, on the permeability of the bubble surface to gas exchange, and on the degree of saturation of the liquid. In micrometre bubbles, the internal pressure is the dominant force, and the gas will rapidly dissolve out of a clean bubble. A stationary air bubble of radius 10 μm in clean water will dissolve completely in 1.2 seconds (Epstein & Plesset, 1950). As the gas diffuses out of the bubble, the radius is reduced and the internal pressure increases. Thus shrinkage is a self-accelerating process. The pressure inside larger bubbles is little affected by the surface tension. The degree of saturation of the liquid surrounding the bubble will be increased by the gas which diffuses out of the small bubbles. The exchange then favours the larger bubbles, so that the gas diffuses into them, and by growing they reduce their internal pressure. Again, bubble growth is a self-accelerating process. So, in a bubbly liquid, bubbles below a certain size tend to dissolve, and the rest of the bubbles grow as they absorb the dissolved gas. The bubble size distribution continuously moves upwards. Disproportionation also acts in foams, and can change the gas cell size distribution even if coalescence is not occurring (Rieser & Lemlich, 1988).

Gas transfer into and out of the bubble has been studied experimentally, and modelled theoretically with some success (Cable & Frade, 1988). The radius of a bubble shrinking in water or seawater is a linear function of time until a critical radius is reached, whereupon the rate of shrinkage increases dramatically (Detsch, 1990). The dissolution rate, *dD/dt*, of a bubble in an aqueous surfactant solution can be predicted by Levich's 'dirty bubble formula'

$$\frac{dD}{dt} = -3.02\,\frac{R_g T(\Delta c)\chi^{2/3}v^{1/3}D^{1/3}}{M_g(1.5DP - 2\sigma)} \qquad [1.5]$$

where D is the diameter of the bubble, R_g is the universal gas constant, T is the temperature, Δc is the concentration difference between the saturated fluid at the bubble surface and the concentration in the bulk liquid, χ is the diffusion constant for the dissolving gas relative to the liquid and M_g is the molecular weight of the gas. This equation is applicable strictly to bubbles with rise velocities which are sufficiently low that the Reynolds number is less than or equal to one. For air bubbles in seawater, there is very good agreement between theory and experimental measurement of bubble radius for bubbles with radii up to 500 μm (Harris & Detsch, 1991).

Disproportionation can be resisted by saturating the liquid with gas, by adding a gas which has a very low solubility in the liquid, by reducing the surface tension and by changing the permeability of the surface to gas exchange. The presence of even a small amount of non-dissolving gas in the bubble can dramatically reduce the rate of bubble shrinkage, and can cause shrinkage to stop at an equilibrium radius (Yung *et al*, 1989, Weinberg *et al*, 1990). The addition of surfactant retards disproportionation by reducing the surface tension and, at high concentrations, by reducing the permeability of the interface.

1.7.4 The existence of stable bubbles

Experimental measurements of the cavitation strength of water have shown that it is much lower than the predicted theoretical value of $\approx 10^4$ atmospheres. Indeed, if the practical cavitation strength of water were this high, it would be practically impossible to induce cavitation ultrasonically. In tap water and distilled water, the cavitation strength is of the order of 1 atmosphere (Sirotyuk, 1970). The reduced cavitation strength is attributed the presence of dispersed air at very low volume fraction, which acts as 'weak spots' or nuclei for the formation of cavitation bubbles[†]. Experiments on decompressed gelatin gels have shown that pre-existing gas nuclei account for at least 99.9% of the bubbles formed on decompression (Yount & Strauss, 1976). The nucleating air is supported in crevices in any particulate matter which is present in the water, and it can also be found in the form of stable bubbles with radii of micrometre order. The presence of stable bubbles in natural waters has been well documented (see for example, Turner, 1961). There has been some speculation about the mechanisms which stabilise these bubbles. Proposals

---

†: Nucleation sites are also responsible for the formation of vapour bubbles when water boils. Completely degassed water will not boil unless it is very strongly superheated.

have been made that there is a rigid impermeable skin of organic matter at the interface (Fox & Herzfeld, 1954), or that bubbles may be stabilised by a skin of charged particles, since bubbles in natural waters are known to carry a net charge. Stabilisation by a skin of solid particles at the interface has also been suggested (Turner, 1961). Crum (1982) has discussed the merits of the various models in some detail. If water containing stable bubbles is subjected to high pressures prior to the measurement of cavitation strength, it is found that cavitation strength increases linearly with the magnitude of the applied pressure, as the bubbles are forced into solution. This disproves the rigid skin hypothesis, because there would be a threshold pressure below which the bubbles would be resistant to crushing. Measurements on very pure solutions of sodium salts have shown that inorganic compounds have practically no effect on the stability of air bubbles with regard to dissolution (Brylyakov & Gorlovskii, 1988).

The best evidence is that free bubbles are stabilised by a thick skin of surfactant material (Yount, 1979, Crum, 1982). This skin increases the mass of the bubble and lowers the mobility of the bubble sufficiently for it to resist creaming. The presence of a large amount of surfactant at the interface makes the interface much less permeable to gas diffusion. Surfactant material is abundant in foods and in natural waters like sea water. In fact, traces of organic material with surfactant properties are found in even the most rigorously purified water (Sirotyuk, 1970), and even at a level of $\approx 2 \times 10^{-8}$ moles per litre the cavitation strength is reduced to ≈ 7.5 atmospheres.

Air is introduced into natural waters by breaking waves, falling rain drops and by dust. The air bubbles formed are initially quite large, and they either cream out rapidly or start to shrink due to diffusion. In the meantime surfactant starts to adsorb at the interface. As the bubble continues to shrink, the surfactant layer becomes more concentrated as the bubble surface is reduced. A point is reached where the bubble has shrunk so much that the surfactant skin is sufficiently condensed to hinder any further escape of gas. It is reasonable to expect then that bubbles in foods will also be primarily stabilised by surfactants (as these are widely found in food liquids) rather than by ionic or particulate material (although these will make a contribution).

1.8 Characterisation of bubbly liquids

The food scientist wants to know the volume fraction of air and the bubble size distribution in bubbly foods. Obtaining this information is not always straightforward. There are several techniques for characterising bubbly liquids. Most of the techniques are destructive or invasive. The following list, which is not claimed to be exhaustive, sets out the features of the main techniques.

1.8.1 Density measurements (gravimetry/densitometry)

The most obvious technique to determine the volume fraction of air is to measure the density of the aerated food. The density of an irregularly shaped solid may be difficult to determine accurately. The density of a liquid food is much easier to measure, but the highly cohesive and viscous nature of many of these liquids limits the accuracy of the measurements which can be made. Thus it is difficult to measure small volume fractions of air, when the density change due to the presence of the air is less than the uncertainty of the measurement.

1.8.2 Rise time

Using Stokes' equation, or one of the many modifications which describe bubble movement in non-Newtonian liquids, it is possible to relate the bubble rise velocity to the radius. The observations of bubble rise velocity may be made by optical or electroresistive techniques (Choi and Lee, 1990). Large bubbles can deform drastically at high rise velocities, and the rise rate of an individual bubble is influenced by the presence of bubbles in close proximity. The rise velocity technique is therefore of limited accuracy.

1.8.3 Photographic measurement

In clear liquids, bubbles may be characterised by high speed cinematographic or video measurements, which are frequently coupled with digital image analysis techniques (Walsh and Mulhearn, 1987, Yianatos *et al*, 1988, Saxena *et al*, 1990). This technique is restricted to bubbles with millimetre radius, and volume fractions of one percent or less.

1.8.4 Light microscopy

Photographic measurement and light microscopy are the most commonly used techniques for characterising the bubble size distribution in bubbly liquids. Bubbles show up very clearly under the microscope, with a thick black outline. The resolution of the light microscope places a lower limit on the bubble sizes which can be measured of a few micrometres. Problems arise when there is a wide distribution of bubble sizes. The thickness of the section of bubbly liquid which is examined under the microscope is limited by the size of the largest bubbles. If many smaller bubbles are also present, then there is a good chance that large bubbles will obscure the smaller ones. In extreme cases, the section may be so thick that it is too opaque to be examined fruitfully. This would require the use of many different magnifications in order to characterise all the different bubbles. In order to achieve statistically meaningful bubble size distributions by light microscopy, it is necessary to count a large number of bubbles from various samples of the bubbly liquid. Light microscopy is therefore more likely to be useful as a semi-quantitative technique rather than as a quantitative technique.

1.8.5 Electron microscopy

Solid foods are relatively easy to characterise using electron microscopy. Thin sections can be prepared, and the observed sectional size distribution can be related to the true size distribution (Piefke, 1976, Kawakami *et al*, 1988). Liquid foods can be examined by freezing them in order to obtain a solid section. However, the freezing process must be very rapid, in order to avoid a change in the bubble size distribution. The sample preparation process for electron microscopy is lengthy, and care must be taken to avoid the generation of artifacts. Because the magnification factor is very high, the area of the sample which is observed is very small. Careful sampling is therefore essential. Sampling considerations, and the tedious nature of the sample preparation, mean that electron microscopy is not generally used to measure bubble size distributions.

1.8.6 Laser light scattering

Laser light scattering is capable of examining bubbles with radii of micrometre dimensions. The technique is limited to very low volume fractions. Observations of the scattering of laser light by an individual bubble can be used to measure the velocity and diameter of the bubble (Hansen, 1985, Yu & Varty, 1988). Very high speed laser holography (up to 69 300 holograms per second) can be used to observe chaotic oscillations of cavitation bubbles (Lauterborn & Koch, 1987). Devices such as the Malvern Mastersizer (which is described in more detail in Chapter Three) are capable of characterising very dilute bubbly systems. The bubbles which are found in bubbly foods do not survive the dilution which is part of the measurement process, so the technique is not useful for real foods.

1.8.7 Capillary suction probe

In this method, a capillary tube is submerged in the liquid of interest (Randall *et al*, 1989, Barigou and Greaves, 1991). Suction is applied to one end of the tube, so that bubbles are drawn through it. A pair of optical detectors surround the capillary, which measure the length of the bubble slug and its rate of passage through the tube. The technique provides an accurate means of determining bubble sizes down to a radius of 0.15 mm.

1.8.8 Electrical resistance

In electrically conducting liquids, bubble size can be determined by measuring the change in resistance of the liquid between two electrodes as a bubble passes through the gap between the wires. An instrument such as the CoulterCounter, which draws bubbles through an orifice of known diameter to pass through the electrodes, is capable of measuring bubble size distributions in systems with stable bubbles. As with the Mastersizer, the dilution which is necessary renders the technique unsuitable for use with real bubbly foods.

1.8.9 Empirical techniques

A variety of empirical techniques are used to characterise foams and concentrated bubbly liquids (see for example Phillips *et al*, 1987, Schott, 1988, Lachaise *et al*, 1990). Most of these methods are based on the sparging of a known volume of liquid. The measured properties are usually the over-run (= 100 × (volume of foam - volume of original liquid) / (volume of original liquid)) and the foam drainage time. Empirical techniques will not be considered in detail in this work.

1.9 Methods of producing gas dispersions

There are three main methods for producing bubbly liquids and foams: production *in situ*, sparging and whipping.

1.9.1 Bubble production in situ

In liquids which are supersaturated with gas, such as carbonated drinks and spray cream, bubbles are spontaneously produced at nucleation sites when the liquid is brought to atmospheric pressure. Gas bubbles may also be produced by chemical reaction, such as the decomposition of baking powder at high temperature, or by biochemical reaction, such as the production of carbon dioxide by yeast.

1.9.2 Sparging

Gas may be blown directly into the liquid through a sparger, which is any device containing one or more small orifices, such as a hypodermic needle or sintered glass filter. Although sparging is well understood (Geary and Rice, 1991) it is not widely used in food production. Sparging is useful as a laboratory technique because it is the most reproducible method (Dickinson, 1992), although all methods of foam production have poor reproducibility. A repeatability of 20% between runs is considered a good figure (Calvert & Nezhati, 1987).

1.9.3 Whipping

This is the principal method used to produce bubbly liquids in the food industry. The whipping process is governed by the beating rod and surfactant concentration in much the same way as emulsification is controlled by the homogeniser type and surfactant concentration. As whipping proceeds, large unstable bubbles are produced, which break up in the shear field produced by the beating rod. The maximum incorporated air volume is fairly quickly achieved, when the whipping rod becomes submerged and cannot add any more air. Further beating merely serves to subdivide the bubbles (Bee *et al*, 1987), although very vigorous agitation can cause coalescence as bubbles collide with one another more often and with more force. The degree to which the bubbles can be reduced in size depends on the shear field that the beating rod can create, and on the surfactant concentration. After lengthy beating, the minimum bubble size is reached, when nearly all the surfactant has moved to the gas-liquid interface.

1.10 Summary

There are a wide variety of foods which contain dispersed gas, almost all of which are created by processing. The majority of bubbly foods are liquid at some point in their existence, and it is on bubbly liquids that this thesis will concentrate. Ultrasound is capable of characterising liquid-in-liquid dispersions. The objective of this work is to assess if it useful for characterising gas-in-liquid dispersions. Bubbly liquids are destabilised by creaming, coalescence and disproportionation. The stability of bubbly liquids can be enhanced by increasing the viscosity of the liquid phase, and by adding surfactants which are charged and/or macromolecular. Bubbly liquids can be characterised by a variety of methods, of which gravimetry and light microscopy are the most suitable for foods. Bubbly liquids can be produced *in situ*, by sparging or, usually, by whipping.

CHAPTER TWO

The ultrasonic behaviour of bubbles

2.1 The behaviour of an individual bubble

2.1.1 Introduction

In this section, the physical processes are considered which occur when an individual bubble resonates and when a bubble is insonified. The means by which bubbles redirect incident ultrasonic energy, and convert it into heat, are considered. The ultrasonic scattering behaviour of the bubble is elucidated.

2.1.2 The bubble as a mass on a spring

Consider a mass *m* suspended on a massless, perfectly elastic spring, which is free to move only in the vertical direction. If the mass is displaced by a small distance *x* from its equilibrium position and then released it will exhibit a simple harmonic oscillation around the equilibrium position. If the oscillations are undamped then the equation of motion of the mass is

$$m \frac{d^2x}{dt^2} + kx = 0 \qquad [2.1]$$

where *k* is the stiffness of the spring. If *x* varies with time, *t*, according to $x = a \sin(2\pi t/T)$, where *a* is the maximum displacement of the mass and *T* is the period of the oscillation, it is simple to solve *Equation 2.1* to give

$$f_{\text{res}} = \frac{1}{2\pi}\sqrt{\frac{k}{m}} \qquad [2.2]$$

Now consider a single bubble performing spherically symmetric radial oscillations (sometimes called 'breathing mode' oscillations) in an infinite sea of liquid. The following approximations are made: there is no heat or mass transfer between bubble and liquid during the oscillations, the liquid is incompressible and inviscid and the pressure is uniform throughout the entire system. The bubble has only one degree of freedom (because of the spherical symmetry) and the equation of motion of the bubble is the same as that of the mass on a spring. The mass is provided by the water which is displaced during the oscillations of the bubble, and the stiffness is provided by the gas in the bubble. In the equation of motion for the bubble, x is replaced by v, where $v = V - V_0$, V is the volume of the bubble at some time t, and V_0 is the equilibrium volume of the bubble. The form of the expression for the resonant frequency of the bubble will thus clearly be that of *Equation 2.2*, where m and k represent generalised mass and stiffness constants for the bubble-liquid system.

2.1.3 The resonant frequency

In a widely quoted paper Minnaert derived an approximate expression for the resonant frequency of a bubble (Minnaert, 1933). The derivation relies on the mass-spring analogy for a vibrating bubble, and is reproduced below. Let the bubble exhibit undamped simple harmonic oscillation at its natural frequency, such that the radius, r, oscillates around the equilibrium value, r_0 according to:

$$r = r_0 + a \sin \left(\frac{2\pi t}{T} \right) \qquad [2.3]$$

where a is the maximum change in the radius (assumed small compared to r) and T is the period of the oscillation. If the oscillations are undamped, the total energy of the system, E, is given by $E = E_{\text{pot}} + E_{\text{kin}}$, where the subscripts 'pot' and 'kin' stand for potential and kinetic respectively. When the bubble has its minimum volume $E = E_{\text{pot}} \big|_{r=r_0-a}$, and when the bubble is at equilibrium volume $E = E_{\text{kin}} \big|_{r=r_0}$. The period of the oscillation, and hence the natural frequency, are found by equating these two energies.

To calculate the potential energy at minimum volume, let the radius decrease by a small amount, x. Assuming that the compression is adiabatic, the volume, V, and pressure inside the bubble, P, are related to their equilibrium values, V_0 and P_0, by

$$\frac{P}{P_0} = \left(\frac{V_0}{V} \right)^{\gamma} = \left(\frac{r_0}{r_0 - x} \right)^{3\gamma} \qquad [2.4]$$

where γ is the ratio of the specific heats of the gas in the bubble. For air, the value of γ at 20 °C is very close to the theoretical value for a diatomic gas of 1.4. Since x

is defined as small compared to r, *Equation 2.4* can be approximated by

$$P - P_0 = \frac{3\gamma Px}{r} \qquad [2.5]$$

E_{pot} is then found from the following integral

$$-\int_{V_0}^{V} (P - P_0)dV = \int_0^a \frac{3\gamma Px}{r} \cdot 4\pi r^2 dx = 6\pi\gamma P_0 r_0 a^2 \qquad [2.6]$$

To calculate the kinetic energy of the system, only the liquid need be considered. The velocity of the bubble wall is easily obtained from *Equation 2.3*

$$\frac{dr}{dt} = \left(\frac{2\pi a}{T}\right) \cos\left(\frac{2\pi t}{T}\right) \qquad [2.7]$$

The velocity, v, of an infinitesimally small volume of fluid at some distance R from the centre of the bubble is given by

$$\mathrm{v} = \frac{r^2}{R^2}\frac{dr}{dt} \qquad [2.8]$$

The maximum kinetic energy of all such volumes surrounding the bubble is now calculated. E_{kin} is maximal when $r = r_0$ and the cosine term in *Equation 2.7* is equal to one. The kinetic energy is given by

$$\frac{1}{2}\int \left(\frac{dr}{dt}\right)\Bigg|^{2}_{r=r_0} dm = \frac{\rho_l}{2}\int_r^{\infty} \frac{r^4}{R^4}\cdot\frac{4\pi^2 a^2}{T^2}\cdot 4\pi R^2\, dR = \frac{8\pi^3 \rho_l r_0^3 a^2}{T^2} \qquad [2.9]$$

where m is the mass of each infinitesimal volume, and ρ_l is the density of the liquid. Setting *Equation 2.6* equal to *Equation 2.9* gives

$$6\pi\gamma P_0 r_0 a^2 = 8\pi^3 \rho_l r_0^3 a^2 T^{-2} \qquad [2.10]$$

$$T^2 = \frac{4\pi^2 \rho_l r_0^2}{3\gamma P_0} \qquad [2.11]$$

$$f_{\text{res}} = \frac{1}{T} = \frac{1}{2\pi r_0}\sqrt{\frac{3\gamma P_0}{\rho_l}} \qquad [2.12]$$

It is seen that k / m for the system is given by $3\gamma P_0 / \rho_l r_0^2$, and it is possible to show that $k = \gamma P_0 / V_0$ and $m = \rho_l / 4\pi r_0$ (Devin, 1959).

Anderson and Hampton (1980) have looked at several experimental measurements of the resonant frequency of air bubbles in water, and compared these measurements with the frequencies predicted by the Minnaert equation. They concluded that Minnaert's expression predicted the resonant frequency for bubble with radii larger than 10 μm to within 5%. Nishi (1975) states that "for most applications where the bubble radii are larger than 10 μm the existing models [*ie the Minnaert equation*] are sufficient to predict the acoustic properties of the bubble."

2.1.4 An improvement on the Minnaert equation

The Minnaert equation fails for small bubbles because the assumptions made in its derivation are violated. In order to improve our description of the bubble, an improved equation of motion is needed. The Rayleigh-Plesset equation allows for surface tension and the viscosity of the liquid. It is a second order differential equation in r, which describes how the bubble behaves when it is placed in a sound field with acoustic pressure amplitude P_a and arbitrary frequency ω ($= 2\pi f$):

$$\rho_l r\ddot{r} + \frac{3}{2}\rho_l \dot{r}^2 = P_{\text{in,eq}}(r_0/r)^{3\gamma} - P_0\left[1 - \frac{P_a}{P_0}\cos(\omega t)\right] - \frac{2\sigma}{r} - \frac{4\eta}{r}\dot{r} \qquad [2.13]$$

where the dots denote differentiation with respect to time, σ is the surface tension, η is the viscosity of the liquid and $P_{\text{in,eq}}$ is the equilibrium pressure acting on the inner side of the bubble surface at equilibrium radius (which thus far has been assumed equal to P_0). Many modifications of the Rayleigh-Plesset equation have been proposed which attempt to account for factors such as the compressibility of the liquid, and non-Newtonian behaviour (see for example De, 1987, Prosperetti, 1987, Shukla, 1987). The most used modifications have been reviewed by Prosperetti (1984). The precise form of the Rayleigh-Plesset equation used is not central to the present analysis of the behaviour of the bubble, so the existence of such modifications is merely noted.

The Rayleigh-Plesset equation can be solved by linearising it. Taking $r = r_0 (1 + x)$, where $|x|$ is very small, results in the equation for a driven damped harmonic oscillator (Devin,1959, Prosperetti, 1977, Prosperetti, 1984).

$$m \frac{d^2v}{dt^2} + b \frac{dv}{dt} + kv + P_a \exp(i\omega t) = 0 \qquad [2.14]$$

or

$$\frac{d^2x}{dt^2} + 2\beta \frac{dx}{dt} + \omega^2 x + \frac{P_0}{\rho_l r_0^2} P_a \exp(i\omega t) = 0 \qquad [2.15]$$

where m is the effective mass of the system and P_a, the amplitude of the driving pressure, is assumed to be small, and to have a harmonic time dependence. The damping constants b and β will be discussed in more detail below.

Before the driven bubble is considered, it is instructive to summarise the improved analysis of the behaviour of a freely resonating bubble (Devin, 1959). The equation for the resonant frequency is improved, by refining the assumptions concerning heat transfer and the pressure within the bubble.

2.1.4.1 Heat transfer between bubble and liquid

The gas in the bubble is much more compressible than the surrounding fluid, so it becomes alternately warmer and cooler than the liquid as its radius changes. It has been assumed thus far that there is no heat transfer between the bubble and the liquid, so that the gas in the bubble follows the adiabatic equation of state, $dP/P_0 = -\gamma dV/V_0$. It could equally have been assumed that heat flows out of the bubble when it is warmer than the liquid, and then into the bubble when it is cooler than the liquid, such that the heat loss and gain by the bubble during each cycle are exactly balanced. Under these conditions the bubble and liquid stay at the same temperature, and the pulsations are isothermal, with $dP/P_0 = -dV/V_0$.

Now consider the situation in a real bubble. The values of the thermal conductivity and specific heat capacity of the gas in the bubble are lower than the corresponding values for the liquid. Near the surface of the bubble, the gas can easily gain heat from, or give up heat to, the surrounding liquid. Towards the centre of the bubble, the gas is insulated from the surrounding liquid by the outer part of the bubble, which is a poor conductor of heat. Thus, in general, the gas at the surface of the bubble follows the isothermal equation of state, and the gas in the centre follows the adiabatic equation of state. Overall the gas in the bubble obeys a polytropic equation of state, $dP/P_0 = -\kappa dV/V_0$, where κ is the polytropic exponent, the value of which lies between 1 and γ (Devin, 1959). The larger the bubble, the more adiabatically it behaves, and the smaller the bubble, the more isothermally it behaves.

At resonance, the polytropic exponent κ is given approximately by (Devin, 1959)

$$\kappa = \gamma / A \qquad [2.16]$$

$$\mathrm{A} = \left[1 + \frac{3(\gamma - 1)}{2\phi_1 r_0} \left[1 + \frac{3(\gamma - 1)}{2\phi_1 r_0} \right] \right] \qquad [2.17]$$

$$\phi_1 = (\omega / 2D_1)^{½} \qquad [2.18]$$

$$D_l = K_l / \rho_l c_{p,l} \qquad [2.19]$$

where K_l is the thermal conductivity of the liquid and $c_{p,l}$ is the specific heat capacity at constant pressure of the liquid. The stiffness of the bubble, previously taken as $\gamma P_0 / V_0$, is thus modified to $\kappa P_0 / V_0$.

2.1.4.2 Surface tension effects

So far, the pressure within the bubble has been assumed to be the same as that in the liquid. When the bubble is at rest, the Laplace equation (*Equation 1.4*) states that pressure within it, $P_{in,eq}$, is increased by an amount $2\sigma / r_0$. The stiffness, k, of the bubble is therefore modified to

$$k = \kappa P_{in,\,eq} / V_0 \qquad [2.20]$$

The surface tension acts as an extra restoring force, increasing the effective stiffness of the bubble, and increasing the resonant frequency by a factor g, where g is given by

$$g = 1 + (2\sigma / P_0 r_0) - (2\sigma / 3\kappa P_0 r_0) \qquad [2.21]$$

Thus the corrected expression for the resonant frequency becomes (Devin, 1959)

$$f_{\mathrm{res}} = f_{\mathrm{M}} \sqrt{\kappa g/\gamma} \qquad [2.22]$$

where f_{M} is the resonant frequency predicted by the Minnaert equation.

2.1.5 Damping mechanisms

If the gas in the bubble follows a polytropic equation of state, then the heat lost by the bubble during compression exceeds the heat gained during expansion. There is a net loss of energy from the bubble, and the amplitude of successive oscillations is reduced by *thermal damping*. In addition to thermal damping, the motions of the bubble are damped by *viscous* damping and *acoustic* damping, which will be described in more detail below. The relative importance of these various damping mechanisms depends on the size of the bubble. The overall damping constant b (or β) can be thought of as a sum of the damping constants from each damping process

$$b = b_{\mathrm{t}} + b_{\mathrm{v}} + b_{\mathrm{a}} \qquad [2.23]$$

where the subscripts t,b and v stand for thermal, viscous and acoustic respectively. Thus the viscosity term in *Equation 2.13* can be thought of an effective viscosity which includes contributions from thermal and acoustic effects.

2.1.5.1 Thermal damping (Devin, 1959)

Thermal damping at resonance can be described by a dimensionless thermal damping constant, δ_t, where

$$\delta_{\mathrm{t}} = \frac{\omega_{\mathrm{res}} b_{\mathrm{t}}}{k} = 2\,\frac{F_1}{F_2} \qquad [2.24]$$

$$F_1 = \left[\frac{16}{9(\gamma - 1)^2} \cdot \frac{Fg}{f_{\mathrm{res}}} - 3\right]^{1/2} - \frac{3\gamma - 1}{3(\gamma - 1)} \qquad [2.25]$$

$$F_2 = \frac{16}{9(\gamma - 1)^2} \cdot \frac{Fg}{f_{\mathrm{res}}} - 4 \qquad [2.26]$$

$$F = 3\gamma P_0 / 4\pi\rho_1 D_1 \qquad [2.27]$$

2.1.5.2 Viscous damping (Devin, 1959)

Whilst retaining the assumption that the liquid is incompressible, it is possible to calculate the damping of the bubble motion due to viscous stresses in the liquid.

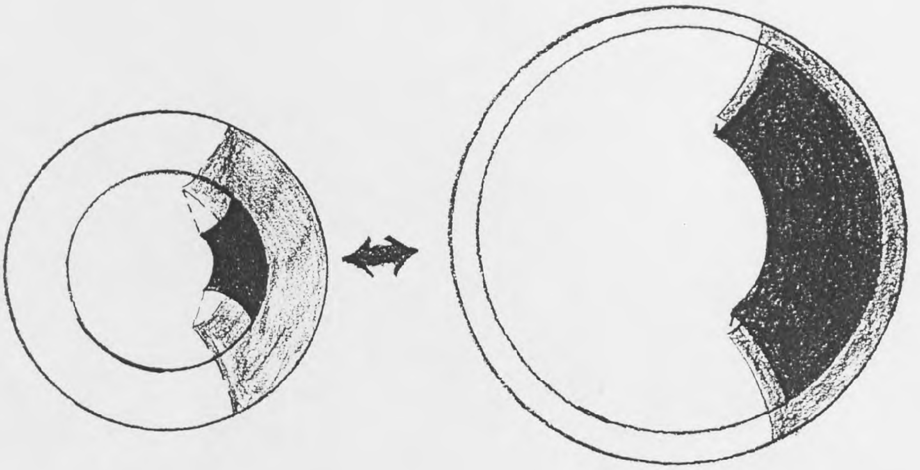

Figure 2.1 An exaggerated illustration of the viscous damping mechanism for an undriven oscillating bubble. An element of the thin spherical shell of liquid at the bubble surface is thicker and squatter when compressed (left) and thinner and flatter when expanded (right).

Consider a small element of a thin spherical shell of the liquid at the bubble surface. This element has a certain shape when the bubble radius is at its equilibrium value. When the bubble expands, the element becomes thinner and more stretched out, whereas when the bubble contracts the element becomes thicker and more squat (see *Fig. 2.1*). If the liquid is incompressible, then the change in shape is not caused by a change in the volume of the element, but by viscous stresses acting within it. More energy is required to compress the bubble than is regained in the subsequent expansion, so the effect of the viscosity of the liquid is to damp the oscillation of the bubble. The dimensionless damping constant at resonance, δ_v, is related to the viscous damping coefficient, b_v, by

$$\delta_v = b_v / \omega_{res} m = 8\pi\eta f_{res} / 3\kappa P_0 g \qquad [2.28]$$

where η is the coefficient of shear viscosity of the liquid, and m is the effective mass of the system ($= \rho_l / 4\pi r_0$).

2.1.5.3 Acoustic damping (Devin, 1959)

So far, the liquid has been considered to be incompressible, because the ratio β_l / β_g is of the order of 10^{-5}, where β_l and β_g represent the compressibility of the liquid and of the gas respectively. However, the liquid does have a finite compressibility, and is thus able to support sound waves. The oscillating bubble therefore acts as a source of sound, and it gives up energy in doing so. If the bubble is considered as a simple sound source, where r_0 is much smaller than the wavelength of the radiated sound, then the acoustic damping constant at resonance is given by

$$\delta_a = b_a / \omega_{res} m = \omega_{res} r_0 / c_l \qquad [2.29]$$

where c_l is the speed of sound in the liquid.

2.1.5.4 Overall damping at resonance

The overall dimensionless damping constant at resonance, δ $(= \delta_t + \delta_v + \delta_a)$ is calculated as a function of the resonant frequency in *Fig. 2.2*. In large bubbles with low resonant frequency, thermal and acoustic damping are the dominant mechanisms. For smaller bubbles, with higher resonant frequencies, which behave polytropically, thermal damping dominates. The smallest bubbles act isothermally, so thermal damping is much less important, and viscous damping effects dominate.

2.1.6 The behaviour of an insonified bubble

The foregoing discussion constitutes a reasonably accurate description of the phenomena occurring at the resonant frequency of the bubble. Clearly, a bubble does not spontaneously start to oscillate at its resonant frequency: an energy input is required. In Minnaert's experiments the bubbles were excited to resonance as they broke away from the nozzle at which they were formed. In ultrasonic experiments, the bubbles are excited into radial oscillation by an incident sound wave of arbitrary frequency, which for convenience will be assumed to be perfectly plane and of infinite extent.

The description of the damping processes is modified somewhat in the presence of a driving sound wave. The thermal behaviour of the bubble depends on the insonifying frequency, and thermal damping is usually the dominant mechanism in driven

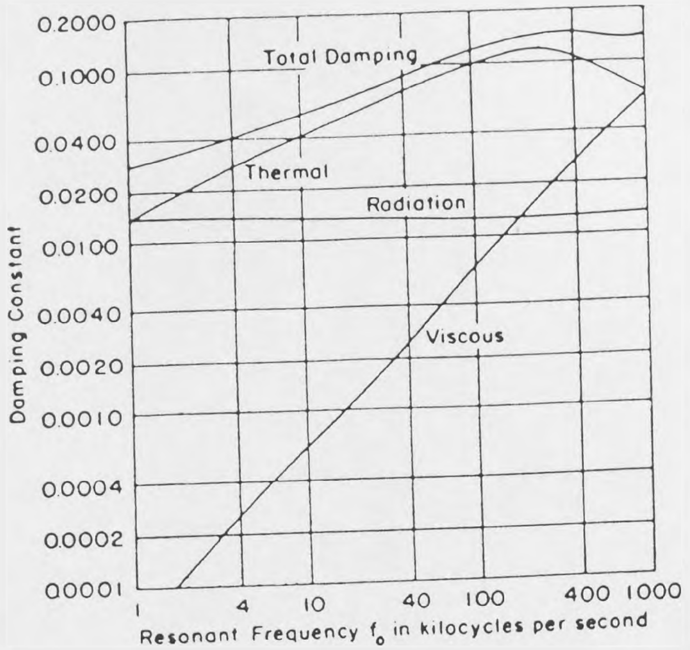

Figure 2.2 The dimensionless damping constant for air bubbles freely resonating in water. The bubble size is inversely proportional to the resonant frequency. The contributions from the individual damping mechanisms are also shown. *From Devin, 1959.*

bubbles. The nature of the viscous damping mechanism also changes, because the bubble moves back and forth along the axis of propagation of the incident wave. The translational motion arises due to the difference in inertia between the bubble and the liquid, and it is resisted by drag due to the viscosity of the liquid. Thus this type of damping is often referred to as visco-inertial damping.

2.1.7 The polytropic exponent

Prosperetti (1977, 1991) has made a perturbation analysis of the behaviour of a bubble which is more detailed than that of Devin, and it drops the assumption that the pressure is uniform within the bubble. His expression for the resonant frequency of the bubble is

$$f_{\mathrm{res}} = \frac{1}{2\pi} \left[\frac{3\kappa P_{\mathrm{in,eq}}}{\rho_l r_0^2} - \frac{2\sigma}{\rho_l r_0^3} + \frac{\omega^2 (\omega r_0 / c_l)^2}{1 + (\omega r_0 / c_l)^2} \right]^{1/2} \qquad [2.30]$$

where ω is the impressed angular frequency and the other terms are defined as previously. The polytropic exponent, κ, is given by

$$\kappa = \frac{1}{3}\left[\frac{\omega^2 \rho_g r_0^2}{P_{\text{in,eq}}}\right] \text{Re}\,(\varphi) \qquad [2.31]$$

where ρ_g is the density of the gas in the bubble and φ is given by

$$\varphi = \frac{k_p f_p(\Gamma_2 - \Gamma_1) + \lambda_2\Gamma_2 - \lambda_1\Gamma_1}{k_p f_p(\lambda_2\Gamma_1 - \lambda_1\Gamma_2) - \lambda_1\lambda_2(\Gamma_2 - \Gamma_1)} \qquad [2.32]$$

$$\Gamma_m = \text{m} + G_1 \pm [\,(\text{m} - G_1)^2 + 4\text{m}G_1 / \gamma\,]^{½} \qquad [2.33]$$

$$\lambda_m = \beta_m \coth \beta_m - 1 \qquad [2.34]$$

$$\beta_m = (½\gamma G_2\,\{\,\text{m} - G_1 \pm [\,(\text{m} - G_1)^2 + 4mG_1 / \gamma\,]^{½}\,\}\,)^{½} \qquad [2.35]$$

$$k_p = k_l / k_g \qquad [2.36]$$

$$f_p = 1 + (\,1 + \text{m}\,)\,(\,½G_3\,)^{½} \qquad [2.37]$$

$$G_1 = M_g D_g \omega / \gamma R_g T \qquad [2.38]$$

$$G_2 = \omega r_0^2 / D_g \qquad [2.39]$$

$$G_3 = \omega r_0^2 / D_l \qquad [2.40]$$

$$\text{m} = 1, 2 \qquad [2.41]$$

where M_g is the molecular weight of the gas in the bubble, D_g is the thermal diffusivity of the gas ($= K_g / \rho_g c_{p,g}$), D_l is the thermal diffusivity of the liquid, R_g is the universal gas constant and T is the absolute temperature of the liquid. The quantity φ describes all the thermal effects associated with small amplitude bubble oscillations. Crum (1983) has verified that these expressions accurately predict the polytropic exponent of the gas in an oscillating bubble. However, at frequencies around $f_{res} / 2$, there is some discrepancy between the theory and the measured value of the polytropic exponent.

Prosperetti (1977) explains the physical significance of the dimensionless parameters G_1 and G_2 by saying that G_1 is essentially the square of the ratio between the thickness of the layer in which conduction causes significant temperature changes and the wavelength of the sound in the gas. The parameter G_2 is essentially the square of the ratio between the bubble radius and the thermal penetration depth. *Fig. 2.3* shows the effective polytropic exponent κ as a function of G_2 for various

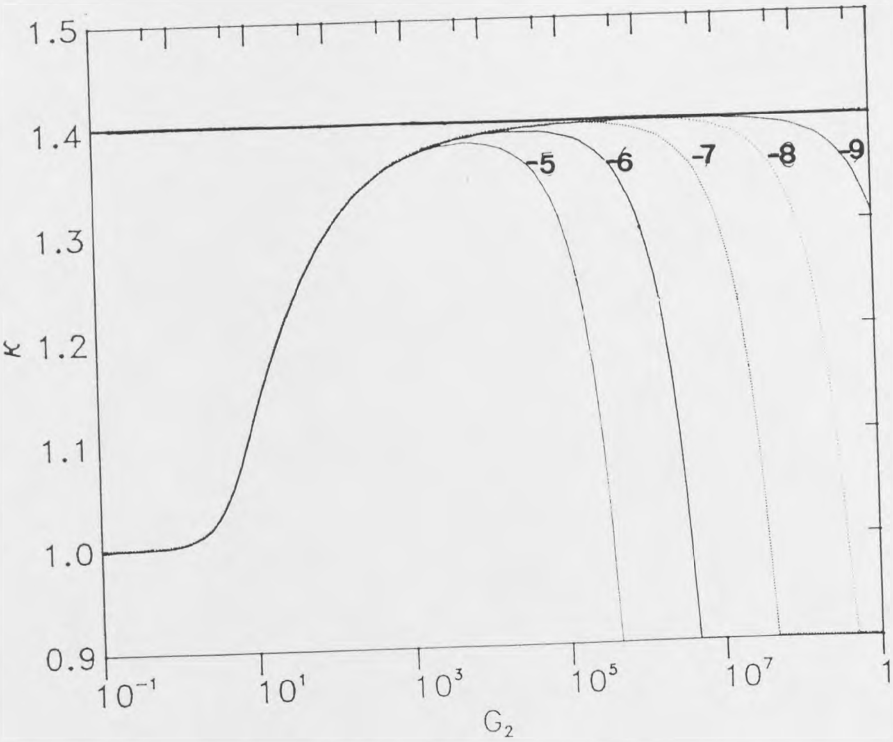

Figure 2.3 The effective polytropic constant, κ, as a function of the dimensionless parameter G_2. The value of G_1 used to calculate each curve is indicated by the label x, where $G_1 = 10^x$. The line shows the value of κ for an ideal diatomic gas.

values of G_1. The value of κ varies from 1.0 for small values of G_2 up to 1.4 for higher values, representing a change in thermal behaviour from isothermal to adiabatic, with an intermediate polytropic region. At very high values of G_2 the value of κ falls very dramatically. This represents the case where the wavelength of the sound in the liquid is small compared to the radius of the bubble. Under these conditions the pressure non-uniformity inside the bubble is very marked, and many of the assumptions made in deriving the expressions for κ are violated.

Fig 2.3 is consistent with the observation made previously that small bubbles act isothermally and large bubbles act adiabatically. If the frequency is fixed at a low value, then the value of G_1 is fixed at a low value such as 10^{-9}. With the frequency fixed, G_2 scales as r_0^2. Inspection of *Fig. 2.3* shows that at small values of G_2 (ie at small values of r_0) the behaviour is isothermal. As the value of r_0 increases the polytropic region is entered, and when r_0 reaches a threshold value the behaviour becomes adiabatic. Alternatively, if the bubble radius is considered as fixed, then as the frequency increases the value of G_1 increases and the range of frequencies over which adiabatic behaviour is possible is reduced. Thus the effect of an impressed frequency is to shift the thermal behaviour of the bubble towards the isothermal.

2.1.8 Variation in damping with frequency

The dimensional damping constants, β_t, β_v and β_a are given by

$$\beta_t = 2\eta_t \,/\, \rho_l r_0^{\,2} \qquad [2.42]$$

$$\beta_v = 2\eta \,/\, \rho_l r_0^{\,2} \qquad [2.43]$$

$$\beta_a = \tfrac{1}{2}\omega \,(\, \omega r_0 / c_l \,)\, [\, (1 + (\, \omega r_0 / c_l \,)^2 \,]^{-1} \qquad [2.44]$$

The quantity η_t can be thought of as an effective thermal contribution to the viscosity, and is given by

$$\eta_t = \tfrac{1}{4}\omega \, \rho_g r_0^{\,2} \, \mathrm{Im}\,(\varphi) \qquad [2.45]$$

The relative contributions of each type of damping to the overall damping is shown as a function of frequency, for a variety of bubble sizes, in *Fig. 2.4*. The system considered is air bubbles in pure water. In large bubbles, (*Fig. 2.4(a)*), viscous damping is unimportant. At frequencies below resonance thermal damping is predominant, and at frequencies above resonance acoustic damping dominates. As the radius of the bubble is reduced (*Fig. 2.4(b)*) the magnitude of the total damping is increased. In small bubbles, viscous damping becomes more important, and thermal damping and acoustic damping are less important. In the smallest bubbles viscous damping dominates at all frequencies.

2.1.9 Partial wave analysis

An alternative way to consider the behaviour of a bubble in a sound field is to examine the scattering behaviour of the bubble. A bubble in a sound field will cause attenuation through elastic scattering and through the damping mechanisms which were outlined above. Damping mechanisms lead ultimately to the conversion of ultrasonic energy into heat. Elastic scattering on the other hand leads to a redirection of ultrasonic energy which is incident on the bubble. In the long wavelength limit the scattering is omnidirectional, so the bubble acts as a monopole sound source. The bubble redirects ultrasound because of the big difference

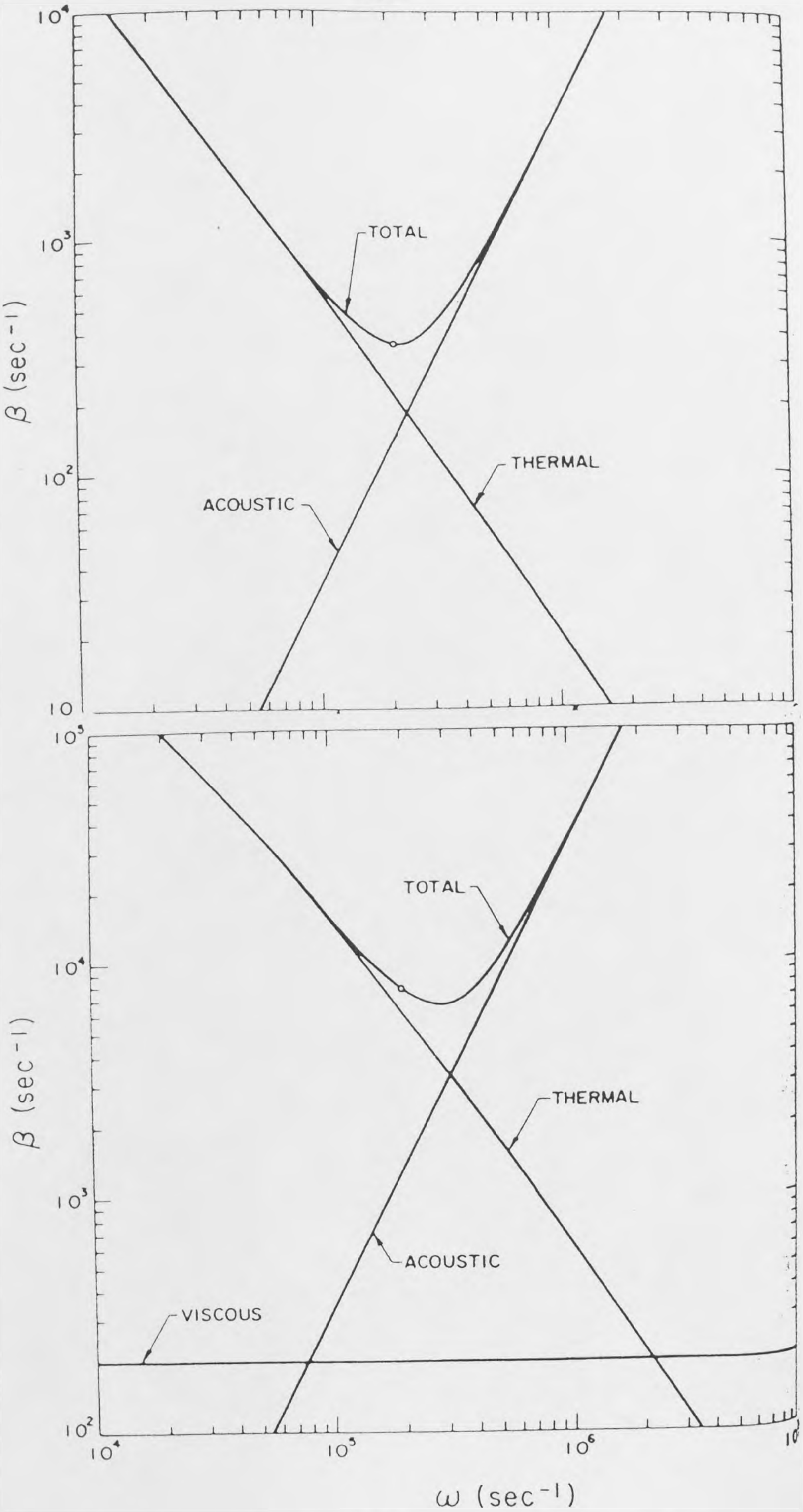

Figure 2.4(a) The total dimensional damping constant *versus* angular frequency for air bubbles in water. The open circle marks the value at resonance.The contributions from individual damping mechanisms are shown. Top: radius = 1000 μm (β_v has the constant value of 2, and is thus off-scale). Bottom: radius = 100 μm. *From Prosperetti, 1977.*

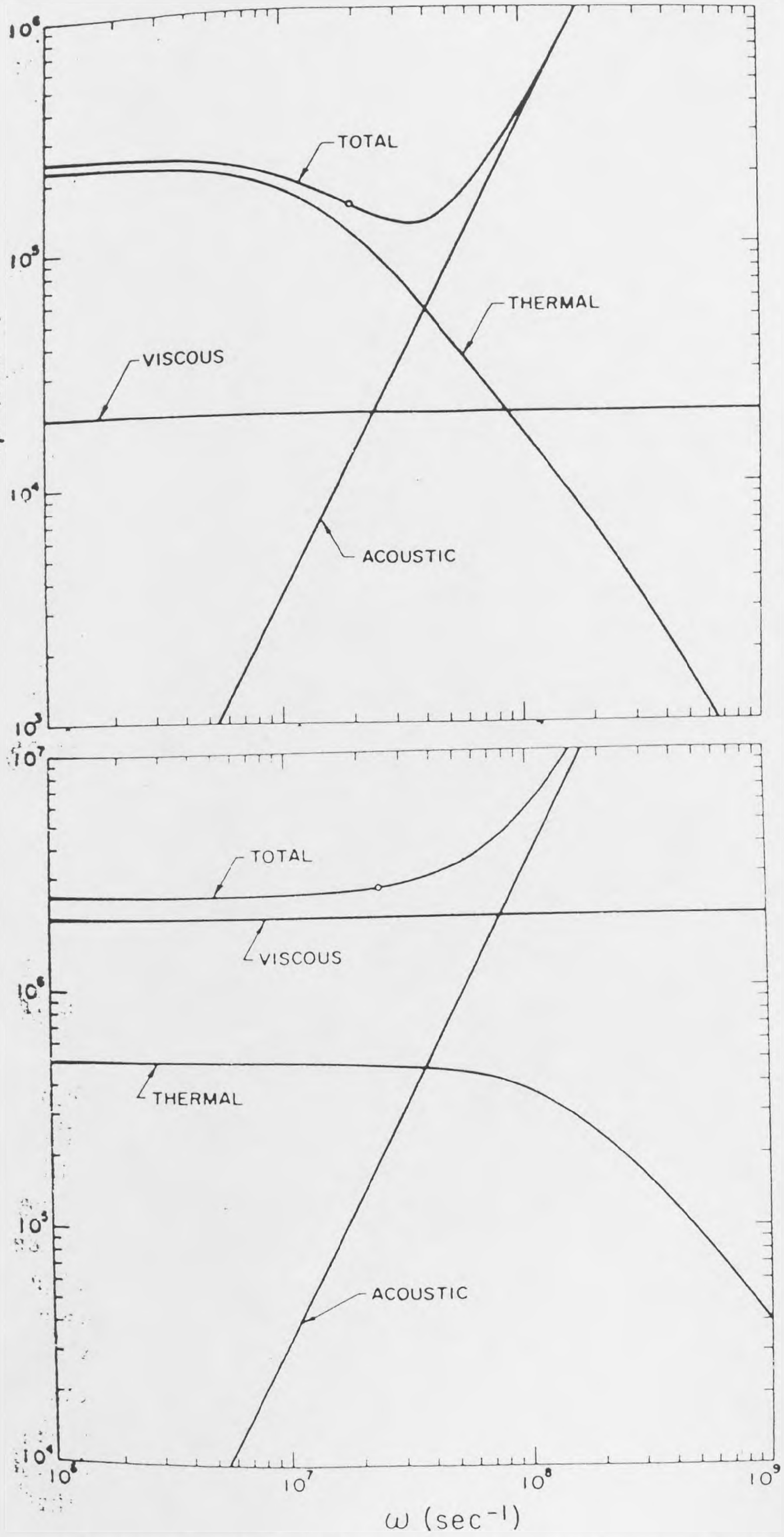

Figure 2.4(b) The total dimensional damping constant *versus* angular frequency for air bubbles in water. The open circle marks the value at resonance. The contributions from individual damping mechanisms are shown. Top: radius = 10 μm. Bottom: radius = 1 μm. *From Prosperetti, 1977.*

between the characteristic acoustic impedances ($= \rho c$) of the gas and the liquid. The amplitude of the scattered sound field is large compared to the amplitude of the incident sound field, so the scattering is described as strong. Elastic scattering constitutes the basic scattering behaviour of the bubble, and it is modulated by the effects of the various damping mechanisms.

The scattering behaviour of a bubble can be quantified by means of partial wave analysis (Epstein and Carhart, 1953, Chow, 1964, Ahuja, 1972, Allegra and Hawley, 1972, Nishi, 1975). The incident sound wave is usually described by

$$\psi_i = \exp(ik_r r \cos\theta - i\omega t) \qquad [2.46]$$

where ψ_i is the potential of the incident wave and k_r is the propagation coefficient in the liquid. The polar coordinates r, θ and φ have their origin at the centre of the bubble, and the polar axis is taken to be in the direction of propagation of the incident wave. *Equation 2.46* can be written as the summation of a series of partial waves (Jones, 1986)

$$\psi_i = \sum_{n=0}^{\infty} i^n (2n + 1) j_n (k_r r) P_n (\cos\theta) \qquad [2.47]$$

where j_n are spherical Bessel functions and P_n are Legendre polynomials. In this equation, and in subsequent equations which describe wave potentials, a common time factor $\exp(-i\omega t)$ has been omitted in order to improve clarity. When a sound wave is incident upon the bubble, there arise a scattered acoustic wave (due to elastic scattering and acoustic damping), a longitudinal thermal wave (due to thermal damping), and a transverse viscous wave (due to viscous damping). These waves originate at the interface between the gas and the liquid, and propagate out in both directions. They can be described respectively by the potentials ψ_r, ψ_t and ψ_v, which satisfy the following linear equations:

$$(\nabla^2 + k_r^2)\, \psi_r = 0 \qquad [2.48]$$

$$(\nabla^2 + k_t^2)\, \psi_t = 0 \qquad [2.49]$$

$$(\nabla^2 + k_v^2)\, \psi_v = 0 \qquad [2.50]$$

where

$$k_r = \frac{\omega}{c}\left\{1 + \frac{i}{2}\left[\frac{N\nu\omega}{c^2} + \frac{D\omega}{c^2}(\gamma - 1)\right]\right\} \tag{2.51}$$

$$k_t = (1 + i)\sqrt{\frac{\omega}{2D}} \tag{2.52}$$

$$k_v = (1 + i)\sqrt{\frac{\omega}{2\nu}} \tag{2.53}$$

$$N = 4/3 + \mu/\eta \tag{2.54}$$

$$\nu = \eta/\rho \tag{2.55}$$

where μ is the compressional viscosity, and the quantity ν is sometimes referred to as the kinematic viscosity. In this section, in order to improve clarity, a different method is adopted for differentiating between quantities which pertain to the gas and quantities which pertain to the liquid. The subscript $_l$ is dropped, and the subscript $_g$ is replaced by a prime. Thus ρ_l and ρ_g become ρ and ρ' respectively. The series expansions for the waves in the liquid (ψ_r, ψ_t and $\boldsymbol{\psi}_v$) and in the gas (ψ'_r, ψ'_t and $\boldsymbol{\psi}'_v$) are given by

$$\psi_r = \sum_{n=0}^{\infty} i^n (2n + 1) A_n h_n (k_r r) P_n (\cos\theta) \tag{2.56}$$

$$\psi_t = \sum_{n=0}^{\infty} i^n (2n + 1) B_n h_n (k_t r) P_n (\cos\theta) \tag{2.57}$$

$$A = \sum_{n=1}^{\infty} i^n (2n + 1) C_n h_n (k_v r) P_n^1 (\cos\theta) \tag{2.58}$$

$$\psi'_r = \sum_{n=0}^{\infty} i^n (2n + 1) A'_n j_n (k'_r r) P_n (\cos\theta) \tag{2.59}$$

$$\psi'_t = \sum_{n=0}^{\infty} i^n (2n + 1) B'_n j_n (k'_t r) P_n (\cos \theta) \tag{2.60}$$

$$A' = \sum_{n=1}^{\infty} i^n (2n + 1) C'_n j_n (k'_v r) P_n^1 (\cos \theta) \tag{2.61}$$

where h_n are Hankel functions, P_n^1 are Legendre polynomials of the first kind and $A = \psi_{v,\varphi}$, $\psi_{v,\theta} = \psi_{v,r} = 0$. The quantities A_n to C'_n represent a series of single scattering coefficients, which are found by considering the boundary conditions. The conditions are governed by the equality of the following quantities:

$u_r = u_r'$ normal velocity component [2.62]

$u_\theta = u_\theta'$ tangential velocity component [2.63]

$T = T'$ temperature [2.64]

$K (\partial T / \partial r) = K'(\partial T' / \partial r)$ heat flux [2.65]

$\pi_{r\theta} = \pi_{r\theta}'$ normal stress [2.66]

$\pi_{rr} = \pi_{rr}' + \delta S$ tangential stress [2.67]

where

$$S = \frac{\sigma}{r_0^2} \left[2r_0 - 2\xi - \frac{1}{\sin \theta} \frac{\partial}{\partial \theta} \left[\sin \theta \frac{\partial \xi}{\partial \theta} \right] \right] \tag{2.68}$$

$\delta = 1$ when n = 0, otherwise $\delta = 0$

The quantity ξ is the deformation of the bubble, and is given by

$$\xi = \sum_{n=0}^{\infty} L_n P_n (\cos \theta) \tag{2.69}$$

The evaluation of ξ will be explained below. The explicit form of the quantities in the boundary conditions is given by

$$u_r = - \frac{\partial \Psi}{\partial r} + \frac{1}{r \sin \theta} \frac{\partial}{\partial \theta} (A \sin \theta) \tag{2.70}$$

$$u_\theta = -\frac{1}{r}\frac{\partial \Psi}{\partial \theta} - \frac{1}{r}\frac{\partial}{\partial r}(Ar) \qquad [2.71]$$

$$T = g(\psi_i + \psi_r) + G\psi_t \qquad [2.72]$$

$$\pi_{r\theta} = \eta \left\{ -\frac{\partial}{\partial \theta}\left[\frac{1}{r}\frac{\partial \Psi}{\partial r} - \frac{\Psi}{r^2}\right] - \left[\frac{\partial^2 A}{\partial r^2} - \frac{2A}{r^2}\right] + \frac{1}{r^2}\frac{\partial}{\partial \theta}\left[\frac{1}{\sin\theta}\frac{\partial}{\partial \theta}(A\sin\theta)\right]\right\} \qquad [2.73]$$

$$\pi_{rr} = \eta\, k_v^2 [M_1(\psi_i + \psi_r) + M_2\psi_t] + 2\eta\left\{-\frac{\partial^2 \Psi}{\partial r^2} + \frac{1}{\sin\theta}\frac{\partial}{\partial \theta}\left[\sin\theta\left(-\frac{A}{r^2} + \frac{1}{r}\frac{\partial A}{\partial r}\right)\right]\right\} \qquad [2.74]$$

$$P = -i\omega\rho_1 [Q_1(\psi_i + \psi_r) + Q_2\psi_t] \qquad [2.75]$$

where $\Psi = \psi_i + \psi_r + \psi_t$ [2.76]

$$\Psi' = \psi'_r + \psi'_t \qquad [2.77]$$

$$\mathbf{u} = -\nabla\Psi + \nabla \times A \qquad [2.78]$$

and approximately

$$g = -i\omega T\alpha_c / c_p \qquad [2.79]$$

$$G = -(\alpha_c D)^{-1} \qquad [2.80]$$

$$M_1 = 1 \qquad [2.81]$$

$$M_2 = 1 - (3N\nu / 2D) \qquad [2.82]$$

$$Q_1 = 1 \qquad [2.83]$$

$$Q_2 = 1 - N\nu / D \qquad [2.84]$$

where α_c is the coefficient of cubical expansion. Substitution of *Equations 2.56-61* into *Equations 2.70-74*, with r set equal to r_0, results in a set of six simultaneous equations in A_n through C'_n. The following abbreviations are introduced: $a = k_r r_0$, $b = k_t r_0$, $c = k_v r_0$ and $a' = k'_r r_0$, $b' = k'_t r_0$, $c' = k'_v r_0$. Note that the first and second derivatives of Bessel and Hankel functions with respect to time are denoted by j'_n, j''_n, h'_n and h''_n respectively. Then for n ≥ 1:

$$\begin{aligned} &aj'_n(a) + A_n ah'_n(a) + B_n bh'_n(b) - C_n n(n+1)h_n(c) = \\ &\qquad A'_n a'j'_n(a') + B'_n b'j'_n(b') - C'_n n(n+1)j_n(c') \end{aligned} \qquad [2.85]$$

$$\begin{aligned} &j_n(a) + A_n h_n(a) + B_n h_n(b) - C_n[h_n(c) + ch'_n(c)] = \\ &\qquad A'_n j_n(a') + B'_n j_n(b') - C'_n[j_n(c') + c'j'_n(c')] \end{aligned} \qquad [2.86]$$

$$g\,[\,j_n(a) + A_n h_n(a)\,] + GB_n h_n(b) = g'A'_n j_n(a') + G'B'_n j_n(b') \qquad [2.87]$$

$$\begin{aligned} &K\,\{\,g\,[\,aj'_n(a) + A_n ah'_n(a)\,] + GB_n bh'_n(b)\,\} = \\ &\qquad K'\,\{\,g'A'_n a'j'_n(a') + G'B'_n b'j'_n(b')\,\} \end{aligned} \qquad [2.88]$$

$$\begin{aligned} &\eta\,\{\,[\,aj'_n(a) - j_n(a)\,] + A_n[\,ah'_n(a) - h_n(a)\,] + B_n[\,bh'_n(b) - h_n(b)\,] - \\ &\qquad \tfrac{1}{2}C_n\,[\,c^2h''_n(c) + (\,n^2 + n - 2\,)h_n(c)\,]\,\} = \\ &\eta'\,\{\,A'_n\,[\,a'j'_n(a') - j_n(a')\,] + B'_n\,[\,b'j'_n(b') - j_n(b')\,] - \\ &\qquad \tfrac{1}{2}C'_n\,[\,c'^2j''_n(c') + (\,n^2 + n - 2\,)j_n(c')\,]\,\} \end{aligned} \qquad [2.89]$$

$$\begin{aligned} &\eta\,\{\,[\,c^2j_n(a) - 2a^2j''_n(a)\,] + A_n\,[\,c^2h_n(a) - 2a^2h''_n(a)\,] + \\ &\qquad B_n\,[\,M_2c^2h_n(b) - 2b^2h''_n(b)\,] + 2n\,(\,n + 1\,)\,C_n\,[ch'_n(c) - h_n(c)\,]\,\} = \\ &\eta'\,\{\,A'_n\,[\,c'^2j_n(a') - 2a'^2j''_n(a')\,] + B'_n\,[\,M'_2c'^2j_n(b') - 2b'^2j''_n(b')\,] + \\ &\qquad 2n\,(\,n + 1\,)\,C'_n\,[\,c'j'_n(c') - j_n(c')\,]\,\} \end{aligned} \qquad [2.90]$$

In the case n = 0, the last equation is modified by the presence of the *S* term in the boundary condition. Using the relationships

$$P_n^1(\cos\theta) = -dP_n(\cos\theta)\,/\,d\theta \text{ and} \qquad [2.91]$$

$$\frac{1}{\sin\theta}\,\frac{d}{d\theta}(\sin\theta\,P_n^1(\cos\theta)) = n\,(\,n + 1\,)\,P_n(\cos\theta) \qquad [2.92]$$

it is seen that when n = 0, the boundary condition specified by *Equation 2.67* is modified to

$$\pi_{rr} = \pi'_{rr} + \frac{\sigma}{r_0^2}(\,2r_0 - 2\xi\,) \qquad [2.93]$$

A tractable form of the equation is found by taking the partial derivative with respect to time. Utilising the relationship $\partial\xi\,/\,\partial t = u_r\,|_{\,r\,=\,r_0}$,gives

$$\frac{\partial}{\partial t}(\pi_{rr}) = \frac{\partial}{\partial t}(\pi'_{rr}) + \frac{2\sigma}{r_0^2}\left.\frac{\partial \Psi}{\partial r}\right|_{r=r_0} \qquad [2.94]$$

and thus the right hand side of *Equation 2.90* gains an extra surface tension term

$$(\,2\sigma / i\omega r_0\,)\,[\,a j'_0 + A_0 a h'_0 + B_0 b h'_0\,] \qquad [2.95]$$

The effects of the surface tension term are insignificant for bubbles with radii which are larger than a few tenths of a micrometre.

In the long wavelength limit, the series expansions for the potentials converge very rapidly, and only the cases n = 0 and n = 1 need be considered. It is possible to calculate from the A_n scattering coefficients quantities such as the scattering and absorption cross-section of the bubble (Nishi, 1975) and the damping constants b_t, b_v and b_a (Allegra & Hawley, 1972). The next section will show how the values of A_n can be used to calculate the velocity and attenuation in a liquid containing many bubbles. The partial wave analysis is therefore a very powerful approach.

The most accurate evaluation of A_0 and A_1 requires the solution of the set of simultaneous equations given by *Equations 2.85* to *2.90*. Approximate analytical expressions for A_0 (Chow, 1964) and A_1 (Allegra & Hawley, 1971) are given by

$$A_0 = \left\{ i\frac{a^3}{3}\left[\rho_r\frac{a'^2}{a^2} - 1\right] + \right. \qquad [2.96]$$

$$\left. ia\frac{g}{G}\left[\rho_r\frac{g'}{g} - 1\right]^2 \frac{bh_1(b)}{h_0(b)\,(1 - K_r Z)} \right\} (1 - FH)^{-1}$$

where $\rho_r = \rho / \rho'$ [2.97]

$K_r = K / K'$ [2.98]

$H = 1 + 3K_r(c'/c)\,(1/a^2)\,(g'/g)\,(1 - ib) / (1 - K_r Z)$ [2.99]

$F = 2\sigma / 3r_0\rho' c'^2$ [2.100]

$Z = [j_0(b')bh_1(b)] / [b'j_1(b')h_0(b')]$ [2.101]

$$3A_1 = \frac{-ia^3\,(\rho_r - 1)\,[h_2(c)\,Q(c') - (\eta_r\,c\,h_1(c)j_2(c')]}{[3\rho_r h_2(c) + 2(\rho_r - 1)h_0(c)]\,Q(c') - \eta_r\,c\,h_1(c)j_2(c)(\rho_r + 2)} \qquad [2.102]$$

where $\eta_r = \eta / \eta'$ [2.103]

$$Q(c') = c'j_1(c') - 2(1 - \eta_r)j_2(c') \quad [2.104]$$

The A_0 term incorporates the scattering due to thermal and acoustic damping, and it accounts for the resonant behaviour of the bubble. Thus the behaviour of the bubble at the resonant frequency is often referred to as the giant monopole resonance. The A_1 dipole term incorporates the scattering due to viscous damping, and for all but the smallest bubbles A_1 is much smaller than A_0. Between them the two terms constitute the most complete description available of an insonified bubble in the long wavelength limit.

2.1.10 The effect of material at the surface

In the foregoing discussion, it has been assumed that the bubble is completely clean. It has been shown that in practice the bubble surface always carries some contamination, and this may affect the resonant frequency of the bubble. For example, the resonant frequency of a bubble of 10 μm radius at a depth of 10 cm increases by about 8% when a film of primary aliphatic alcohol is adsorbed at the bubble surface (Glazman, 1983). Although the restoring force which is associated with the surface tension is reduced in the presence of a surfactant, there is an additional restoring force associated with the dilational elasticity of the surfactant film, which increases the resonant frequency. This effect will be more marked in the presence of a film which is strongly self-associated, such as a cross-linked protein.

Transport of surfactant between the bubble surface and the bulk liquid can also contribute to damping (Glazman, 1984). As the bubble oscillates, the surface concentration of surfactant rises and falls. If the period of oscillation is long compared with the time taken for thermodynamic equilibrium to be established, the surfactant can migrate away from or to the surface in response to the change in concentration. The change in entropy associated with the transport of surfactant results in a dissipation of energy. The magnitude of the effect depends on the whether the surfactant exchange is controlled by adsorption kinetics (which promotes damping) or by diffusion in the bulk liquid (which suppresses damping due to surfactant exchange). These effects are significant for bubbles with micrometre radii at frequencies well below resonance. Quantitative determination of the effects of surfactants is hampered by the lack of knowledge of surfactant exchange rates and dilational elasticity of surfactant films.

It is possible to extend the partial wave analysis to account for the presence of a thin uniform shell of material around the bubble (Anson & Chivers, 1989(a)). The boundary conditions at the gas/shell and shell/liquid interfaces are evaluated using the partial wave expansions of the scattered waves in the bubble, the shell and the liquid. This leads to a set of 12 equations of 12 unknowns which can be solved to give the single scattering coefficients A_n. A problem in applying such an approach to bubbly liquids is that the properties of the shell (such as the thickness and the density) are nearly always unknown.

2.1.11 *T*-matrix theory

It should be noted that a different type of partial wave analysis is widely used to obtain the single scattering coefficients, A_n. The transition matrix (usually abbreviated to the *T*-matrix) theory was introduced by Waterman (1969, 1976), and can be applied to the scattering of acoustic, elastic and electromagnetic waves. Three wave potentials are postulated: a total wavefield, ψ_t, an incident wavefield, ψ_i and a scattered wavefield, ψ_s, such that $\psi_t = \psi_i + \psi_s$. The total wavefield follows the scalar Helmholtz equation

$$(\nabla^2 + k^2)\psi_t = 0 \qquad [2.105]$$

where k is the propagation coefficient (sometimes called the wavenumber). The incident and scattered wavefields are expanded according to

$$\psi_i = \Sigma a_n \operatorname{Re} \psi_n \qquad [2.106]$$

$$\psi_s = \Sigma f_n \psi_n \qquad [2.107]$$

where $\{\psi_n; n = 1,2...\}$ is the set of functions consisting of the outgoing partial wave solutions of *Equation 2.105*, and Re ψ_n is the set of functions which are regular at the origin. The *T*-matrix has dimensions n × n, and it relates the coefficients a_n to the coefficients f_n by

$$f_n = \Sigma a_{T_{nn'}} a_{n'} \qquad [2.108]$$

The scheme for solving the equations and obtaining the *T*-matrix is quite involved, and will not be reproduced here. The interested reader is referred to the many publications on *T*-matrix theory (Peterson & Strom, 1974, Varatharajulu & Pao, 1976, Varadan VK *et al*, 1979, Visscher, 1980, Ma *et al*, 1987). It will suffice to note that the elements of the *T*-matrix contain the scattering coefficients. In the long wavelength regime analytical expressions can be found for the elements T_{00} and T_{11}, which are analogous to A_0 and A_1. These expressions have been shown to be identical to those yielded by the partial wave analysis due to Epstein & Carhart (1953) which was used in Section 2.1.9 (Varadan VV & Varadan VK, 1979). A problem with the method of Epstein & Carhart is that the equations become ill-conditioned at high values of the acoustic radius, *kr*, because it is necessary to calculate the Bessel and Hankel functions of large numbers. Waterman's original version of the *T*-matrix method suffers from the same problems of ill-conditioning at high frequencies (Tobocman, 1985) but more recent versions can work up to very high frequencies (Varadan VV *et al*, 1988[†]). Thus in a general sense the *T*-matrix method is the superior method for the calculation of scattering coefficients. In the long wavelength limit either partial wave analysis could be used. The justification for preferring the Epstein & Carhart method in this work is that it is more comprehensible, and more easily mounted as a computer model.

2.1.12 Summary

The expression due to Minnaert for the resonant frequency of the bubble is a reasonable description for large bubbles. The Rayleigh-Plesset equation provides a more general description of the behaviour of an oscillating bubble, which accounts for the damping of the bubble by three mechanisms: thermal, viscous and radiative. The relative importance of these mechanisms depends primarily on the size of the bubble. The behaviour of an oscillating bubble can also be analysed using partial wave analysis, leading to a description in terms of single scattering coefficients. The theory associated with partial wave analysis is well developed, and it provides the most useful description of the bubble.

[†]: This paper contains an extensive bibliography of 151 references on the *T*-matrix method.

2.2 Propagation in bubbly liquids

2.2.1 Introduction

In this section, the theoretical calculation of velocity and attenuation in bubbly liquids is considered. Two theoretical approaches, effective medium theory and multiple scattering theory are discussed in some detail. Finally, reported measurements of velocity and attenuation in bubbly liquids are discussed.

2.2.2 The Wood equation

Wood (1964) proposed a simple description of propagation in a bubbly liquid, which is commonly referred to as the Wood equation, or sometimes as the Urick equation. If the wavelength of the sound is assumed to be very large compared to the radius of the bubbles, then scattering can be disregarded, and the velocity, c^*, of sound in the bubbly liquid is related to the volume average of the properties of the component phases by:

$$c^* = (\beta^* \rho^*)^{-1/2}, \quad \text{where} \quad \beta^* = \phi\beta_g + (1-\phi)\beta_l, \qquad [2.109]$$
$$\rho^* = \phi\rho_g + (1-\phi)\rho_l$$

where β is the compressibility and ϕ is the volume fraction of dispersed gas. The Wood equation is applicable only at frequencies which are at least an order of magnitude lower than the resonant frequency. A modified version of the Wood equation has been proposed (Floyd, 1981) which attempts to incorporate two additional thermodynamic degrees of freedom of the bubble which are associated with the surface tension and depth of the bubbles. The predictions from the corrected theory differ very little from those from the Wood equation. In order to predict the velocity and attenuation in bubbly liquids over a wide range of frequencies, a more sophisticated analysis is necessary.

2.2.3 Theories of bubbly liquids

There are many theories available in the literature which predict the velocity and/or attenuation coefficient in bubbly liquids with small volume fractions of gas (Crespo, 1969, van Wijngaarden, 1972, Drumheller & Bedford, 1979, Caflisch *et al*, 1985, Cheng *et al*, 1985, Rubinstein, 1985, Miksis & Ting, 1987, Mond, 1987, Belyayev, 1988, Yildiz, 1988, Commander & Prosperetti, 1989, Nigmatulin *et al*, 1989, Temkin, 1990, Schmitt-von Schubert, 1991, Ruffa, 1992). These theories are based on a variety of physical approaches, and few of them are completely rigorous in derivation. Although the different theories account to varying degrees for the many physical processes which occur when a bubbly liquid is insonified, in practice they give very similar predictions of the velocity and attenuation at low volume fraction. In this work, two theories have been chosen, one relatively simple and the other relatively complex.

2.2.4 Effective medium theory

The effective medium theory (EMT) due to Gaunaurd and Uberall (1981) has proved to be very useful for the description of bubbly liquids. The approach is an extension of the work of Kuster and Toksöz (1974). In the EMT the scattering behaviour of bubbles in a sphere of radius R is equated to the scattering behaviour of a sphere of homogeneous effective medium of radius R (*Fig. 2.5*). This approach leads to a dispersion relation which includes terms in R, which is an arbitrary parameter. In order to achieve a valid dispersion relation, terms in R must be eliminated, and the means by which this elimination is effected have been the subject of some criticism (Scharnhorst, 1987, Anson & Chivers, 1989(b), McClements *et al*, 1990, Kerr, 1992(a,b)). The physical arguments used by Gaunaurd and Uberall to justify the removal of R from their formulations are not valid. However, it is reasonable to define the properties of the sphere of effective medium to be independent of its radius *a priori*.

The accuracy of the predictions of velocity and attenuation arising from the EMT are limited mainly by the choice of the expressions chosen for A_0 and A_1 by Gaunaurd and Uberall. The A_0 term is derived from the explicit expressions given by Nishi (1975) for the long wavelength limit. The A_1 term is a static expression. It can be shown that the accuracy of the EMT can be improved by employing a dynamic expression for A_1 (McClements *et al*, 1990). In fact, by employing the full expressions for A_0 and A_1, the EMT can be shown to yield the same dispersion relation as the multiple scattering theory of Waterman and Truell (which will be discussed below). The EMT is useful because it is relatively simple, and yet it yields reasonably accurate results.

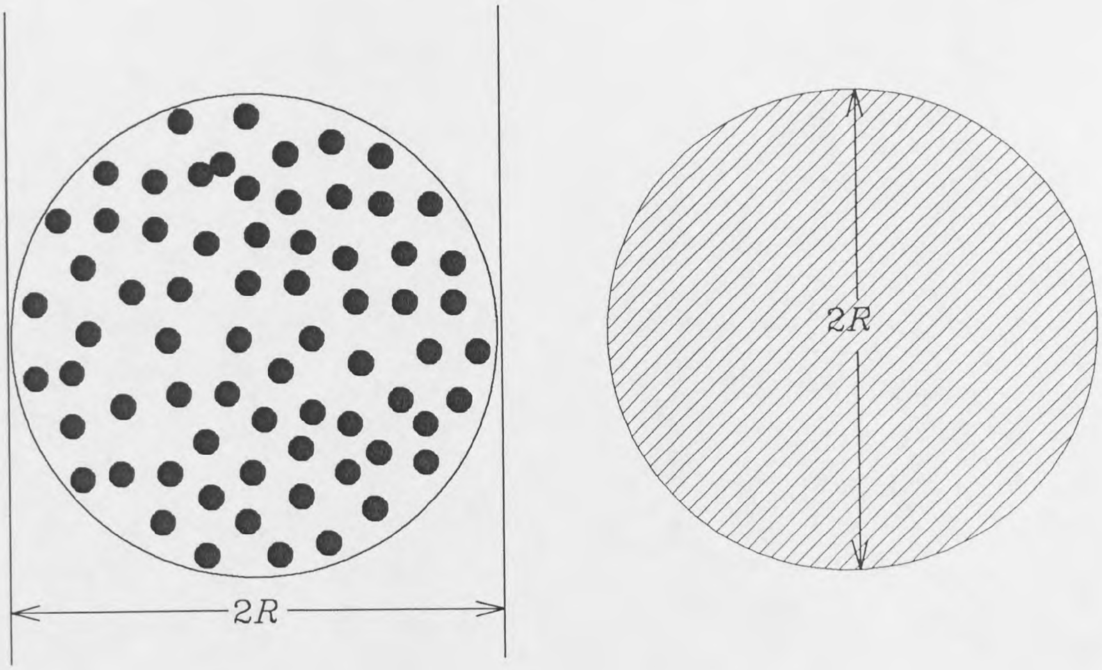

Figure 2.5 A spherical volume of scatterers, of radius R, and the equivalent imaginary sphere of effective medium, with the same radius and scattering behaviour.

In the EMT, the effective velocity, c_{eff} and effective attenuation, α_{eff} are given by

$$c_{\text{eff}} / c_1 = \{(\rho_{\text{eff}} / \rho_1)\ [(\hat{\rho} + \hat{x}) / 2]\}^{-1/2} \qquad [2.110]$$

$$\alpha_{\text{eff}} = -k_1\hat{\sigma}\{(\rho_{\text{eff}} / \rho_1)[(\hat{\rho} - \hat{x}) / 2]\}^{1/2} \qquad [2.111]$$

where

$$\frac{\rho_{\text{eff}}}{\rho_1} = \frac{1 - \phi[(\varepsilon - 1) / (\varepsilon + 2)]}{1 + 2\phi[(\varepsilon - 1) / (\varepsilon + 2)]},\ \varepsilon = \frac{\rho_1}{\rho_g} \qquad [2.112]$$

$$\hat{\rho} = (\hat{x}^2 + \hat{y}^2)^{1/2} \qquad [2.113]$$

$$\hat{x} = 1 - \frac{4\pi}{3}\int_0^\infty r^3 g(r)dr\,\frac{(1 - 3rz)(1 - rzx^2)}{(1 - rzx^2)^2 + r^2x^6y^2z^2} \qquad [2.114]$$

$$\hat{y} = -\frac{4\pi}{3}\int_0^\infty r^3 g(r)dr\,\frac{(1 - 3rz)(1 - rzx^3y)}{(1 - rzx^2)^2 + r^2x^6y^2z^2} \qquad [2.115]$$

$$\phi = \frac{4\pi}{3}\int_0^\infty r^3 g(r)dr \qquad [2.116]$$

$$\hat{\sigma} = -|\hat{y}| / \hat{y} \qquad [2.117]$$

$$x = k_l r \qquad [2.118]$$

$$y = 1 + \frac{1}{x^3}\left[\frac{\delta_t}{r\varepsilon}\left[1 + \frac{2\gamma\sigma}{r\rho_g c_g^{\,2}}\right] + \frac{4x\eta_l}{r\rho_l c_l}\right] \qquad [2.119]$$

$$z = \varepsilon / g \qquad [2.120]$$

$$g = 1 + (2\gamma\sigma / r\rho_g c_g^{\,2})(1 - \varepsilon / 3\gamma) \qquad [2.121]$$

$$\varepsilon = (1 + \delta_t^{\,2})\left[1 + \frac{3(\gamma - 1)}{d}\left[\frac{\sinh d - \sin d}{\cosh d - \cos d}\right]\right] \qquad [2.122]$$

$$\delta_t = \left[\frac{(\sinh d + \sin d)}{(\cosh d - \cos d)} - \frac{2}{d}\right]\left[\frac{(\sinh d - \sin d)}{(\cosh d - \cos d)} + \frac{d}{3(\gamma - 1)}\right]^{-1} \qquad [2.123]$$

$$d = (2\gamma r c_l x / D_l)^{1/2} \qquad [2.124]$$

In *Equations 2.114* to *2.116* the function *g(r)* describes the size distribution of the bubbles.

2.2.5 Multiple Scattering Theory

As the concentration of particles in a scattering system increases, the scatterers become more closely spaced. It becomes increasingly likely that the wave scattered by an individual particle will propagate as far as another particle before it is completely absorbed. The scattered wave can then be scattered again, and the resulting wave may go on to experience yet another scattering event. This process of scattering and rescattering continues until the scattered waves are completely absorbed. Since each particle has many neighbours, the number of scattering events can rapidly become very large, and the scattering behaviour of the system becomes very complex. The degree to which this process, known as *multiple scattering*, occurs depends on the intensity of the incident wave, on how strongly the particles scatter ultrasound, how closely spaced the particles are, and on how strongly the scattered waves are absorbed. Air bubbles are very strong scatterers, especially around resonance, and multiple scattering effects start to become important at concentrations as low as a fraction of a per cent. Every time a scattering event occurs, the scattered wave is slightly out of phase with the wave from which it arises. Thus the ultrasonic signal becomes more incoherent as the degree of multiple scattering increases. This can make measurements very difficult in concentrated systems of scatterers.

Many formulations are available in the literature which attempt to describe multiple scattering mathematically (see for example Foldy, 1945, Waterman & Truell, 1961, Lloyd & Berry, 1967, Twersky, 1962, 1964, 1977, 1978, Varadan VK, 1979, Varadan VK *et al* 1979, Tsang & Kong, 1981, Ishimaru & Kuga, 1982, Tsang *et al*, 1982, Varadan VK *et al*, 1983, Mehta, 1983, Ma *et al*, 1984(a,b), Varadan VK *et al*, 1985(a,b), Varadan VV *et al* 1985, Javanaud & Thomas, 1988, Ma *et al*, 1990, Liu, 1991(a,b)). The theories are necessarily complex, because the events which they attempt to describe are also complex. Inevitably some approximations have to be made in the evaluation of the multiple scattering events, but even so the multiple scattering formalism is soluble analytically only in the long wavelength regime. A very widely used result is that due to Waterman and Truell (1961). They consider a plane wave incident normally on an infinite half-space containing a uniform random distribution of identical scatterers. When considering the ultrasonic field at an individual scatterer, they assume that the exciting field at the particle can be replaced by the field which would exist if the scatterer in question (and its effects) were removed. This results in the following dispersion relation (using the notation of McClements (1992))

$$(k / k_1)^2 = (1 + \phi a)(1 - 3\phi b) \qquad [2.125]$$

where k is the propagation coefficient in the bubbly liquid, k_1 is the propagation coefficient in the bubble-free liquid, ϕ is the volume fraction of gas and the coefficients a and b are given by

$$a = -3i A_0 / (k_1 r_0)^3 \qquad [2.126]$$

$$b = 3i A_1 / (k_1 r_0)^3 \qquad [2.127]$$

where A_0 and A_1 are the single scattering coefficients (see previous section). Although the multiple scattering theory is derived for scatterers of identical radius, in polydisperse systems the particle size distribution can be accounted for to some extent by dividing the distribution into j size classes, and modifying the terms a and b according to

$$a = -3i\,\Sigma(\Phi_j A_{0,j} / (k_1 r_j)^3) \qquad [2.128]$$

$$b = 3i\,\Sigma(\Phi_j A_{1,j} / (k_1 r_j)^3) \qquad [2.129]$$

where Φ_j represents the ratio of the volume fraction of particles in the jth size class to the total volume fraction, r_j is the radius corresponding to the midpoint of the jth size class, and $A_{0,j}$ and $A_{1,j}$ are the values of the single scattering coefficients for particles of radius r_j.

Measurements of velocity and attenuation in *n*-hexadecane in water emulsions have shown that the predictions from the MST of Waterman and Truell agree very well with experiment at a dispersed phase volume fraction of 10 %, but the agreement is poorer at volume fractions of 30 and 50 % (McClements, 1992). Lloyd and Berry (1967) have shown that the theory of Waterman and Truell is a limiting case of their theory, which includes a higher order term in the volume fraction

$$(k / k_1)^2 = (1 + \phi a)(1 - 3\phi b) + 6\phi^2 b^2 \qquad [2.130]$$

where the terms in the equation have the same meaning as above. Alternatively an MST due to Ma *et al* (1990) can be employed

$$\left[\frac{k}{k_1}\right]^2 = \frac{(1 + \phi a)(1 - \phi b)}{(1 + 2\phi b)} \times \qquad [2.131]$$
$$\left[1 + \frac{i(k_1 r_0)^3 \phi w}{6}\left[\frac{a^2}{(1 + \phi a)} + \frac{3b^2}{(1 + 2\phi b)(1 - \phi b)}\right]\right]^2$$

where $w = (1 - \phi)^4 / (1 + 2\phi)^2$. In the long wavelength limit the term in $(k_1 r_0)^3$ becomes very small compared to unity, so that to a good approximation the second line of the equation can be discarded. The formulations of Lloyd and Berry and those of Ma *et al* both show good agreement with measurement in *n*-hexadecane in water emulsions with volume fractions of 30 and 50 %, but the agreement is not perfect (McClements, 1992).

2.2.5.1 Predictions of the velocity and attenuation in bubbly water

Having set out the theory relating to bubble behaviour in some detail, it is possible to demonstrate the way in which the most commonly measured ultrasonic parameters, the velocity and the attenuation, relate to the bubble size, the ultrasonic frequency and the volume fraction of dispersed air.

Figure 2.6(a) shows the predicted velocity and attenuation in bubbly water, calculated using the EMT and the various MST formulations, utilising the properties of air and water given in *Table 2.1*. The volume fraction of air is 2 %. At low frequencies, the velocity of sound is very low, and it is modelled accurately by the Wood equation. As the frequency increases, the velocity passes through a minimum, which marks the resonant frequency. The resonant frequency is inversely related to the bubble size. Over the next decade of frequency the velocity climbs and reaches very high values. At higher frequencies still the velocity drops back to the value in air-free water. At low frequencies the attenuation is quite low, but it rises steeply, reaching a very large peak value at the resonant frequency. The attenuation remains high over the decade of frequency above resonance, and then it drops back to low values. There is little quantitative difference between the predictions given by the various theories. The MST gives the more accurate values, but the predictions at high frequency suffer from the ill-conditioning mentioned previously. Note that the Waterman & Truell and the Lloyd & Berry formulations are

Table 2.1 *The thermophysical properties of distilled water and air at 20 °C, as required for calculations of effective medium theory and multiple scattering theory*

Property	*Distilled water*	*Air*
Velocity of sound/ m s^{-1}	1482.3	344.0
Density/ kg m^{-3}	998.2	1.21
Dynamic (shear) viscosity/ Pa s	1.002×10^{-3}	1.82×10^{-5}
Thermal conductivity/W m^{-1} K^{-1}	0.561	0.00241
Specific heat capacity/J kg^{-1} K^{-1}		
at constant pressure	4181.6	1010
at constant volume	4167.6	721.4
Coefficient of cubical expansion/ K^{-1}	2.1×10^{-5}	3.6728×10^{-3}
Compressional viscosity/ Pa s	10^{-8}	10^{-10}
Surface tension/ N m^{-1}	7.275×10^{-2}	
Bulk modulus/ Pa	2.193×10^{9}	1.432×10^{5}
Ambient pressure/ Pa	1.01×10^{5}	

From Kaye & Laby, 1986

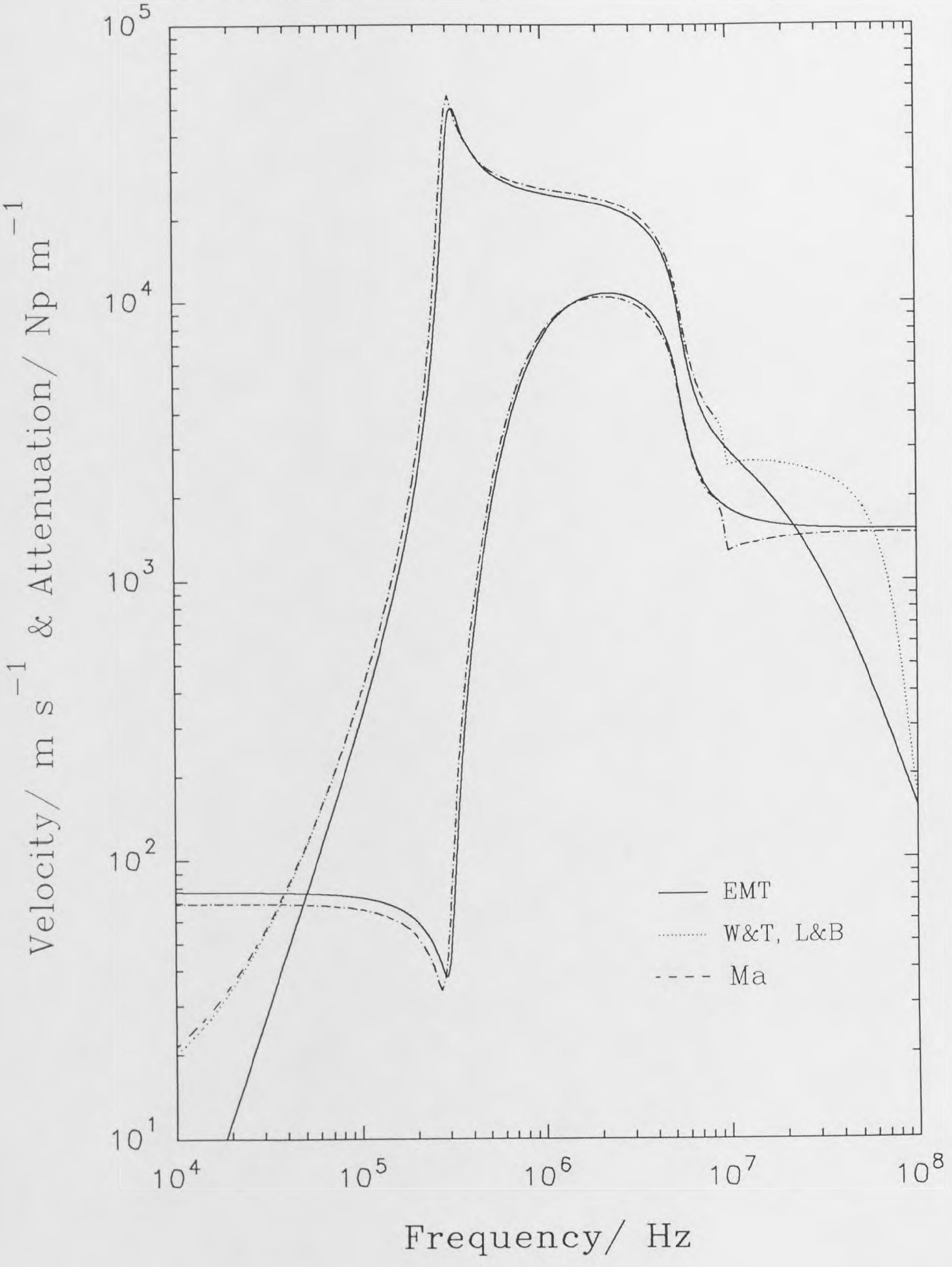

Figure 2.6(a) The velocity (lower curves) and attenuation (upper curves) in a monodisperse system of air bubbles in water (radius = 10 μm, volume fraction = 2 %). The curves are labelled according to the theory used to generate them. EMT: effective medium theory (Gaunaurd & Uberall, see text), WT: Waterman & Truell, LB: Lloyd & Berry, Ma: Ma et al.

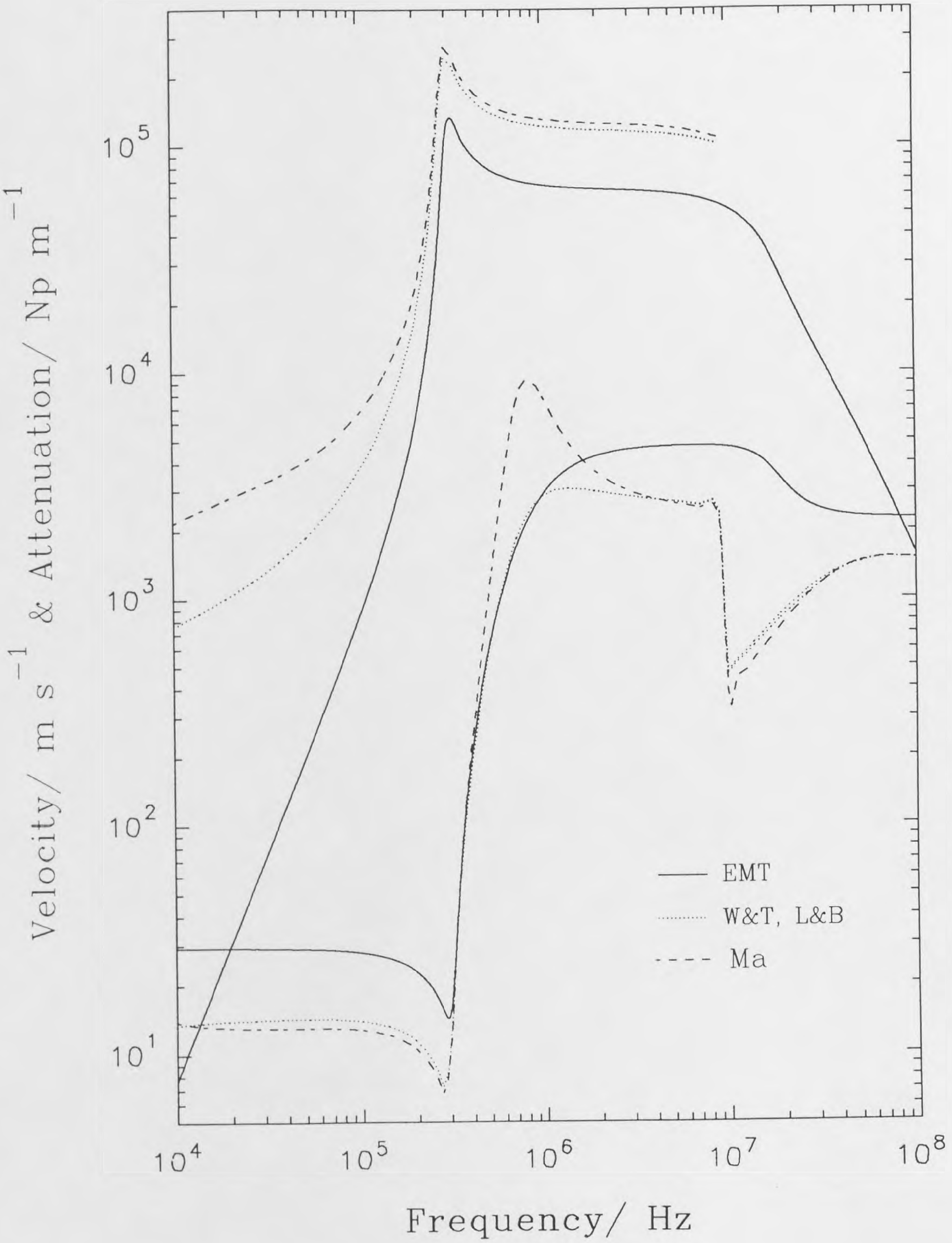

Figure 2.6(b) The velocity (lower curves) and attenuation (upper curves) in a monodisperse system of air bubbles in water (radius = 10 μm, volume fraction = 10 %). The curves are labelled according to the theory used to generate them. EMT: effective medium theory (Gaunaurd & Uberall, see text), WT: Waterman & Truell, LB: Lloyd & Berry, Ma: Ma et al.

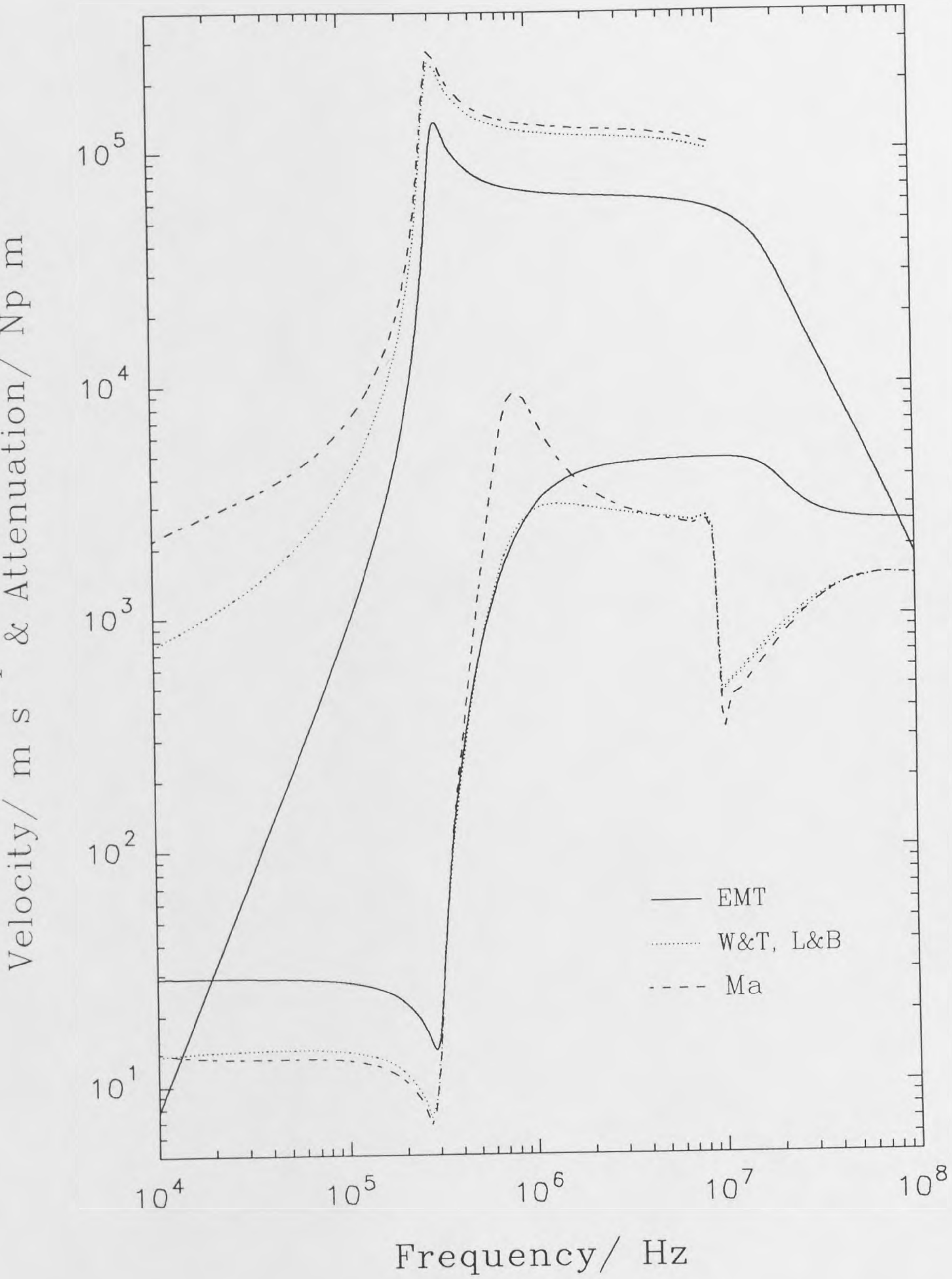

Figure 2.6(c) The velocity (lower curves) and attenuation (upper curves) in a monodisperse system of air bubbles in water (radius = 10 μm, volume fraction = 40 %). The curves are labelled according to the theory used to generate them. EMT: effective medium theory (Gaunaurd & Uberall, see text), WT: Waterman & Truell, LB: Lloyd & Berry, Ma: Ma et al.

indistinguishable. This is because A_0 is very much bigger than A_1, so the term $\phi^2 b^2$ in *Equation 2.130* is negligible.

Fig. 2.6(b) shows the predicted velocity and attenuation in the same system when the volume fraction is increased to 10 %. The resonant frequency is not affected by the volume fraction. The velocity is very strongly depressed at frequencies below resonance, but the elevation at frequencies above resonance is not as marked. The difference between the various theories is much more marked, especially in the prediction of the attenuation, which is again very high. As the volume fraction is increased further, the predictions do not change very greatly. *Fig. 2.6(c)* shows the predicted velocity and attenuation in the bubbly system with a volume fraction of 40 %. The predictions are only marginally different from those for a system with a volume fraction of 10 %. Even at this high volume fraction the Waterman & Truell and the Lloyd & Berry predictions are indistinguishable. It is likely that the assumptions made in the derivation of the multiple scattering theory are violated even at volume fractions of 10 % (this will be discussed in more detail below).

2.2.5.2 The effects of polydispersity

Real bubbly systems are never monodisperse. The effects of polydispersity can be examined by introducing a bubble size distribution into the calculations, using the approach described in *Equations 2.128* and *2.129*. *Fig. 2.7* shows the predicted velocity and attenuation in the bubbly system described above, calculated using EMT. The monodisperse prediction is shown, and the prediction for a system with the same total volume fraction, log normally distributed about a mean bubble size of 10 μm, with a log standard deviation of 0.25. Therefore very nearly all the bubbles fall within the size range 1-100 μm. The effects of polydispersity are quite subtle. The resonant minimum in the velocity disappears, and the range of frequencies over which the velocity is elevated is reduced somewhat. The resonant peak in the attenuation also disappears, and the attenuation is increased over the value in a monodisperse system.

2.2.6 Limitations of multiple scattering theory

Although multiple scattering theory is the most complete description available for scattering from bubbles and emulsion droplets, it has been shown that it does not

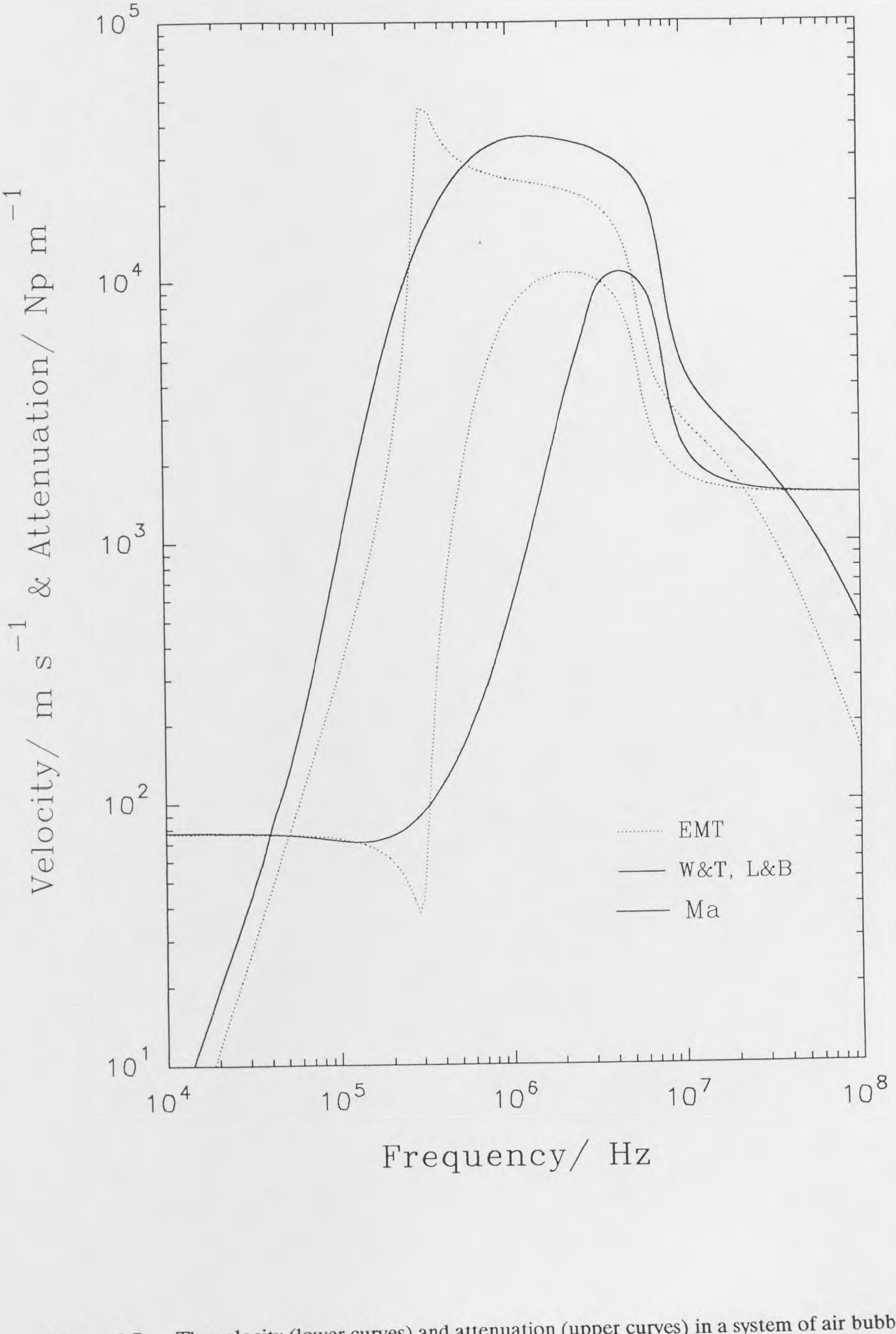

Figure 2.7 The velocity (lower curves) and attenuation (upper curves) in a system of air bubbles in water (volume fraction = 2 %). The dotted curves are the prediction from EMT for a monodisperse system with radius 10 μm. The solid curves are the prediction from EMT for a polydisperse system (see text for details).

give a perfect fit to experimental measurements of velocity and attenuation at high volume fractions. There are a number of reasons for this disagreement.

2.2.6.1 Incoherency

The discrepancy may be partly due to incoherence in the ultrasonic signal. The EMT and MST account for coherent scattering, but the transducers used in ultrasonic measurements are sensitive to the spatial distribution of the phase of the wave which they detect. When the signal becomes incoherent, the phase of the wave may differ across the face of the transducer, which will affect the apparent values of the velocity and attenuation. This effect is more pronounced with larger transducers.

2.2.6.2 The radial distribution function

Consider a particle within the ensemble of scatterers. If the centre of this particle is taken as fixed, a number of concentric spheres can be drawn around the particle, so that the volume interval between neighbouring spheres is constant (*Fig. 2.8*). The radial distribution function (hereafter abbreviated to $g(R)$ or rdf) is the average number of scatterers contained between each spherical shell (Tabor, 1991). As an illustration, the rdf is plotted as a function of R, the distance from the centre of the particle, in *Fig. 2.9* for liquid argon. The rdf is an indicator of the degree of structure in the ensemble (sometimes referred to as the degree of correlation). It is used in the MST to describe the spatial distribution of the scatterers. As the volume fraction increases, the degree of correlation increases and the structure becomes more regular. At high volume fractions the particles are forced into regular packing and the structure becomes crystalline.

The rdf has been of particular interest to workers trying to model liquids and concentrated gases at the molecular level. Various expressions for the rdf are available in the literature, and much attention has been paid to the choice of expression for $g(R)$ in the development of MST (see for example Twersky, 1978, Varadan VK *et al*, 1983). The simplest form of rdf is the Hole Correction Approximation (HCA), which states that the rdf is zero when $R \leq r_0$ (because the particles are impenetrable) and is equal to x for all $R > r_0$, where x is a constant which depends on the volume fraction of particles. The HCA is a good approximation for

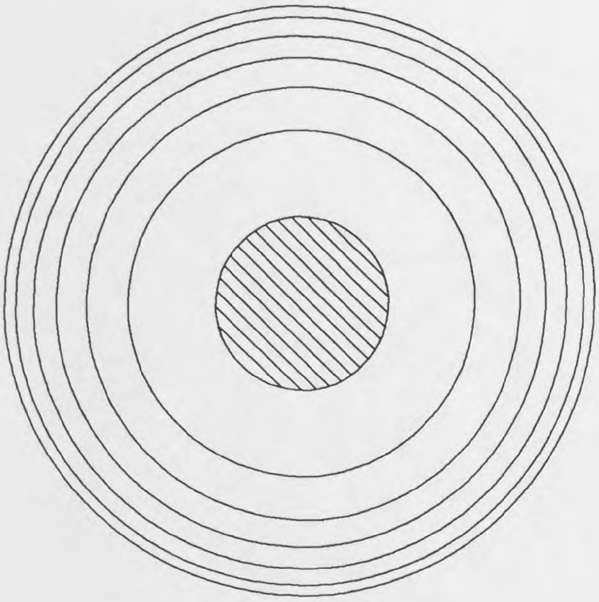

Figure 2.8 A particle in an ensemble of scatterers. Conceptual spheres are drawn around the particle at regular intervals. The radial distribution function predicts the number of neighbouring particles to be found in each shell.

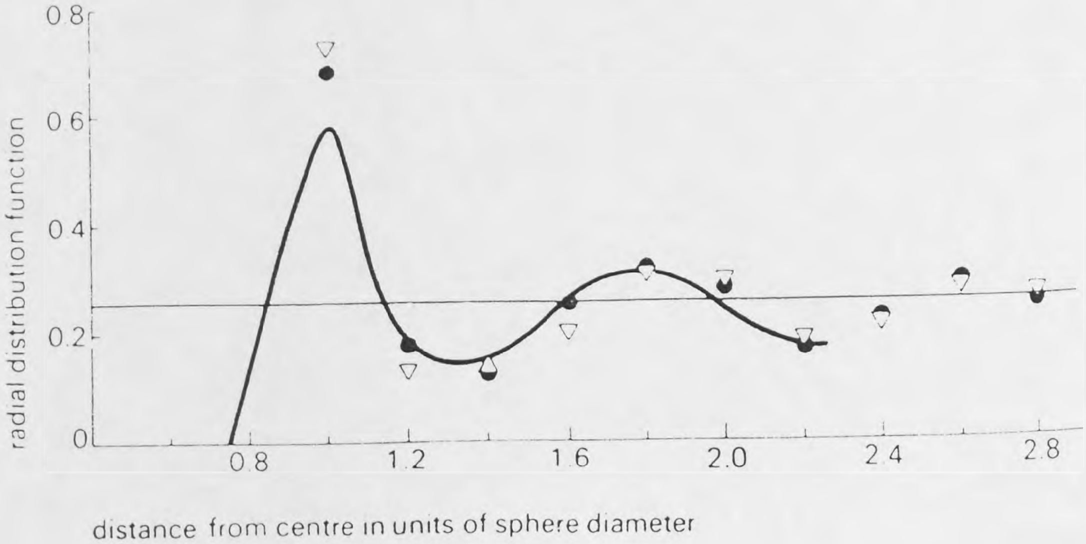

Figure 2.9 The radial distribution function for liquid argon as a function of R. The solid line represents the results from neutron diffraction, and the symbols are values calculated using a random packing model. *Taken from Tabor, 1991, p 262.*

volume fractions up to about 10 % (Ishimaru & Kuga, 1982). As the volume fraction increases, the degree of short range order in the ensemble increases, and a more sophisticated rdf is required.

In multiple scattering formulations, the most commonly used rdf is that due to Percus and Yevick (1958) (hereafter abbreviated to PY-rdf). The exact analytical solution of the expressions in the PY-rdf is available (Wertheim, 1963, Thiele, 1963)[†], and tables of values of the PY-rdf have been compiled (Throop & Bearman, 1965, Mandel *et al*, 1970). The PY-rdf is known to be inaccurate at volume fractions in excess of 40 % (Verlet & Weis, 1972). The closest approach to the exact rdf has been made using Monte Carlo simulation techniques (Barker & Henderson, 1971). This approach is computationally intensive, but, in common with many previously expensive and laborious computations, is becoming increasingly feasible with desk-top computers. Nevertheless, the formulations of MST to be found in the literature employ the PY-rdf, and therefore the accuracy of the MST will necessarily be reduced at volume fractions above 40 %.

The radial distribution function is calculated for particles which are monodisperse. Whilst the effects of polydispersity on the scattering coefficients can be accounted for (as in *Equations 2.128, 2.129*), the effects of polydispersity on the form of the radial distribution function are much harder to account for. It would seem likely that a numerical approach such as the Monte Carlo method would be able to account for polydispersity more easily.

2.2.6.3 The single scattering coefficients

The single scattering coefficients, A_n, which are used in the MST (and effectively in the EMT) are calculated under the assumption that the scatterer is situated in an infinite sea of liquid. Now, when multiple scattering occurs, the particles are, by definition, experiencing an effect due to the presence of neighbouring particles. The conditions experienced by the particle are not the same as those experienced by the particle which is considered in the calculation of the single scattering coefficients. McClements (1992) has suggested that the proximity of the particles

---

[†]: The *w* term in *Equation 2.131* arises from the use of the Wertheim-Thiele solution of the Percus-Yevick equation.

becomes an important factor when the distance between the particles becomes comparable with twice the thermal and viscous skin depths, d_t and d_v (ie $d_t \geq R/2$ and/or $d_v \geq R/2$). The thermal skin depth is defined as the distance over which the scattered wave generated by thermal conduction decreases in amplitude to 1/*e* of its value at the interface:

$$d_t = \sqrt{(2K_l / \omega\rho_l c_{p,l})}. \qquad [2.132]$$

where the terms on the right hand side of the equation are defined as previously. The viscous skin depth is defined as the distance over which the shear wave generated by visco-inertial damping decreases in amplitude to 1/*e* of its value at the interface

$$d_v = \sqrt{(2\eta_l / \omega\rho_l)} \qquad [2.133]$$

This condition is likely to be fulfilled at high volume fraction, and at low frequencies. Although multiple scattering theory is the most sophisticated description of propagation in scattering systems, it would seem that it is of limited use when the volume fraction of scatterers is above about 30 %. There is no theory available which fully describes propagation in concentrated systems. Given the complex behaviour of bubbles at resonance, it may well be impossible to model multiple scattering in a concentrated polydisperse bubbly liquid[†].

2.2.7 Reported measurements on bubbly liquids

In contrast to the extensive literature on the theoretical behaviour of bubbles, rather fewer investigations of bubbly liquids have been reported (Carstensen & Foldy, 1947, Laird & Kendig, 1952, Meyer & Skudrzyk, 1953, Fox *et al*, 1955, MacPherson, 1957, Silberman, 1957, Gibson, 1970, Medwin, 1974, Kol'tsova *et al*, 1979, Dontsov *et al*, 1989, Hall, 1989, Coste *et al*, 1990). The literature has recently been reviewed by Commander & Prosperetti (1989), and the salient features of some of the experiments are summarised in *Table 2.2*. All the experiments employed very low volume fractions of gas (not more than 1 %), and a wide range of bubble sizes (from tens of micrometres up to millimetres) have been studied. All

---

†: In concentrated bubbly liquids collective effects occur which are hard to account for in MST. These will be discussed in more detail in the next section.

Table 2.2 *Some experimental investigations of bubbly liquids. Methods for measuring the radius and volume fraction are indicated by superscripts*

Experimenter(s)	Bubble radii (mm)	Volume fraction (%)	Frequency range (kHz)	System examined
Carstensen & Foldy, 1947	0.1-0.4^{do,rt}	0.4^{c}	10-35	a/fw
Laird & Kendig, 1952	0.02-0.10^{p}	0.045^{c}	2-16	a/fw
Meyer & Skudrzyk, 1953	not reported	0.01	5-100	a/sw
Fox *et al*, 1955	0.02-0.12^{do,rt,p}	0.02^{c}	10-1000	a/pw
MacPherson, 1957	0.08-0.25^{p}	0.01-0.04	15-100	a/pw
Silberman, 1957	1-3.3^{p}	0.03-1^{m}	0.06-20	a/pw
Gibson, 1970	not reported	0.2-0.8	not reported	a/pw
Medwin, 1974	0.0002-0.05	not reported	10-110	a/sw
Kol'tsova *et al*, 1979	0.007-0.045^{p}	0.002-0.04^{py}	30-30000	e/NaCl
Dontsov *et al* 1989	0.6-1.8	0.6-1	not reported	a/pw
Coste *et al*, 1990	<0.5	0.5	0.2-0.9	v/de

Key
do: direct optical observation, rt: rise time, p: photographic measurement
c: collection of bubbles, m: manometer, py:pycnometer
a/fw: air bubbles in fresh water, a/pw: air bubbles in pure water, a/sw: air bubbles in sea water, e/NaCl: electrolysis in sodium chloride solution, v/de: vapour bubbles in diethyl ether

the experimenters studied air bubbles in water except Kol'tsova *et al* (1979) who electrolysed sodium chloride solution and Coste *et al* (1990) who produced vapour bubbles in diethyl ether by heating it. The vapour bubbles were modelled well by the Wood equation at low frequencies.

The most common method for producing bubbles was sparging, and the bubbles were characterised by rise velocity, by direct observation, or by photographic measurement. The volume fraction of gas was measured by collecting the bubbles as they rose to the top of the measurement vessel, or by calculation from the gas flow rate or the electrolytic current. Many of these techniques were of relatively limited accuracy, especially when measuring very small volume fractions of gas.

In many experiments there was a great deal of scatter in the ultrasonic measurements, and the quality and usefulness of the reported data differ widely. The most widely quoted results are those due to Silberman (1957), who reported a series of experiments in large tubes of water employing a standing wave technique and rather large bubbles (up to 3.3 mm radius). For example, Varadan VK *et al* (1985(b)), compare the predictions from their *T*-matrix multiple scattering approach with the experimental values from Silberman's paper. They found excellent agreement between theory and experiment, and the predictions of the MST and EMT can also be shown to be in excellent agreement with Silberman's work. Unfortunately, in Silberman's experiments (indeed in all the experiments reported in the literature), the very high attenuation at frequencies just above resonance prevented experimental verification of the greatly elevated velocity which is predicted at those frequencies. There is still a need for an investigation of velocity and attenuation in a fully and accurately characterised bubbly liquid over the complete frequency range of interest. Given the practical difficulties associated with ultrasonic measurements on bubbly liquids, it may be that no such experiment will ever be performed. It would seem reasonable nevertheless to conclude from the reported measurements that the Wood equation and MST or EMT are accurate descriptions of bubbly liquids at volume fractions of a few percent or less.

2.2.8 Summary

When scattering can be neglected, the velocity of sound in bubbly liquids is given by the Wood equation. When scattering is important, ultrasonic propagation can be described by effective medium theory or by multiple scattering theory. Although multiple scattering theory is the more rigorous of the two theories, and may be expected to provide a more accurate description, both theories suffer from drawbacks when there is a high concentration of scatterers. For strong scatterers like air bubbles, the concentration can be considered to be high at levels above a few per cent. The literature contains few examples of well controlled experiments which compare theory with experiment. Such experiments as have been reported suggest that theory and experiment are in very good agreement at volume fractions below one or two per cent.

2.3 Nonlinear behaviour

2.3.1 Introduction

There are a number of aspects of the interaction between ultrasound and bubbles which have not been touched on so far, which should be included for a fuller understanding of the behaviour of bubbly liquids. These aspects, although quite varied in character, all arise from nonlinear behaviour.

2.3.2 Nonlinear solution of the Rayleigh-Plesset equation

In Section 2.1, the Rayleigh-Plesset equation (which describes the radial oscillations of a bubble in a sound field) was solved by linearising it. This is a reasonable approach, because the majority of experiments involve incident sound fields of low amplitude, and the change in bubble radius caused by the field is extremely small. However, at resonance the oscillations of the bubble can become very large, and the pulsation regime becomes nonlinear (Prosperetti, 1984, Eatock *et al*, 1985). Nonlinear oscillations of the bubble can increase the effective nonlinearity parameter of the liquid (B/A) by several orders of magnitude (Wu & Zhu, 1991). This dynamic effect on the value of B/A supplements a static effect which can be attributed to the high compressibility of the dispersed gas. Thus in bubbly water the value of B/A may be of the order of 10^4 to 10^5 (Wu & Zhu, 1991) around the resonant frequency of the bubbles (*cf* the values for pure air and water of ≈ 0.4 and 5 respectively).

Nonlinear behaviour will occur across the entire frequency range when the amplitude of the incident acoustic wave is sufficiently high. A classic example of nonlinear behaviour is the occurrence of cavitation. Another interesting example is the excitation of transients, when a bubbly liquid is first exposed to an ultrasonic wave. A transient is an initial extremely nonlinear oscillation, which is usually succeeded by stable oscillations (which may be linear or nonlinear) as the bubble reaches equilibrium. The excitation of transients can lead to *sonoluminescence*, a weak emission of light, associated with the very high temperatures which are momentarily reached within the bubble (Leighton, 1989).

It is usually necessary to solve the Rayleigh-Plesset equation numerically in the nonlinear regime (Keller & Miksis, 1980, Shima *et al*, 1985, Prosperetti *et al*, 1988, Tsujino *et al*, 1988, Matsumoto & Watanabe, 1989, Miksis & Ting, 1984). An approximate analytical solution is also possible (Francescutto & Nabergoj, 1983, Samek, 1987, Smereka *et al*, 1987, Samek, 1989, Du & Wu, 1990). For oscillations of small amplitude, the results of the analytical solution agree with the linear theory (Miksis & Ting, 1984). Crum & Prosperetti (1983) have examined the nonlinear behaviour of an individual bubble which was acoustically levitated by a standing wave in a glycerine and water mixture. They defined a quantity, called the levitation number, as the ratio of the hydrostatic pressure gradient to the acoustic pressure gradient. They measured the levitation number as a function of the bubble radius, and found excellent agreement between their measurements and the predictions of the nonlinear solution of the Rayleigh-Plesset equation. The nonlinear solution correctly predicted the existence of the subharmonic resonance which was observed at a frequency near to $f_{res}/2$. The inability of the linear theory to account for subharmonic resonances explains the deviation between the measured value of the polytropic exponent and the value predicted by linear theory (see Section 2.1.7).

2.3.3 Shape oscillations

Thus far, it has been assumed that the bubble remains spherical as it oscillates. It was mentioned briefly that bubbles with radii greater than a few millimetres can undergo shape oscillations. Bubbles which are formed by whipping must undergo a significant deviation from sphericity as they are formed. The bubbles entrained by waves breaking in the ocean will start out with an arbitrary shape and undergo several oscillations before settling down into a spherical shape (Longuet-Higgins, 1990). These oscillations make a significant contribution to the noise spectrum associated with bubbles in the ocean (Longuet-Higgins, 1991).

Spherical bubbles can support standing waves on their surfaces, which can be thought of as analogous to standing waves on water (see *Fig. 2.10*). These vibrational modes are particularly promoted when one point on the bubble surface is immobilised (Gorskii *et al*, 1989). The pressure field associated with these oscillations is negligible in the linear regime, but may become appreciable when the oscillations of the bubble become nonlinear (Longuet-Higgins, 1989(a,b,c), Brooke Benjamin, 1989), especially if there is a resonant interaction between the funda-

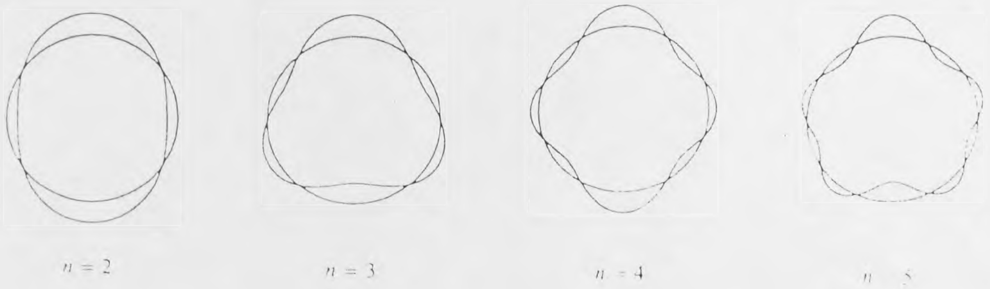

Figure 2.10 Axial sections of the axisymmetric normal modes: n = 2, 3, 4 and 5. *From Longuet-Higgins, 1989.*

mental breathing mode oscillation and shape oscillations (Longuet-Higgins, 1992). Non-spherical oscillations generate a monopole sound field which has a frequency twice the fundamental frequency of the shape oscillation. Shape oscillations are not significant for the bubbles examined in this work, because the bubbles are examined some time after formation, and the bubble oscillations are linear.

2.3.4 Cavitation

In our discussion of bubbly liquids so far, it has been assumed that the dispersed gas is permanent *ie* non-condensing. Cavitation is caused by high power ultrasound or by boiling, and is therefore not expected in low power unfocussed ultrasonic systems. Cavitating liquids are highly non-linear, and are described well by the non-linear solution of a modified form of the Rayleigh-Plesset equation (Vokurka, 1987, 1989, Gurikov, 1989).

2.3.5 Rectified diffusion

At moderately elevated power levels, the shrinkage of some bubbles can be reversed ultrasonically. As the bubble is compressed and expanded during forced oscillations there is a transport of gas into and out of the bubble. During the expansion part of the ultrasonic cycle gas can diffuse into the bubble, and during the compression part of the ultrasonic cycle gas can diffuse out. The interfacial area for gas exchange is lower during compression, and hence a net influx of gas can occur. This influx can be sufficient to counter disproportionation, and is termed rectified diffusion. Rectified diffusion is promoted in dirty bubbles. The surface film is patchy when the bubble is expanded, so influx is possible. The film is relatively compact when the bubble is compressed, so efflux is hindered. For a given acoustic pressure there is a threshold bubble radius below which rectified diffusion will not occur (Crum, 1980, Church, 1988(a)), because the Laplace pressure cannot be overcome. Gas transport into and out of the bubble is significantly enhanced by *acoustic microstreaming* (Church, 1988(b)). Microstreaming occurs when the bubble surface supports standing waves. This leads to local mixing in the shell of liquid around the bubble, bringing fresh gas-rich liquid to the bubble surface.

2.3.6 Acoustic pressure and Bjerknes forces

At high power levels, the translational oscillation of the bubble associated with visco-inertial damping under the influence of a travelling ultrasonic wave can lead to a net movement, because the two halves of the oscillation are not perfectly balanced. In a high power standing wave field there exist pressure nodes and antinodes, with concomitant pressure gradients. Depending on the frequency of the standing wave in relation to the resonant frequency of the bubble, the bubble may be driven to move to a node or antinode.

When two bubbles are oscillating next to one another, they experience an interaction force called the Bjerknes force, F_B, which in an incompressible liquid is given by

$$F_B = \rho_l \langle \dot{V}_1 \dot{V}_2 \rangle \; / \, 4\pi d_{12}^2 \qquad [2.134]$$

where V_1 and V_2 are the volumes of the two bubbles, d_{12} is the distance between the bubbles, and the dots denote differentiation with respect to time (Kobelev & Ostrovskii, 1989). When the bubbles oscillate in phase with each other, F_B is an attractive force, and when they oscillate out of phase with each other it is a repulsive force. Allowing for the effects of the compressibility of the liquid makes the expression for F_B rather more complex (Doinikov & Zavtrak, 1990), and introduces a long range component into the Bjerknes force (Doinikov & Zavtrak, 1988, 1989). In an ensemble of bubbles, the Bjerknes forces are complex, and it is not always straightforward to predict the effects which may occur. One notable effect is the spontaneous gathering of bubbles into swarms under the influence of a powerful sound field at a frequency near to the resonant frequency of the bubbles. If the swarm moves out of the ultrasonic beam, it can break up again into individual bubbles. If however it is continuously insonified, the bubbles in the swarm may coalesce and cream out of the liquid. The attenuation of the liquid is thus lowered, and this phenomenon is known as *acoustic self-induced transparency* (Zavtrak, 1988) or *self-illumination* (Kobelev *et al*, 1980). At the low sound intensities used in the experiments reported in this work, the volume changes are sufficiently small that Bjerknes forces can be disregarded.

2.3.7 Collective behaviour

Bjerknes forces are an example of collective behaviour between bubbles. Collective behaviour is a phenomenon which is not fully understood. When two bubbles are oscillating near one another, each bubble is sensitive to the pressure fields which arise as the other bubble pulsates (Snyder & Mord, 1990). Tolstoy (1986) has shown that in a system of three identical bubbles, the oscillations of the bubbles become coupled when the bubbles are positioned at the corners of an equilateral triangle of a certain dimension. This arrangement of bubbles has its own resonant frequency which is 1.0022 times the resonant frequency of the bubbles. Tolstoy terms this a super-resonance to distinguish it from the resonance of the individual bubbles.

Clearly in a real bubbly liquid the bubbles are not identical, and there is very little chance that they will all be arranged in a suitable configuration for super-resonances to occur. Nevertheless, collective behaviour is observed in bubble clouds. A bubble cloud has a series of resonant frequencies which are much lower than the resonant frequencies of the bubbles within the cloud (Omta, 1987), and these resonances are thought to contribute to the noise spectrum of natural bubbles in the ocean (Yoon *et al*, 1991, Kozhevnikova & Bjφrnφ, 1992). The acoustical absorption and scattering cross sections of spherical bubble clouds can be shown to be very different to the values for the individual bubbles in the cloud, and to the value for a single large bubble with the same volume of gas (d'Agostino & Brennen, 1988). The behaviour of a spherical bubble cloud depends on the exciting frequency, and can be divided into sub-resonant, trans-resonant and super-resonant regimes (d'Agostino & Brennen, 1989). The bubble cloud has a cut-off frequency which is equal to the resonant frequency of the bubbles within it (Smereka & Banerjee, 1988). Above the cut-off frequency the inner core of the bubble cloud is shielded by the outer layer. The degree to which collective effects occur depends on the void fraction and the geometry of the bubble cloud.

A bubble which is surrounded by other bubbles must experience a different mass loading to a bubble which is surrounded by bubble-free water, and consequently there will always be some collective effects in a bubble cloud. Collective effects are clearly hard to predict, and thus to model mathematically. It would seem reasonable to surmise that they will influence the velocity and attenuation in a bubbly liquid more and more as the volume fraction increases. Collective effects constitute yet another factor which make propagation in concentrated bubbly liquids hard to model.

2.3.8 Ultrasonic characterisation of bubbly liquids

A number of ultrasonic techniques for the characterisation of bubbly liquids have been reported in the literature. These publications indicate which workers, other than food scientists, have an interest in bubbly liquids and foams (see *Table 2.3*). There would be some justification for listing these publications along with the other measurements on bubbly liquids given in Section 2.2.7. However, those measurements were chiefly aimed at confirming the theoretical predictions of velocity and attenuation. The measurements described here aim to relate ultrasonic measurements to some property of the bubbly system, such as the gas volume fraction or the bubble size distribution. In some cases, little or no recourse is made to theory. Straightforward measurements of velocity and attenuation in the long wavelength regime are rarely used. The measurement systems can be broadly divided into active and passive types, according to whether or not an external

Table 2.3 *Research workers with an interest in bubbly liquids*

Category	*Type of bubbly system*
Medicine	Bubbles in the blood produced by decompression ('the bends'). Bubbles in the blood introduced for imaging of the heart (echocardiography).
Naval Oceanography	Bubbles in the sea introduced by rainfall and breaking waves. Bubbly wakes caused by entrainment from the air or by cavitation.
Chemical Engineering	Bubbles in gas-liquid reactors which control reaction rates and the characteristics of slug flow.
Biochemical Engineering	Bubbles in suspensions of cells performing aerobic reactions.
Nuclear power	Vapour bubbles in the cooling flow in liquid cooled reactors, which reduce the heat transfer efficiency.
Paper manufacture	Bubbles in the slurry used to produce paper which reduce the wet web strength and cause problems on the production line.

source of ultrasound is employed.

2.3.8.1 Passive systems

When a bubble is initially formed, it is very frequently excited into resonant vibrations. Using a transducer, the ultrasonic field associated with a resonating bubble can be detected. By simply registering the emissions associated with bubble formation, it is possible to construct an acoustical neutron counter, which detects the bubbles formed in a material which is specially formulated to produce a bubble each time a neutron passes through it (Biro *et al*, 1990). By registering the sound produced every time a bubble bursts at the surface of a liquid in which bubbles are being produced, it is possible to measure bubble nucleation rates (Lubetkin, 1989). If the frequency of the sound emitted by a bubble is measured, then it can be related to the bubble size via the Minnaert equation. This procedure is employed in a technique which measures the volume flow rate of gas in a system which produces bubbles sufficiently slowly that the pulses associated with each bubble can be resolved (Oosterwegel & de Groot, 1980). This technique can also be applied to the underwater detection of the signals from bubbles being formed by breaking waves (Medwin & Daniel, 1990), although care must be taken to account for the signals from bubbles oscillating off-resonance (Commander & Moritz, 1989).

2.3.8.2 Active systems

When the wavelength of ultrasound is much smaller than the bubbles (or other dispersed objects), the propagation regime is referred to as the optical regime. This analogy is employed because each scatterer casts a 'shadow', a region where the sound pressure level is zero. A measurement zone can be created between a source transmitter which produces pulses of ultrasound, and a receiver transducer. When a bubble is present in the measurement zone, the attenuation in the optical regime is proportional to the maximum cross-sectional area of the bubble. This arrangement can be used to measure the interfacial area in gas-liquid dispersions (Stravs & von Stockar, 1985, Bugmann & von Stockar, 1989(a)) and in bioreactors (Bugmann & von Stockar, 1989(b), Bugmann *et al*, 1991). In papermaking, the paper pulp contains air at a level of 1 % or so. Bubble formation is suppressed by the addition of chemical defoamer. Overdosage with the defoamer is costly, reduces paper strength and cause deposits to form on the machinery. Defoamer feed rates can be controlled by measuring the ultrasonic attenuation, which is a direct function of the air content (Karras *et al*, 1988).

In the optical regime it is relatively straightforward to utilise ultrasound for tomographic measurements. A circular array of transducers is arranged around the diameter of a pipe through which bubbly liquid flows. The bubbles must be sufficiently large that there are only one or two bubbles in the cross section of the flow which is analysed. Each transducer produces a pulse of ultrasound which propagates through the pipe and is reflected by the bubble or bubbles in the liquid. The time taken for the reflected pulse to return to the transducer is recorded by a a computer, which stimulates each of the transducers in turn. The computer combines all the time delays and constructs an image of the flow in cross-section. This measurement procedure can be used to detect vapour bubbles in the coolant in nuclear reactors (Kolbe *et al*, 1986, Turko *et al*, 1986). It could also be used to monitor natural gas in off-shore pipes used to transport crude oil, in order to optimise the control of the pumps (Wolf, 1988).

Stravs & von Stockar (1985) and Stravs *et al* (1987) have reported a system which fires pulses of ultrasound at megahertz frequencies into a liquid containing bubbles which are rising. By monitoring the backscatter from each bubble as it passes through the ultrasonic beam, it is possible to size bubbles with radii of several millimetres. The measurement system is only successful if the bubbles pass through the beam singly or in pairs.

In active systems, it is possible to employ a double frequency technique which gives unambiguous values for the radii of the bubbles which are in the imaging volume. The system consists of a pumping transducer and an imaging transducer, which acts as a transmitter/receiver. The imaging transducer works at its natural frequency, which is much higher than the resonant frequencies of the bubbles in the liquid. The pumping transducer is swept through a range of frequencies, which are chosen to cover the resonant frequencies of the bubbles which are to be imaged. The imaging transducer produces pulses of ultrasound which are scattered by the bubbles and subsequently detected by the imaging transducer. When the frequency of the pumping field is near to the resonant frequency of the bubbles, the scattered ultrasound contains components at the frequencies $(f_i - f_p)$, $(f_i - f_p/2)$, $(f_i + f_p/2)$ and $(f_i + f_p)$, where f_p and f_i are the frequencies of the pumping and imaging fields respectively. Of course, the major component of the scattered signal is at the frequency f_i. These sum and differences frequencies arise as a result of the nonlinear behaviour of the bubble around resonance. If the scattered signal is analysed in the frequency domain (by applying the Fourier transform or by using a spectrum analyser), the sum and difference frequencies can be quantified (see *Fig. 2.11*). Because they appear at either side of the main frequency peak, they are often referred to as side band frequencies, or just side bands. The amplitude of the side band frequencies is maximal when f_p is equal to the resonant frequency of the bubbles. Successful bubble sizing techniques have been described, which utilise the $(f_i \pm f_p/2)$ sidebands (Leighton *et al*, 1991) and the $(f_i \pm f_p)$ sidebands (Chapelon *et al*, 1985, Chapelon *et al*, 1988).

A rather different technique has been described (Medwin & Breitz, 1989, Breitz & Medwin, 1989, Wu & Hwang, 1991) which utilises a resonator. A large, flat Mylar capacitive transducer is mounted parallel to a flat reflector plate. The transducer is

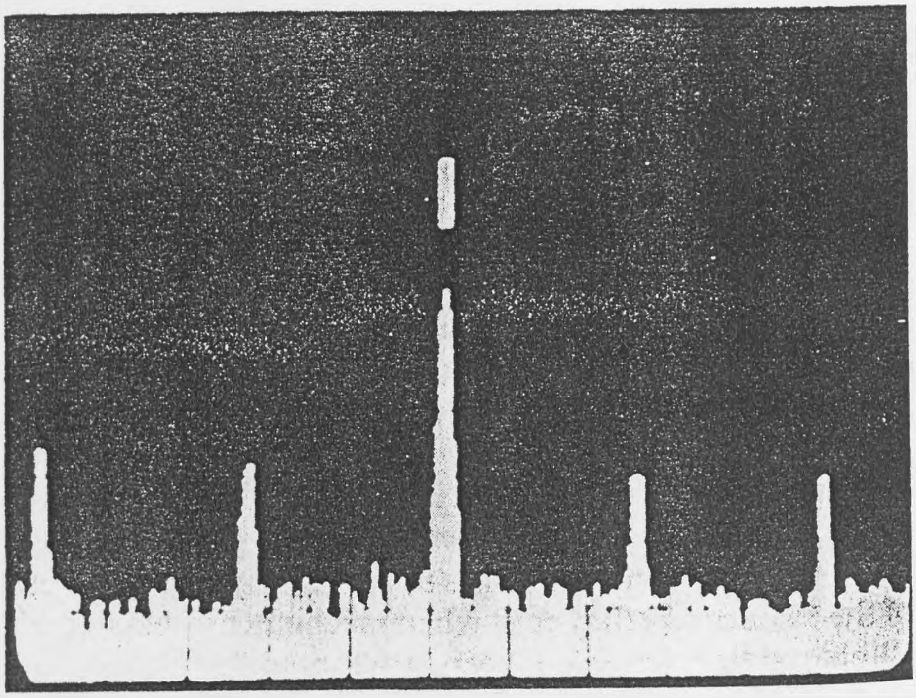

Figure 2.11 Output from spectrum analyser, with frequency plotted on the x-axis. Running from left to right, the peaks correspond to the frequencies $f_i - f_p$, $f_i - f_p/2$, f_i, $f_i + f_p/2$ and $f_i + f_p$. *Taken from Leighton* et al, *1991.*

stimulated with electrical white noise, which excites the system into resonance. The transducer / reflector system has a series of resonances which correspond to the existence of standing waves within the space between the transducer and the reflector plate. A hydrophone is situated on the face of the transducer, which detects the multiresonant field. The standing wave behaviour of the system is different when it is submerged in water and when it is submerged in bubbly water. By taking the Fourier Transform of the signal from the hydrophone, it is possible to measure the change of Q of the resonant modes when the resonator is located in bubbly water, which can be related to the size distribution of the bubbles. The system has been successfully employed to measure bubble spectra under breaking waves in real time.

2.3.8.3 Disadvantages of the reported techniques

All the systems reported here have drawbacks, the principal one being the restricted range of volume fractions which can be dealt with. Most of the systems are only reliable when there are at most two or three bubbles in the volume of the bubbly liquid which is characterised. Unless an array of transducers is employed, this places a severe restriction on the volume fraction of gas, because to ensure that only a few bubbles are in the sensitive volume, the volume fraction must be low. Even in the resonator system, which can cope with large numbers of bubbles, the total volume fraction cannot be too high, because the highly attenuating nature of bubbly water will completely damp out the resonances of the system.

Most of the systems are invasive, which is a big disadvantage for use in the food industry, where it is very important that all the surfaces which are in contact with food can be rigorously cleaned. Given the restriction on volume fraction, and the invasive nature of some techniques, it would seem that the existing systems are inadequate for characterising bubbly food liquids.

2.3.9 Summary

Nonlinear behaviour leads to a rich variety of behaviour in bubbly systems. High intensity ultrasound, through processes such as rectified diffusion, cavitation and self-induced transparency, is an extremely effective means by which bubbly liquids can be degassed. At lower intensities, the coupling of bubble oscillations leads to collective behaviour and resonant behaviour of the entire bubble ensemble.

Dilute bubbly liquids can be characterised using low intensity ultrasound, using a number of different approaches. So far, no technique has been reported which can characterise concentrated bubbly liquids. The invasive nature of most of the reported techniques for ultrasonic characterisation renders them unsuitable for use in food processing applications.

CHAPTER THREE

Materials and methods

3.1 Materials

3.1.1 Introduction

In this section, the materials are discussed which were used in the ultrasonic experiments. The following systems were examined†: a model bubbly liquid (in concentrated and diluted forms), bubbled gel, yogurt, cream, bread dough and beer foams. Concentrations of Sweetose should be taken as ± 0.2 wt%, concentrations of surfactant should be taken as ± 0.01 wt%, and temperatures should be taken as ± 0.1 °*C*, unless otherwise stated. Other figures are quoted to the appropriate number of significant places ie 10.0 implies 10.0 ± 0.1, 10.00 implies 10.00 ± 0.01.

3.1.2 An aerated food model

As was seen in Chapter One, aerated foods are quite diverse in their physical and chemical nature. In order to establish the usefulness of ultrasound as a technique for the characterisation of aerated foods, a model aerated food is needed. The ideal model would be simple, controllable, reproducible, consistent and easily characterised by conventional means. Clearly, no such model presently exists, but a system which exhibits all these properties to a reasonable degree is available (Bee *et al*, 1987). It consists of a highly viscous syrup, Sweetose, which is aerated in the presence of a surfactant (Hyfoama or P1670). The components of the food model, which are discussed in more detail below, were kindly supplied by Unilever Research plc.

3.1.2.1 Sweetose syrup

Sweetose syrup (Ragus Sugars Ltd, Slough, UK) is produced by the hydrolysis of corn starch. It is optically clear and near Newtonian. It is supplied at a strength of 80-82 wt%, with a dextrose equivalence of 63. The syrup is highly viscous and shows a pronounced tendency to form a skin. Sweetose is composed principally of glucose and maltose (see *Table 3.1*), with small amounts of higher order oligosaccharides. The syrup is too viscous for whipping experiments at the concentration at

---

†: The chronological order of the experiments was not necessarily the same as the order in which they are listed.

Table 3.1 *Composition of Sweetose syrup*

number of glucose units per molecule	1	2	3	4	5	6	7	8	9
percentage composition	37.2	43.4	6.3	2.2	3.4	3.2	2.4	1.2	0.6

based on data from Hodges, 1990

which it is supplied (see *Fig. 3.1*), so batches of stock syrup were diluted to a concentration of 70 wt% prior to whipping. There is an excellent correlation between the refractive index of the syrup and the total sugar content. It was therefore straightforward to determine the concentration of the stock syrup, and to check the concentration of the syrup batches following dilution. The syrup is hygroscopic, so the refractive index of the diluted batches was checked from time to time. The decrease in sugar concentration due to the absorption of water from the atmosphere was not very marked (0.2 wt% over six months). At a concentration of 70 wt%, the syrup has a viscosity of ≈ 1.0 Pa s at 20 °*C* (Hodges, 1990), which is about 1000 times the viscosity of water.

3.1.2.2 Hyfoama

Hyfoama DSN (Quest International, Zwijndrecht, Netherlands) is manufactured by the hydrolysis of soya protein. The resulting polypeptide fragments are highly surface active, and promote bubbly systems with high volume fractions of air. Sweetose foams which are made with Hyfoama are vulnerable to drainage and collapse in a matter of days (Hodges, 1990).

3.1.2.3 P1670

Ryoto Sugar Ester P1670 (Mitsubishi-Kasei Food Corporation, Tokyo, Japan) is a sucrose ester of palmitic acid (see *Fig. 3.2*). The name is derived from the fatty acid used for esterification (P for palmitic acid), the HLB number (16) and the purity of the fatty acid (70%). The ester composition is approximately 80% monoester with the remaining 20% made up by di- and tri- polyester (Ryoto Sugar Ester Technical Information, 1987). By varying the fatty acid type, sucrose esters can be prepared with any desired HLB number. In addition to their use as emulsifiers, sucrose

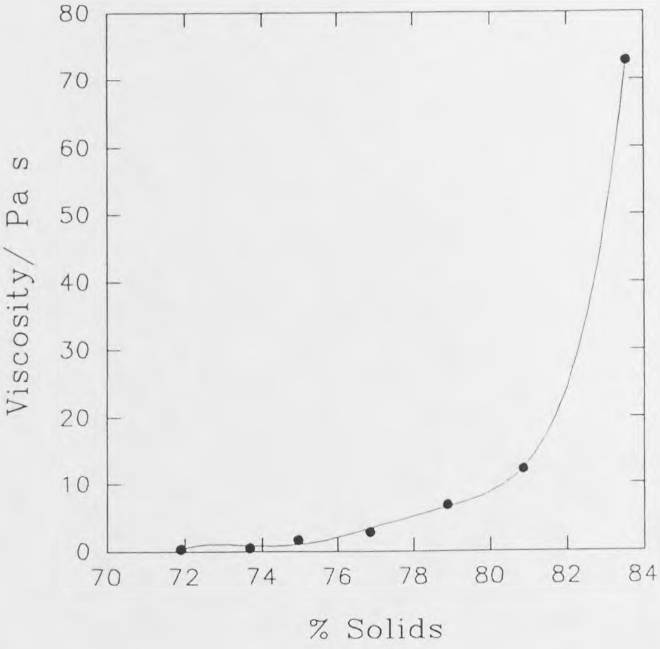

Figure 3.1 Viscosity of Sweetose syrup *vs* sugar content. *From Bee* et al, *1987.*

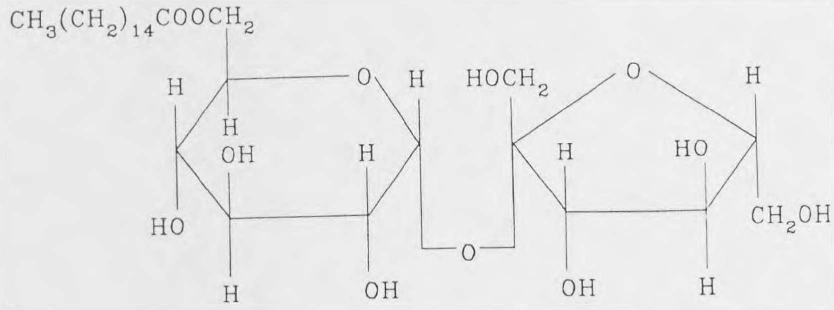

Figure 3.2 Structure of P1670 sucrose ester surfactant. *From Ryoto Sugar Ester Technical Information, 1987.*

esters can be used to control crystallisation in oils and to inhibit thermal and freezing denaturation of proteins. They have a useful anti-microbial action, and they are tasteless, odourless and non-toxic (Ryoto Sugar Ester Technical Information, 1987).

In Sweetose syrup, sucrose esters P1670 and S1670 (the sucrose ester of stearic acid) promote bubbly liquids which have very small bubbles and which are very stable compared to bubbly liquids prepared with Hyfoama (Hodges, 1990). This is presumably due in part to the affinity between the hydrophilic sucrose head group of the surfactant and the continuous phase. At high concentrations of surfactant, the sucrose esters can form a liquid crystal mesophase at the bubble surface (Hodges, 1990).

3.1.2.4 Electron microscopy *(carried out by Unilever Research Ltd, Colworth)*

Electron microscopy was used in order to examine the model bubbly liquid. Three different versions of the model were examined, each employing a different surfactant (Hyfoama, P1670 and S1670) at a level of 0.5 wt% in 70 wt% Sweetose syrup. Thin strands of the liquid were allowed to fall into liquid nitrogen contained in a Dewar flask. The rapidly frozen strands were then transferred to beakers packed in solid carbon dioxide for storage until they were prepared for microscopy. The samples were examined in a transmission electron microscope, so considerable sample preparation was necessary. The frozen sample was fractured using a microtome, and the fractured surface was 'shadowed' with osmium tetroxide to produce a very thin layer of metal atoms with the same topography as the fractured sample. The sample was then washed away using chromic acid, leaving behind a fragile metal replica of the sample which was suitable for examination in a transmission electron microscope.

The electron microscope revealed a high degree of structure at the surface of bubbles which were stabilised by S1670 and P1670 (*Fig. 3.3*). This structure was extremely regular and may be due to surfactant micelles, tightly packed at the bubble surface, and consequently deformed into hexagonal shapes. The hexagons which can be discerned on the bubble surface are about 40 nm across, although there are some examples which are rather larger. This scale is consistent with the

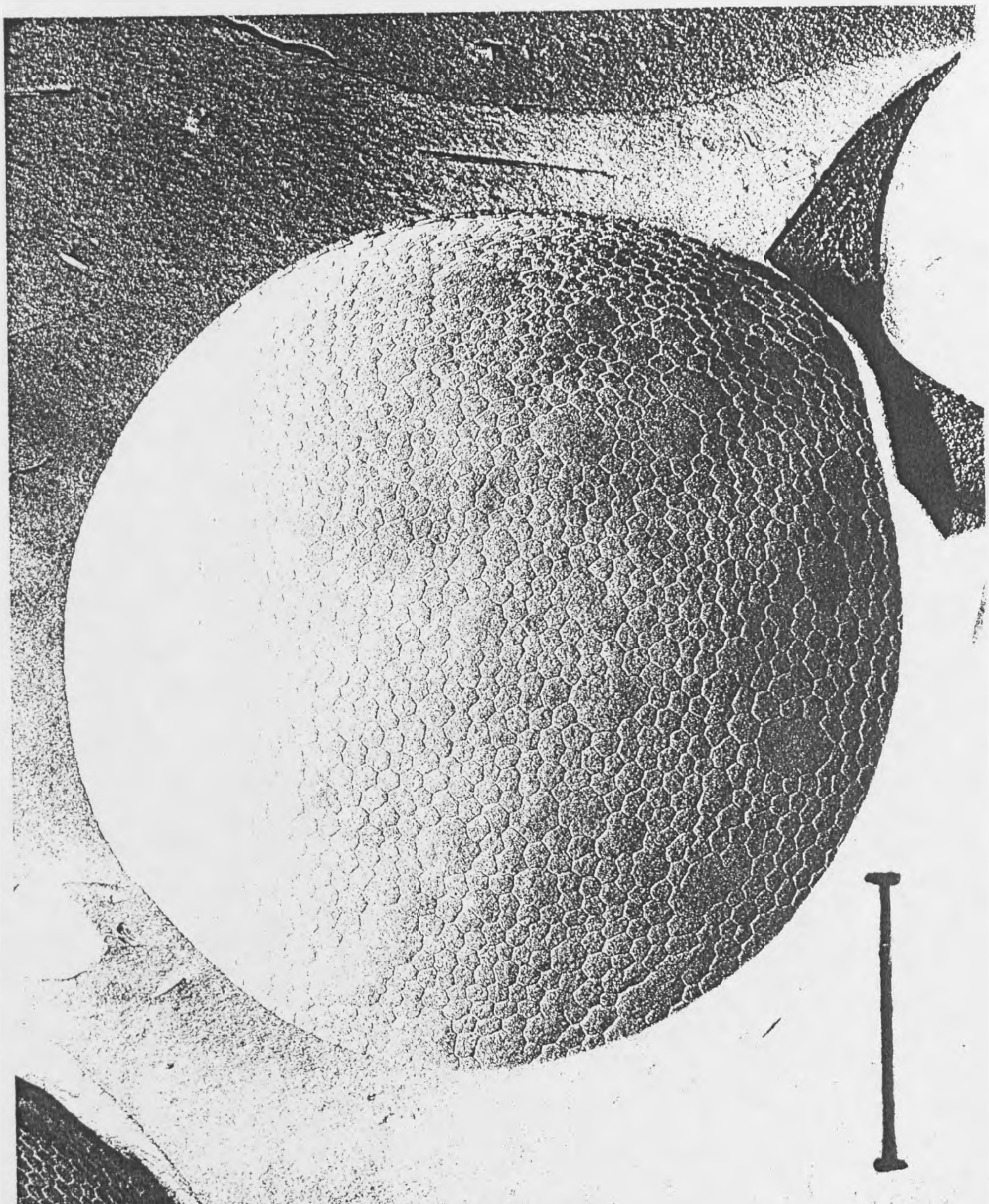

Figure 3.3 Transmission electron micrograph of a bubble in Sweetose syrup, stabilised with S1670 sucrose ester. Bar = 0.5 μm. Note the extremely regular structure at the interface.

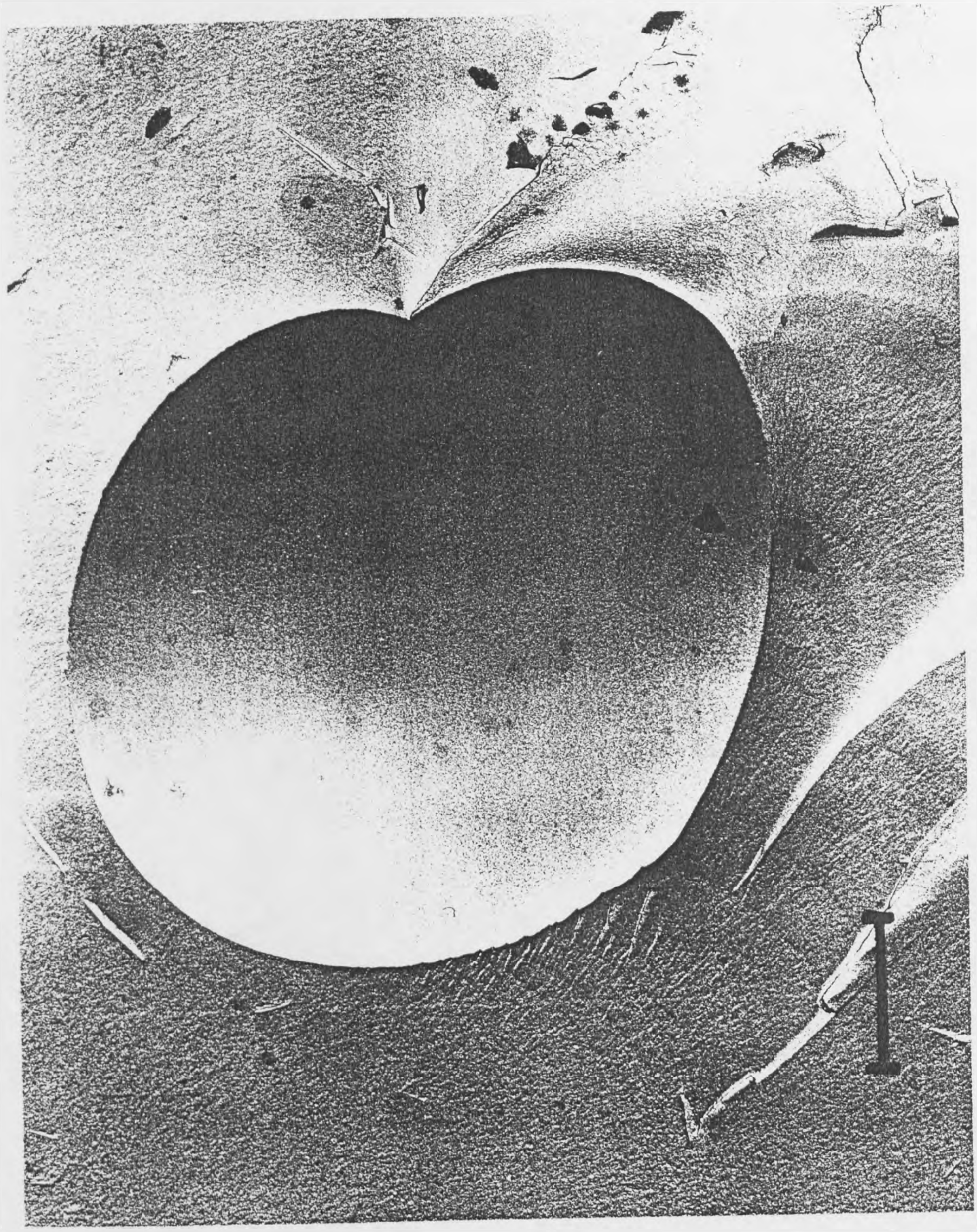

Figure 3.4 Transmission electron micrograph of a bubble in Sweetose syrup, stabilised with Hyfoama. Bar = 0.5 μm. Note the absence of structure at the surface.

dimensions of surfactant micelles. The structure was seen principally on the smallest bubbles, such as the one pictured, which had a radius of just 0.75 μm. In the absence of surfactant such a bubble would dissolve in a fraction of a second, so the surfactant must have had a very strong stabilising influence. Bubbly liquid prepared with S1670 lasts for several weeks (Hodges, 1990). In this work, bubbly liquids prepared with P1670 at high concentrations were observed to persist for several months.

No structure was seen on large bubbles, or on bubbles stabilised by Hyfoama (*Fig. 3.4*). Several samples were prepared and examined, and the structure was repeatedly observed, so it was not an artifact generated by the preparation process which is necessary for electron microscopy. The structure is almost certainly associated with the ability of the sucrose ester molecules to adopt a highly ordered configuration at the bubble surface.

The structure at the interface is believed to arise through an aging process, similar to that discussed in Section 1.7.4., which is explained as follows: the bubbles formed during whipping were initially quite large, and the surfactant film may not have covered them completely. The bubbles shrank due to disproportionation, and the surfactant film became more closely packed. As the local surfactant concentration rose, and the available surface area was reduced, the formation of a mesophase (and possibly micelles) was promoted, and the diffusion of gas out of the bubble was greatly hindered, so that further shrinkage of the bubble was greatly retarded. The controlling factor in foam stability would then be the film drainage and rupture. Drainage was retarded by the high viscosity of the syrup, the low surface tension and the Gibbs-Marangoni effect. The enhanced dilational elasticity due to the surfactant layer at the bubble surface meant that the critical thickness for film rupture was reduced.

The key factor seems to be the configuration of the surfactant molecules. The aging process will occur with any surfactant, but only the sucrose ester is known to form liquid crystals. Transient stabilisation of bubbles by liquid crystal layers has previously been observed in the production of solid foams from aqueous systems of polymerizable surfactants (Friberg & Fang, 1987). The use of liquid crystals to stabilise bubbles in a food system appears to be novel. The ability to prepare stable bubbles meant that the bubbles did not have to be prepared by continuous sparging, and the experimental equipment could therefore be much more compact.

3.1.2.5 Preparation of the model bubbly liquid

The bubbly liquid was prepared by whipping in a Kenwood Chef Excel KM210 food mixer, fitted with a stainless steel bowl and clear plastic bowl cover, using the stainless steel balloon whisk attachment. The bowl, bowl cover and whisk were always thoroughly cleaned before use to remove any grease which might destabilise the bubbly liquid. Neither Hyfoama nor P1670 were very soluble in 70 wt% Sweetose, because of the low water activity of the syrup. Dispersion was greatly improved by forming a pre-mix of surfactant in absolute ethanol[†]. The surfactant dispersion was placed in the mixer bowl, and sufficient 70 wt% Sweetose was added to give a total weight of 500.0 g (not counting the ethanol). The mixture was stirred thoroughly with a spatula until the mixture appeared to be homogeneous. The surfactant concentration was in the range 0.5 to 5 wt% in the total mixture before whipping. The mixture was whipped for 60 minutes at speed 5.0 in a covered bowl. The resulting concentrated bubbly liquid was used as it stood, and as a base for the preparation of the bubbled gel and the dilute bubbly liquid.

The temperature of the whipped mixture rose by several degrees over the course of whipping. In some experiments the bowl was cooled by tap water running through a water jacket around the bowl. The effect of the cooling jacket was found to be rather limited, because of the very low thermal conductivity of the foam. Therefore in the majority of the experiments whipping was performed at ambient temperature. This can be expected to have had a small effect on the reproducibility of the model, through the variable effects of evaporation. Nevertheless, the reproducibility of the whipping experiments was acceptable. Much better temperature control would be achieved by controlling the temperature of the air which is incorporated, and by cooling the beater and the motor of the mixer. The viscous

---

†: It is well known that alcohols can enhance the stability of foams prepared with chemically similar surfactants. For example, lauric alcohol enhances the stability of foams prepared with sodium lauryl sulphate. However, it is not likely that the ethanol used in this work to prepare the model bubbly liquid acted as a co-surfactant, because nearly all of it evaporated over the course of whipping.

nature of the system meant that considerable heat production was inevitable on prolonged vigorous mixing. This heat produced within the bubbly liquid would have been difficult to remove without a more drastic cooling system. A big disadvantage of using a lower temperature for the cooling liquid is the effect that this will have on the viscosity of the liquid which is in contact with the surface of the mixing bowl. Some evaporation was therefore inevitable, because of the long whipping time and concomitant rise in temperature.

3.1.2.6 Characterisation of the concentrated model bubbly liquid

In the simplest experiments, bubbly liquids prepared with P1670 or Hyfoama were transferred from the mixing bowl directly to the ultrasonic equipment, known as the UPER or FSUPER, which are described in detail in Sections 3.2.3 and 3.2.4. The liquid was allowed to equilibrate to 20 °*C* (which usually took several hours), and ultrasonic and density measurements were then performed. The bubble size distribution was determined using a Malvern Mastersizer (which is described in more detail in Section 3.2.6). The light microscope was found to have insufficient resolution to characterise the bubbly liquid.

3.1.3 Dilute model bubbly liquid

A dilute model bubbly liquid was prepared using concentrated bubbly liquid made with P1670, and distilled water. Most of the bubbles from the concentrated liquid dissolved on the addition of water, but a small proportion of the bubbles were sufficiently stable to survive for many days.

3.1.3.1 Preparation of dilute model bubbly liquid

Dilute bubble systems were prepared by adding a known quantity of concentrated bubbly liquid (typically 25-100 g) to 500.0 g of distilled water in a beaker. The beaker was covered, and the mixture was stirred vigorously for at least an hour to disperse the foam. When dispersion appeared complete, 500.0 ± 0.25 ml of the solution was measured into a volumetric flask, and 50.00 ± 0.04 ml of solution was removed from the flask using a pipette, and discarded. The remaining 450.0 ml of solution was transferred to the FSUPER and allowed to equilibrate to 20 °*C*. The solution was stirred constantly whilst in the FSUPER by means of a submersible magnetic stirrer. The ultrasonic properties of the sample were determined, and then 50.00 ± 0.04 ml of the solution were removed using a pipette. The total volume of the liquid in the FSUPER was made up to 450.0 ml using 50.00 ± 0.04 ml of distilled water, taken from a large beaker which was kept at the temperature of the water bath. Thus the dilute bubbly liquid was diluted by a factor of 8/9. The liquid which was removed from the FSUPER was used for a density determination in the Paar densitometer.

The dilution process was repeated several times in order to obtain measurements over a range of bubble concentrations. In the later stages of the dilution process the amount which was removed was increased to 100.00 ± 0.04 ml, with 100.00 ± 0.04 ml of water being added in order to top up the FSUPER. This gave a dilution factor of 7/9. The dilutions were performed as quickly as possible, because the more dilute solutions were not stable to disproportionation for more than a few hours.

In order to determine the effect of the presence of air in the dilute bubbly liquid, it was necessary to repeat each run using a source sample which contained no air. A duplicate sample was therefore prepared, which was heated whilst it was stirred, taking care not to lose any water due to evaporation. The solution was held at 70-80 °*C* for about two hours, and then it was allowed to cool back to room temperature. This solution was then measured out and diluted in exactly the same way as the bubbly sample.

3.1.3.2 Albunex

The Sweetose model used in this work is not the only one which can provide bubbles which have unexpectedly long lifetimes. *Albunex* is the trade name of an ultrasonic contrast agent used for echocardiology. It consists of bubbles with micrometre radii, stabilised by a surface film of human serum albumin, which is a naturally occurring blood protein. Albunex bubbles have been characterised in a Malvern Mastersizer and a CoulterCounter (see Sections 1.8.6 and 1.8.8) and they have also been characterised ultrasonically (Schneider *et al*, 1992, de Jong *et al*, 1991).

Albunex bubbles are formed by sonication of a 5 wt% solution of human serum albumin. The mean diameter of the bubbles so formed is typically 2-4 μm, and the thickness of the protein film is around 20-25 nm. Native human serum albumin has molecular dimensions of approximately $4 \times 4 \times 14$ nm (de Jong *et al*, 1992). If the protein is not denatured at the bubble surface[†], this would suggest that the protein film is 5-6 molecules thick (de Jong *et al*, 1992). The protein film has elasticity, which adds an extra restoring force, increasing the resonant frequency. Measurements of the scattering and absorption cross-sections of Albunex bubbles agree well with theoretical predictions, taking into account the influence of the protein film (de Jong *et al*, 1992), and resonance behaviour of the bubbles has been observed (Bleeker *et al*, 1990). Ultrasonic measurements have also been made on another type of echocardiographic contrast agent, termed *polymeric microballoons* by the inventors. Bubbles with a skin of a biodegradable polymer, tert-butyloxycarbonylmethyl polyglutamate, are more stable under pressure than Albunex bubbles, and they are slightly smaller (Schneider *et al*, 1992). These bubbles show similar ultrasonic behaviour to Albunex bubbles, but the polymer skin has a more pronounced effect on the resonant frequency. The volume fraction of air in the bubbly liquids was measured using a density meter similar to the one used in this work.

In further studies on model bubbly liquids, it may be instructive to investigate Albunex or polymeric microballoons as alternatives to the bubbles used in this study. The advantage of these contrast agents is that they are available commercially and they appear to be very stable.

3.1.4 Bubbled gel

Some ultrasonic measurements were performed upon bubbled gel. The intention was to add a gelling agent to a bubbly liquid, and by allowing the mixture to cream whilst the gelling agent set, to produce a fractionated bubbly system. Gelling agents such as gelatin, pectin and alginate were examined, but agar gave the best results. It was necessary to reduce the Sweetose concentration to 50 wt%, because the gelling agents would not dissolve in concentrated syrup. At concentrations of 2-

---

†: Protein molecules usually adsorb irreversibly at the air-water interface. This implies that they are denatured. Protein molecules in the outer part of the shell need not be denatured.

2.5 wt% in 50 wt% Sweetose, agar formed firm, rather brittle gels which did not exhibit significant syneresis. In practice, the disparity between the bubble creaming rate and the gelling rate was so large that few of the envisioned experiments were possible.

Bubbled gel was prepared by diluting the concentrated model bubbly liquid with a solution containing Sweetose (50 wt%), Agar (2.5 wt%) and P1670 (0.5 wt%). In preparation, this solution was heated in order to dissolve the agar, and then cooled to blood heat. The bubbly liquid was added and thoroughly mixed in using a glass rod. The bubbly molten gel was poured into a beaker and allowed to set. The gel set in 2-3 hours at room temperature. The finished gels were removed from the beaker, and cut into cylindrical sections which were typically 10-30 mm long. The ultrasonic properties of bubbled and unbubbled gel were determined in a specially constructed ultrasonic rig, which is described in detail in Section 3.2.2.

3.1.5 Yogurt

In addition to the model systems described above, the ultrasonic properties of several different real aerated foods were examined. The simplest of these was yogurt, which is described in more detail below.

Yogurt is a relatively simple liquid, prepared by the fermentation of milk. It is chiefly water, with small amounts of dispersed fat, protein and sugar. Native yogurt can be whipped, but the resulting dispersion is extremely unstable. In order to prepare stable bubbly yogurt it is necessary to add a surfactant. The use of Hyfoama resulted in a reasonably stable bubbly yogurt, presumably because the Hyfoama was well solvated at the low pH found in yogurt. Whipped yogurt prepared using Hyfoama was stable for around 24 hours at 5 °*C*. Two different types of yogurt, low fat natural yogurt and full fat set yogurt, were obtained from a local supermarket and stored in a domestic refrigerator at 4-5 °*C* prior to use. The composition of the yogurts, as supplied by the manufacturers, is set out in *Table 3.2*. The density and ultrasonic properties of the yogurts were determined in both whipped and unwhipped forms.

Table 3.2 *The composition of the yogurts examined here (manufacturer's data).*

Composition (g/100g):	Carbohydrate	Fat	Protein
Low fat natural yogurt (Own label, Morrison Supermarkets plc, Bradford, BD8 9AX, UK)	8.4	1.2	5.9
Full fat set yogurt (*Biogarde*, Capital Foods Ltd, Barrow-upon-Soar, LE12 8LP, UK)	3.5	5.5	3.9

3.1.5.1 Preparation of whipped yogurt

The Kenwood bowl, balloon whisk and bowl cover were thoroughly cleaned and dried. Hyfoama (5.00 g) was weighed into the Kenwood bowl, and yogurt (420 g) was added. The mixture was stirred thoroughly by hand in order to disperse the Hyfoama, and it was then whipped (6.0 minutes at speed setting 3.0). The bubbly yogurt was placed in the FSUPER, and in the density cup, both of which were located in a waterbath at 5 *°C*. Temperature equilibration was usually complete within 30 to 40 minutes. The ultrasonic properties of the whipped yogurt were dynamic, so they were assessed 60 minutes after the yogurts had been transferred to the FSUPER. In this way, all samples would be sure to have reached thermal equilibrium, and one source of inter sample variation could be reduced. Some samples of whipped yogurt were also examined under the light microscope.

3.1.5.2 Light Microscopy

Small samples of yogurt were withdrawn from the mixing bowl using a suction tube. Each sample was placed in a Howard mould count cell, which is similar to a haemocytometer slide. It consisted of circular well, 100 μm deep, which was surrounded by a moat. The cell was covered with a thick coverslip which was supported on coverslips placed either side of the well, giving a total cell depth of 260 μm. This placed an upper limit of 240 μm on the bubble sizes which could be determined. A small proportion of the bubbles were beyond this size limit and hence could not be accounted for. A total of around 400 bubbles were sized from photomicrographs of the yogurt samples. This number was a compromise between the requirements of statistical rigour and the practical difficulties in sampling the system, which was changing with time. The observed size distribution was assumed to be a reasonable approximation to the true size distribution, with a bias toward the smaller bubbles. No structure other than the presence of bubbles was observed in the whipped yogurt.

3.1.6 Cream

Cream is a more complex liquid than yogurt. It is typically prepared by the centrifugation of milk. It contains small amounts of protein and sugar, and large amounts of dispersed fat. Three types of cream were obtained from a local supermarket: whipping cream, double cream and 'spray' cream. These were stored in a domestic refrigerator at 4-5 °*C* prior to use. Whipped whipping cream and whipped double cream were stable for several days at 5 °*C*. The spray cream was stable for only a few hours at 5 °*C*. The composition of the creams, as supplied by the manufacturers, is set out in *Table 3.3*. The density and ultrasonic properties of the creams were determined, where possible, in both whipped and unwhipped forms.

3.1.6.1 Unwhipped cream

Considerable creaming occurs during storage within the containers of whipping cream and double cream. The flocculated fat globules can however be redispersed by stirring. It was necessary to gently but thoroughly stir the whipping cream and double cream, taking care not to introduce any air. Attempts were made to prepare an air-free version of the spray cream. The spray cream was allowed to collapse naturally at room temperature, then the resulting liquid was centrifuged. The centrifugate was gently stirred to redisperse the fat which had risen to the top of the centrifuge tubes.

3.1.6.2 Preparation of whipped cream

The Kenwood bowl, balloon whisk and bowl cover were thoroughly cleaned and dried. Whipping cream or double cream (560 g) was weighed into the Kenwood bowl, and whipped for 6.0 minutes at speed setting 3.0. This yielded a stiff cream, with a dry appearance. The whipped cream was carefully spooned into the FSUPER, and into the density cup, both of which were located in a waterbath at 5 °*C*. Temperature equilibration was quite slow, usually taking 3-4 hours. The

Table 3.3 *The composition of the creams examined here (manufacturer's data)*

Composition (g/100g):	Carbohydrate	Fat	Protein
Whipping cream (Own label, Morrison Supermarkets plc, Bradford, BD8 9AX, UK)	3.0	40.0	2.0
Double cream (Own label, Morrison Supermarkets plc, Bradford, BD8 9AX, UK)	2.6	48.0	1.7
'Spray' cream (Anchor)	Composition not provided. Stated ingredients: Cream, sugar, emulsifier E471 (mono- and diglycerides of fatty acids), stabiliser E407 (carrageenan), propellant nitrous oxide.		

whipped creams were quite stable, so density and ultrasonic properties were determined once thermal equilibration was complete.

The 'spray' cream was taken from the refrigerator and sprayed directly into a clean Kenwood bowl, keeping the nozzle of the can under the surface of the emerging cream, in order to avoid the entrapment of extra air. The cream was then spooned into the FSUPER and density cup in the same way as the other creams had been. The cream was measured 30 minutes after being sprayed into the FSUPER, because it was much less stable, and the temperature of the freshly formed whipped cream was close to 5 °*C*.

3.1.6.3 The structure of whipped cream

Cream does not require the addition of a surfactant in order to be successfully whipped. The events which occur during whipping are well understood (Anderson & Brooker, 1988). The fat is dispersed as globules which are surrounded by a strong membrane which protects them from coalescence. As whipping starts, the bubbles which form are stabilised by the highly surface active protein. Hydrophobic fat globules start to move to the newly created interface, where they displace protein from the interface. The membrane surrounding the larger fat globules is damaged in the shear field of the whipping rod. If the temperature is sufficiently low, the damaged globules can agglomerate with any other globules with which they collide. Within a few minutes, the surface of the bubbles is completely covered in fat globules, which are linked together in a network which extends throughout the whipped cream. The fat globules hinder the diffusion of gas out of the bubbles, and they provide structural stability. The structure of whipped cream and spray cream cannot be observed under the light microscope. It is however elucidated perfectly by electron microscopy (*Fig. 3.5(a)*). Fat globules are located at the bubble surface, and they protrude into the lumen of the bubble. The agglomerated fat network is clearly visible in cross-section. The bubbles typically have radii of 5-10 μm, and some of the larger ones (not shown) are non-spherical. The structure of spray cream is similar (*Fig. 3.5(b)*), although the bubbles are larger and the lamellae are thinner.

If the temperature in the whipped cream is allowed to rise above 10 °*C*, the fat within the globules melts and becomes partly liquid. This liquid fat escapes from globules with damaged membranes, and is very strongly adsorbed at the bubble surface, displacing protein and the more loosely adsorbed intact fat globules. The liquid fat confers no stability on the bubbles and they rapidly coalesce. For successful whipping therefore, the temperature of the cream must be kept at 10 °*C* or less.

3.1.7 Bread dough

Bread is a commercially important food product, and consequently it has been very well studied. A large battery of empirical tests are used to classify flours according to their suitability for bread-making, and to characterise bread dough and baked bread. In this work, the properties of bread dough merit no more than a brief consideration. The interested reader is referred to Pyler (1973) for more information.

3.1.7.1 Preparation of dough

Strong bread flour dough was prepared by mixing flour (400.0 g), salt (12.7g) and water (255.0g) in a Kenwood Chef Excel mixer at speed 2.0 for 2.0 minutes, using a dough hook attachment. The dough was carefully transferred to the FSUPER, and allowed to equilibrate to 20 °*C*. This took several hours, so the size distribution of bubbles within the dough can be expected to have reached a quasi-equilibrium state. Once equilibration was complete, the density and the ultrasonic properties of the dough were measured. A fermented version of the dough was also exam-

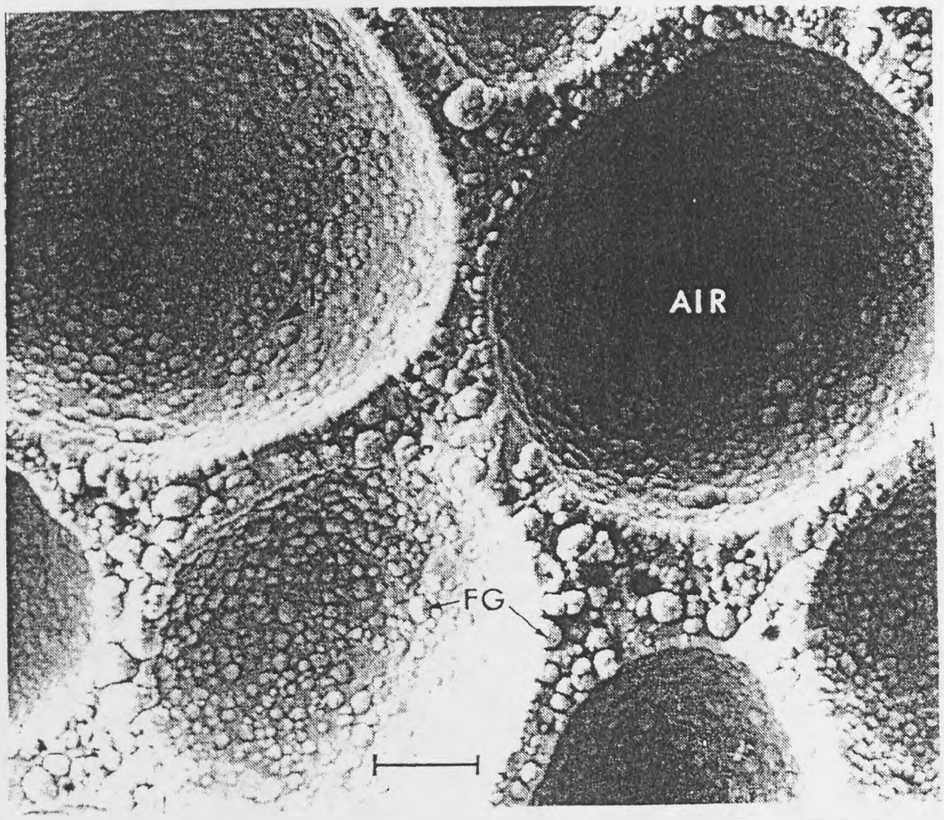

Figure 3.5(a) Scanning electron micrograph of whipped cream (bar = 10 μm). The fat globules (FG) are clearly visible at the interface (I). *From Anderson & Brooker, 1988.*

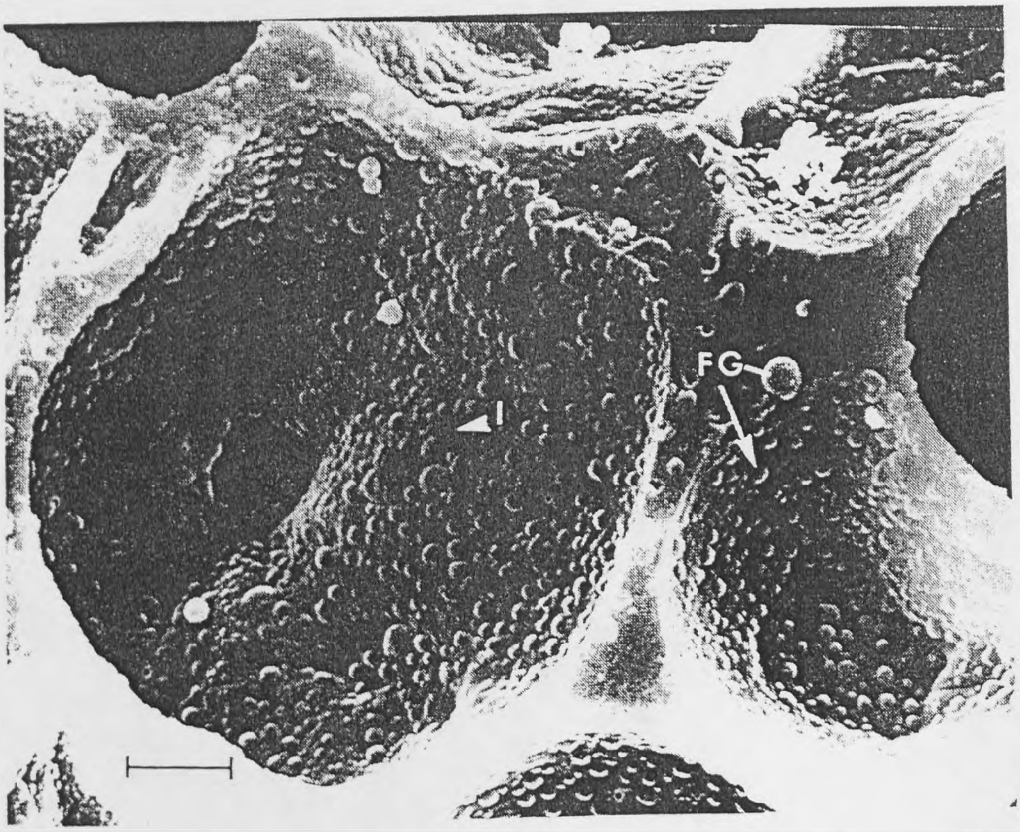

Figure 3.5(b) Scanning electron micrograph of spray cream (bar = 10 μm). Again, fat globules (FG) are visible at the interface (I). Note the thinner lamellae. *From Anderson & Brooker, 1988.*

ined. This was prepared in exactly the same way as before, with the addition of 7.6g of fresh yeast to the mixture. The dough was covered and allowed to ferment for 24 hours after being placed in the FSUPER at 20 °*C*. The fermentation was then deemed complete and ultrasonic measurements were made.

3.1.7.2 The structure of bread dough

Flour and water are transformed into bread dough by the input of a large amount of mechanical energy. The unique structure of wheat flour dough is due to the protein in the flour, which exists as a complex called gluten. In the presence of water, neighbouring protein molecules form disulphide bonds when the dough is worked. This cross-linking results in the formation of an elastic network, which is able to retain the gas produced during leavening. The bread-making quality of flour is directly related to its gluten content. Flours which are low in gluten (8-10 wt%) are termed 'weak' and are suitable for cake and biscuit manufacture. Flours which are high in gluten (11-13%) are termed 'strong' and are most suitable for bread manufacture. Dried, extracted gluten is produced commercially as a supplement for weak flour in order to improve its bread-making potential. There is still a need for a universal test of the suitability of gluten and flour for breadmaking (Czuchajowska & Pomeranz, 1990).

Ultrasound may offer a technique for the characterisation of bread dough, through its interaction with the bubbles which are entrained in the dough. During mixing, many air bubbles are entrained in the gluten matrix. These bubbles are thought to be stabilised by the surfactant materials which are present in the dough liquor[†] (Kumagai *et al*, 1991, Sahi, 1992). After mixing ends, the bubble size distribution in the dough is governed by disproportionation. Bubbles which are below a critical radius (about 15 μm) shrink as the gas diffuses out of them (Shimiya & Yano, 1988). The rate of shrinkage is well described by a modified version of the Epstein-Plesset equation (Epstein & Plesset, 1950). Bubbles in wheat flour dough shrink at about one thousandth of the rate at which bubbles in water shrink (Shimiya & Yano, 1987). This can be attributed to the presence of surfactant material at the interface and to the low diffusion rate of dissolved gas through the dough. Never-

---

†: This is the liquid phase which can be separated from dough by centrifugation.

Table 3.4 *The beers examined in this project*

Name of Beer	Packaging	Number of Samples
Swan Light	Can	2
Michelob	Can	2
Smithwick's	Bottle	2
John Smith's	Can	1
Bodington's	Can with insert	1

theless, bubbles which have radii below the critical radius have shrunk completely within 15 minutes at 3 °*C* (Kumagai *et al*, 1991) and within an hour at 42 °*C* (Shimiya & Yano, 1988). As expected, the bubbles which are larger than the critical radius grow at the expense of the smaller bubbles. However, the rate of growth is very much lower than expected. This can again be attributed to the slow diffusion of gas through the dough, and also to the elasticity of the gluten network.

The existence of stable bubbles (with radii typically in the range 40-140 μm) in the dough is essential for successful leavening. The yeast cells produce carbon dioxide, but they cannot initiate a gas bubble within the dough. Pre-existing nuclei are required which can be expanded by the diffusion of carbon dioxide through the dough. The volume fraction of gas in doughs made with strong and weak flours is different both before and after fermentation (Pyler, 1973). It may therefore be possible to assess the bread-making potential of a flour by determining the volume fraction of gas and/or the bubble size distribution in unyeasted dough. The determination of these parameters is, at present, difficult to perform quickly, accurately and non-destructively. Ultrasound might be useful for just such a purpose.

3.1.8 Beer foam

Several packaged beers were kindly supplied by Dr Roger Hammond of the Brewing Research Foundation. The names of the beers and the type of packaging are listed in *Table 3.4*. Unopened beer was equilibrated to 5 °*C* in the same water bath which contained the FSUPER. The beer was poured from a height of around

60 cm directly into a large beaker, in order to generate a frothy mixture. This mixture was immediately used to fill the FSUPER to the brim. Ultrasonic measurements were made immediately, the beer was allowed to settle for 30 seconds and then a second set of measurements were made.

3.2 Methods

3.2.1 Introduction

The purpose of this section is to describe the equipment which was used over the course of this investigation. The ultrasonic measurements were made in devices which were developed in the Department of Food Science, and these are listed in order in which they were developed. The most useful devices were the ultrasonic pulse echo reflectometer (UPER) and the frequency scanning ultrasonic pulse echo reflectometer (FSUPER). These devices were designed and developed by Dr Julian McClements whilst working in the Physical Measurement Group of the Food Science Department with Dr Malcolm Povey. The application of densitometry and light scattering is also described.

3.2.2 Measurement rigs for bubbled gel

In this investigation, a bubbled gel was the first bubbly food system to be examined ultrasonically. Two different measurement systems were employed in order to examine the bubbled gel.

A float glass rig (*Fig. 3.6*) was constructed in the Procter department workshop. Two float glass plates (approximately 1 m × 1m) were held parallel at a known spacing (5-10 mm) by a set of brass spacers. The gel was sealed in between the glass plates by a circular length of rubber tubing. Each of the transducers (Sonatest, centre frequency 500 kHz, diameter 20 mm) was supported by a holder bar containing a number of holes which were machined to the diameter of the transducer. The holder bars were aligned so as to keep the transducers coaxial with their faces parallel. The transducers acted as a transmitter/receiver pair, with the transmitting transducer excited by an electrical spike from an ultrasonic flaw detector (Balteau Sonatest UFD 1). The receiving transducer was connected to a digital storage oscilloscope (LeCroy 9420).

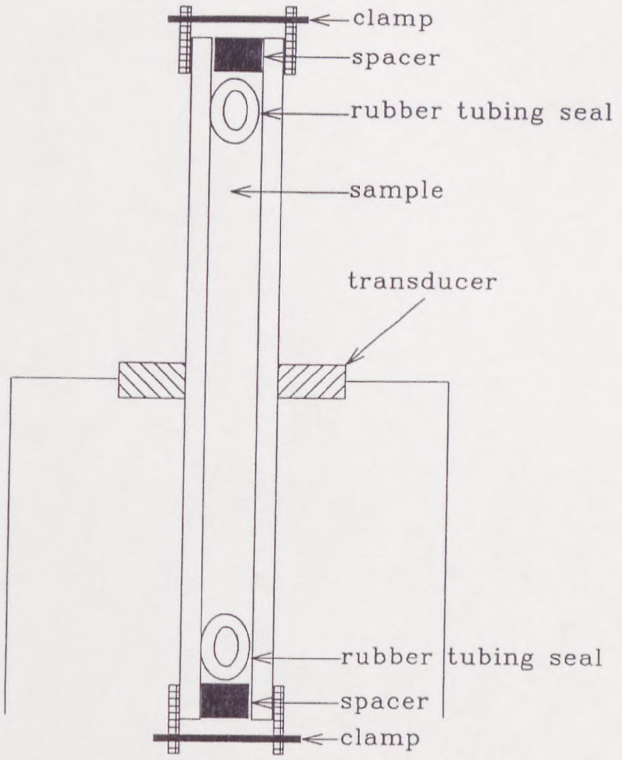

Figure 3.6 The first ultrasonic measurement rig for gel samples constructed by the Procter Workshop.

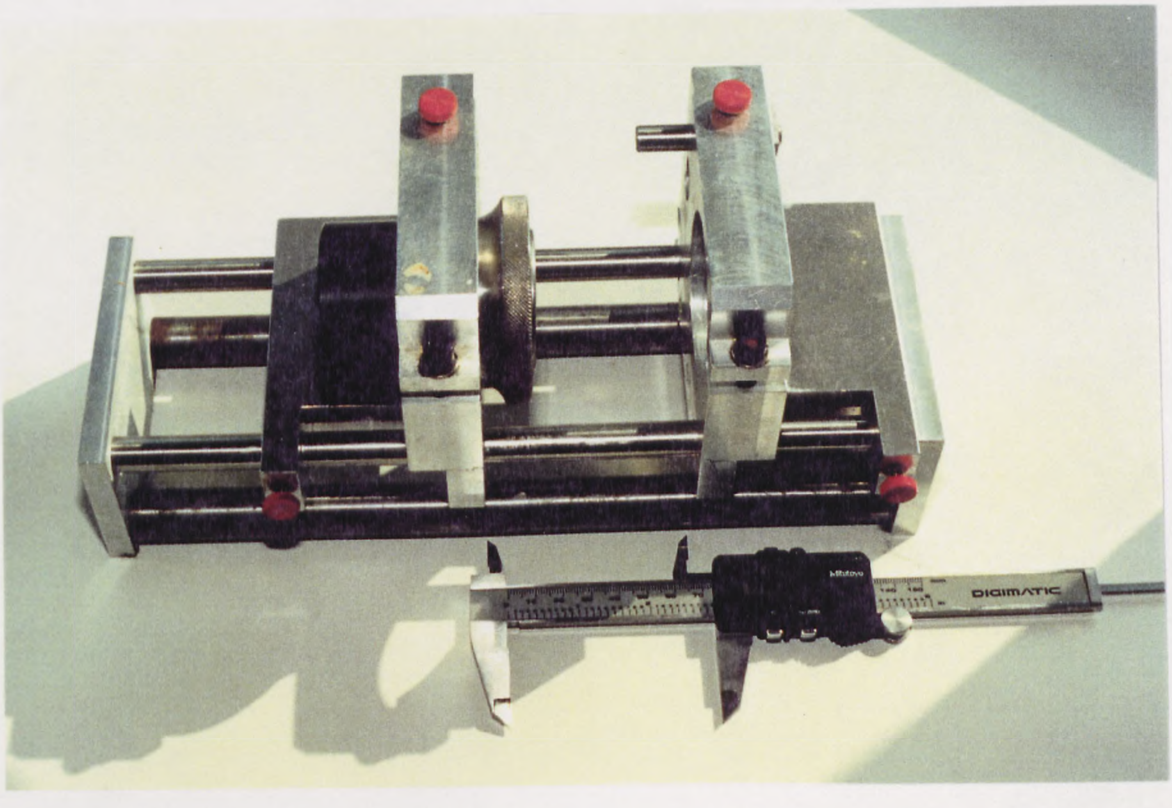

Figure 3.7 The second ultrasonic measurement rig for gel samples constructed by the Procter Workshop.

Strength considerations required the use of fairly thick (approximately 5 mm) glass plates. There was an acoustic impedance mismatch between the glass and the transducer and sample, so that the signal reverberated within the glass plates. This gave rise to a severe phase shift in the received signal, rendering the equipment useless for accurate measurements.

A revised measurement rig for the gel samples was constructed by the Workshop (*Fig. 3.7*). The rig consisted of holders for two pairs of transducers, arranged so that the transducer pairs were coaxial, and the transducer faces were parallel. The transducers used covered the frequency range 0.3 to 1 MHz (Karl Deutsch S40 HB 0.3-1, diameter 40 mm) and 1 to 8 MHz (Karl Deutsch S12 HB 1-8, diameter 12 mm). One holder was fixed at one end of the rig, and the other was free to move on guide rails, but could be fixed in position if desired. The gel slice which was to be assessed was placed between the transducers, and the movable holder was positioned so as to gently squeeze the gel and hold it in place. The holder was then fixed in position, and the transducer separation was determined to ± 0.2 mm using digital callipers (Mitutoyo Digimatic 500-321).

The measurement set-up is represented schematically in *Fig. 3.8*. Measurements were made using one pair of transducers at a time, with one transducer acting as a transmitter and the other acting as a receiver. The transmitter was excited by a toneburst containing at least 8 cycles, generated by a function generator (Hewlett Packard HP3312A or Hewlett Packard HP8116A). The function generators produced signals of modest amplitude (16V peak to peak maximum), so the technique could only accommodate samples with low attenuation coefficients. The receiving transducer was connected to a digital storage oscilloscope (LeCroy 9420). Each pair of transducers was swept through its operating frequency range in a number of discrete steps. The apparent time of flight of a pulse through the system consisted of the time taken to traverse the gel plus a delay due to the transducer wearplates and a small delay due to the electronic equipment. This system delay was determined by measuring the time of flight with the probes pushed fully together. The true time of flight through the gel samples was thus found by subtracting the system delay time from the apparent time of flight.

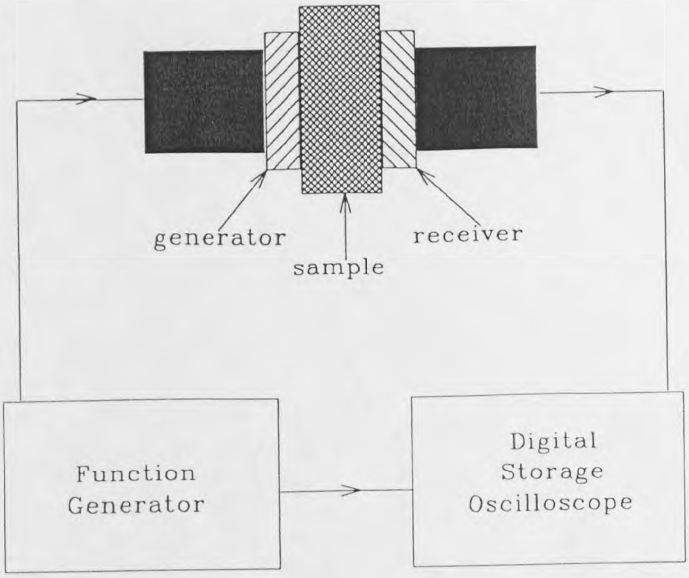

Figure 3.8 Schematic representation of the ultrasonic measurement rig for gel samples.

3.2.3 The Ultrasonic Pulse Echo Reflectometer

Because the bubbled gel was highly attenuating, it was not possible to make transmission measurements without increasing the intensity of the signal to the extent where the propagation would become non-linear. The success of the impedance technique employed by Leatherhead (Randall *et al*, 1987, Manetou, 1990) suggested that reflection measurements would be useful for systems which were very highly attenuating. A device incorporating a Perspex buffer rod was therefore employed, which could be used to measure the velocity, attenuation coefficient and acoustic impedance of a liquid sample at a fixed frequency of 2.1 MHz (McClements & Fairley, 1991). This device was used to measure air-free Sweetose, air-free Sweetose gel, and the model bubbly liquid.

The ultrasonic pulse echo reflectometer (or UPER) consisted of a cylindrical polymethylmethacrylate (Perspex) buffer rod set into an aluminium cell, which contained the sample (*Figs. 3.9* and *3.10*). An ultrasonic transducer (Balteau Sonatest, nominal centre frequency 2 MHz, diameter 10mm) was bonded to one end of the buffer rod, and the other end was fixed parallel to the inside face of the

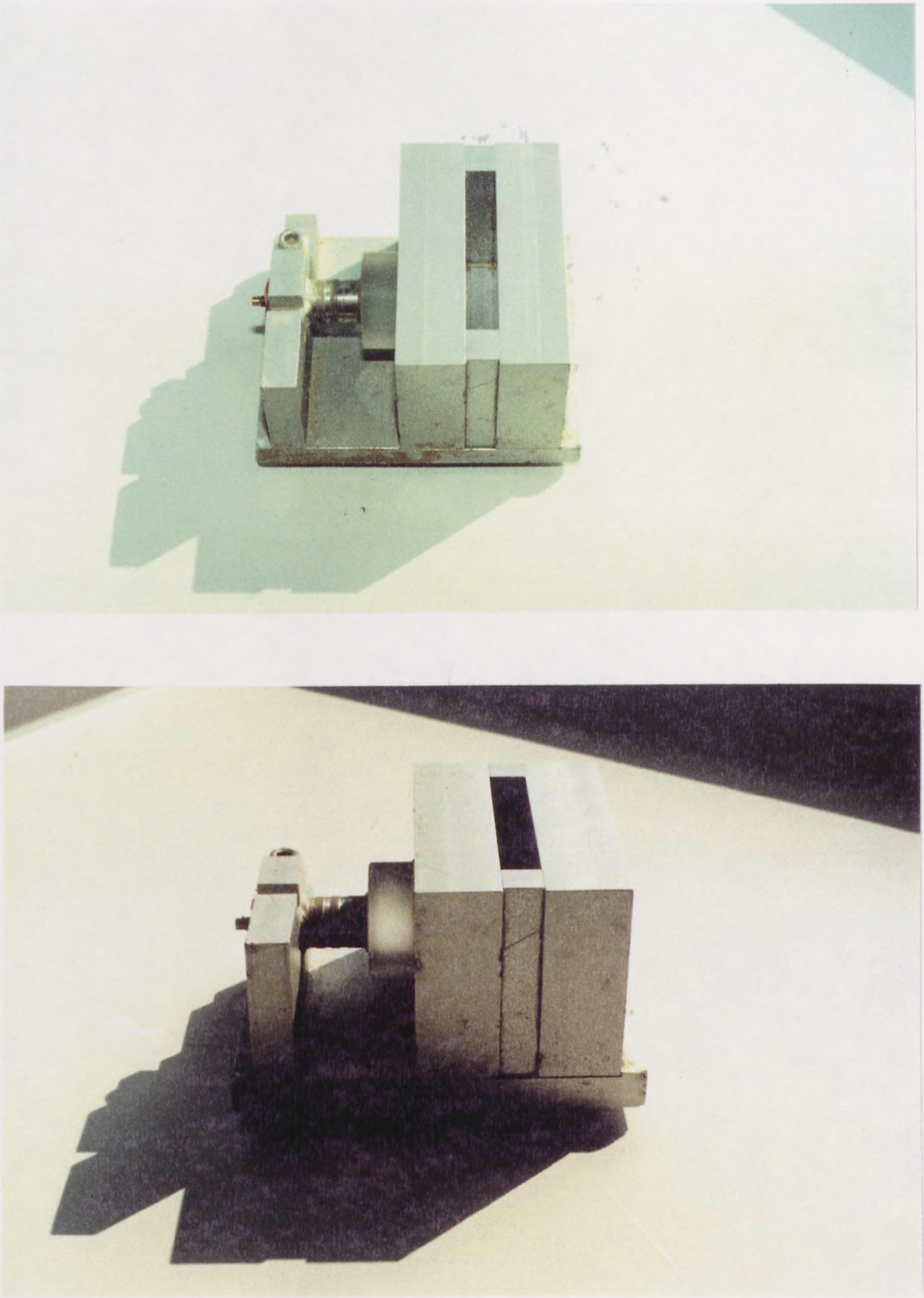

Figure 3.9 The Ultrasonic Pulse Echo Reflectometer.

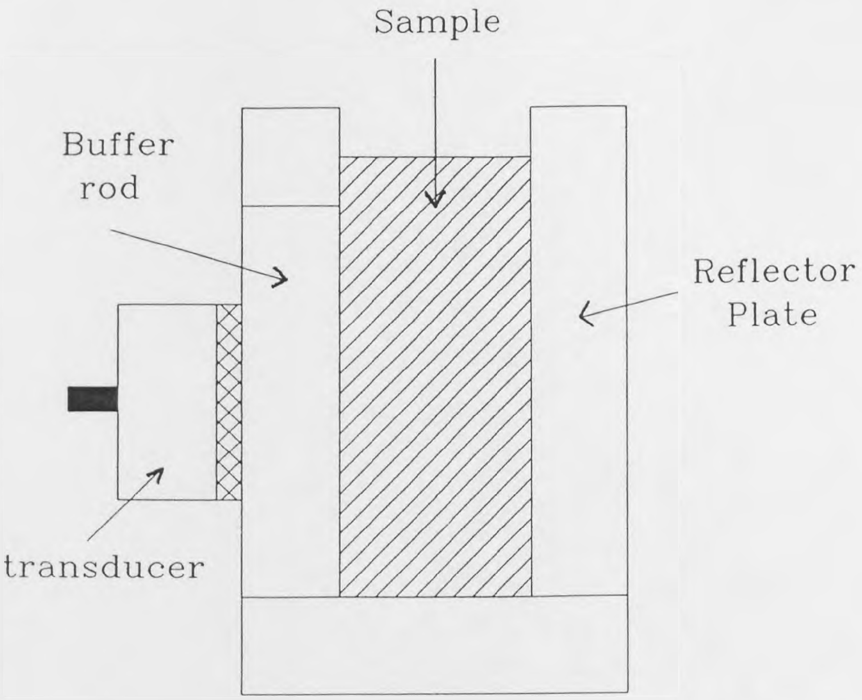

Figure 3.10 Schematic representation of the Ultrasonic Pulse Echo Reflectometer.

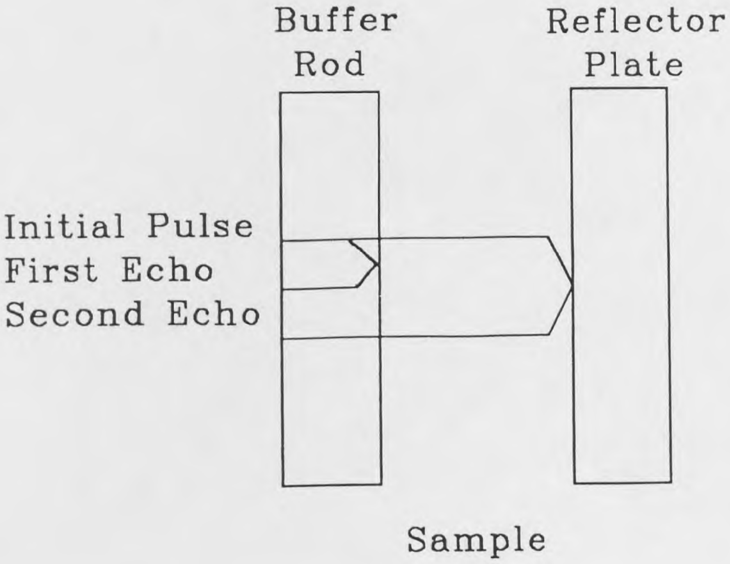

Figure 3.11 Diagram of the echoes occurring within the UPER. Echo one arises due to reflection at the buffer rod/sample interface. Echo two arises due to reflection at the sample/reflector plate interface.

opposite wall of the cell, which acted as a reflector plate. The transducer was medium damped, and it was excited by a toneburst of 5-10 cycles at 2.1 MHz from a function generator (Hewlett Packard HP 8116A). The ultrasonic signals which returned from the sample were analysed using a digital storage oscilloscope (LeCroy9420). The instrument was thermostatted in a waterbath to ± 0.1 *°C*. The transducer produced a pulse of ultrasound which travelled along the buffer rod to the rod/sample interface where it was partly reflected, giving rise to echo one, and partly transmitted (*Fig. 3.11*). The transmitted portion travelled on through the sample until it reached the sample/reflector plate interface, where it was again partly reflected, giving rise to echo two, and partly transmitted. The echoes reflected from both interfaces returned to the transducer, where they were detected and displayed on the oscilloscope.

3.2.3.1 Design Considerations

There are a number of important factors which were considered in the design of the UPER. The transducer, the buffer rod and the reflector plate had smooth faces and were aligned parallel to each other. The diameter of the buffer rod was large enough to ensure that beam spreading (see Appendix I) of the ultrasonic pulse did not lead to side wall reflections. The time the pulse took to travel the length of the buffer rod was greater than the time the pulse took to travel through the sample, so that the second echo displayed on the oscilloscope was the one which travelled through the sample and not a multiple echo in the Perspex rod. This placed a lower limit on the velocity of the material which the UPER could measure of about 400 ms^{-1}. The majority of liquids have velocities considerably larger than this lower limit. The reflector plate was sufficiently thick that no reverberations within it interfered with the pulse reflected from it.

3.2.3.2 Impedance measurements

The specific acoustic impedance of the sample liquid was determined by comparing the (complex) amplitude of echo one when the sample was placed in the cell with the amplitude when a liquid calibrant (a material whose ultrasonic properties are known), was placed in the cell. These amplitudes are given by

$$A_{1,s} = R_{1,s} \cdot A_i \cdot e^{-2\alpha' d'} \qquad [3.1]$$

$$A_{1,c} = R_{1,c} \cdot A_i \cdot e^{-2\alpha' d'} \qquad [3.2]$$

where A_1 refers to the amplitude of echo one, and the subscripts s and c refer to the sample and the calibrant respectively. R_1 is the (complex) reflection coefficient at the buffer rod/sample interface, A_i is the amplitude of the ultrasonic pulse when it initially enters the buffer rod, α' is the attenuation coefficient of the buffer rod and d' is the length of the buffer rod. Dividing *Equation 3.1* by *Equation 3.2* and rearranging gives

$$R_{1,s} = R_{1,c} \cdot A_{1,s}/A_{1,c} \qquad [3.3]$$

Distilled water was used as a calibrant, because its ultrasonic properties are well known (del Grosso & Mader, 1972) and for our Perspex buffer rod the value of $R_{1,water}$ was 0.374 ± 0.001 at 20 °C. The specific acoustic impedance of the sample, Z_s, was found from the reflection coefficient using

$$Z_s = Z_p \cdot (1 - R_{1,s})/(1 + R_{1,s}) \qquad [3.4]$$

where Z_p is the impedance of the Perspex buffer rod, which was measured as 3.245 $\pm$ 0.005 $\times 10^6$ kg m^{-2} s^{-1} at 20.0 °*C*, and can be treated as completely real without significantly affecting accuracy.

3.2.3.3 Attenuation measurements

The attenuation coefficient of the sample can be determined from the amplitudes $A_{1,s}$ and $A_{2,s}$ of echoes one and two respectively, which are given by

$$A_{1,s} = e^{-2\alpha' d'} \cdot R_{1,s} \cdot A_i \qquad [3.5]$$

$$A_{2,s} = e^{-2\alpha' d'} \cdot (1 - R_{1,s}^{\,2}) \cdot R_{2,s} \cdot A_i \cdot e^{-2\alpha d} \qquad [3.6]$$

where $R_{2,s}$ is the reflection coefficient at the sample/reflector plate interface, *d* is the length of the sample, α is the attenuation coefficient of the sample, and A_i is the amplitude of the pulse when it initially enters the buffer rod. Dividing *Equation 3.6* by *Equation 3.5*, and rearranging gives

$$\alpha = (1/2d) \cdot \ln\{[A_{1,s} \cdot (1 - R_{1,s}^{\,2}) \cdot R_{2,s}]/[A_{2,s} \cdot R_{1,s}]\} \qquad [3.7]$$

$R_{2,s}$ was determined by reference to $R_{2,c}$ in the same manner as $R_{1,s}$. It was then possible to determine α by measuring $R_{1,s}$, $R_{2,s}$, $A_{1,s}$ and $A_{2,s}$. In order to obtain accurate results the measurements were corrected for diffraction effects (see Appendix I).

3.2.3.4 Velocity measurements

The velocity, c_s, of the sample was determined from the equation

$$c_s = c_c \delta_c / \delta_s \qquad [3.8]$$

where c_c is the velocity in the calibrant, and δ is the time of flight in the UPER. The time of flight was determined using the central peak in echo one and echo two, taking into account a phase shift of 180° in echo two. This phase shift occurred because the acoustic impedance of the sample was lower than the impedance of the reflector plate. The velocity measurements were also corrected for diffraction effects (see Appendix I).

3.2.3.5 Accuracy

The principal sources of error in the measurements were temperature fluctuations, non-parallelism between the face of the buffer rod and the reflector plate, imperfections in the corrections applied to account for diffraction, and variability in the output of the function generator. The UPER can measure the velocity to $\pm$ 0.5 $\mathrm{ms^{-1}}$, the attenuation to $\pm$ 1 Np $\mathrm{m^{-1}}$ and the acoustic impedance to $\pm 0.01 \times 10^6$ kg $\mathrm{m^{-2}\,s^{-1}}$, with temperature control to $\pm$ 0.1 °*C*. Measurements made in the UPER on a number of liquids agreed very well with literature values (McClements & Fairley, 1991).

3.2.4 The Frequency Scanning Ultrasonic Pulse Echo Reflectometer

The UPER was very useful, but it was limited by the fact that it worked at only one frequency. The properties of bubbly liquids, and of course many other systems, are frequency dependent. The Frequency Scanning Ultrasonic Pulse Echo Reflectometer (or FSUPER) was developed from the UPER, in order to determine the acoustic impedance, velocity and attenuation of liquid samples as a function of frequency (McClements & Fairley, 1992). The FSUPER was used to examine the model bubbly liquid (in concentrated and diluted forms), and to examine whipped yogurt, whipped cream, bread dough and beer foam.

The FSUPER consisted of two cylindrical polymethylmethacrylate (Perspex) buffer rods set into an aluminium cell, which contained the sample (*Figs. 3.12* and *3.13*). An ultrasonic transducer was water-coupled to one end of each buffer rod, and the other ends were fixed parallel to the inside face of the opposite wall of the cell, which acted as a reflector plate. Both transducers were highly damped, and each one was operated in the same way. The transducer was excited by an electrical spike from an ultrasonic flaw detector (Balteau Sonatest UFD1) and it produced a broad band pulse of ultrasound. The ultrasonic signals returning from the sample were analysed using a digital storage oscilloscope (Lecroy 9420), and the whole measurement procedure was controlled using a personal computer (Amstrad PC2086 or PC1512). The entire measurement setup is illustrated in *Fig. 3.14*. The transducers covered the frequency ranges 0.3-1 MHz (Karl Deutsch STS 40 WB, diameter 40 mm or Sonatest SLH 1-25, diameter 25 mm) and 1-8 MHz (Sonatest SLH 5-20, diameter 20 mm). The instrument was thermostatted in a waterbath to ± 0.1 *°C*.

Each transducer produced a pulse of ultrasound which travelled through the sample in exactly the same way as in the UPER, giving rise to two echoes. In order to extract the frequency information from the pulses, echoes one and two were subjected to a Fast Fourier Transform, yielding magnitude and phase information in the frequency domain (*Fig. 3.15*).

The ultrasonic velocity was calculated from the phase difference between the transforms, and the attenuation coefficient and specific acoustic impedance were calculated from the ratio of the magnitudes of the transforms. As with the UPER, the device was carefully designed so that side-wall reflections due to beam spreading, and reverberations within the buffer rod and reflector plate did not interfere with the signals from the samples. This required the use of rods with larger diameters and shorter pathlengths than in the UPER. The sample pathlength in the FSUPER was rather larger than in the UPER, so the reverberations in the buffer rod were seen in the time interval between the two echoes (see *Fig. 3.15*). There was therefore no lower limit on the velocity of the liquids which could be examined in the FSUPER.

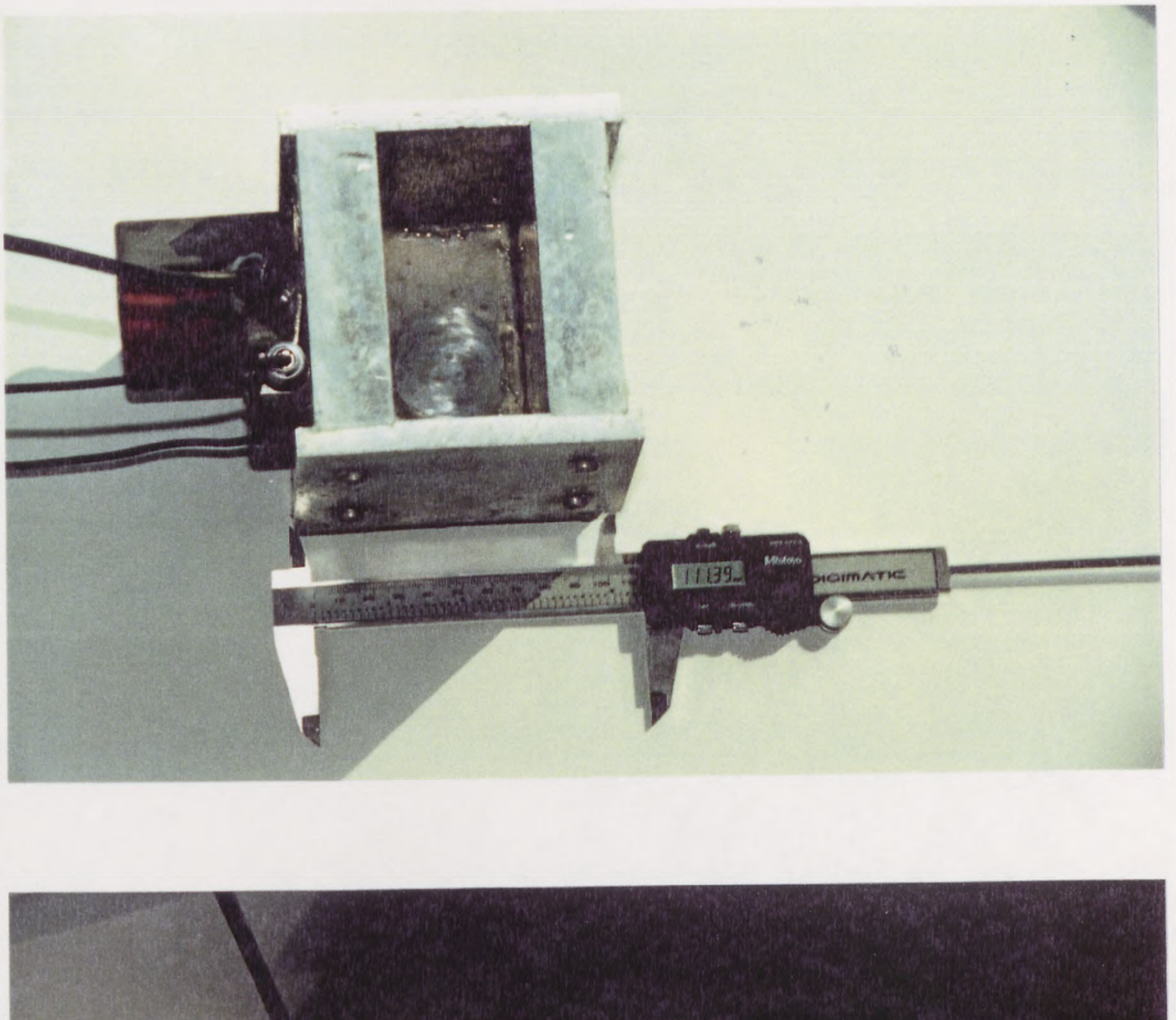

Figure 3.12 The Frequency Scanning Ultrasonic Pulse Echo Reflectometer.

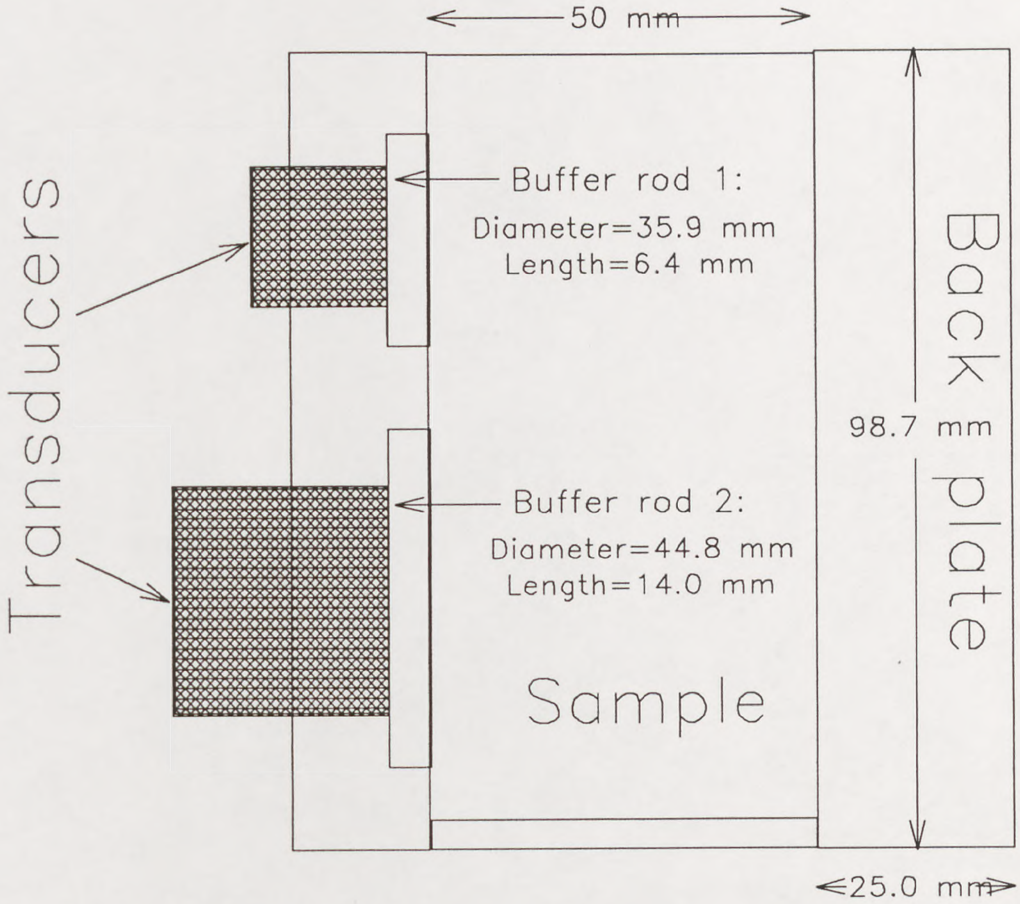

Figure 3.13 The Frequency Scanning Ultrasonic Pulse Echo Reflectometer (schematic).

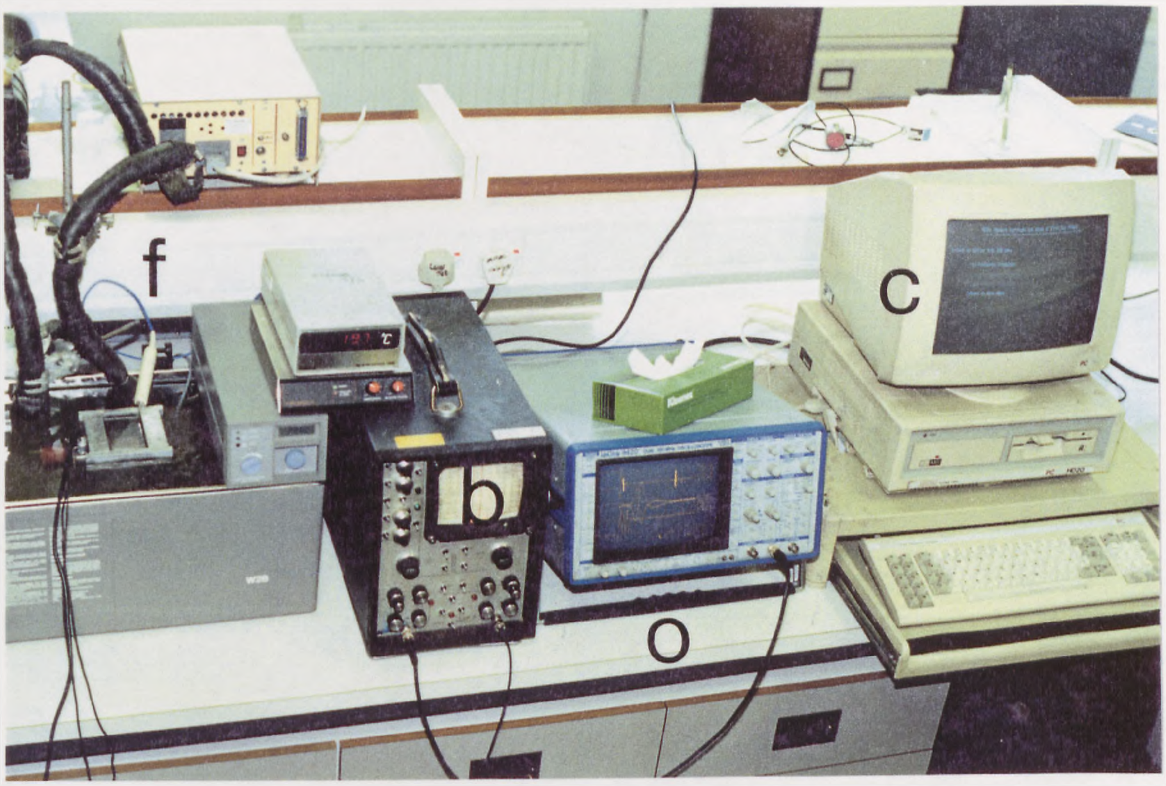

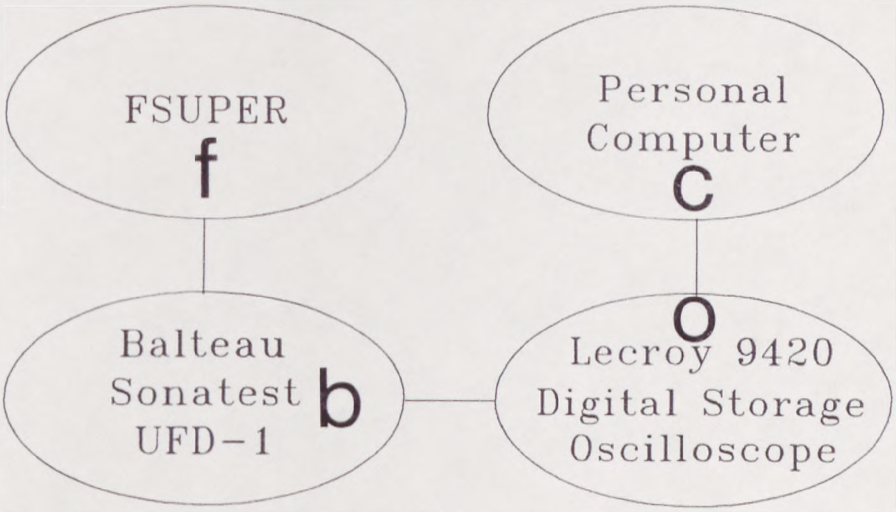

Figure 3.14 The FSUPER and associated equipment are shown in a photograph (top) and in schematic representation (bottom).

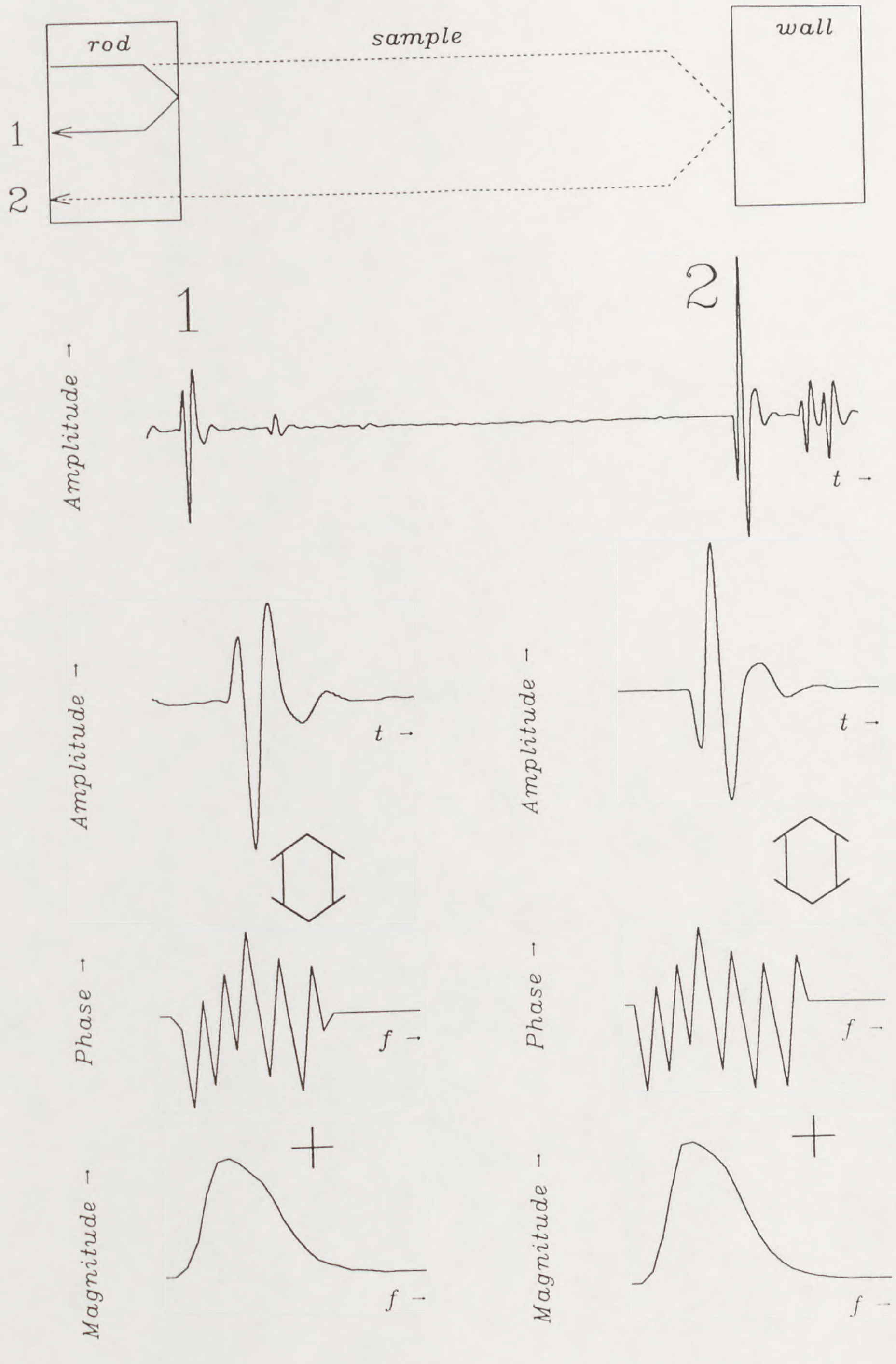

Figure 3.15 A voltage/time trace recorded in the FSUPER. The broadband pulse is reflected at the buffer rod/sample and sample/back wall interfaces, giving rise to echoes 1 and 2. Reverberations in the buffer rod can be seen shortly after echo one. Reverberations in the back plate are seen shortly aver echo two. The echoes are shown individually, on an expanded time scale. The 180° phase shift is obvious. The Fourier transform of each echo is shown in stylised form.

3.2.4.1 Measurement principles

The measurement principles in the FSUPER are broadly similar to those in the UPER. In the following discussion, quantities which are a function of frequency, *f*, are denoted as X(*f*) in the text, but the notation is dropped within equations in order to improve clarity.

3.2.4.2 Impedance measurements

The specific acoustic impedance of a liquid sample is again determined from the ratio of the amplitudes of the signals reflected from the sample and from a calibrant. These amplitudes are given by

$$A_{1,s} = R_{1,s}\cdot A_i\cdot e^{-2\alpha' d'} \quad [3.9]$$

$$A_{1,c} = R_{1,c}\cdot A_i\cdot e^{-2\alpha' d'} \quad [3.10]$$

where $A_1(f)$ refers to the amplitude of echo one, and the subscripts s and c refer to the sample and the calibrant respectively. $R_1(f)$ is the (complex) reflection coefficient at the buffer rod/sample interface, $A_i(f)$ is the amplitude of the ultrasonic pulse when it initially enters the buffer rod, α' is the attenuation coefficient of the buffer rod and d' is the length of the buffer rod. The amplitude of echo one is related to its Fourier transform by $A = M\cdot(\cos(\Theta)+i\cdot\sin(\Theta))$, where M(*f*) is the magnitude, Θ(*f*) is the phase and *i* is √(-1). Dividing *Equation 3.9* by *Equation 3.10* and rearranging, gives

$$R_{1,s} = R_{1,c}\cdot A_{1,s}/A_{1,c} \quad [3.11]$$

Distilled water was again used as a calibrant. The specific acoustic impedance of the sample is given by

$$Z_s = Z_p\cdot(1 - R_{1,s})/(1 + R_{1,s}) \quad [3.12]$$

where Z_p is the impedance of the Perspex buffer rod, which was not found to depend significantly on frequency in the range 0.3 to 8 MHz.

3.2.4.3 Predicted values of the reflection coefficient

In order to illustrate the value of reflection measurements (or impedance measurements), *Fig. 3.16* shows the predicted reflection coefficient (in the FSUPER) of the bubbly water systems considered in Section 2.2.5.1. The value of the reflection coefficient depends on the impedance of the buffer rod, so these predictions are device-specific. The predicted acoustic impedance could have been plotted instead, which would make the predictions independent of the device (although they would still depend on the expression which was chosen for the effective density). It was felt however that using the reflection coefficient made for clearer presentation.

Consider the most dilute system, with a volume fraction of 2 % (*Fig. 3.16(a)*). At low frequencies, the velocity is depressed and the attenuation is very low. Correspondingly, the real part of the reflection coefficient is large and the imaginary part is very small. At the resonant frequency the velocity is at a minimum and the real part of the reflection is at a maximum. At frequencies above resonance the velocity and attenuation are greatly elevated. The real part of the reflection coefficient drops to a minimum and then recovers to the value of the bubble free water. The imaginary part of the reflection coefficient passes through a maximum and drops back to zero as the frequency increases. The frequency at which the real and imaginary parts of the reflection coefficient are equal is approximately ten times the resonant frequency.

As the volume fraction is increased (*Figs 3.16(b)* and *3.16(c)*) the real part of the reflection coefficient increases in value across the frequency range, and the value of the imaginary part decreases. The value of the real part of the reflection coefficient remains elevated at frequencies well above resonance, and the curves describing the real and imaginary parts of the reflection coefficient do not cross.

The reflection coefficient of the polydisperse system postulated in Section 2.2.5.2 is compared with the predicted reflection coefficient of a monodisperse system in *Fig. 3.17*. The bubbles are distributed log normally around a mean radius of 10 μm, with a log standard deviation of 0.25, such that the majority of the bubbles are within four standard deviations of the mean ie within the range 1 to 100 μm. The effects of polydispersity on the predicted reflection coefficient are not very marked. The peak in the real part of the reflection coefficient which occurs in monodisperse systems is not seen in polydisperse systems, and real part remains

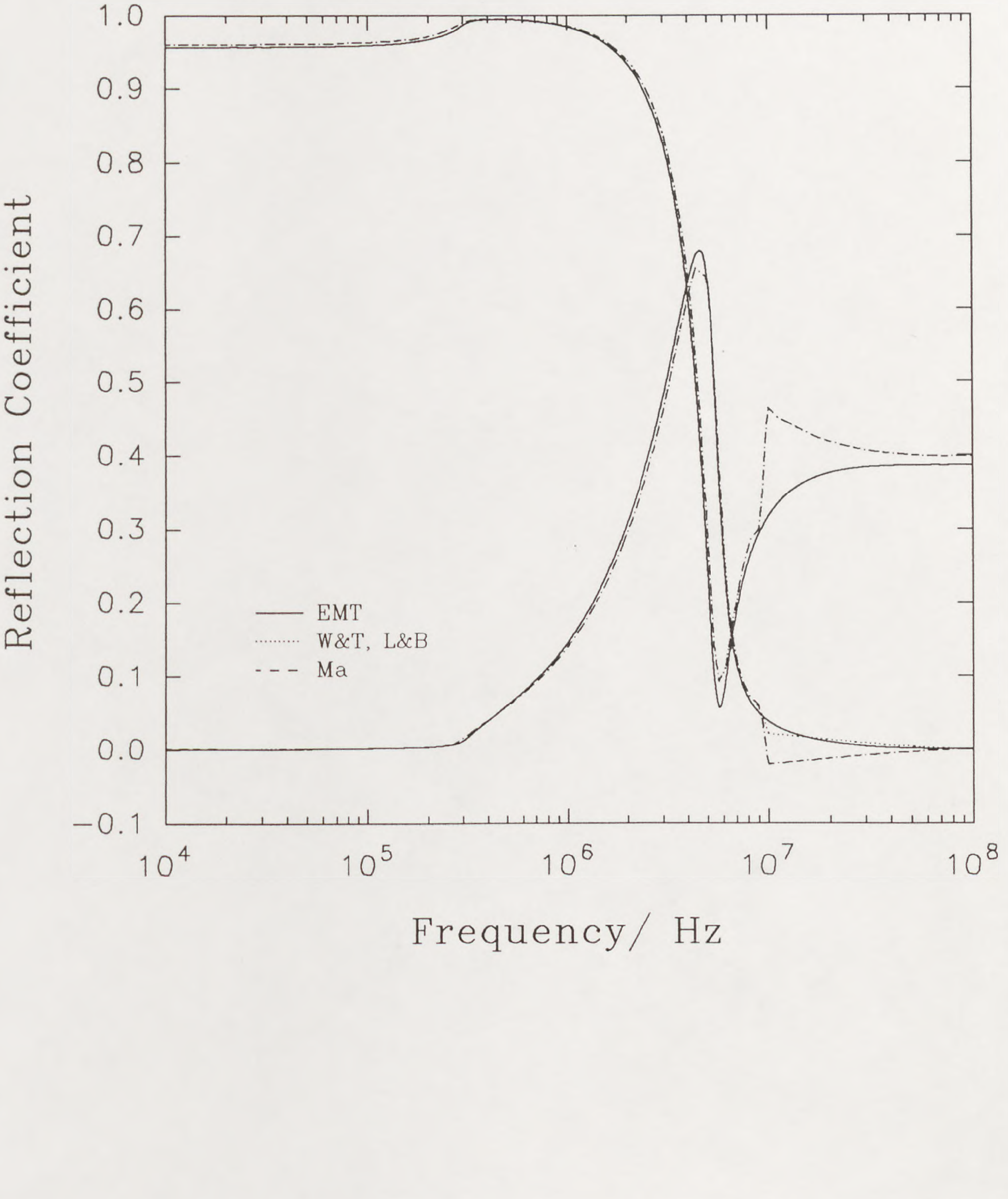

Figure 3.16(a)The predicted real part (upper curves) and imaginary part (lower curves) of the reflection coefficient in the FSUPER of a monodisperse system of bubbles in water (radius = 10 μm, volume fraction = 2 %). The curves are labelled according to the theory used to generate them. EMT: Gaunaurd & Uberall, W&T: Waterman & Truell, L&B: Lloyd & Berry, Ma: Ma *et al.*

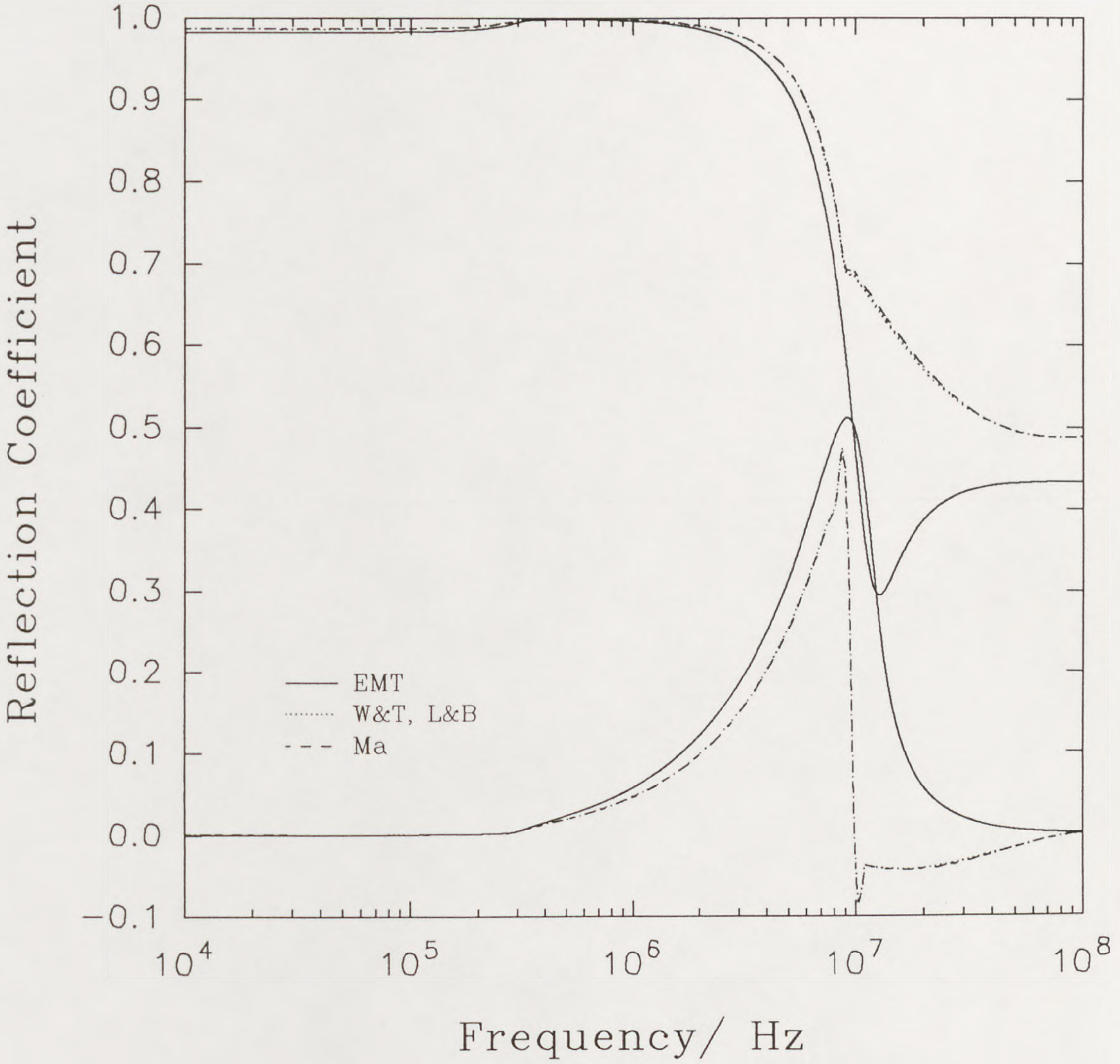

Figure 3.16(b)The predicted real part (upper curves) and imaginary part (lower curves) of the reflection coefficient in the FSUPER of a monodisperse system of bubbles in water (radius = 10 μm, volume fraction = 10 %). The curves are labelled according to the theory used to generate them. EMT: Gaunaurd & Uberall, W&T: Waterman & Truell, L&B: Lloyd & Berry, Ma: Ma *et al.*

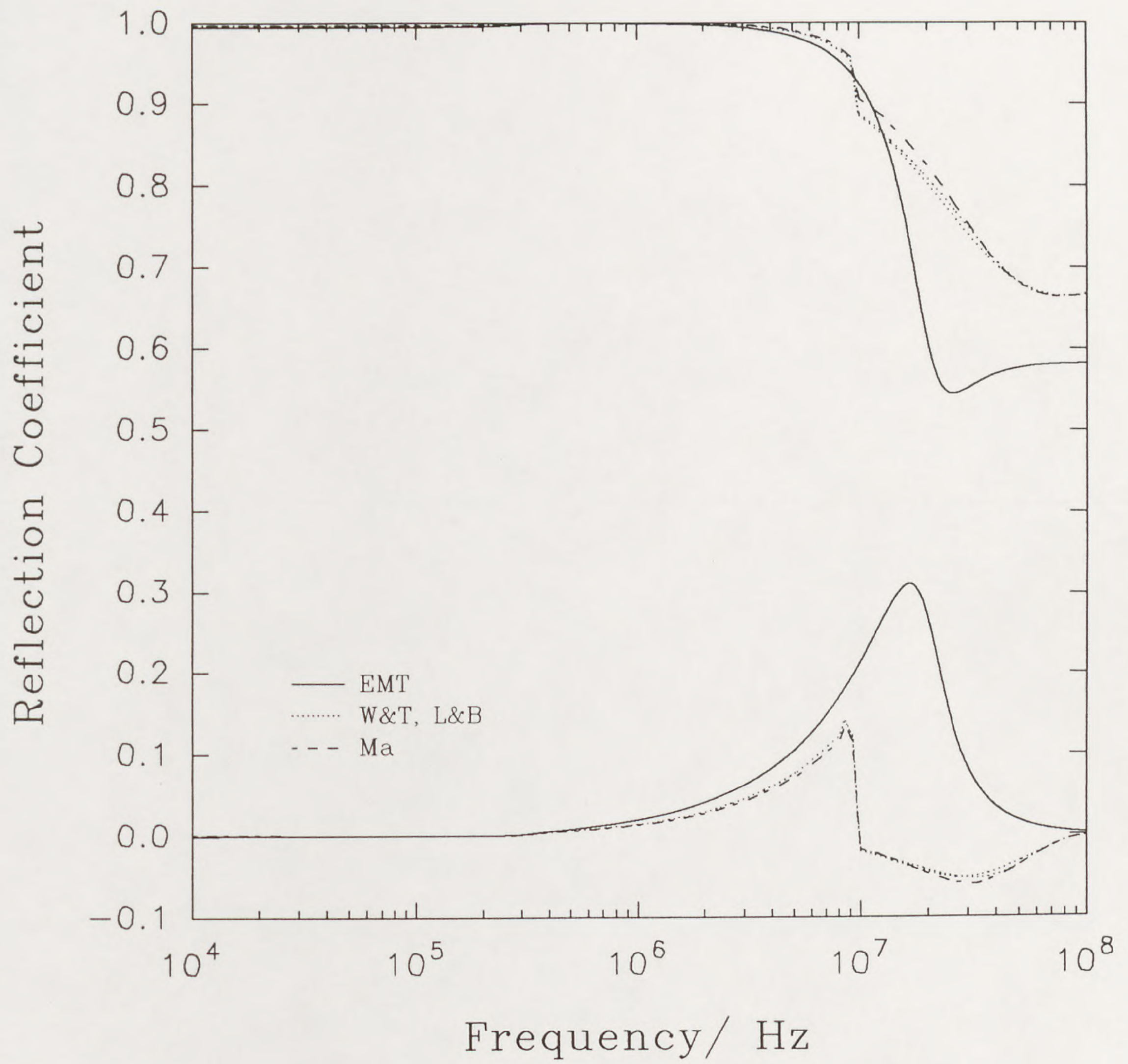

Figure 3.16(c)The predicted real part (upper curves) and imaginary part (lower curves) of the reflection coefficient in the FSUPER of a monodisperse system of bubbles in water (radius = 10 μm, volume fraction = 40 %). The curves are labelled according to the theory used to generate them. EMT: Gaunaurd & Uberall, W&T: Waterman & Truell, L&B: Lloyd & Berry, Ma: Ma *et al.*

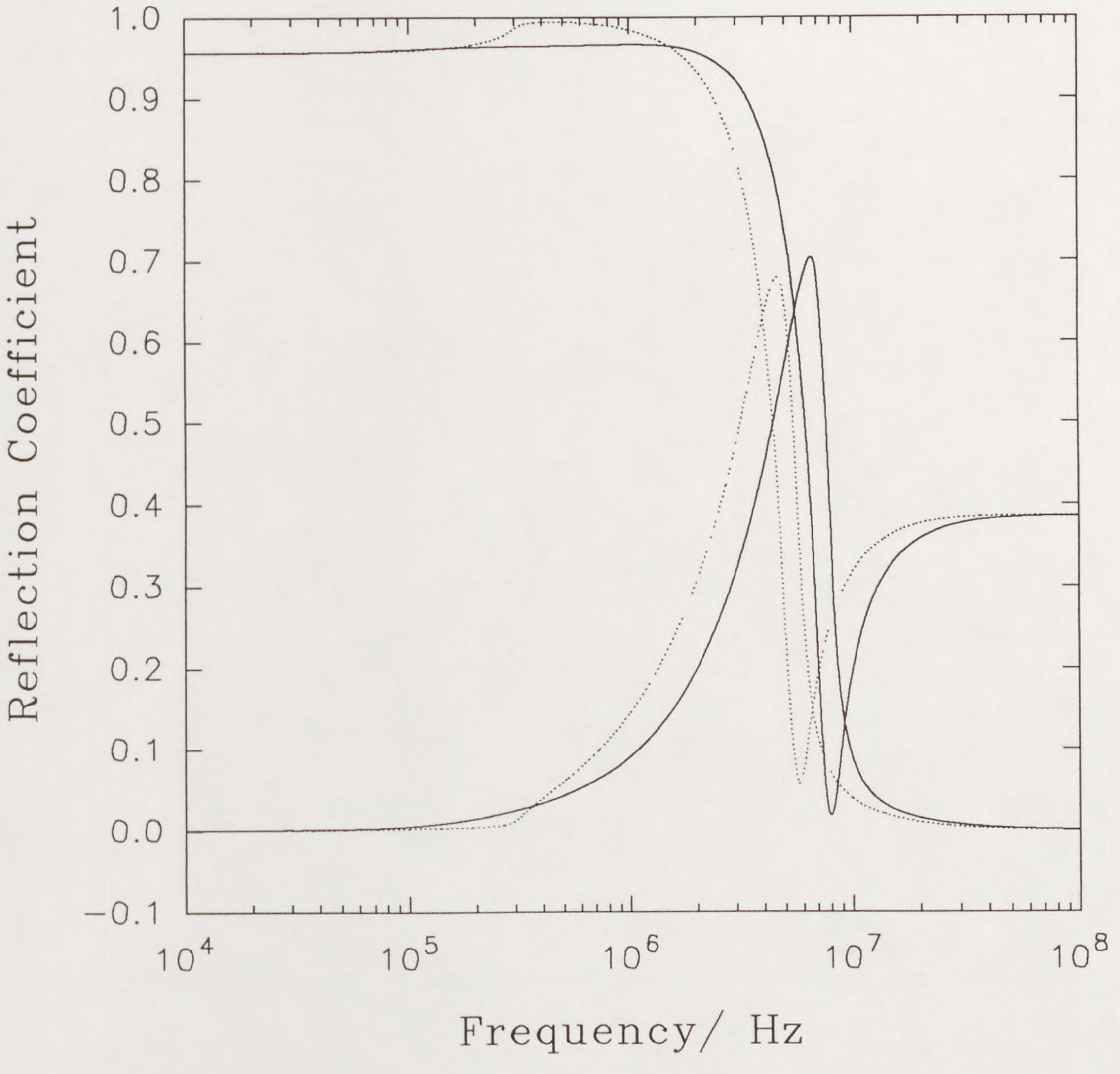

Figure 3.17 The predicted real part (upper curves) and imaginary part (lower curves) of the reflection coefficient in the FSUPER of bubbly water (volume fraction = 2 %). The dotted lines are for a monodisperse system with radius 10 μm. The solid lines are for a polydisperse system with mean radius 10 μm (see text for details).

elevated up to slightly higher frequencies. The minimum in the real part of the reflection coefficient, and the maximum in the imaginary part of the reflection coefficient are both shifted to slightly higher frequencies by the effects of polydispersity.

3.2.4.4 Attenuation measurements

The attenuation coefficient was determined from the Fourier transforms of echoes one and two. The relationships needed are

$$\mathrm{M}_{1,s} = \mathrm{e}^{-2\alpha' d'}\cdot\mathrm{R}_{1,s}\cdot\mathrm{M}_{i} \qquad [3.13]$$

$$\mathrm{M}_{2,s} = \mathrm{e}^{-2\alpha' d'}\cdot(1 - \mathrm{R}_{1,s}^{2})\cdot\mathrm{R}_{2,s}\cdot\mathrm{M}_{i}\cdot\mathrm{e}^{-2\alpha d} \qquad [3.14]$$

where $\mathrm{R}_{2,s}(f)$ is the reflection coefficient at the sample/reflector plate interface, d is the length of the sample, $\alpha(f)$ is the attenuation coefficient of the sample, and $\mathrm{M}_{i}(f)$ is the magnitude of the pulse when it initially enters the buffer rod. Dividing *Equation 3.13* by *Equation 3.14*, and rearranging gives

$$\alpha = (1/2d)\cdot\ln\{[\mathrm{M}_{1,s}\cdot(1 - \mathrm{R}_{1,s}^{2})\cdot\mathrm{R}_{2,s}]/[\mathrm{M}_{2,s}\cdot\mathrm{R}_{1,s}]\} \qquad [3.15]$$

$\mathrm{R}_{2,s}(f)$ was determined by reference to $\mathrm{R}_{2,c}(f)$ in the same manner as $\mathrm{R}_{1,s}(f)$. It was then possible to determine $\alpha(f)$ by measuring $\mathrm{R}_{1,s}(f)$, $\mathrm{R}_{2,s}(f)$, $\mathrm{M}_{1,s}(f)$ and $\mathrm{M}_{2,s}(f)$. The results were corrected in order to account for diffraction effects (see Appendix I).

3.2.4.5 Velocity measurements

The velocity, $c_{s}(f)$, of the sample was determined from the equation

$$c = 2d/t_{s} \qquad [3.16]$$

where d is the sample pathlength and $t_{s}(f)$ is the time difference between echo one and echo two. The pathlength was determined by measuring $t_{c}(f)$ when the calibrant was in the instrument. The time $t_{s}(f)$ was calculated as a function of frequency using the phase information from the Fourier transforms of echoes 1 and 2

$$t_{s} = (\mathrm{n}_{s}\cdot 360 + \Delta\Theta_{s} - \phi_{d} - 180)/(360\cdot f) \qquad [3.17]$$

where $\mathrm{n}_{s}(f)$ is an integer, $\Delta\Theta_{s}(f)$ is the difference in phase between the transforms of echo 1 and echo 2, and $\phi_{d}(f)$ is the phase shift due to diffraction. The -180 appears in *Equation 3.17* because the acoustic impedance of the sample was less than that of the reflector plate.

The velocity dispersion in the sample was not large, i.e. $(c_{max} - c_{min})/c_{max} < 1/(f \cdot t_s)$, so that $n_s(f)$ could be determined by measuring the time difference, Δt between similar positions within the two echoes ($n_s \approx \Delta t \cdot f$). If the samples had been highly dispersive then it would have been necessary to make measurements at two different sample path lengths, d_1 and d_2. By solving the simultaneous equations $c = 2d_1/t_1 = 2d_2/t_2$, the values of $n_s(f)_1$ and $n_s(f)_2$ needed in *Equation 3.17* could be calculated.

3.2.4.6 Accuracy

The sources of error in the measurements were essentially the same as those in the UPER. There was a small additional error due to phase shifting in the wear plate and in the coupling layer, which was most pronounced at frequencies below the centre frequency of the transducer (Jackson *et al*, 1981, Vincent, 1987). Taking into account the variability in our measurements, and comparing literature values with FSUPER measurements on liquids whose properties are known, such as a silicone reference fluid (Zeqiri, 1989), it is estimated that the FSUPER can determine the velocity to better than 0.5 m s^{-1}, the specific acoustic impedance to better than 1% and the attenuation coefficient to better than 5%, with an absolute accuracy of 1-2 Np m^{-1}.

3.2.4.7 Applications

The FSUPER has proven very useful for examining emulsions and suspensions. Some of the applications of the FSUPER have recently been described (McClements, 1992), and a description of the FSUPER itself is to be published (see Appendix III).

3.2.5 Density measurements

Density measurements were used in order to determine the volume fraction of air in the bubbly systems. A fairly crude system was employed when the volume fraction was high. A more sensitive device such as a density bottle or densitometer was employed when the volume fraction was low.

3.2.5.1 'Measuring cup' system

The volume of a Perspex box was determined by weighing the box, and then filling it with water and reweighing. This vessel of known volume (approximately 164 cm^3) and weight (approximately 64 g) was carefully filled with the liquid of interest, taking care not to introduce any extraneous air. When necessary, the liquid was made level with the top of the box by drawing the flat blade of a knife across it. The outside of the box was cleaned and dried, and the box was then weighed again. This yielded the density of the sample, ρ_s, which in turn yielded the volume fraction of dispersed gas, ϕ_g, according to

$$\phi_g = 1 - \rho_s / \rho'_s \qquad [3.18]$$

where ρ_s is the density of the sample, and ρ'_s is the density of the gas-free sample. In the measurements on the bubbly liquid model, ρ'_s was taken as the density of the Sweetose syrup from which the bubbly liquid was prepared. The density of Sweetose depended on the solids content according to ρ_{syrup} / kg m^{-3} = 6.307×(Solids content in wt%) + 923.16 (based on data supplied by Unilever Research Ltd). Using this technique the volume fraction could be measured to ± 0.02 in most cases.

The measuring cup technique was useful for the concentrated bubbly liquid, yogurt cream and, to a lesser extent, dough. The accuracy was reduced when measuring dough, because it was not possible to level the top of the dough properly. In all cases, it was necessary to fill the Perspex box very carefully.

3.2.5.2 The densitometer

The densitometer employed in this work was of the vibrating U-tube type (Anton Paar Digital Density Meter DMA 40). A glass U-tube is mounted horizontally inside a sealed glass cylinder containing a gas of high thermal conductivity, which is in turn contained within a glass water jacket. Thermostatting water is pumped through the water jacket from a waterbath. The liquid which is to be characterised is introduced into the U-tube, using a disposable pipette. The progress of the sample through the tube can be observed because the working parts of the instrument are made of glass. The sample must completely fill the U-tube, which has a volume of approximately 0.7 cm^{-3}. Over-filling does not affect the measurement but under-filling does. The U-tube is caused to oscillate at its natural frequency, and the machine displays the period of the oscillation. The period of the oscillation depends on the mass of the tube and hence on the density of the sample liquid. In order to relate the period of oscillation to the density of the sample, it is necessary to calibrate the device for the measurement temperature of interest. This is achieved by obtaining readings for distilled water and air. This enables the calculation of two temperature- and device-dependent constants, A and B, which are given by (Paar DMA 45 Instruction Manual)

$$A = (\mathrm{T}_w^2 - \mathrm{T}_a^2) / (\rho_w - \rho_a) \qquad [3.19]$$

$$B = \mathrm{T}_a^2 - A\rho_a \qquad [3.20]$$

where T is the reading given by the densitometer, and the subscripts a and w refer to air and water respectively. The densities of air and water are tabulated as a function of temperature in reference books (see for example CRC Handbook, 1987). A and B are required in the calculation of the density of the sample according to

$$\rho_{\text{sample}} = (\mathrm{T}^2_{\text{sample}} - B) / A \qquad [3.21]$$

The thermostatting water was pumped from the waterbath which held the FSUPER. The temperature was controlled to within ± 0.1 °C, so the densitometer could determine the density to within ± 0.1 kg m^{-3}. It could therefore measure the volume fraction of air to approximately ± 0.0002.

The concentrated bubbly liquid was very viscous, and it was very difficult to introduce the liquid into the narrow densitometer U-tube. It was however possible to measure the air-free syrup in the densitometer. The densitometer was most useful for measuring the dilute bubbly liquid, which was easily introduced into the densitometer.

3.2.6 The Malvern Mastersizer

The Malvern Mastersizer is a device for measuring the particle size distribution in dispersions. A small amount of the dispersion is greatly diluted in an optically clear

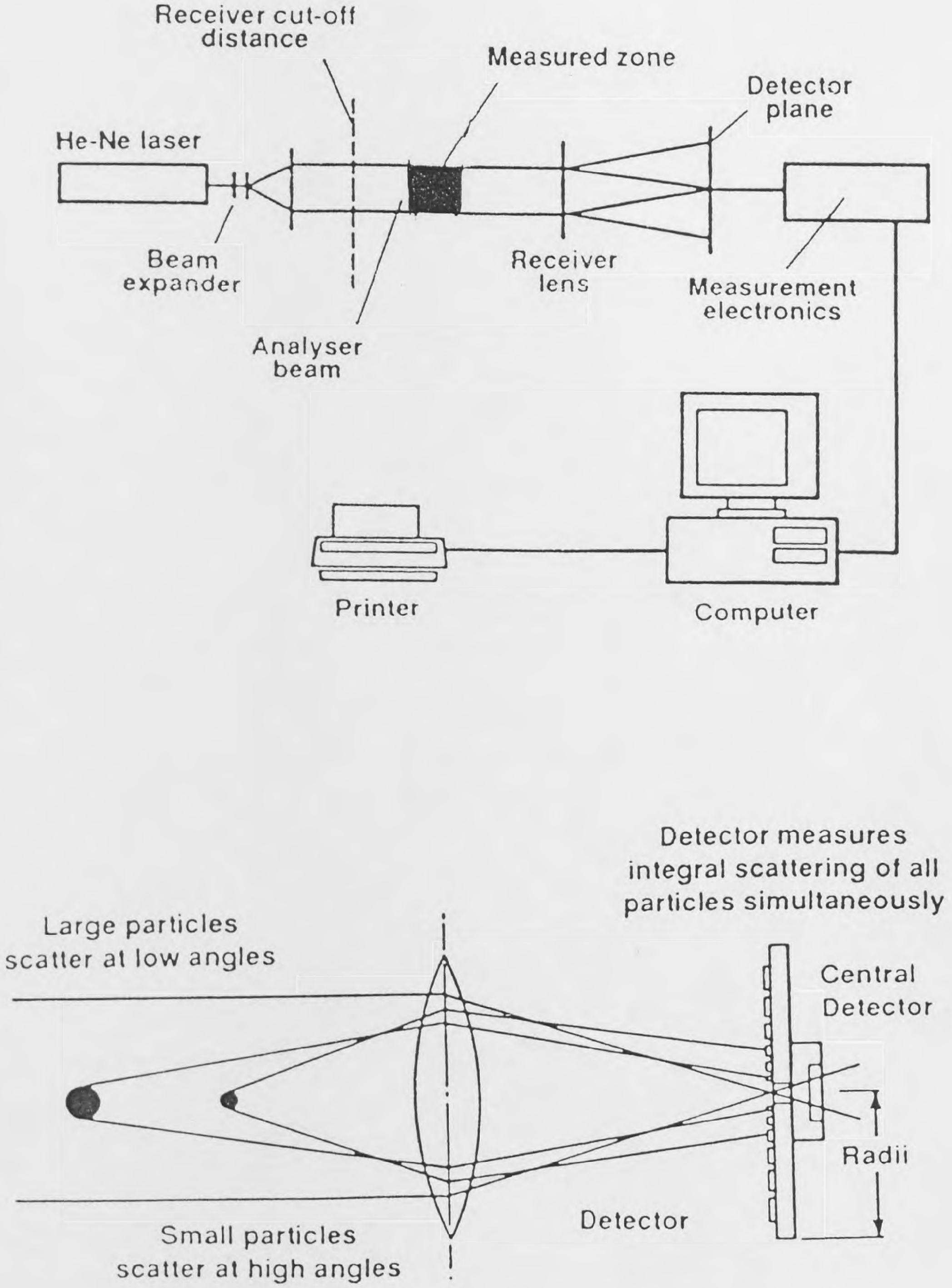

Figure 3.18 The Malvern Mastersizer. In a computer controlled measurement process, laser light is scattered by a dilute dispersion of particles (top). The scattered light falls upon a circular detector (bottom). The scattering angle is inversely proportional to the radius of the particle. *From the Malvern Mastersizer User Manual, 1989.*

diluent. A pump circulates the dilute dispersion from a stirred storage tank into the measurement cell and back to the tank. A laser beam shines through the measurement cell, and the scattering of the laser light by the particles is measured. The device is illustrated schematically in *Fig. 3.18.* The concentration of scatterers in the dispersant must be very low, so that multiple scattering of the laser light does not occur, because the theory used to relate the optical measurements to the particle size distribution is valid only in the single scattering regime. The need for dilution of the sample, and the need to pump the sample through the measurement cell, make the Mastersizer unsuitable for real food systems.

A computer controls the measurement process, and converts the optical measurements into a derived particle size distribution. The fundamental property measured by the Mastersizer is particle volume. Other properties, such as the surface area and radius of the particles, are calculated from the particle volume distribution. By means of different lenses, the Mastersizer can characterise particles with diameters in the range 0.1 μm to 1000 μm.

In order to derive the correct particle size distribution, the refractive index, η_D^{20}, of the dispersant and the particles must be known, as must the optical absorption of the particles. The *relative refractive* index of the system may be taken as the refractive index of the particles divided by the refractive index of the dispersant. The relative refractive index and the absorption of the particles are used to select the correct value for an instrumental parameter, known as the *presentation code*, from a table supplied with the instrument (*Fig. 3.19*). Bubbles are treated as a special case† in the calculation of the relative refractive index. In a reversal of the usual procedure, the refractive index of the diluent is divided by the refractive index of air (taken as 1). Thus the appropriate presentation codes are 1400 when the diluent is water (η_D^{20} = 1.333) and 1600 when the diluent is 50wt% Sweetose syrup (η_D^{20} = 1.425). The value of the relative refractive index has more influence on the calculated particle size distribution than the value of the absorption of the bubbles (taken as 0).

†: As advised by Malvern Instruments Ltd.

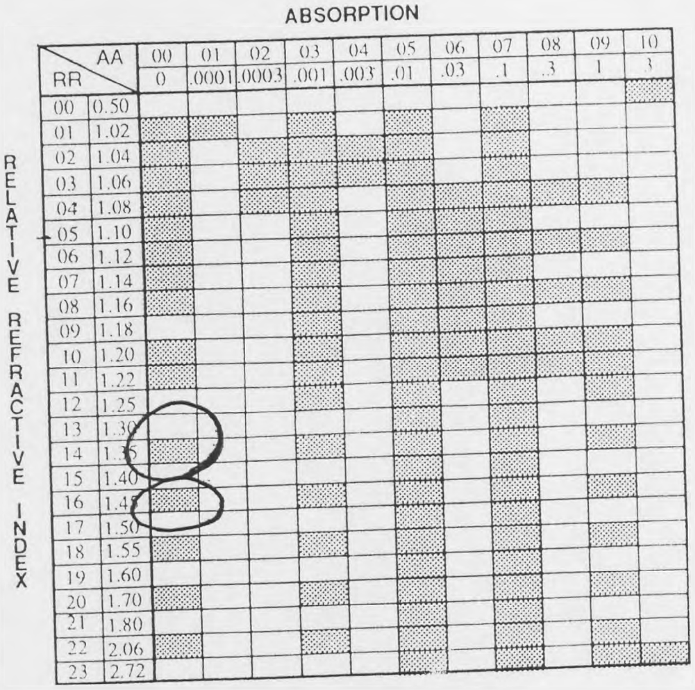

ABSORPTION

RELATIVE REFRACTIVE INDEX

RR	AA	00	01	02	03	04	05	06	07	08	09	10
		0	.0001	.0003	.001	.003	.01	.03	.1	.3	1	3
00	0.50											
01	1.02											
02	1.04											
03	1.06											
04	1.08											
05	1.10											
06	1.12											
07	1.14											
08	1.16											
09	1.18											
10	1.20											
11	1.22											
12	1.25											
13	1.30											
14	1.35											
15	1.40											
16	1.45											
17	1.50											
18	1.55											
19	1.60											
20	1.70											
21	1.80											
22	2.06											
23	2.72											

Figure 3.19 The presentation codes used by the Malvern Mastersizer. *From the Malvern Mastersizer User manual, 1989.*

3.2.6.1 Measuring the bubbly model in the Mastersizer

The bubbles created in the model bubbly liquid were characterised in the Mastersizer, using two different approaches to the dilution of the bubble mixture within the instrument.

When the concentrated bubbly liquid was characterised, a small tank (the so-called Small Sample Presentation Unit) was connected to the Mastersizer. This was filled with approximately 100 ml of 50 wt% Sweetose syrup, taking care not to introduce any air bubbles. Sweetose syrup was used as the diluent in order to minimise the loss of bubbles through creaming. A small amount of concentrated bubbly liquid (typically 300-500 μl) was taken up into an automatic pipette, and carefully introduced below the surface of the syrup, with vigorous stirring. The actual amount of bubbly liquid added was adjusted according to the *obscuration* indicated by the computer which controlled the Mastersizer. The obscuration is a measure of the number of scatterers in the measurement cell. The computer monitors the obscuration as the sample is added, and the user adjusts the concentration of the scatterers until the obscuration falls within the range which is considered ideal. Alternatively, the user can add an excess of scatterers and allow the computer to adjust the concentration. This option was not used here, because it was not sensitive enough. Once sufficient bubbly liquid had been added, the computer measured the light scattering, and calculated the size distribution.

The dilute bubbly liquid was characterised using the built in tank (volume approximately 1800ml), which was filled with tap water. Two different approaches were adopted. In the first approach, the dilute bubbly liquid was added, with stirring, until the obscuration fell within the ideal range, whereupon the sample was characterised. It was found that this method led to fouling of the measurement cell, because P1670 seemed to adsorb rather easily on the glass walls of the measurement cell. The adsorbed surfactant interfered with subsequent measurements, and rigorous cleaning was necessary in order to remove it. Therefore a second approach was employed. The Mastersizer was filled with tap water, and small amounts of the source concentrated bubbly liquid were added, with vigorous stirring. The mixture was stirred for some time, and the size distribution was measured at half hour intervals. It was found that the size distribution was stable after about two hours, and this measurement was taken as the size distribution in the liquid. This method led to much less fouling of the measurement cell, and the results agreed very closely with the measurements made using the first approach.

It was not possible to check the bubble size distribution in the serial dilutions of the dilute model bubbly liquid, because it was found that there were insufficient bubbles in the dilutions to enable a reliable measurement.

3.2.7 Summary

Several different ultrasonic measuring systems were constructed in the Procter Department Workshop. Some of these were of little use, but the ultrasonic pulse echo reflectometer, and the frequency scanning version, were capable of accurate measurements of ultrasonic velocity, attenuation and acoustic impedance, at a fixed frequency or over a range of frequencies. The measuring cup and the densitometer were useful for measuring the volume fraction of air, in concentrated and dilute systems respectively. Laser light scattering was used to measure the bubble size distribution in the concentrated and dilute forms of the model bubbly liquid, but it is of no use in real food systems.

CHAPTER FOUR

Results and Discussion

4.1 Introduction

In this chapter, the experimental results are presented and discussed. The results are given in the order which it was felt makes for the clearest interpretation, which is: dilute model bubbly liquid, concentrated model bubbly liquid, bubbly gel, yogurt, cream, dough and beer foam. The samples were prepared using to the techniques described in the previous chapter, unless otherwise specified. Note that averages, where given, are shown ± the standard deviation. Concentrations of P1670 and Hyfoama should be taken as ± 0.01 wt%, concentrations of Sweetose should be taken as ± 0.1 wt%. Temperatures should be taken as ± 0.1 *°C*.

4.2 Dilute model bubbly liquid

The dilute model bubbly system is considered first, because it should in theory be the easiest to characterise. The volume fraction of the dilute system was deliberately set at a very low value, in order to make transmission measurements possible. The bubble size distribution was measured in the Mastersizer, and the density of the bubbly liquid was measured in the Paar densitometer. The theory has been shown to work at low volume fraction (see Chapter Two), so it should be possible to use the measured bubble size distribution and volume fraction to calculate the predicted velocity and attenuation in the dilute model bubbly liquid.

4.2.1 Preparation of the dilute model bubbly liquid

Concentrated model bubbly liquid was prepared, using P1670 at concentrations of 2, 3, 4 and 5 wt%. The bubble size distribution in a dilute version of each liquid was measuring in the Mastersizer using the second approach described in Section 3.2.6.1 (*Fig. 4.1*). A selected size distribution is a sample measured using the first approach is also shown for comparison. This sample was stirred in the beaker for 24 hours.

The dilute bubbly liquid was prepared as described in Section 3.1.3.1. The amounts of concentrated liquid and water which were used are detailed in *Table 4.1*. Each of the samples of dilute bubbly liquid was serially diluted, and the ultrasonic

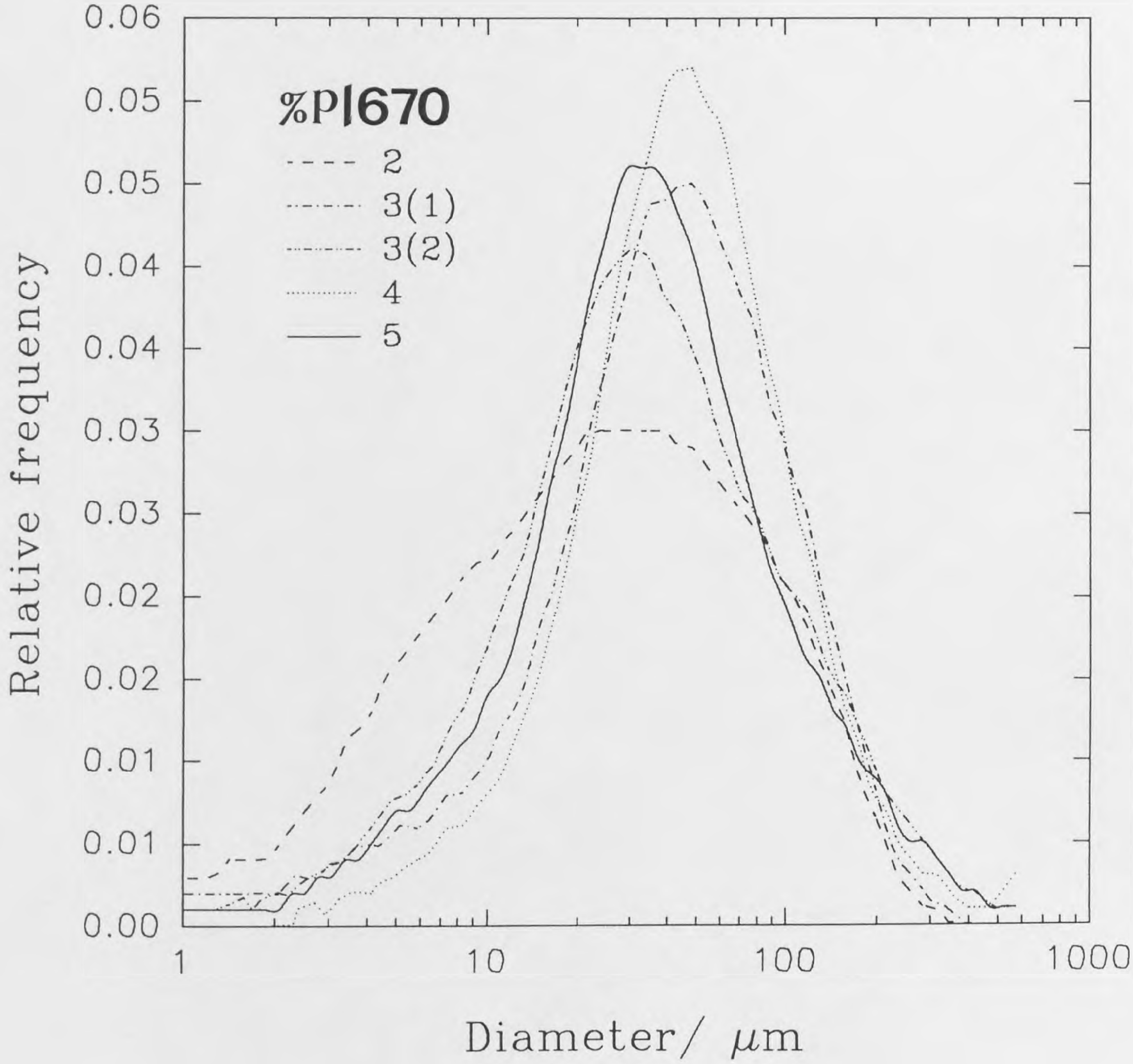

Figure 4.1 The bubble size distribution (measured using the Mastersizer) in the dilute model bubbly liquids. The numbers in the legend indicate the concentration of P1670 in the concentrated bubbly liquid from which the dilute samples were prepared. The figures in parentheses for the samples prepared from bubbly liquid containing P1670 at 3 wt% indicate which approach was used (for details see text).

Table 4.1 *Initial composition of dilute model bubbly liquids*

Sample	Concentration of P1670 (wt%) in original concentrated bubbly liquid	Mass of concentrated liquid used/ g	Mass of water in which diluted/ g
1	4 (in distilled water)		
2	3	25	500
3	3	50	500
4	4	100	500
5	5	100	500

properties and the density were determined at each stage. The dilution regime employed for each sample is detailed in *Table 4.2*. Note that Sample 1 contained no air, and was prepared using P1670 in distilled water, rather than using concentrated bubbly liquid. The purpose of Sample 1 was to ascertain if P1670 had any unusual ultrasonic properties which should be taken into account.

The volume fraction of air in each of the samples was very small, and it will become clear shortly that its value was not certain. Therefore each of the serial dilutions prepared from the stock dilute samples will be referred to by its dilution number, which can be obtained from *Table 4.2*. The stock dilute solutions from which the serial dilutions were prepared will be referred to as dilution zero.

4.2.2 The density and the apparent volume fraction of air

Table 4.3 shows the measured densities of the serial dilutions, prepared both with and without air ($\rho_{\text{with air}}$ and $\rho_{\text{without air}}$). The difference between these two figures should yield the volume fraction of air in the liquid. Unfortunately, in order to make transmission measurements, it was necessary to use such low volume fractions that the density change due to the presence of air was beyond the sensitivity of the instrument in most cases.

In samples three and five it was possible to calculate the apparent volume fraction of air, ϕ_{app}, in dilution zero. The uncertainty in this measurement was of the order of 50-100 %. The volume fraction of gas in the serial dilutions was calculated from the volume fraction in dilution zero, using the known dilution factor, and assuming that no further air dissolved during the serial dilution process. The validity of this

Table 4.2 *Dilution regimes used to prepare serial dilutions. The number of the sample appears in the column which corresponds to the dilution factor used. For example, sample 1 was diluted 13 times, by a factor of 8/9 each time, and sample 5 was diluted 14 times by a factor of 8/9, then a further four times by a factor of 7/9.*

Dilution number	Dilution Factor 8/9	Dilution Factor 7/9
1	1 2 3 5	4
2	1 2 3 5	4
3	1 2 3 5	4
4	1 2 3 5	4
5	1 2 3 5	4
6	1 2 3 5	4
7	1 2 3 5	4
8	1 2 3 5	4
9	1 2 3 5	4
10	1 2 3 5	4
11	1 2 5	4
12	1 2 5	4
13	1 2 5	4
14	2 5	4
15	2	5
16	2	5
17	2	5
18	2	5
19	2	

assumption is of course open to doubt, but it is necessary in the absence of a more sensitive conventional technique. The apparent volume fraction was calculated in order to enable calculations of the predicted ultrasonic properties of the dilute bubbly liquids. Note that the values of ϕ_{app} in sample two were calculated from the properties of sample three (dilution zero), on the assumption that the volume fraction of air was proportional to the mass of concentrated bubbly liquid which was used to prepare dilution zero. This assumption is also questionable, and all the values of volume fraction obtained using the densitometer must be treated with caution.

4.2.3 Measurements on pure P1670 solutions (sample one)

The measurements on pure P1670 show that the solutions were not dispersive in the frequency range measured by this technique (*Fig. 4.2*) and the effects of the serial dilution were well within the sensitivity of the ultrasonic technique. The P1670 elevated the ultrasonic velocity by just over 1 m s^{-1} per wt% added. P1670 solutions were weakly attenuating at frequencies above 1 MHz (*Fig 4.3*). Solutions

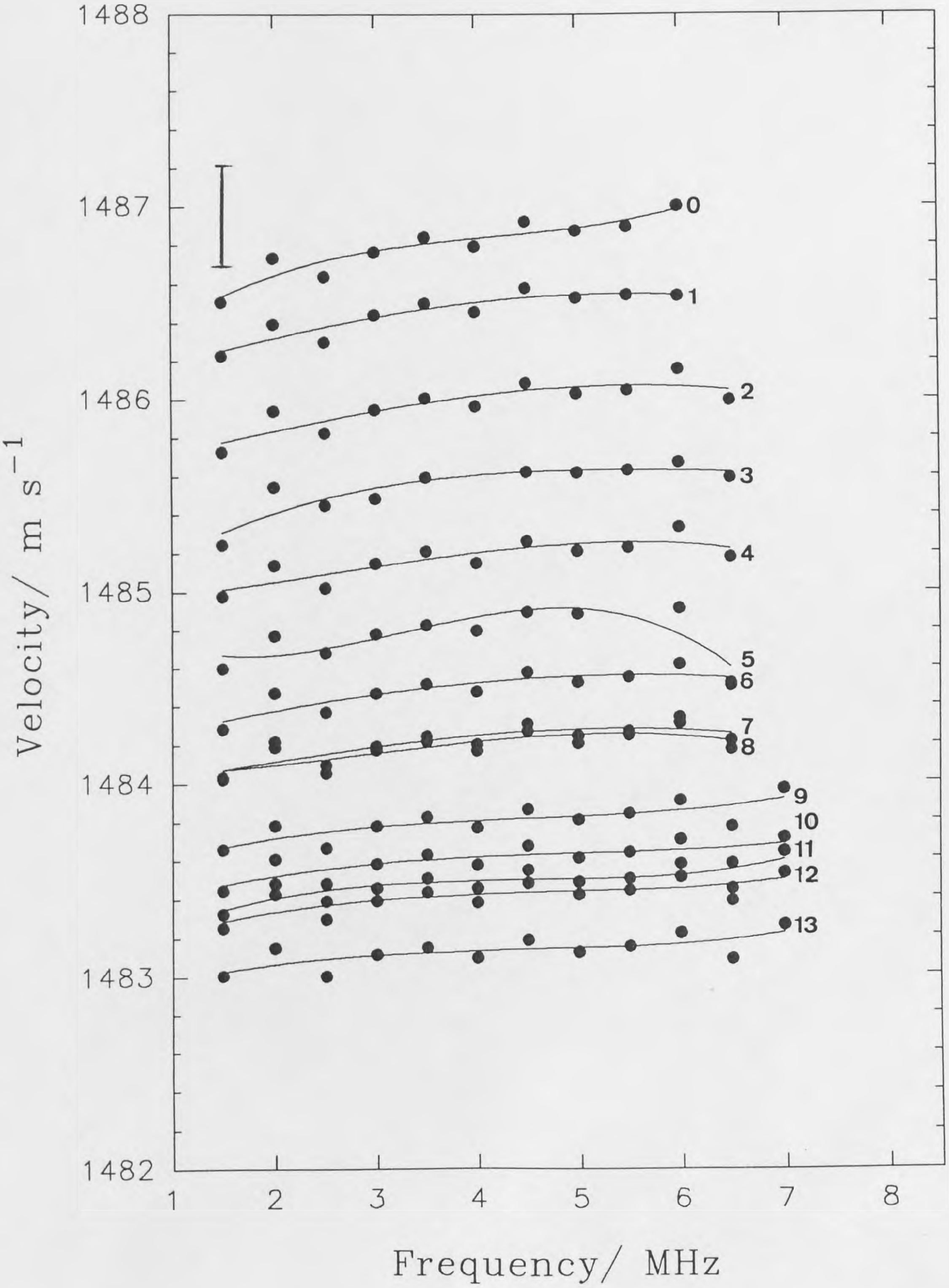

Figure 4.2 The ultrasonic velocity in pure P1670 solutions (sample one) as a function of frequency. Regression lines are drawn through the data points, which are labelled with the appropriate dilution number. The bar indicates the estimated accuracy of the measurement, when applied to standard liquids under controlled conditions.

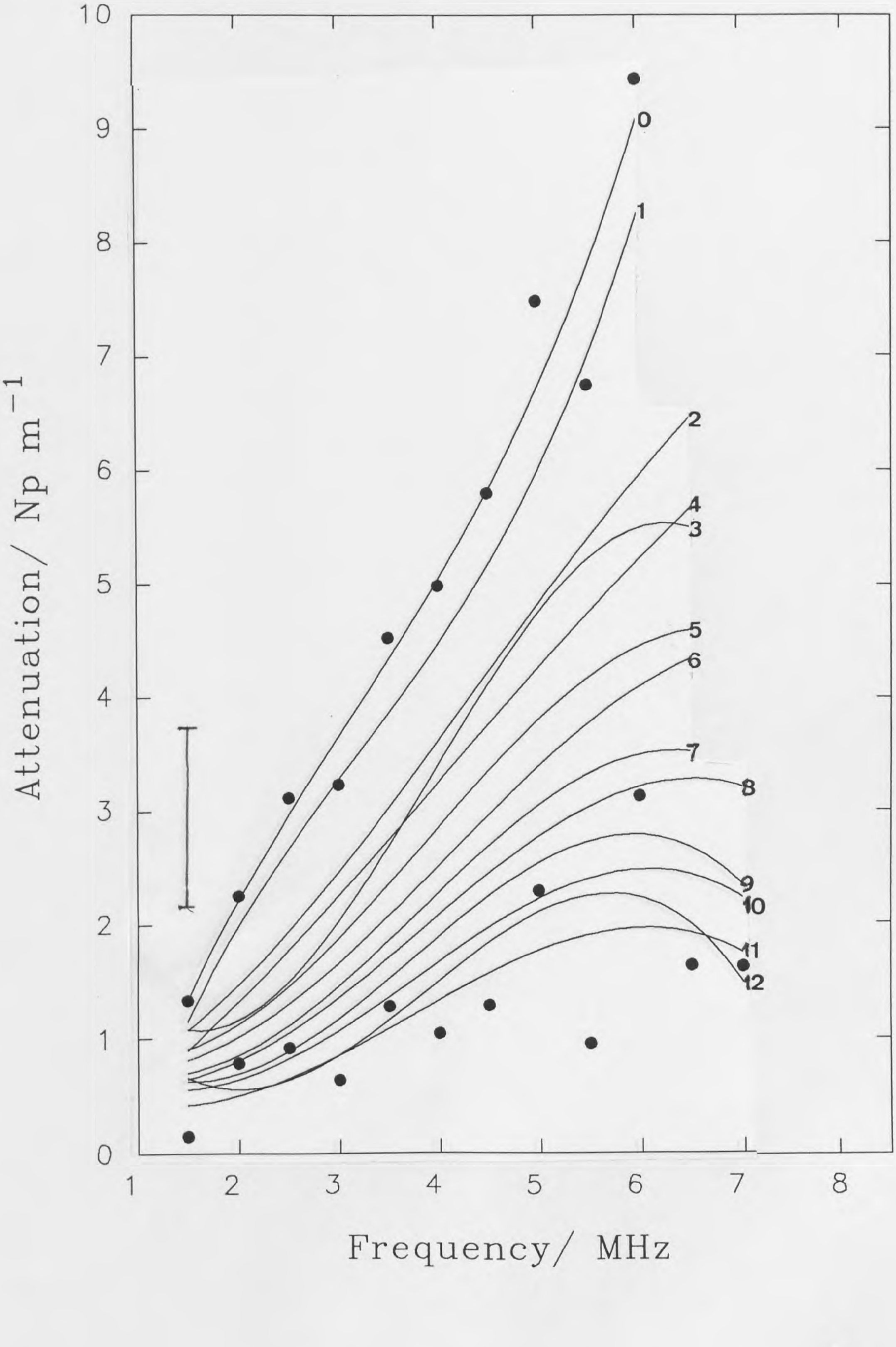

Figure 4.3 The attenuation coefficient in pure P1670 solutions (sample one) as a function of frequency. Regression lines are drawn through the data points, which are labelled with the appropriate dilution number. The actual data points have been omitted for dilutions one to eleven, to improve clarity. The bar indicates the estimated accuracy of the measurement, when applied to standard liquids under controlled conditions.

of P1670 did not appear to exhibit any unusual ultrasonic properties.

4.2.4 Sample Two

The remaining samples are numbered according the amount of concentrated bubbly liquid used to prepare them, and the concentration of P1670 in that concentrated liquid. Thus the aerated version of sample two ought to contain the least amount of air out of samples two to five.

Consider the velocity in the air free version of sample two (*Fig 4.4*). The solution was not dispersive in the frequency range examined, and the highest numbered dilutions were poorly resolved. The velocity was elevated over the value seen in pure P1670 solutions (*Fig 4.2*) because of the added sugar from the concentrated bubbly liquid. The attenuation was very low in all dilutions (*Fig. 4.5*), at around 1-2 Np m^{-1}, which is the limit of the accuracy of the measurement technique. The attenuation coefficients of the various dilutions were therefore poorly resolved.

The presence of air, even at the very low volume fractions used here, had a large effect on the velocity (*Fig. 4.6*). The velocity was depressed by several metres per second in the lowest numbered dilutions. The attenuation in the lowest numbered dilutions was too high to permit measurements of velocity at high frequencies. There was some frequency dependence in the results, but it was not very marked. The depression of the velocity suggests that the measured frequencies were below the resonant frequency of the bubbles, and this is also suggested by the attenuation (*Fig. 4.7*). The attenuation increased very strongly as the frequency increased, and it was much larger than in the air-free version of this sample. Because there was little frequency dependence in the measured velocity values, it would not be possible to measure the bubble size using the FSUPER. It is possible however to measure the volume fraction of air. This will be dealt with more fully in a subsequent section.

Firstly, consider the *predicted* velocity in aerated sample two (*Fig. 4.8*). Note that the frequency scale is logarithmic, and covers the operating frequency range of the FSUPER. The velocity was predicted using the particle size distribution determined in the Mastersizer, the apparent volume fraction of air, and the MST of

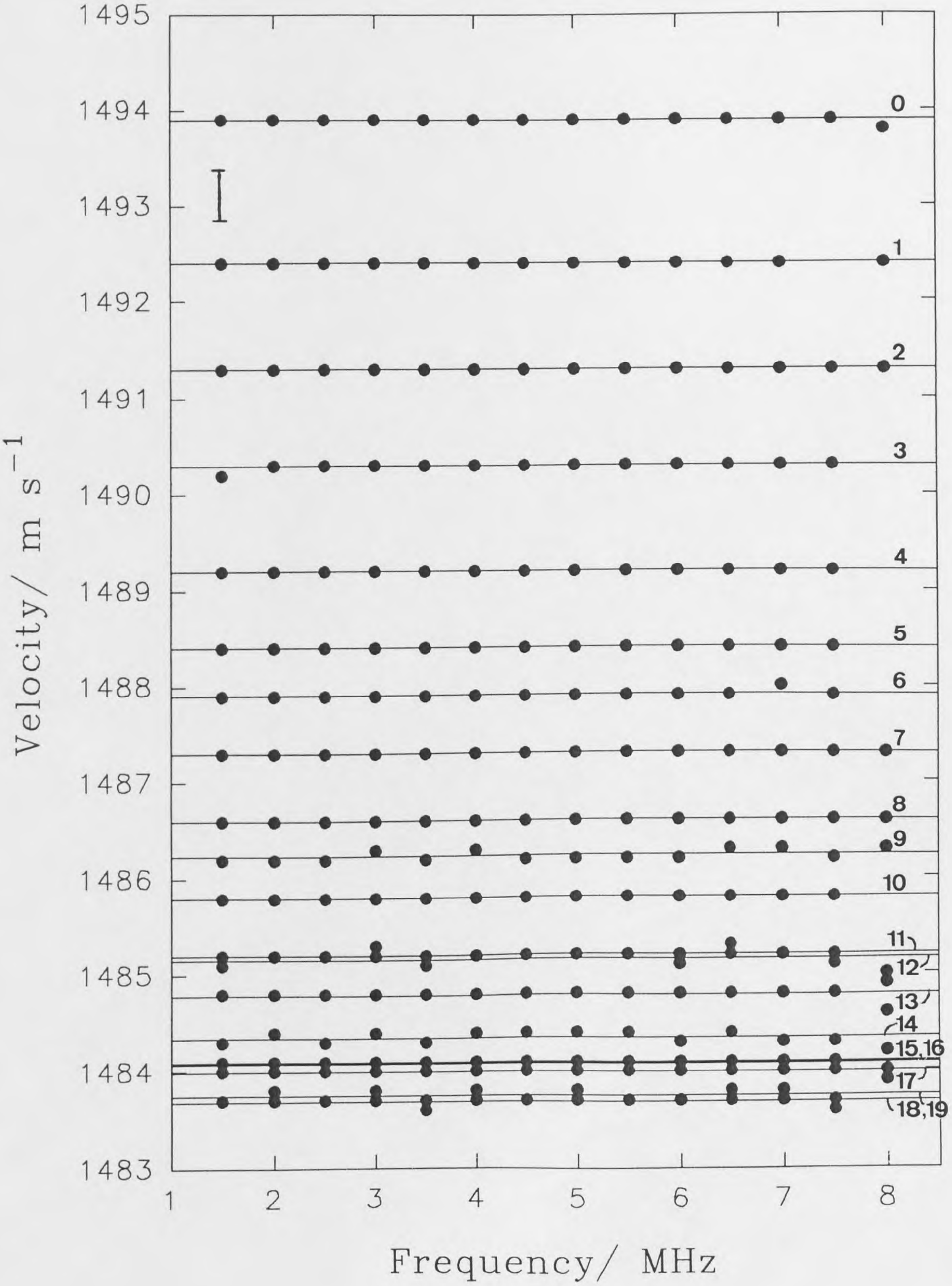

Figure 4.4 The ultrasonic velocity in air-free sample two as a function of frequency. Regression lines are drawn through the data points, which are labelled with the appropriate dilution number. The bar indicates the estimated accuracy of the measurement, when applied to standard liquids under controlled conditions.

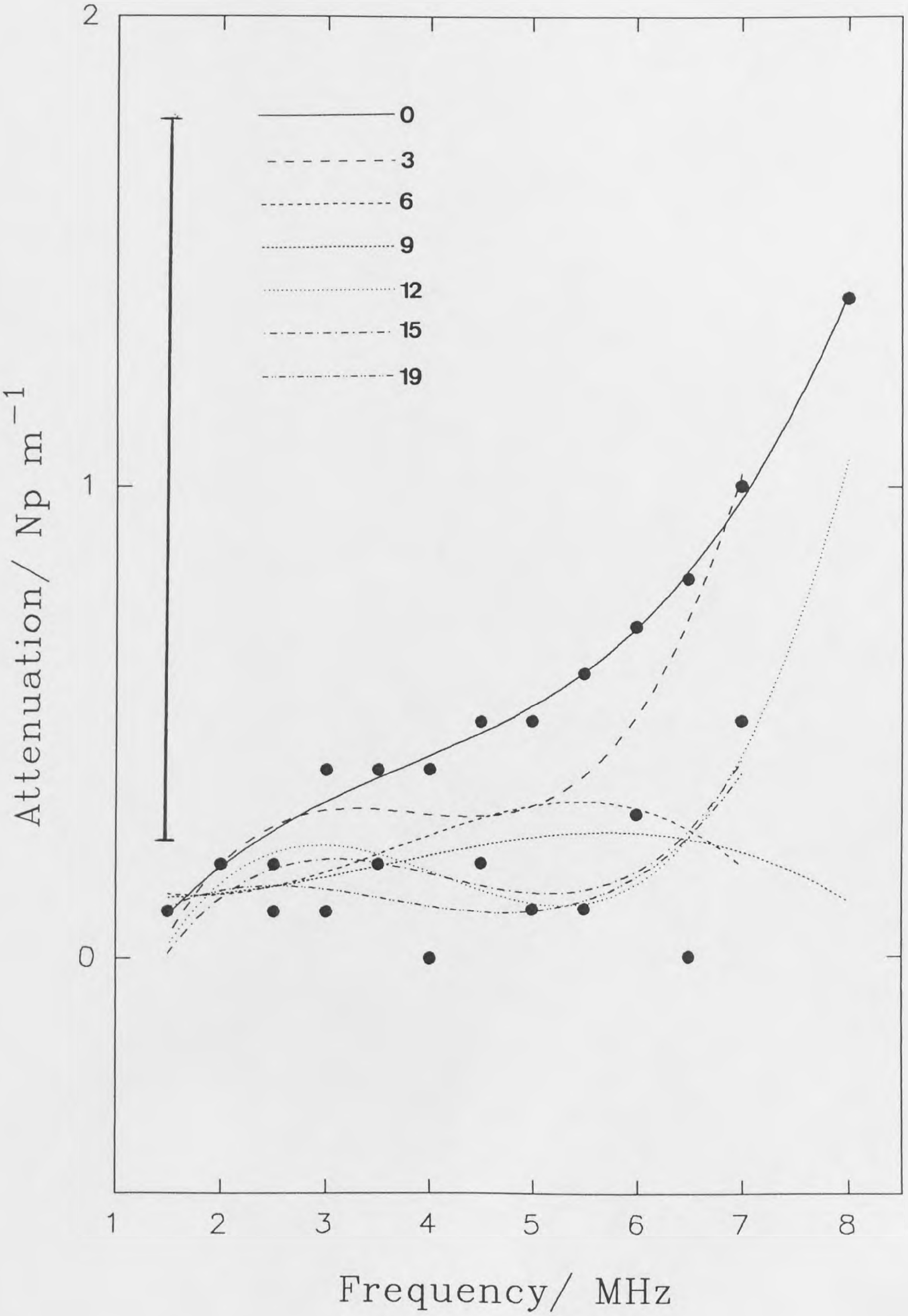

Figure 4.5 The attenuation coefficient in air-free sample two as a function of frequency. Regression lines are drawn through the data points, which are labelled with the appropriate dilution number. Data points are shown only for the highest and lowest dilutions. The bar indicates the estimated accuracy of the measurement, when applied to standard liquids under controlled conditions.

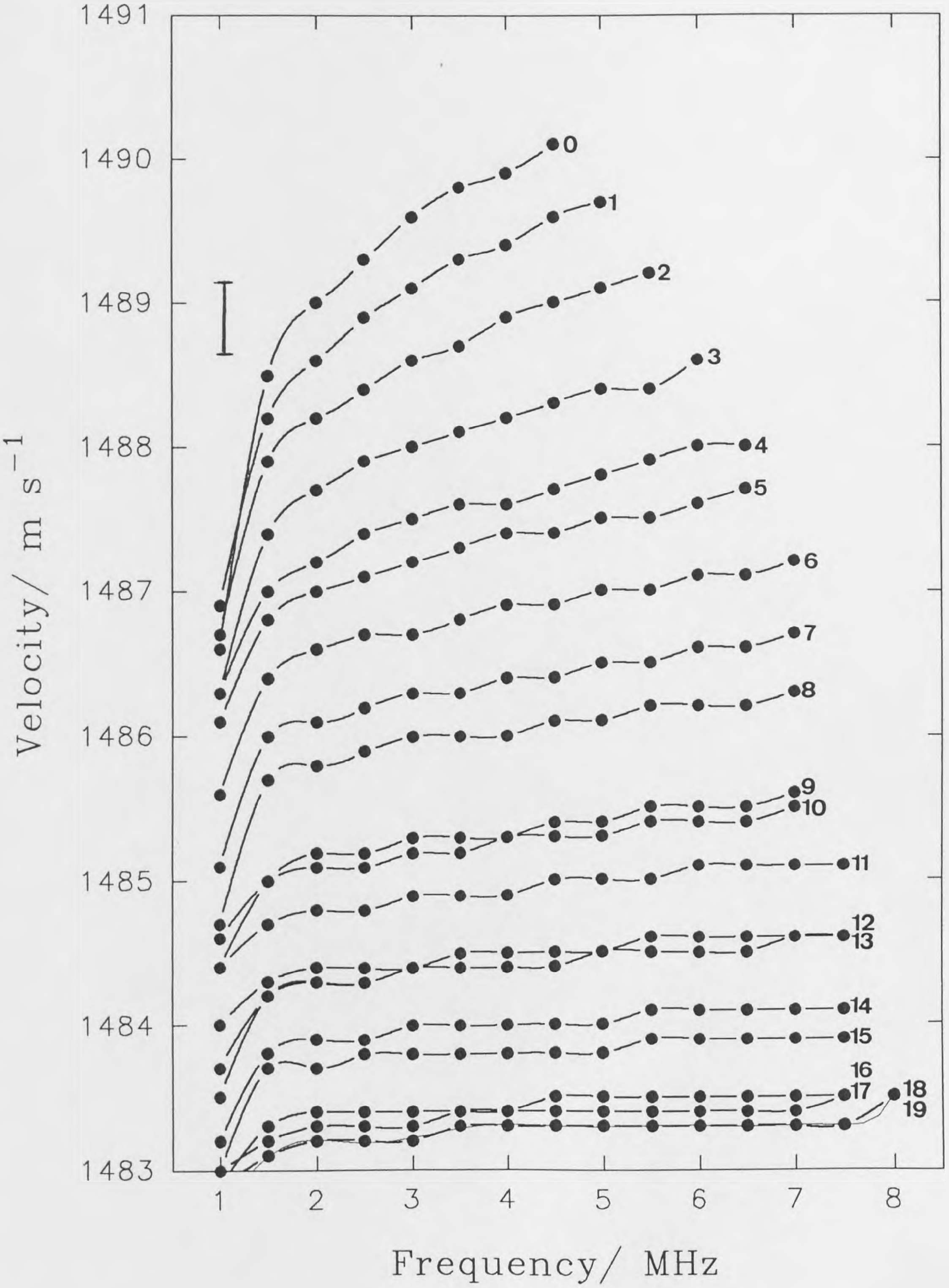

Figure 4.6 The ultrasonic velocity in aerated sample two as a function of frequency. The data points are joined by fitted splines, which are labelled with the appropriate dilution number. The bar indicates the estimated accuracy of the measurement, when applied to standard liquids under controlled conditions.

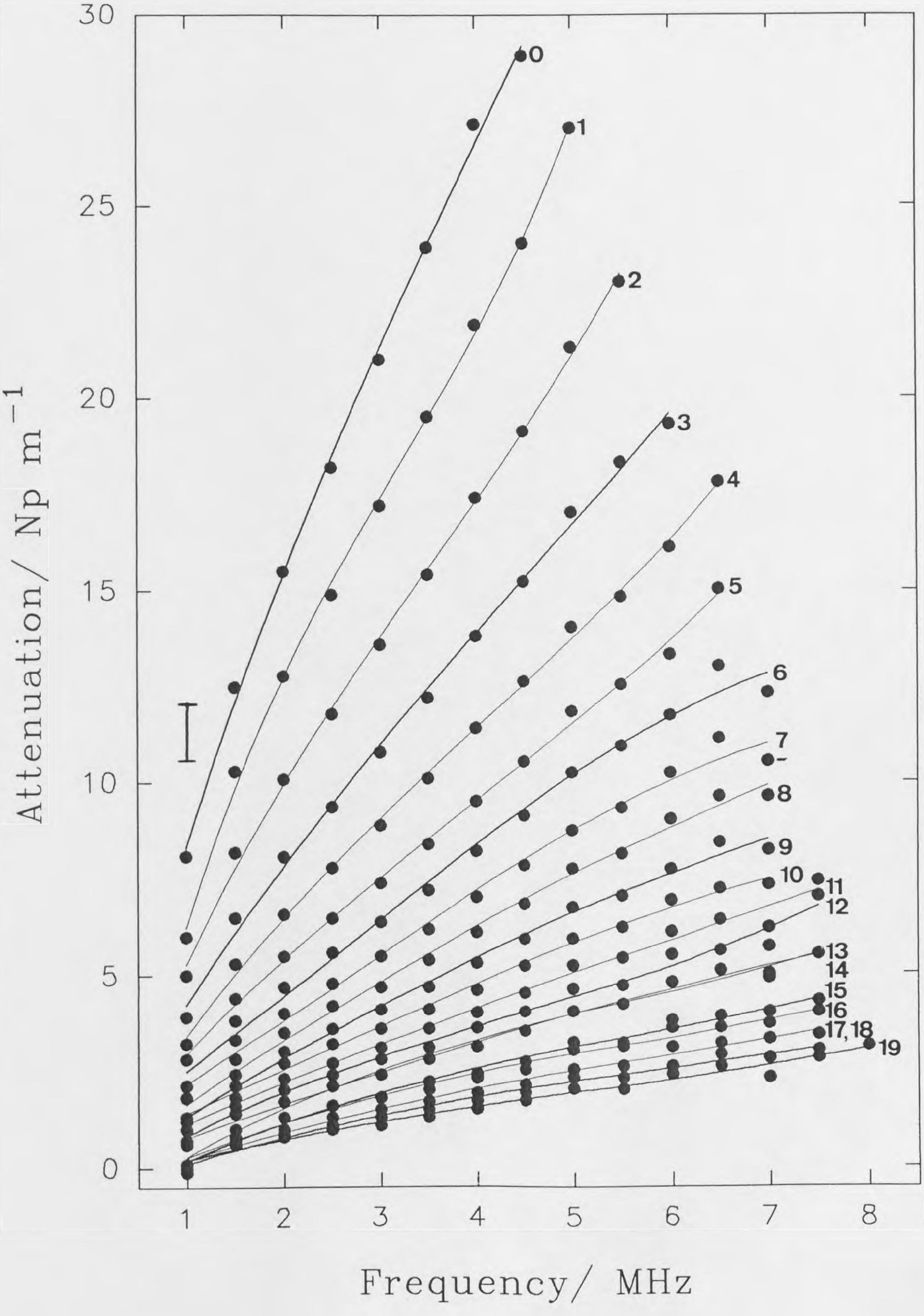

Figure 4.7 The attenuation coefficient in aerated sample two as a function of frequency. Regression lines are drawn through the data points, which are labelled with the appropriate dilution number. The bar indicates the estimated accuracy of the measurement, when applied to standard liquids under controlled conditions.

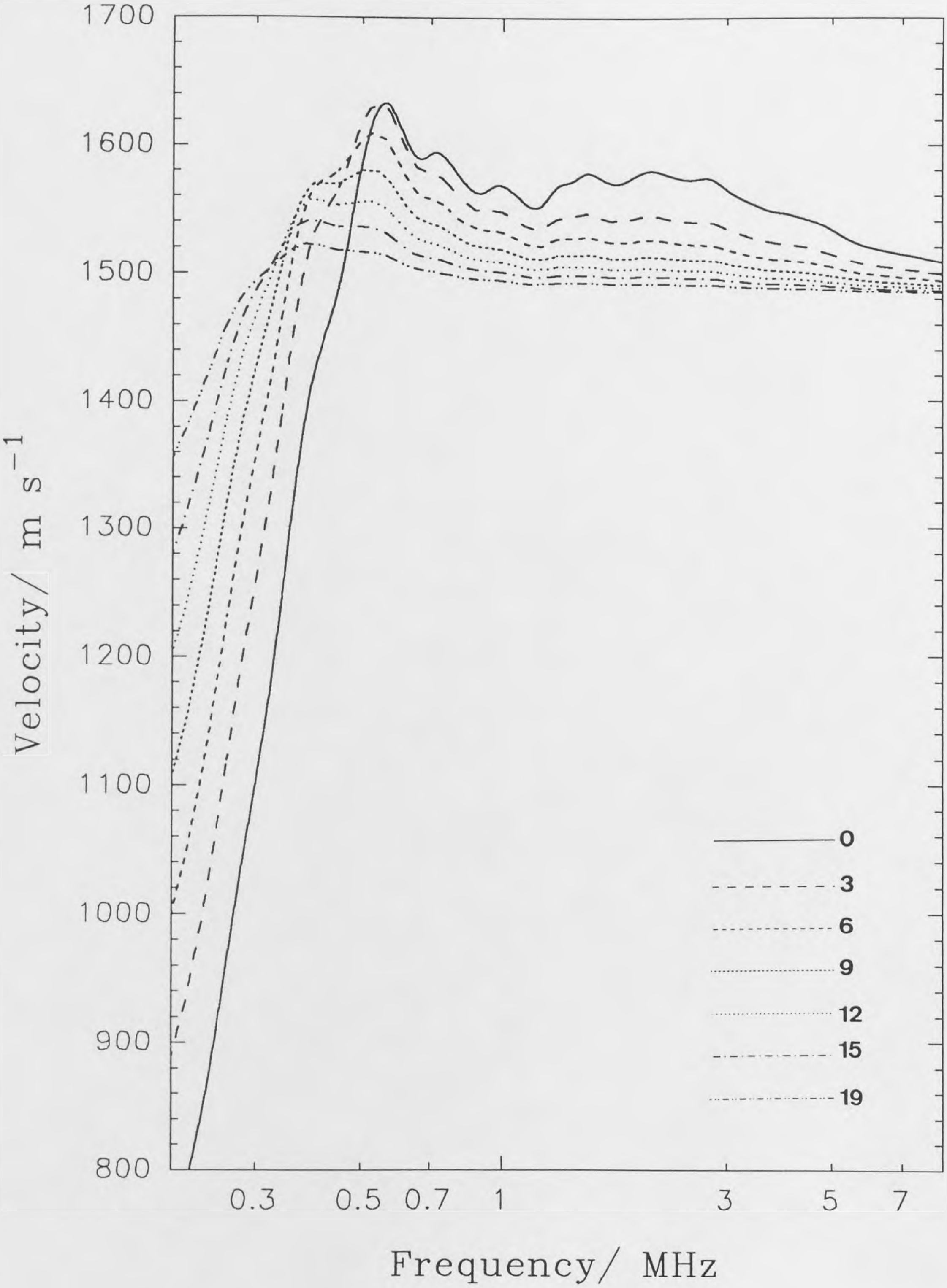

Figure 4.8 The ultrasonic velocity in aerated sample two as a function of frequency, predicted using multiple scattering theory. Selected dilutions are shown (see labels). The jitter is due to the use of a particle size distribution which is divided into discrete size bands.

Table 4.3 *The measured density*(kg m^{-3}) *of the dilute solutions, and the apparent volume fraction of air,* ϕ_{app}.

Dilution number	Sample 2			Sample 3		
	with air	without air	ϕ_{app} / 10^{-4}	with air	without air	ϕ_{app} / 10^{-4}
0	1012.1	1012.0	2.438	1024.8	1025.3	4.876
1	1010.6	1010.5	1.950	1022.1	1022.3	4.334
2	1009.3	1009.2	1.734	1019.5	1019.6	3.853
3	1008.8	1008.0	1.541	1017.0	1017.3	3.425
4	1006.9	1006.9	1.370	1015.0	1015.1	3.044
5	1006.0	1005.9	1.218	1013.2	1013.1	2.706
6	1005.2	1005.1	1.082	1011.5	1011.5	2.405
7	1004.4	1004.3	0.962	1010.1	1010.0	2.138
8	1003.7	1003.6	0.855	1008.7	1008.7	1.900
9	1003.1	1003.1	0.760	1007.6	1007.6	1.689
10	1002.5	1002.6	0.657	1006.5	1006.6	1.502
11	1002.0	1002.0	0.601			
12	1001.7	--	0.534			
13	1001.2	1001.2	0.475			
14	1000.9	1000.9	0.422			
15	1000.6	1000.5	0.375			
16	1000.3	1000.3	0.333			
17	1000.1	1000.1	0.296			
18	999.9	999.9	0.263			
19	999.7	999.7	0.234			

Dilution number	Sample 4			Sample 5		
	with air	without air	ϕ_{app} / 10^{-4}	with air	without air	ϕ_{app} / 10^{-4}
0	1048.3	1048.3	not known	1048.5	1048.8	3.814
1	1037.6	1037.5		1043.0	1043.4	3.390
2	1028.9	1028.8		1038.1	1038.4	3.013
3	1022.3	1022.1		1033.9	1034.0	2.679
4	1017.0	1016.9		1029.9	1031.0	2.381
5	1012.9	1012.8		1026.3	1026.7	2.116
6	1009.7	1009.5		1023.1	1023.4	1.881
7	1007.2	1007.1		1020.5	1020.8	1.672
8	1005.2	1005.1		1018.1	1018.3	1.486
9	1003.6	1003.6		1015.8	1016.1	1.321
10	1002.5	1002.5		1013.8	1014.2	1.175
11	1001.5	1001.5		1012.1	1012.4	1.044
12	1000.8	1000.8		1010.6	1010.9	0.928
13	1000.2	1000.3		1009.3	1009.5	0.825
14	999.8	999.8		1008.0	1008.2	0.733
15				1006.0	1006.1	0.570
16				1004.2	1004.4	0.444
17				1002.9	1003.1	0.345
18				1001.9	1001.9	0.268

Waterman and Truell (Section 2.2.5). The simultaneous equations *2.85* to *2.90* were solved, using the measured density (see *Table 4.3*) and velocity of air-free sample two. All other physical quantities were assumed equal to those of water.

Resonant behaviour is strikingly obvious in the predicted velocity, and a huge change in the velocity is indicated at low frequencies. The jitter in the value of the predicted velocity at high frequency is due to the relatively broad size classes which are employed by the Mastersizer. The velocity in the frequency range 1-8 MHz is predicted to be super-resonant, and in the range 1480-1580 m s^{-1}. The attenuation is accordingly predicted to be very high (*Fig 4.9*), although it decreases at higher frequencies. The disagreement between theory and experiment is very marked indeed, and the reasons why will be considered below.

There are two main reasons why the theory might disagree with experiment (assuming that the experiment has yielded the 'true' values of velocity and attenuation). The theory itself could be inadequate to describe the system, or simply wrong. Alternatively the theory could be right and the values which have been put into it could be wrong. The first possibility is easily dismissed, because the theory is known to work in dilute bubbly liquids and in emulsions (see Chapter Two). The second possibility is therefore strongly suspected, and will be discussed in more detail below.

4.2.4.1 Reasons for the disagreement between experiment and theory

The quantities which could be in error are the apparent volume fraction, the measured bubble size distribution and the thermophysical parameters used in the theoretical calculations.

The apparent volume fraction The apparent volume fraction is clearly open to question. There was a small but real difference in density between the aerated and unaerated versions of some of the samples (see *Table 4.3*). This difference gave an order-of-magnitude estimate of the volume fraction as 0.01 % (10^{-4}). The ultrasonic measurements did not however bear this out. Even a volume fraction of gas as low as 10^{-4} would be expected to depress the velocity by 500-600 m s^{-1} at frequencies below resonance. The relatively small depression in the velocity seen here between the unaerated and aerated versions of the sample indicated a volume fraction which was very much smaller than 10^{-4}.

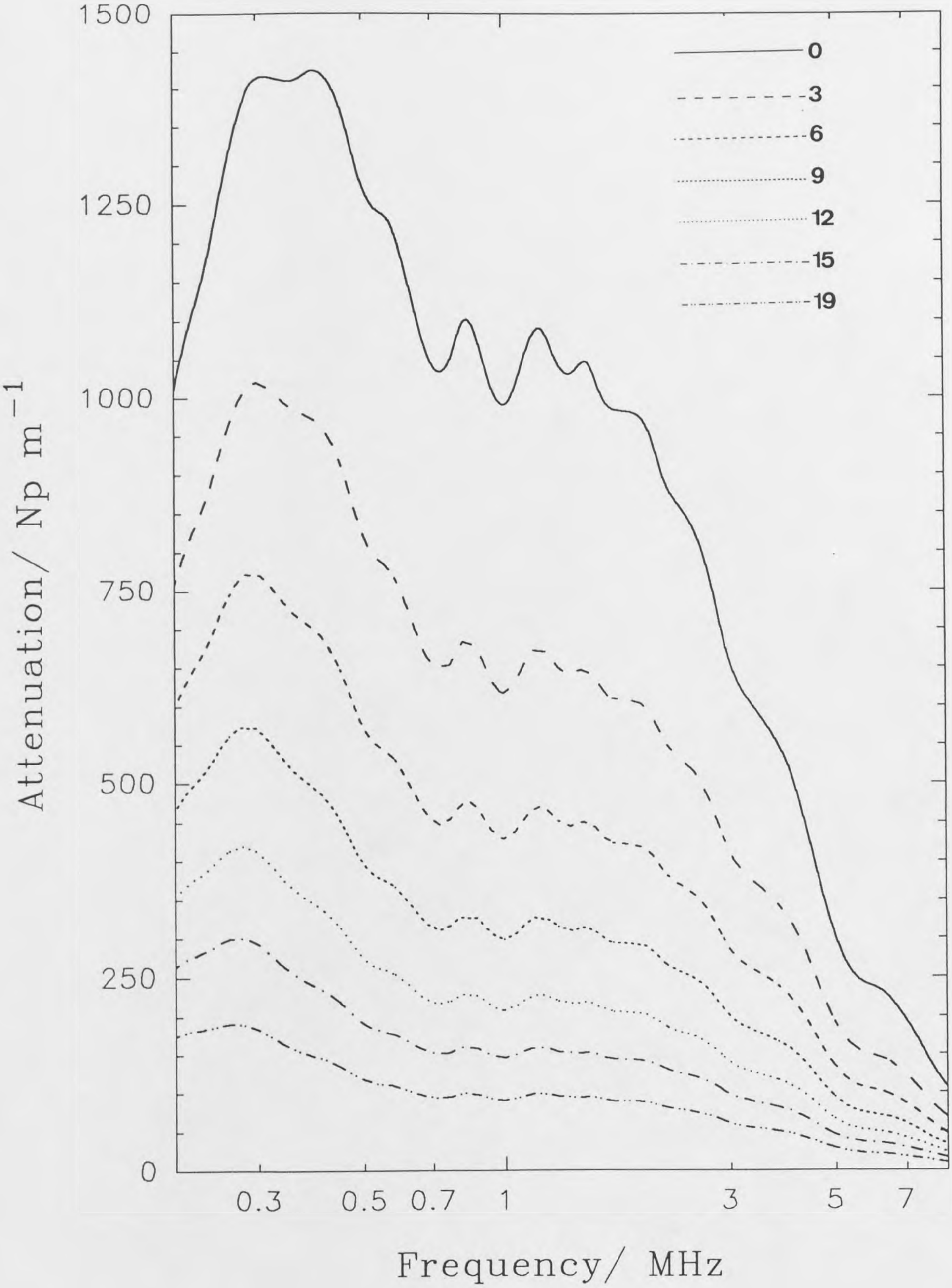

Figure 4.9 The attenuation coefficient in aerated sample two as a function of frequency, predicted using multiple scattering theory. Selected dilutions are shown (see labels). The jitter is due to the use of a particle size distribution which is divided into discrete size bands.

The measured size distribution The measured size distribution suggested that the r_{32} value of the bubbles in the dilute bubbly liquid was typically 15-20 μm. Once again, this was not borne out by the experimental measurements. The experimental measurements showed a depressed velocity in the aerated samples, indicating that the measured frequency range was below the resonant frequency of the bubbles. This would indicate that the bubbles which were measured in the FSUPER were considerably smaller than 15-20 μm, and consequently had higher resonant frequencies. Even so, a bubble with a radius as low as 0.75 μm (as seen in *Fig. 3.3*) has a resonant frequency of 4.3 MHz according to *Equation 2.22*, and resonant behaviour would be expected to be apparent in the experimental measurements.

It is possible that the structured surfactant layer at the surface of the bubbles had a much more dramatic effect on the resonant frequency than expected, shifting it to very much higher frequencies. Measurements of stable bubbles in the sea show that the thickness of the surfactant coat can be equal to the bubble radius, at values around 1 μm (Turner, 1961). Nevertheless, this does not seem to hamper the bubble sizing techniques used in oceanography (see Section 2.3.8). However, the surfactant in the system studied here is known to be highly structured at the interface, which is not the case for bubbles in sea water (where the surfactant material is a hotch-potch of organic materials and particulate matter). Clearly, the precise nature of the structured surfactant layer will need to be elucidated in future work.

An equally plausible explanation for the discrepancy between the bubble size which was apparent in the FSUPER and the bubble size given by the Mastersizer is that the sizing was in error. The choice of presentation code (see Section 3.2.6), a parameter selected by the experimenter to account for the optical properties of the system, has an effect on the bubble size which is calculated from the measured light scattering. It is possible that the use of an inappropriate presentation code could have introduced an error of several per cent into the measured size distribution. It is not possible, however, that a discrepancy of the order seen here could be accounted for solely by the choice of presentation code. There were definitely scatterers present in the light beam, the majority of which were in the size range of tens to hundreds of micrometres. These scatterers were not present in the air-free version of sample two, so it seems therefore that they were almost certainly air bubbles. This does not rule out the presence of small bubbles - indeed some small bubbles are evident in the size distributions shown in *Fig. 4.1*. However, the Mastersizer measures the particle volume and was therefore biased towards bigger particles. Where large particles make up the bulk of the volume, they swamp the effects of any small bubbles. For example, consider a hypothetical mixture made up of bubbles with radii 0.75 μm and 20 μm. Let the large bubbles make up 99 % of the volume, so that there are 50 times as many small bubbles as large bubbles. The r_{10} of such a system is about 1.1 μm, whereas the r_{32} is about 18.8 μm. However, r_{32} is usually taken to be the representative mean radius for use in ultrasonic measurements, so this is not usually a problem. There would seem to be some crucial difference in the bubbles which were sampled by the FSUPER and those which were sampled by the Mastersizer. Large bubbles were present in the dilute bubbly liquid which were detected by the Mastersizer but not by the ultrasonic equipment. These bubbles made up the bulk of the air in the bubbly liquid, and were presumably responsible for the measured density difference between the aerated and air-free versions of some samples. The ultrasonic measurements did not seem to be sensitive to these large bubbles.

The thermophysical properties of the sample The only known thermophysical properties of the sample were the density and ultrasonic velocity at each dilution. All the other properties, such as thermal conductivity and viscosity, were assumed to be equal to the properties of water. This is a source of uncertainty in the predictions, but compared to the uncertainties discussed above it is a rather small one. Trial calculations were made using different values for the assumed parameters. The key parameters turned out to be the volume fraction, the bubble size and the density and ultrasonic veloci+1Xty of the air-free sample. Of the parameters which were given assumed values, only the viscosity had a significant effect on the predictions. Even so, this effect was not nearly enough to account for the discrepancy between the predicted and the measured values of ultrasonic velocity and attenuation.

4.2.4.2 Measuring the volume fraction of air in sample two

The depression of the ultrasonic velocity which occurred in the aerated version of sample two can be used to measure the volume fraction of air. It is assumed that the velocity measurements covered a frequency range which was below the resonant frequency of the bubbles, so that the Wood equation (*Equation 2.109*) can therefore be applied. It is also assumed that no further air dissolved during the serial dilutions.

It should in theory be possible to determine the volume fraction of air using just one dilution of both the aerated and air-free versions of sample two. The velocity of ultrasound was measured in the aerated and air-free versions, and the density of the air-free versions was determined. The Wood equation gives

$$c_0^{-2} = (\phi\rho_a + (1 - \phi)\rho_0)(\phi\beta_a + (1 - \phi)\beta_0) \qquad [4.1]$$

$$c_1^{-2} = (x\phi\rho_a + (1 - x\phi)\rho_1)(x\phi\beta_a + (1 - x\phi)\beta_1) \qquad [4.2]$$

where c_0 and c_1 are the velocities in dilution zero and dilution one of the aerated sample, ϕ is the volume fraction of gas and x is the factor by which the solution has been diluted (8/9). The quantities $\rho_{0,1}$ and $\beta_{0,1}$ are the density and compressibility of the corresponding dilutions in the air-free version. The compressibility of the air-free dilutions can be calculated using the relationship $c'^{-2}_0 = \rho_0\beta_0$, where c'_0 is the velocity in air-free dilution zero. Thus the only unknown is the volume fraction, which could be found from the simultaneous solution of *Equations 4.1* and *4.2*. In practice, the solution is not possible, because ϕ is very small and the uncertainties in ρ, β and c are too large.

This problem is overcome by the use of serial dilutions, and by a consideration of the properties of the air-free solution. Starting with *Equation 4.2*, the full expression for any dilution, n, is given by

$$c_n = (x\phi)^2(\mathrm{A} - \mathrm{B} - \mathrm{C} + \mathrm{D}) + x\phi(\mathrm{B} + \mathrm{C} - 2\mathrm{D}) + \mathrm{D} \qquad [4.3]$$

where $\mathrm{A} = \rho_a\beta_a$ [4.4]

$\mathrm{B} = \rho_a\beta_0$ [4.5]

$\mathrm{C} = \rho_0\beta_a$ [4.6]

$\mathrm{D} = \rho_0\beta_0$ [4.7]

where the subscript a refers to air, the subscript 0 refers to the solution known as dilution zero, and x is the factor by which dilution n has been diluted from dilution zero (in this case, $(8/9)^n$). Note that by setting $x = 1$, *Equation 4.1* is recovered. Note also that the velocity in the air-free solution is equal to $D^{-0.5}$, and the factors B, C and D are affected by the serial dilution process. As distilled water is added to the serial dilutions, the density and compressibility of the continuous phase can be considered as the volume average of the properties of air-free dilution zero and water. Thus ρ_0 is replaced by ρ_n, where

$$\rho_n = x\rho_0 + (1 - x)\rho_w \qquad [4.8]$$

and β_0 is replaced by β_n, where

$$\beta_n = x\beta_0 + (1 - x)\beta_w \qquad [4.9]$$

Equation 4.3 is thus modified to

$$c_1^{-2} - c'^{-2}_1 = ax^4 + bx^3 + cx^2 + dx \qquad [4.10]$$

where $a = D_1\phi^2$ [4.11]

$b = (D_2 - B_1 - C_1 - 2D_1)\,\phi^2$ [4.12]

$c = (A - B_2 - C_2 + D_3)\,\phi^2 + (B_1 + C_1 - 2D_2)\,\phi$ [4.13]

$d = (B_2 + C_2 - 2D_3)\,\phi$ [4.14]

and $B_1 = B - B_2$ [4.15]

$B_2 = \rho_a\beta_w$ [4.16]

$C_1 = C - C_2$ [4.17]

$C_2 = \rho_w\beta_a$ [4.18]

$D_1 = D - F - G + D_3$ [4.19]

$D_2 = F + G - 2D_3$ [4.20]

$D_3 = \rho_w\beta_w$ [4.21]

$F = \rho_0\beta_w$ [4.22]

$G = \rho_w\beta_0$ [4.23]

where the subscript w refers to distilled water. The quantities c and c' have been measured as a function of the dilution, x. The quantity x can be thought of as a relative volume fraction. In dilution zero, the relative volume fraction is 1, after one dilution it is 8/9, after two dilutions it is $(8/9)^2$ and so on. Therefore, if the quantity ($c^{-2} - c'^{-2}$) is plotted as a function of x, it should be possible to fit a fourth degree polynomial in x to the data.

This operation is performed for sample two in *Fig 4.10*, using the measured velocity at 4 MHz in the aerated and air-free versions. The coefficients of the polynomial which can be fitted to the data are: a = -4.84×10^{-9}, b = 1.16×10^{-8}, c = -6.62×10^{-9} and d = 2.26×10^{-9}. *Equation 4.14* gives $2.26 \times 10^{-9} = (\rho_a\beta_w + \rho_w\beta_a - 2\rho_w\beta_w)\phi$. Using the thermophysical properties of air and water given in *Table 2.1*, this yields a value for ϕ of 3.2×10^{-7}.

This value of the volume fraction should be taken as an order of magnitude estimate. Nevertheless, it is very much lower than the value given by the densitometer. In order to check the accuracy of the calculated volume fraction, it was used in the Wood equation, with the properties of dilution zero, in order to calculate the velocity in aerated dilution one. The measured value at 4 MHz was 1489.9 m s^{-1}, and this agrees very well with the predicted value of 1489.5 m s^{-1}. Clearly then the ultrasonic technique is extremely sensitive to small amounts of air. It is the only method known to the author which is capable of measuring the volume fraction of dispersed air at a level of 10^{-7}.

4.2.4.3 An explanation for the observed ultrasonic properties

The ultrasonic measurements indicated that the solution in the FSUPER had a much lower volume fraction of air than indicated by the densitometer, and the bubbles in it were much smaller than those seen in the Mastersizer. A possible explanation is that the majority of the bubbles in dilution zero had radii in the region 15-20 μm, and these bubbles made up the bulk of the air. The densitometer gave a reasonable order of magnitude estimate for the volume fraction (10^{-4}) in dilution zero.

Now, the FSUPER was stirred by a magnetic flea, driven by a submersible stirrer. It is proposed that the stirring was not adequate to prevent the larger bubbles from creaming out. *Equation 1.1* gives a rise velocity of around 0.8 mm s^{-1} for bubbles of radius 20 μm. The Mastersizer is equipped with a reasonably powerful pump and a stirrer, which kept these bubbles from creaming out, so that they were observed in

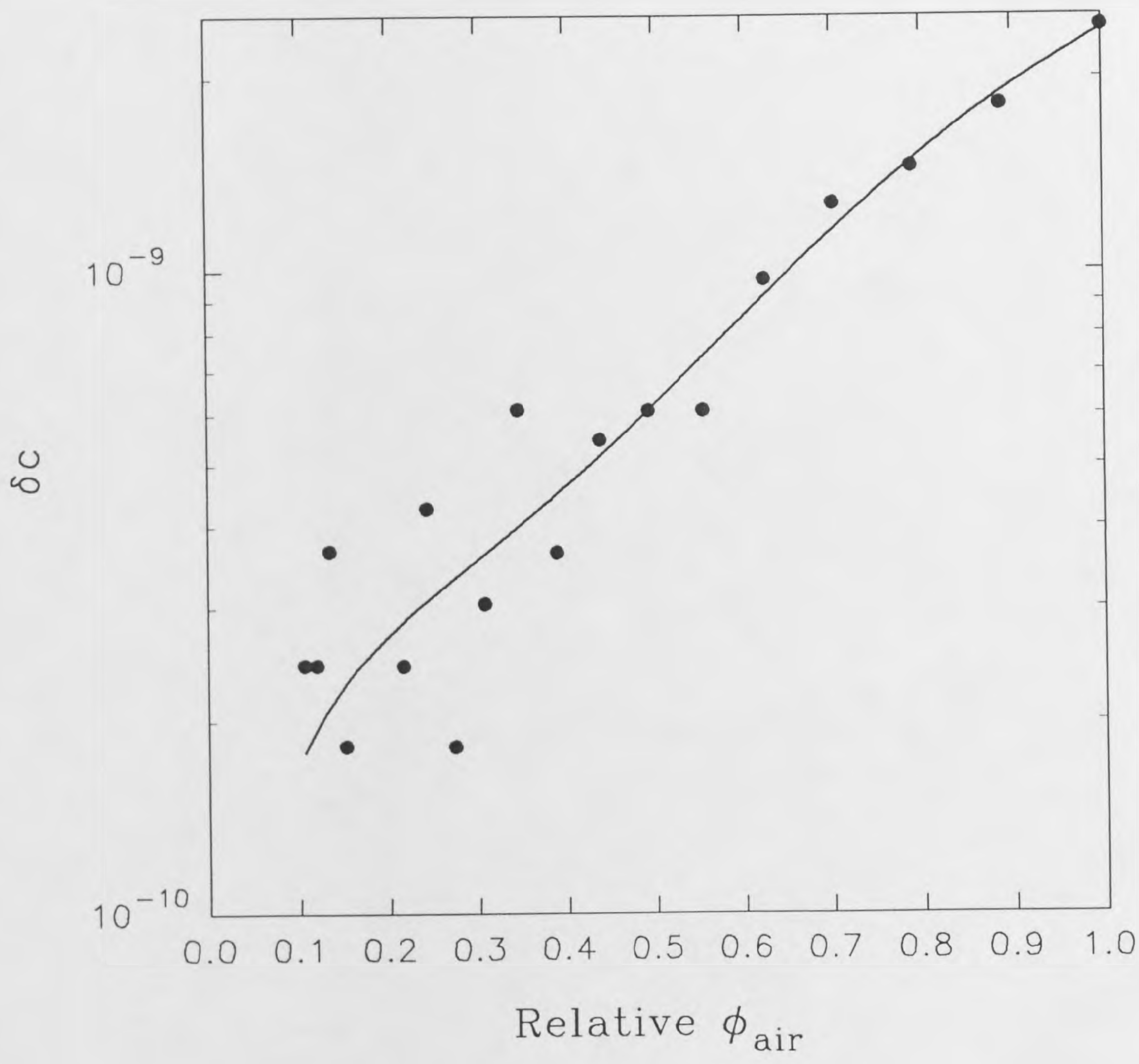

Figure 4.10 The difference in the velocities of aerated and air free versions of sample two (c and c' respectively) are plotted as a function of the relative volume fraction. The quantity δc is given by $1/c^2 - 1/c'^2$. The line is the least squares fit of the polynomial given by *Equation 4.10.*

the light scattering measurements. Once the larger bubbles had creamed out of the FSUPER, only the smallest bubbles remained. These were the bubbles seen in the electron microscope, with radii of the order 0.5 - 1.0 μm. They contributed only a very small proportion of the total volume fraction, because they were so tiny. The structured surfactant at the interface caused these bubbles to have rather higher resonant frequencies than expected. It provided them with an unexpectedly high degree of stability, so that they survived the dilution process without changing size. This enabled the application of the serial dilution technique for the determination of the volume fraction. The ultrasound propagated through a bubbly liquid containing highly stable small bubbles at very low fraction, at frequencies which were below resonance.

4.2.4.4 The reflection coefficient

The reflection coefficient of aerated sample two was measured at each dilution (*Fig. 4.11*). The reflection coefficient was much less sensitive to the slight changes in velocity and density which occurred when the sample was serially diluted. The majority of the dilutions were not resolved. There appeared to be a slight peak in the real part of the reflection coefficient at a frequency of about 3 MHz, but this could have been due to scatter in the data. The fall in the value of the imaginary part at high frequencies is probably due to calibration errors. It will become apparent from other measurements that the technique tended to give a negative value for the imaginary part of the reflection coefficient in solutions which were weakly attenuating at high frequencies. The predicted velocity and attenuation were used in order to predict the value of the real and imaginary parts of the reflection coefficient (*Fig. 4.12*). Unsurprisingly, the predicted reflection coefficient did not model the observed reflection coefficient very well. Notice that the volume fraction of air chosen for the model calculations (10^{-4}) had a dramatic effect on the predicted value of the reflection coefficient. The effect of serial dilutions is also poorly resolved in the predicted values of the reflection coefficient at high frequencies. The reflection coefficient is therefore of limited interest in very dilute systems.

4.2.5 Sample three

Sample three was prepared using twice as much concentrated bubbly liquid as

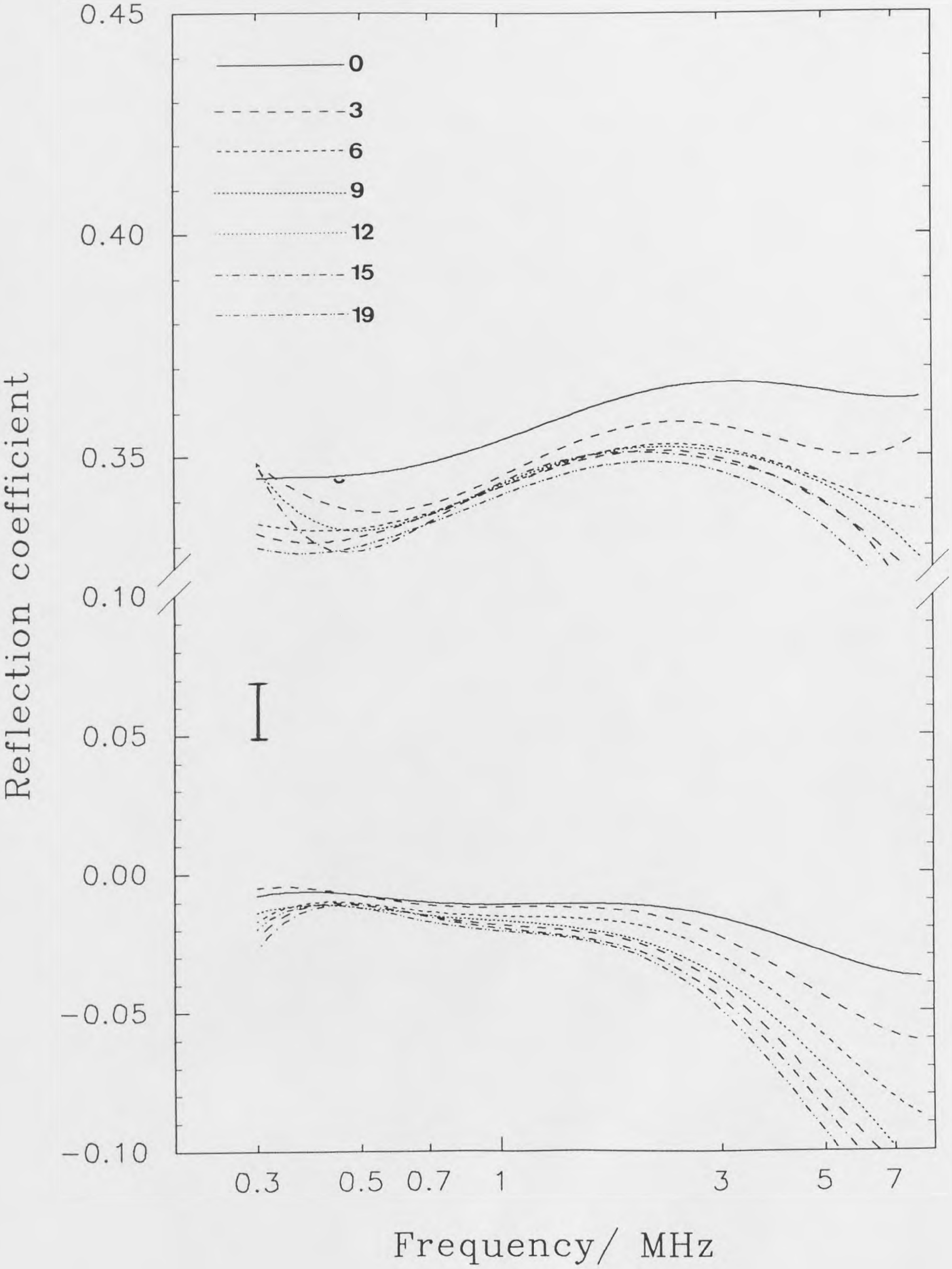

Figure 4.11 The measured real part (upper curves) and imaginary part (lower curves) of the reflection coefficient of aerated sample two. Regression lines are drawn through the data for selected dilutions, which are indicated by the labels. The bar indicates the estimated accuracy of the measurement, when applied to standard liquids under controlled conditions. The data points themselves have been omitted for clarity.

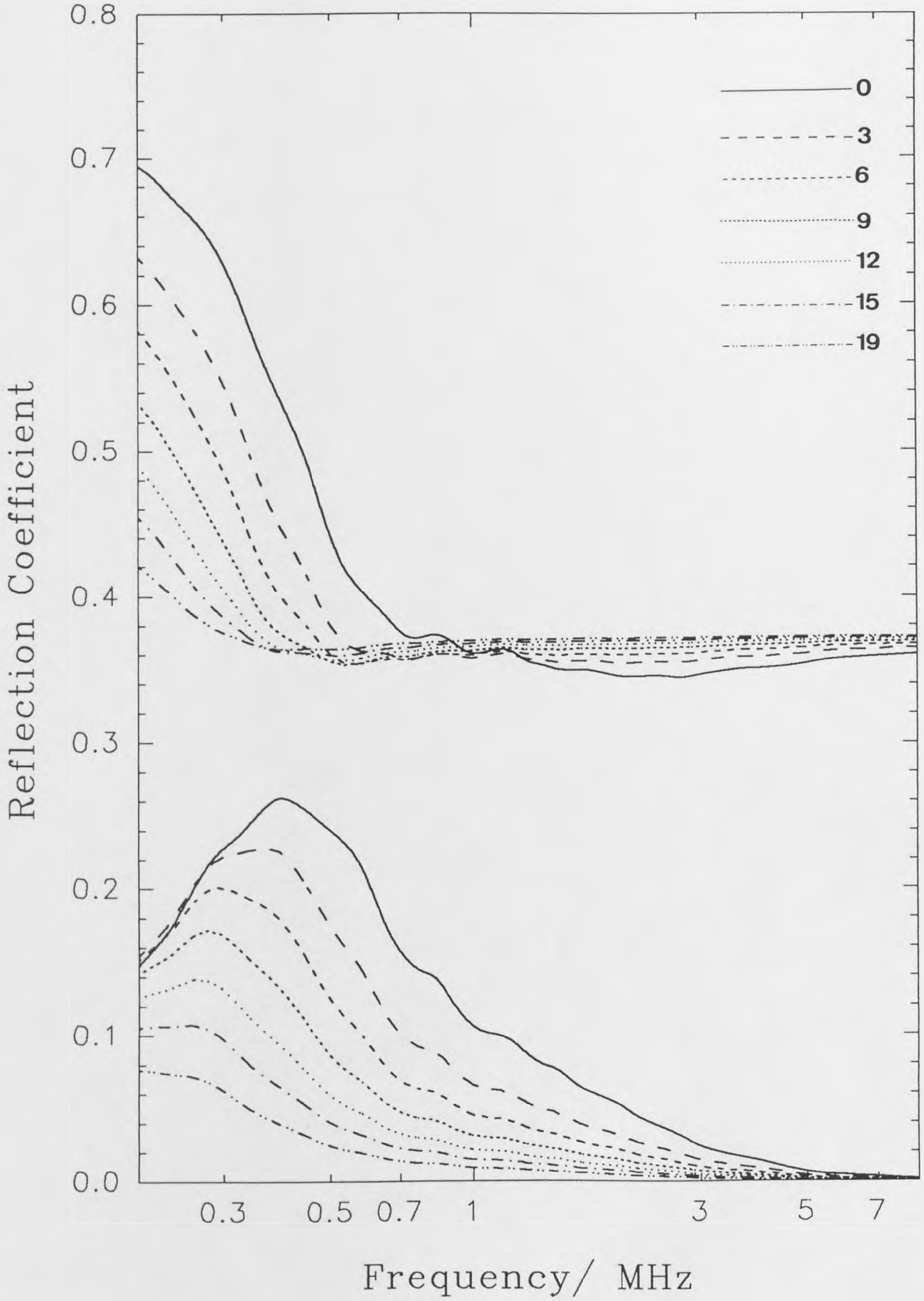

Figure 4.12 The predicted real part (upper curves) and imaginary part (lower curves) of the reflection coefficient of aerated sample two. The labels indicate the dilutions shown, which are the same as those in *Fig. 4.11*. Note that the jitter seen in the predicted values of velocity and attenuation is less evident in the predicted reflection coefficient.

sample two, so it contained more air. The air-free version of sample three showed similar behaviour to sample two. The velocity (*Fig. 4.13*) was not dispersive in the frequency range examined, and the effect of the serial dilutions was well resolved. The low frequency measurements seemed to show rather more scatter than the high frequency results, which were extremely regular. The attenuation (*Fig. 4.14*) in the air-free sample was extremely low, and the various dilutions were not resolved.

The attenuation in the aerated version of sample three was rather high, so it was not possible to make measurements of velocity and attenuation. The velocity and attenuation were *predicted* using the scheme described above. The predicted velocity (*Fig. 4.15*) shows very similar behaviour to the predicted velocity for sample two. The predicted attenuation (*Fig. 4.16*) is also similar to the predicted attenuation in sample two. In the light of the observed behaviour of sample two, these predictions must be treated with extreme caution.

4.2.5.1 The reflection coefficient

Although it was not possible to measure the velocity and attenuation in aerated sample three, it was possible to measure the reflection coefficient (*Fig. 4.17*). The reflection coefficient was sensitive to the extra air which was present in sample three, because the dilutions were much more clearly resolved than in the measurements on sample two (*Fig. 4.11*). There was a definite negative slope in the real part of the reflection coefficient, and a discernible peak in the imaginary part, although this peak was less obvious in the measurements for the highest numbered dilutions. On comparing the measured reflection coefficient with the predicted reflection coefficient (*Fig. 4.18*), it is obvious that there is a good agreement in form between the two sets of curves. However, the measured values of the reflection coefficient did not vary as dramatically as the predicted values, and resonant behaviour was seen at higher frequencies in the measured values than in the predicted values. This is consistent with the presence of smaller bubbles, at a much lower volume fraction, than the conventional measurements would suggest. This is also consistent with the behaviour of sample two.

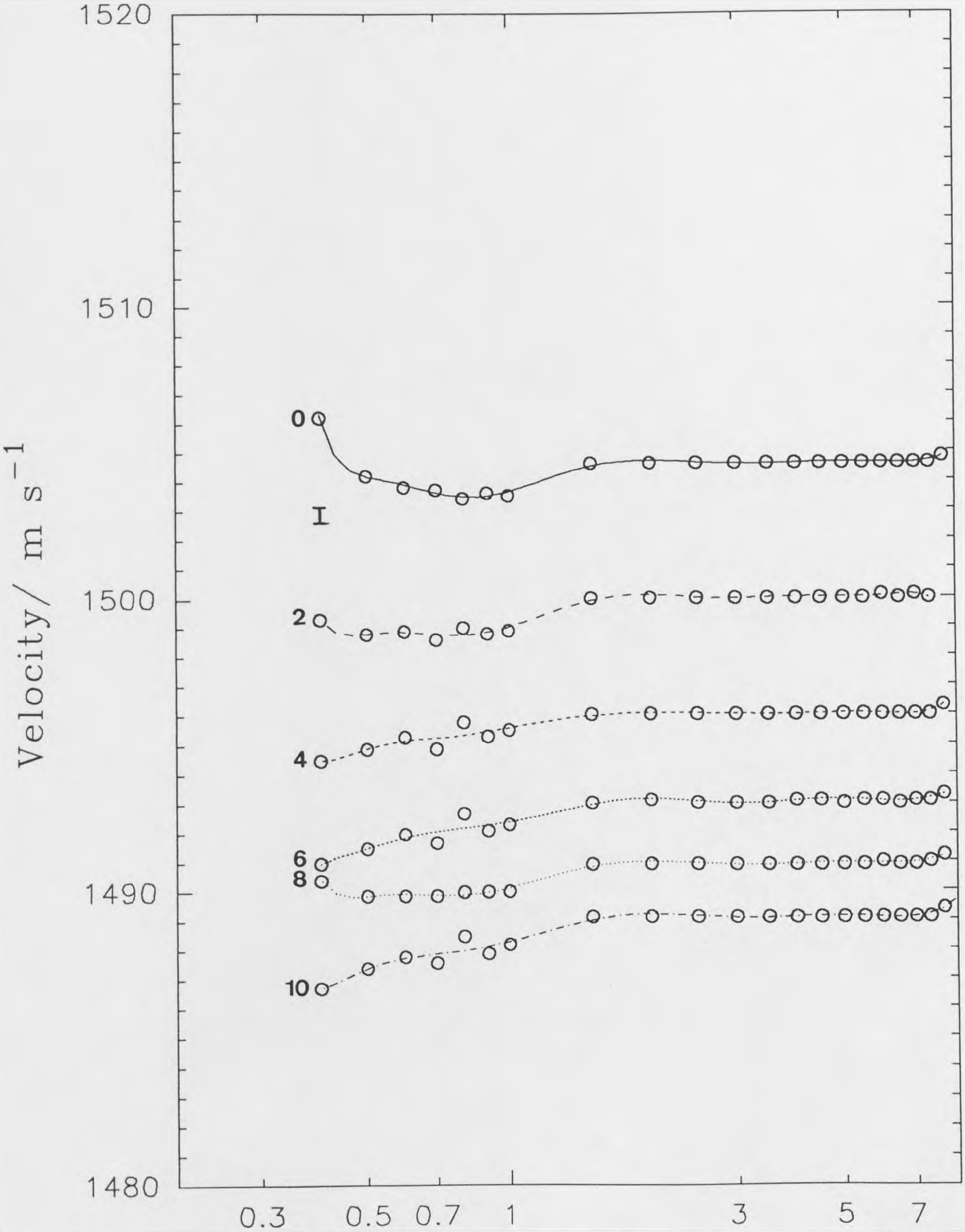

Figure 4.13 The ultrasonic velocity in air-free sample three as a function of frequency. Regression lines are drawn through the data points for selected dilutions, which are labelled with the appropriate dilution number. The bar indicates the estimated accuracy of the measurement, when applied to standard liquids under controlled conditions.

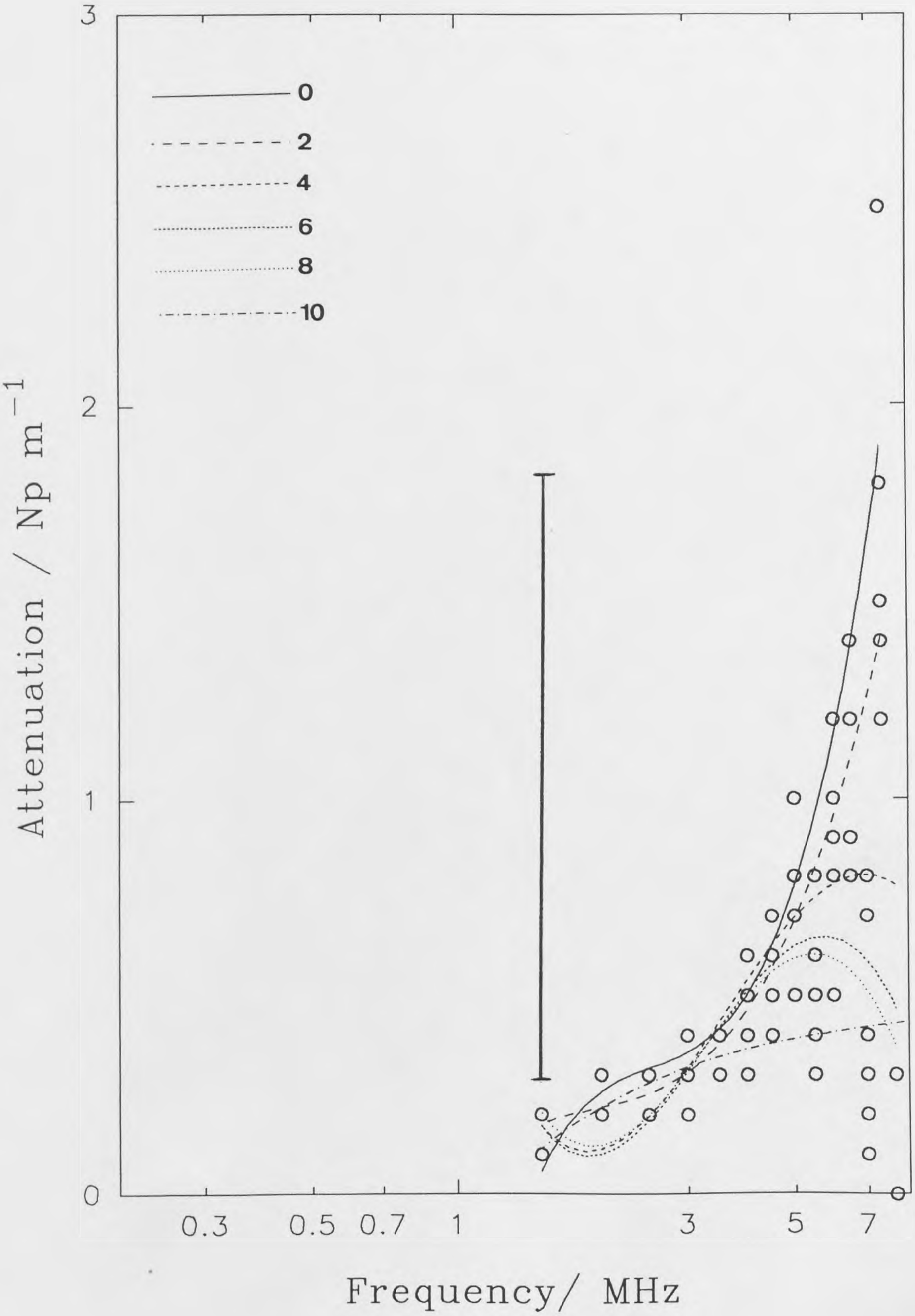

Figure 4.14 The attenuation coefficient in air-free sample three as a function of frequency. Regression lines are drawn through the data points for selected dilutions, which are labelled with the appropriate dilution number. The bar indicates the estimated accuracy of the measurement, when applied to standard liquids under controlled conditions. Note that the dilutions are not resolved, leading to an apparent jumble of data points.

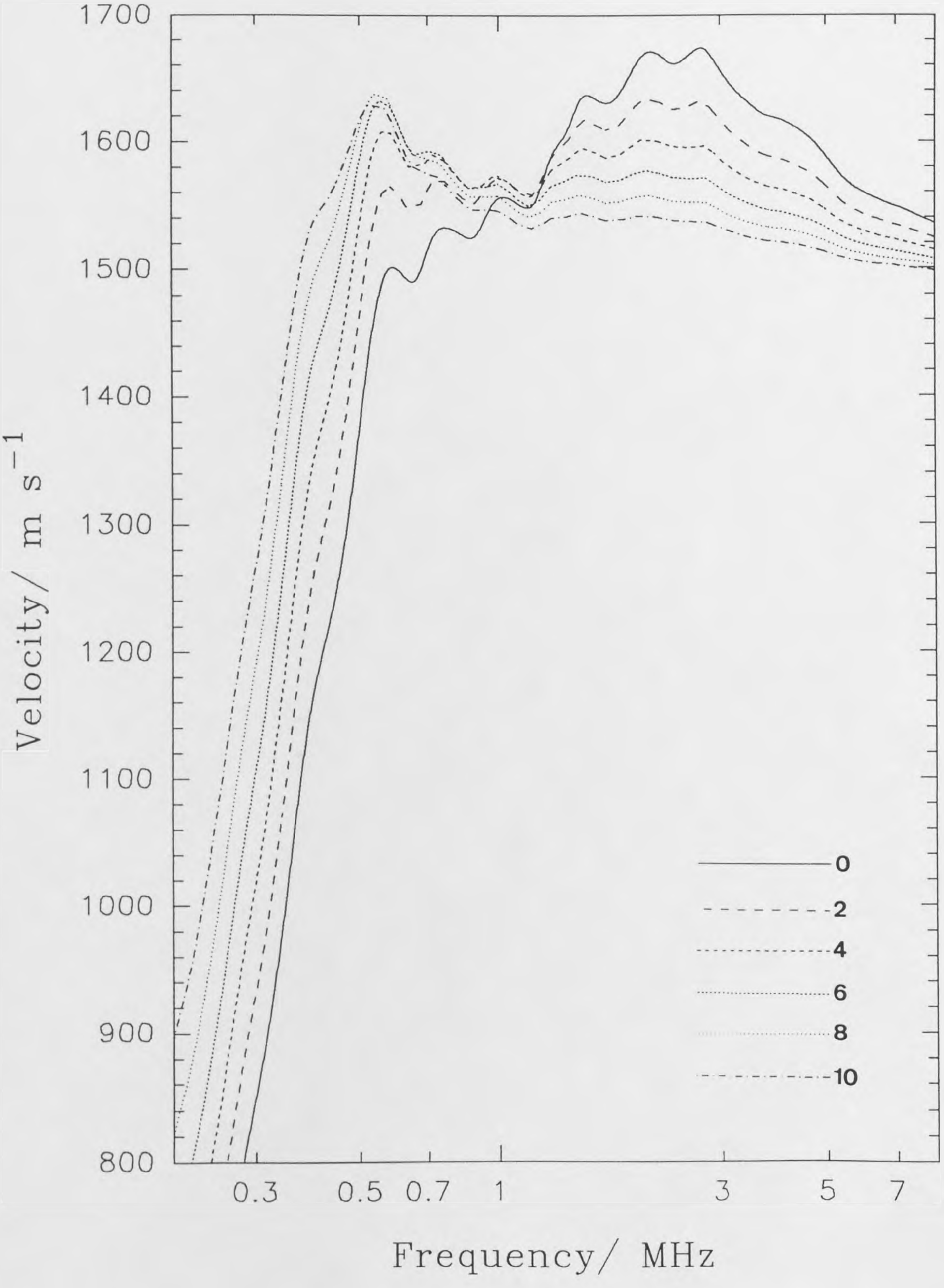

Figure 4.15 The predicted ultrasonic velocity in aerated sample three as a function of frequency. The predictions for selected dilutions are shown, which are labelled with the appropriate dilution number. The jitter is due to the width of the size classes in the bubble size distribution provided by the Mastersizer.

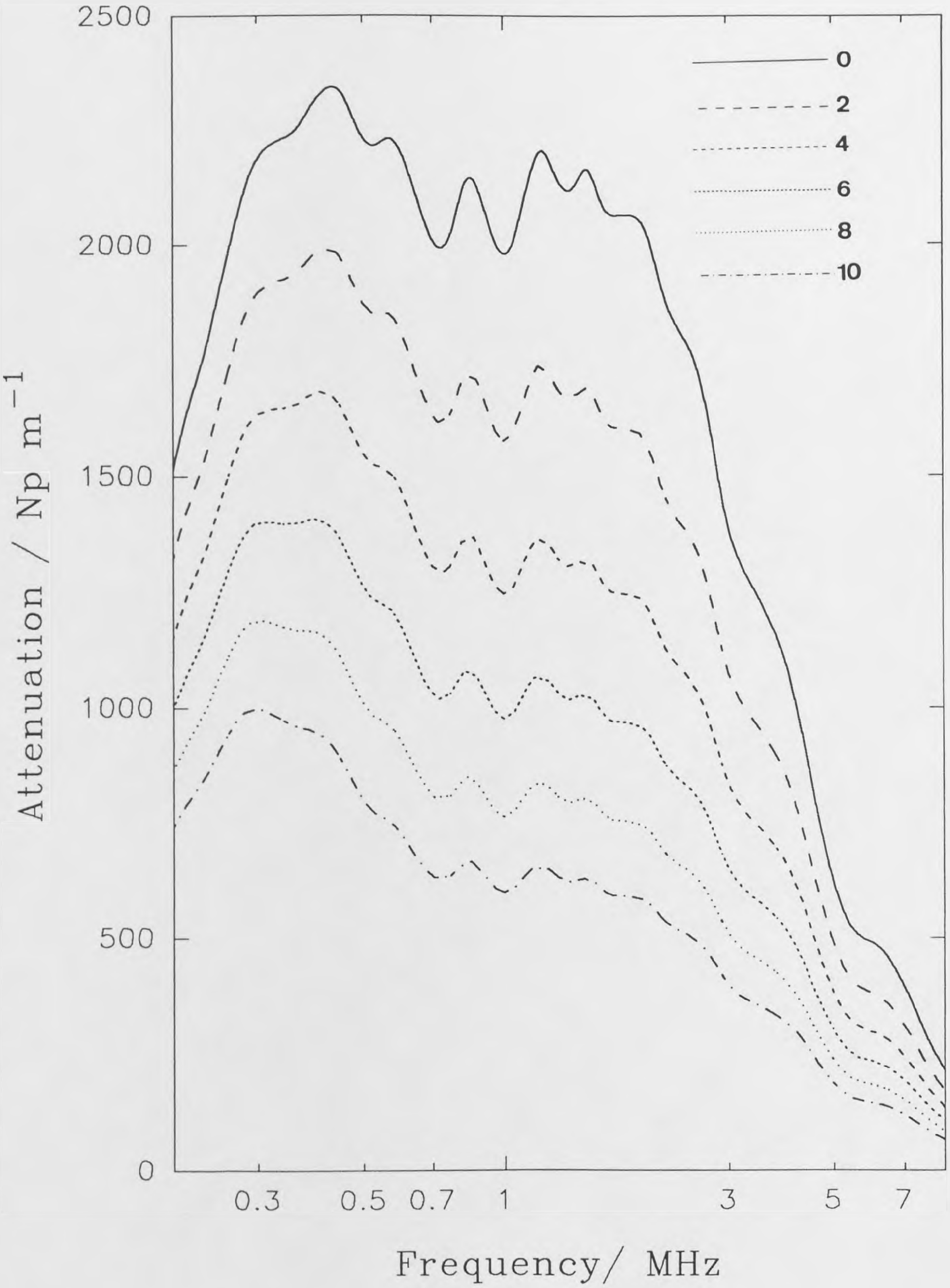

Figure 4.16 The predicted attenuation coefficient in aerated sample three as a function of frequency. The predictions for selected dilutions are shown, which are labelled with the appropriate dilution number. The jitter is due to the width of the size classes in the bubble size distribution provided by the Mastersizer.

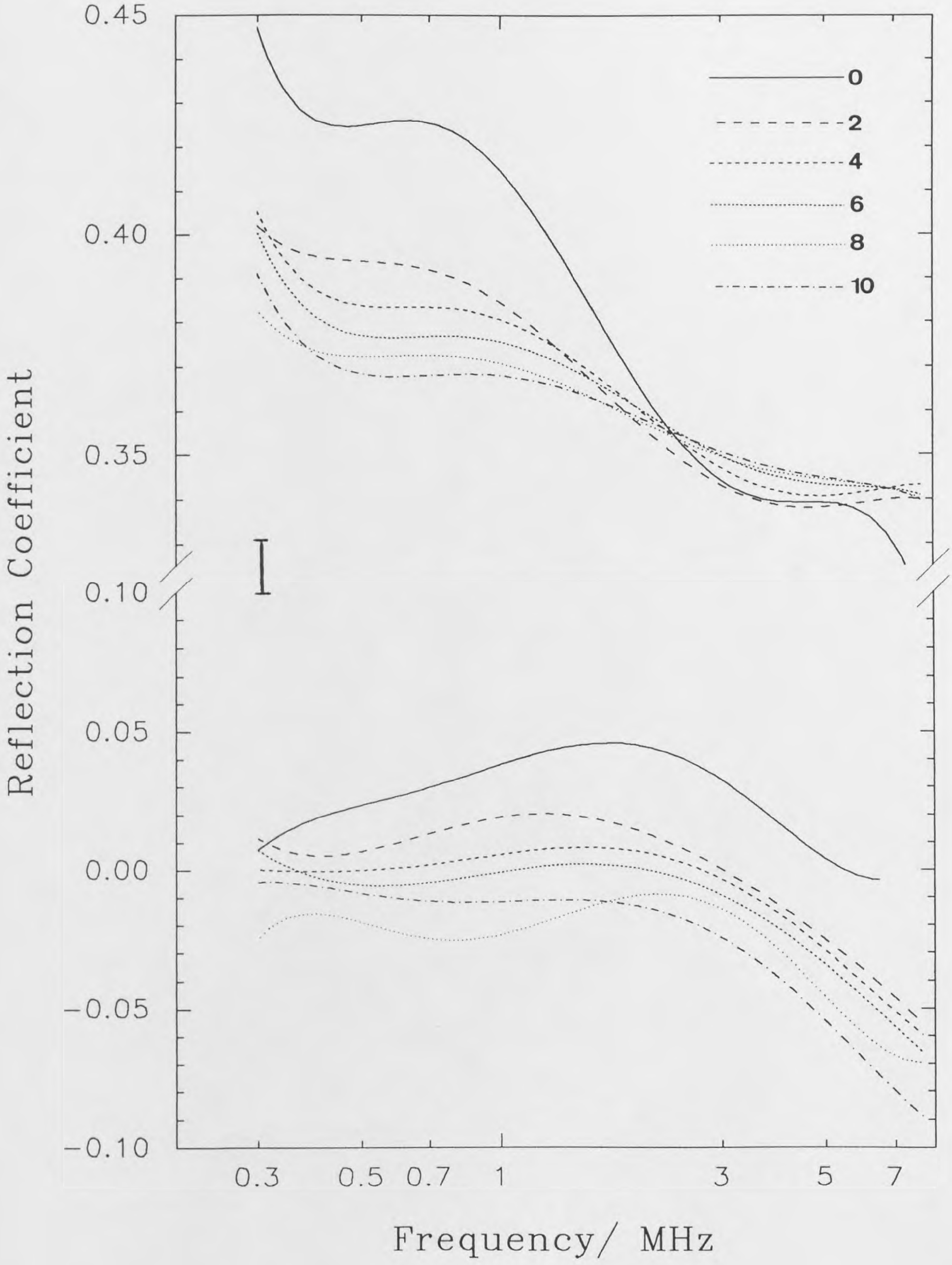

Figure 4.17 The measured real part (upper curves) and imaginary part (lower curves) of the reflection coefficient in aerated sample three. The lines are regressions through the data points, and are labelled with the appropriate dilution number. The data points themselves are omitted for clarity. The bar indicates the estimated accuracy of the measurement, when applied to standard liquids under controlled conditions.

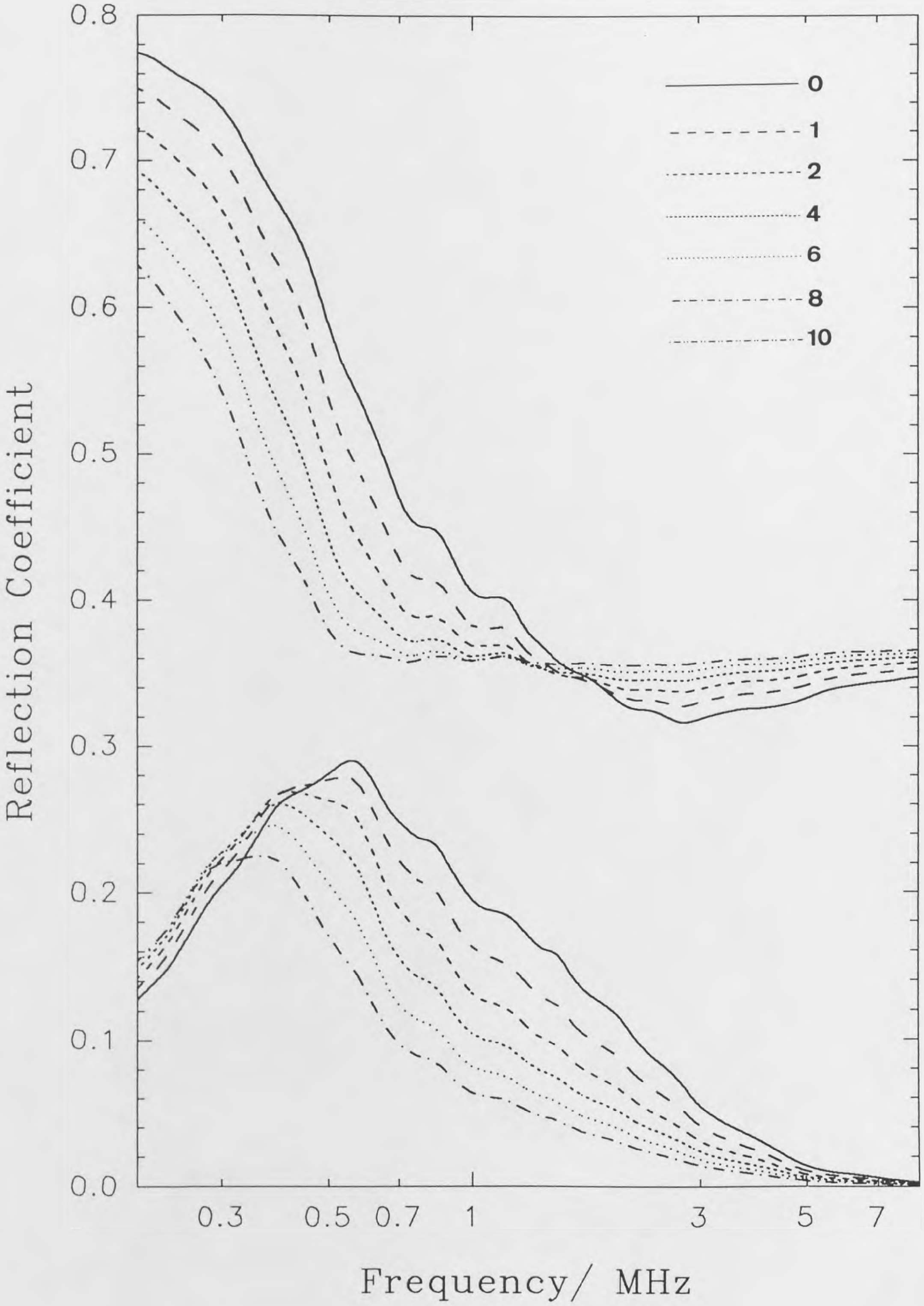

Figure 4.18 The predicted real part (upper curves) and imaginary part (lower curves) of the reflection coefficient in aerated sample three. The lines are labelled with the appropriate dilution number. Note the similarity in form to *Fig. 4.17*.

4.2.5.2 Trends in the ultrasonic measurements

The results from sample three, although they are not as complete as the results for sample two, are in keeping with the behaviour of sample two. In the absence of air the dilutions had very low attenuation coefficients, and they were non-dispersive. On the addition of a very small amount of air the attenuation increased dramatically. The reflection coefficient suggested that the bubbles characterised in the FSUPER were smaller than those seen in the Mastersizer, and they were present at a much lower volume fraction than the densitometer suggested.

4.2.6 Sample four

Sample four was prepared using twice as much concentrated bubbly liquid as sample three, and there was a higher concentration of surfactant in the concentrated bubbly liquid. The attenuation in the lowest numbered dilutions was too high to allow measurements of velocity and attenuation. However, the dilution factor was changed to 7/9 for this sample, so that transmission measurements were possible in the higher numbered dilutions, albeit over a restricted frequency range.

Starting once again with the velocity in the air-free version of sample four (*Fig. 4.19*), the expected lack of dispersion was seen. The dissolved sugar had a noticeable effect on the velocity, which in dilution zero was about 40 m s^{-1} higher than the velocity in distilled water. The dilutions were well resolved. Again the attenuation was very low and thus poorly resolved between dilutions (*Fig. 4.20*), although it was slightly higher than the attenuations in samples two and three.

The measured velocity in the aerated version of sample four was depressed by greater amounts than seen previously (*Fig. 4.21*). The change was about 20 m s^{-1} in dilution eight, which was the lowest numbered dilution which could be characterised in transmission. Some dispersion was evident in the measurements for the lowest numbered dilutions. The dispersion suggested that the velocity was increasing with frequency, which indicated that the measurement frequency was below the resonant frequency of the bubbles. This evidence gives added weight to the argument that the bubbles which persisted in the FSUPER were rather smaller than those which predominated in the Mastersizer. The velocity in the highest numbered dilutions was poorly resolved.

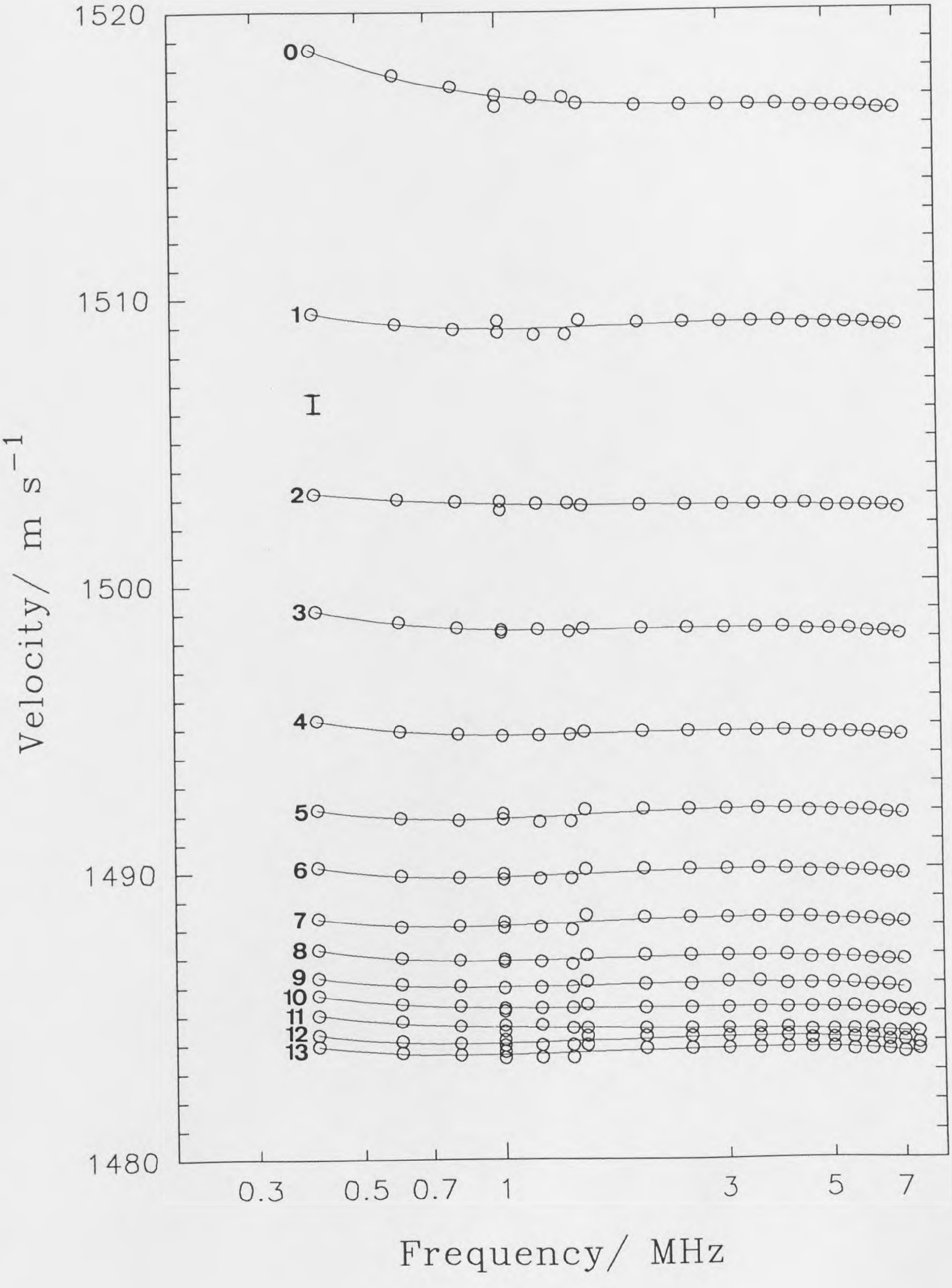

Figure 4.19 The measured ultrasonic velocity in air-free sample four as a function of frequency. Regression lines are drawn through the data, which are labelled with appropriate dilution number. The bar indicates the estimated accuracy of the measurement, when applied to standard liquids under controlled conditions. The data points at 1 MHz are shown for the low and high frequency transducers. There is agreement to within 0.5 m s^{-1}.

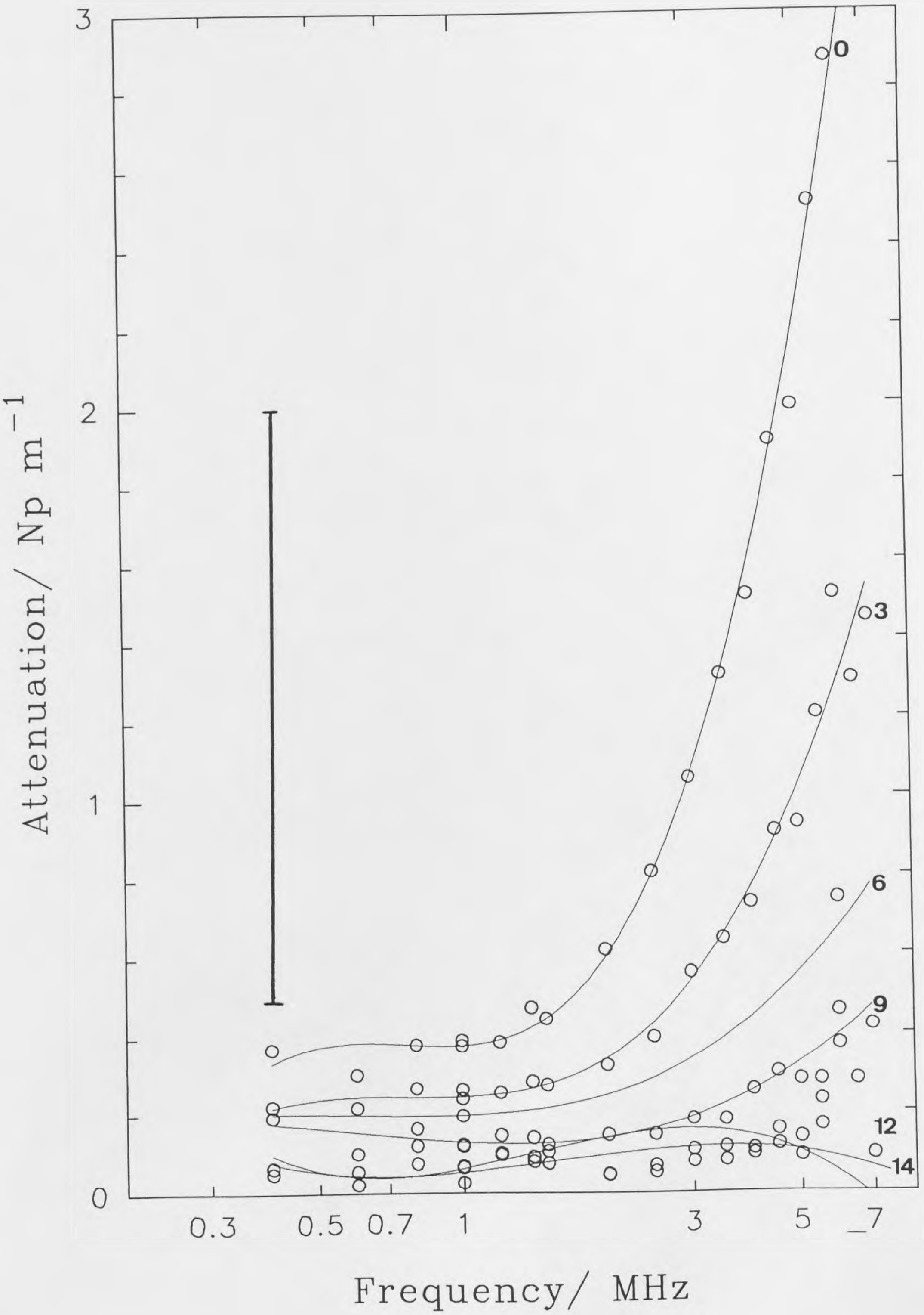

Figure 4.20 The measured attenuation coefficient in air-free sample four as a function of frequency. Regression lines are drawn through the data for selected dilutions, which are indicated by the labels. The bar indicates the estimated accuracy of the measurement, when applied to standard liquids under controlled conditions. Notice the good agreement between the measurements from different transducers.

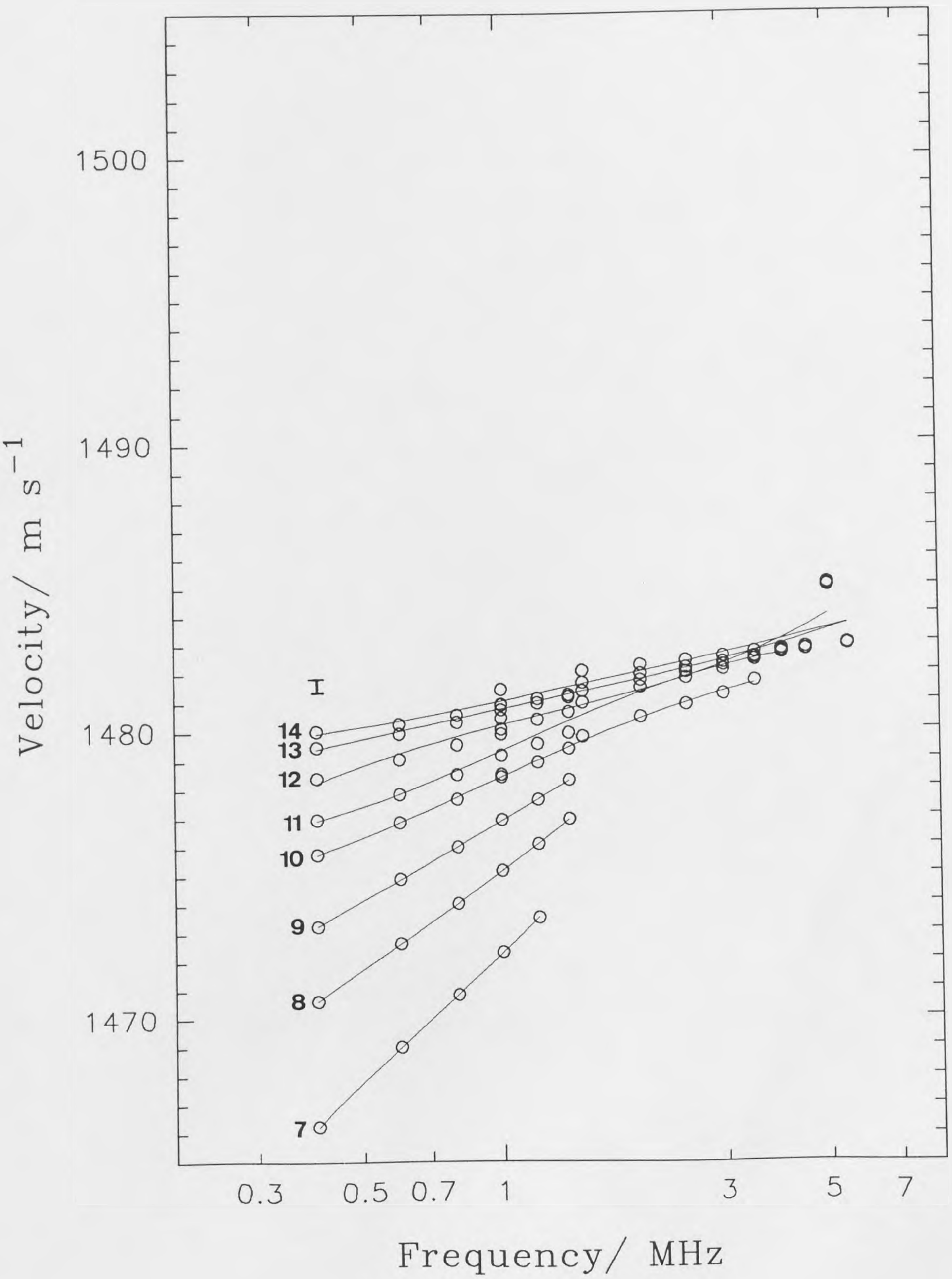

Figure 4.21 The measured ultrasonic velocity in aerated sample four as a function of frequency. Regression lines are drawn through the data for the dilutions which could be characterised. The labels indicate the dilution number. The bar indicates the estimated accuracy of the measurement, when applied to standard liquids under controlled conditions.

The attenuation was high in all the dilutions of aerated sample four (*Fig. 4.22*) and the dilutions were well resolved. This is in keeping with the larger volume fraction of air which is expected in the sample (because it was prepared with a lot of concentrated bubbly liquid). Notice that both the transducers in the FSUPER seemed to have an upper limit of attenuation of about 40 Np m^{-1}, above which they were unable to characterise bubbly liquid using transmission measurements.

The densitometer was not able to discriminate between the air-free and aerated versions of sample four, even though the higher volume fraction of air should have been easier to detect. In the absence of any value for the volume fraction it was decided not to perform any theoretical calculations for sample four.

The volume fraction in the liquid examined by the FSUPER can be calculated from the ultrasonic measurements, assuming that the Wood equation can be applied and that no air dissolved during the dilutions, using the technique described in Section 4.2.4.2. Accordingly, a fourth degree polynomial was fitted to the difference in the reciprocal squares of the velocities at 0.6 MHz in aerated and air-free sample four (*Fig. 4.23*). There was a very good fit to the data, because the differences between the two velocities were bigger, and the scatter in the measurements was thus smaller. The coefficient d in *Equation 4.10* was given here by 6.32×10^{-8}, which yielded a volume fraction of 9.0×10^{-6}. This was rather higher than the volume fraction seen in sample two, and was in accordance with the larger amount of concentrated bubbly liquid used to prepare sample four. It would seem that, for this sample, the liquid in the densitometer was more like the liquid which was probed by the ultrasound. The higher volume fraction of air probably accounted for the dispersion which was seen in the results.

The reflection coefficient of aerated sample four (*Fig. 4.24*) was markedly different from the reflection coefficient of the unaerated sample (*Fig. 4.25*). The form of the reflection coefficient of the aerated sample was similar to that of sample three (*Fig. 4.17*). The real part of the reflection coefficient had a negative slope, and a slight peak was discernible in the imaginary part, suggesting the presence of small bubbles. There was a lot of scatter in the measurements at frequencies below 0.5 MHz, especially in the higher numbered dilutions. This scatter was also present in

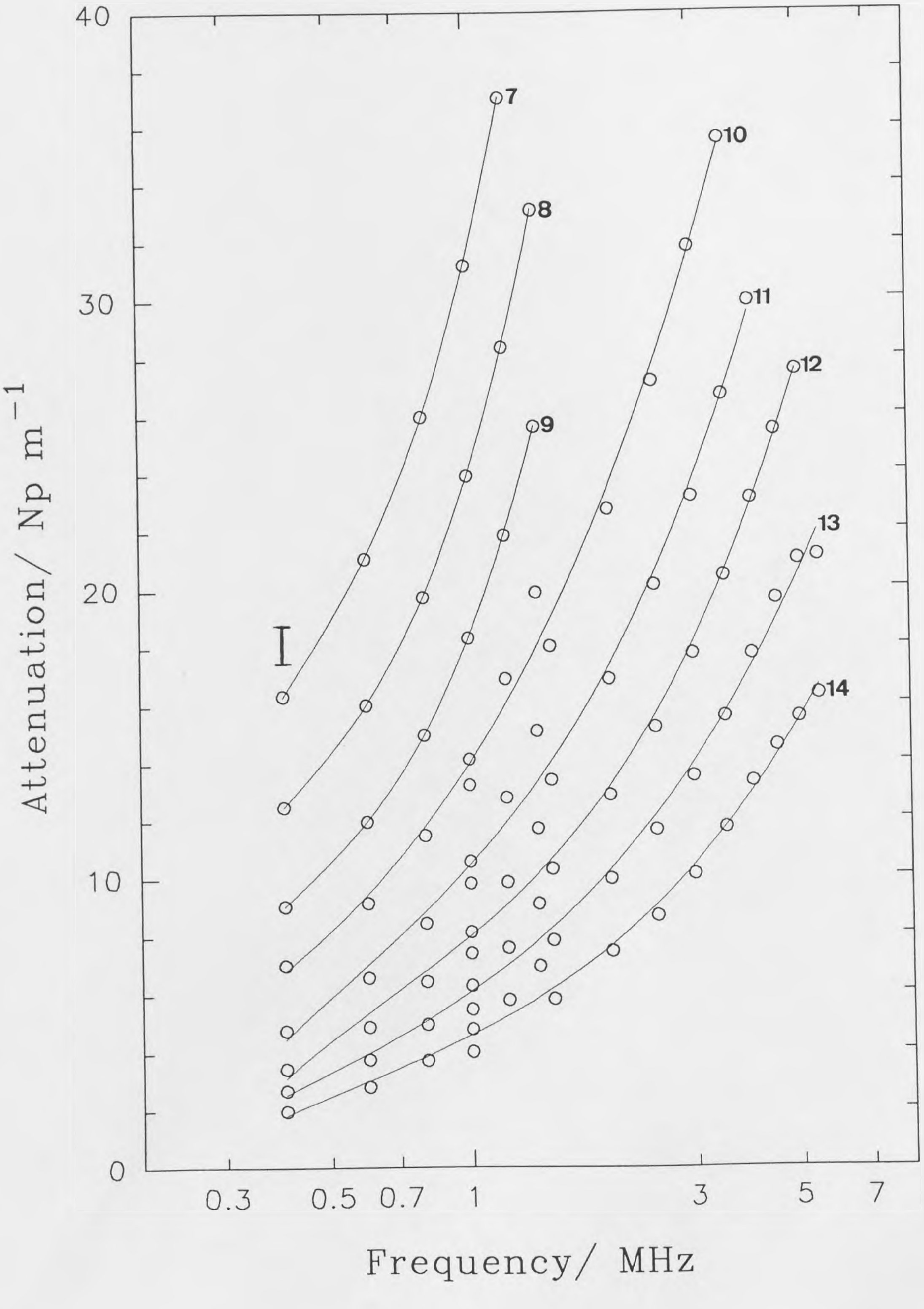

Figure 4.22 The measured attenuation coefficient in aerated sample four as a function of frequency. Regression lines are drawn through the data for the dilutions which could be characterised. The labels indicate the dilution number. The bar indicates the accuracy of the measurement, when applied to standard liquids under controlled conditions.

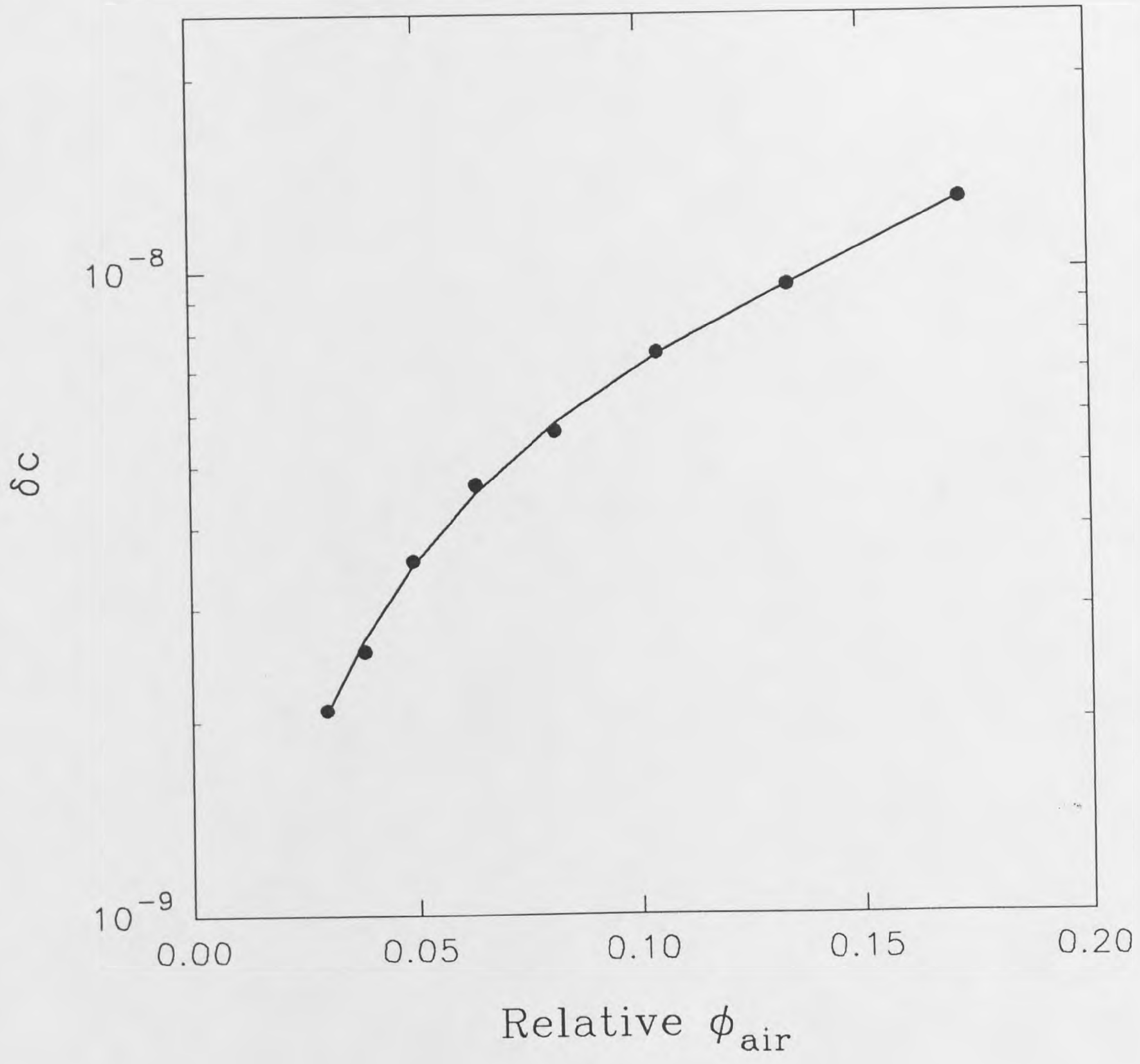

Figure 4.23 The difference in the velocities of aerated and air free versions of sample four (c and c' respectively) are plotted as a function of the relative volume fraction. The quantity δc is given by $1/c^2 - 1/c'^2$. The line is the least squares fit of the polynomial given by *Equation 4.10*.

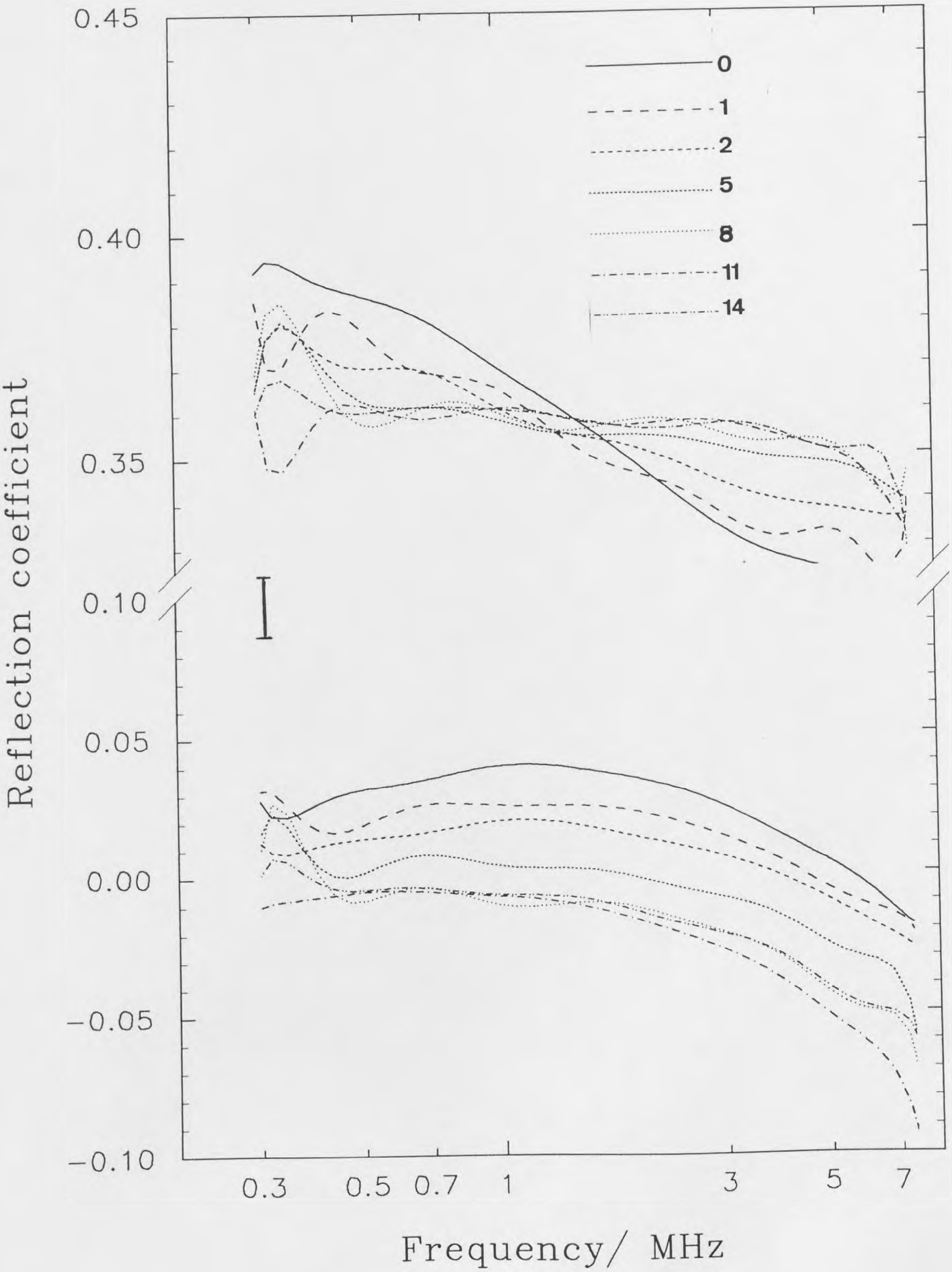

Figure 4.24 The measured real part (upper curves) and imaginary part (lower curves) of the reflection coefficient of aerated sample four as a function of frequency. Regression lines are drawn through the data, which are labelled with the appropriate dilution number. The data points have been omitted in order to improve clarity. The bar indicates the estimated accuracy of the measurement, when applied to standard liquids under controlled conditions.

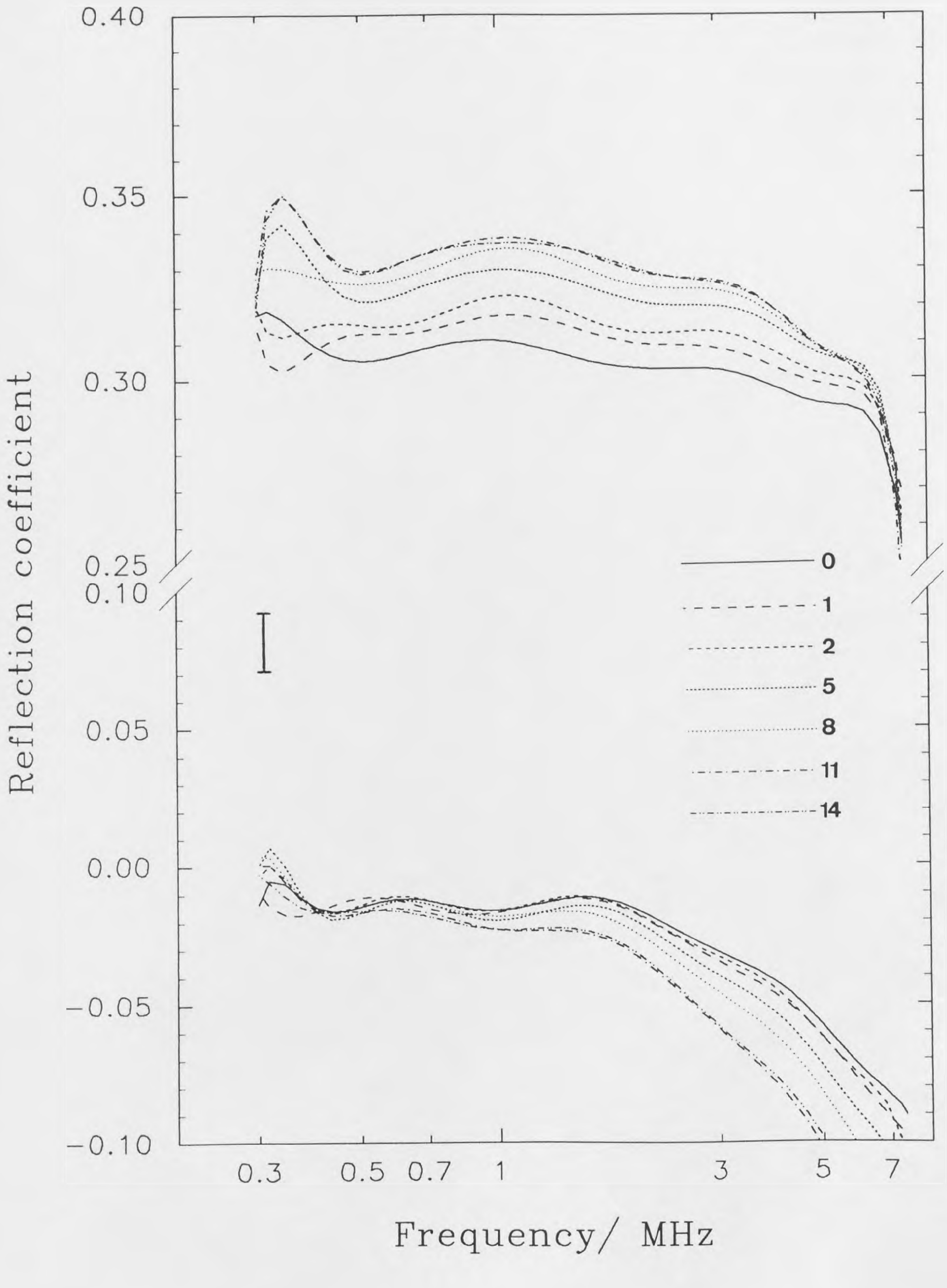

Figure 4.25 The measured real part (upper curves) and imaginary part (lower curves) of the reflection coefficient of air-free sample four as a function of frequency. The curves are labelled with the appropriate dilution number. The bar indicates the estimated accuracy of the measurement, when applied to standard liquids under controlled conditions.

the measurements on the unaerated sample (*Fig. 4.25*). The reason for this scatter in the data is not known. The tendency for the imaginary part of the reflection coefficient to apparently become negative at high frequencies, which was noted in previous samples, was seen again for sample four.

4.2.7 Sample five

Sample five was prepared with same amount of concentrated bubbly liquid as sample four, but the concentrated bubbly liquid contained more P1670. Sample five might reasonably be expected to have contained approximately the same amount of air as sample four.

The measured velocity in air-free sample five is shown in *Fig. 4.26*. The velocity in dilution zero was very close the velocity in dilution zero of sample four (cf *Fig. 4.19*). A different dilution regime was followed for sample five, however, with the dilution factor being returned to 8/9 for all but the highest numbered dilutions. Dilutions two, four, six and so on should have corresponded approximately to dilutions one, two, three and so on of air-free sample four. Comparison of *Figs. 4.26* and *4.19* shows that this was indeed the case. The attenuation in air-free sample five was however slightly higher than in air-free sample four (*Fig. 4.27*). This can presumably be attributed to the presence of extra P1670.

The measured velocity in aerated sample five was, surprisingly, little different from the velocity in the air-free version (*Fig. 4.28*). The main difference between the two sets of curves was the slight dispersion seen in the aerated version. The various dilutions were therefore well resolved. As in sample four, the dispersion suggested that the measurement frequencies were below the resonant frequency of the bubbles, which were therefore small. The attenuation in aerated sample five was rather higher than in the air-free version (*Fig. 4.29*), but it was somewhat lower than the values seen in sample four (*Fig. 4.22*) and was more like the attenuation in aerated sample two (*Fig. 4.7*). This suggested that the volume fraction of air in sample five was very low.

The predicted velocity in aerated sample five is shown in *Fig. 4.30*. This prediction seems to be in slightly better agreement with the observed data than the predic-

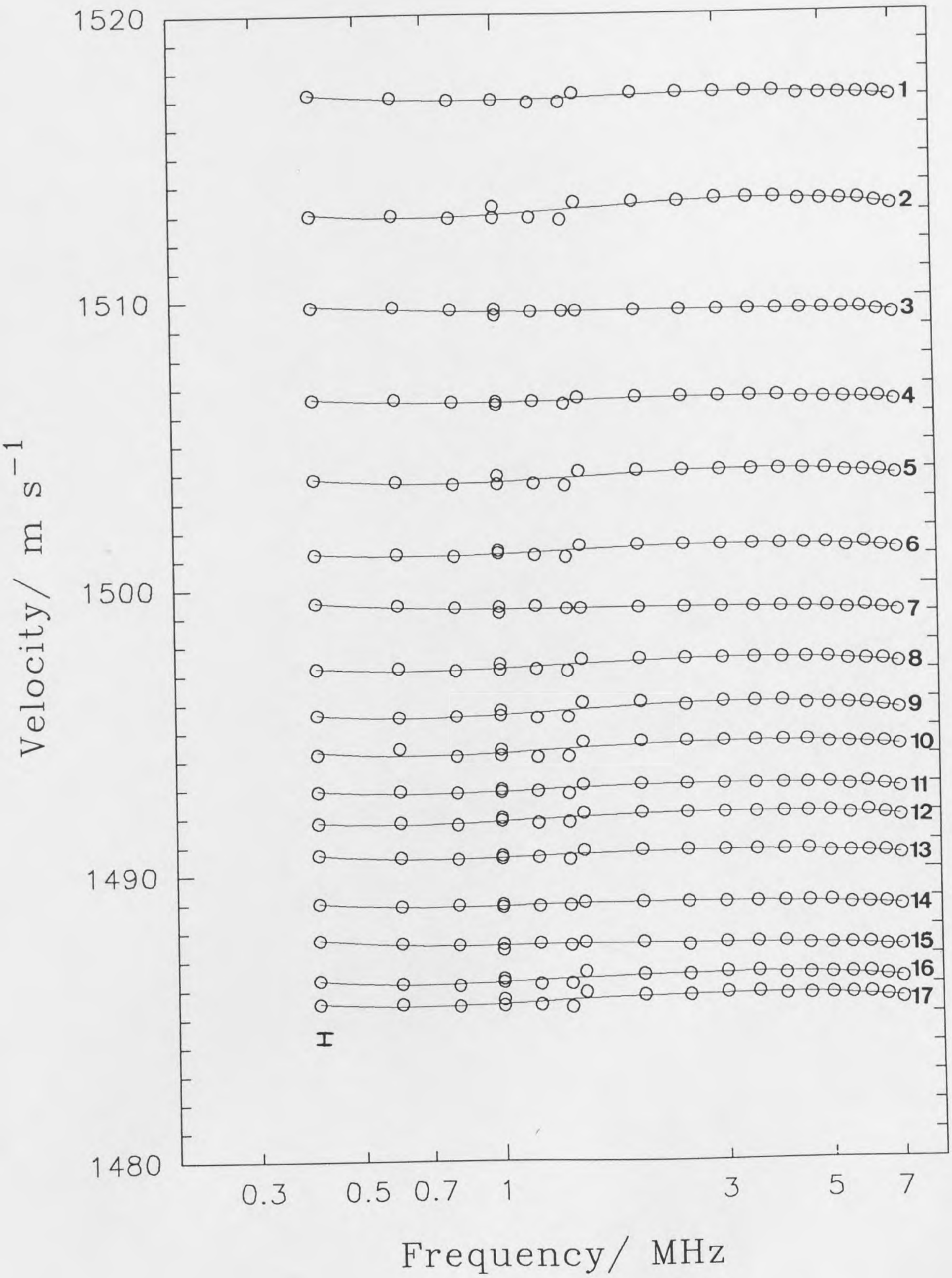

Figure 4.26 The measured ultrasonic velocity in air-free sample five as a function of frequency. Regression lines are drawn through the data, which are labelled with the appropriate dilution number. The bar indicates the estimated accuracy of the measurement, when applied to standard liquids under controlled conditions.

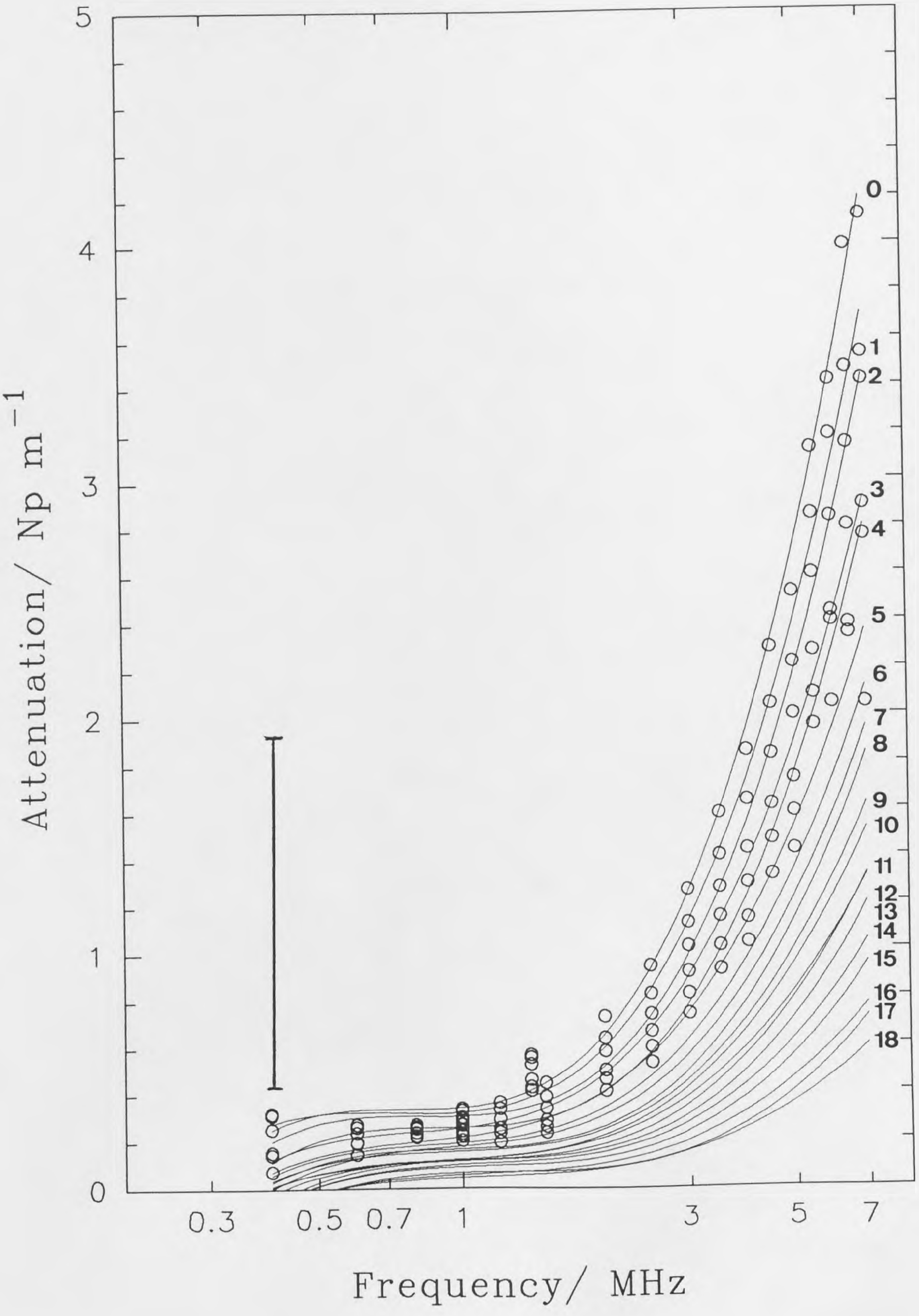

Figure 4.27 The measured attenuation coefficient in air-free sample five as a function of frequency. Regression lines are drawn through the data, which are labelled with the appropriate dilution number. Data points for higher numbered dilutions have been omitted to improve clarity. The bar indicates the estimated accuracy of the measurement, when applied to standard liquids under controlled conditions.

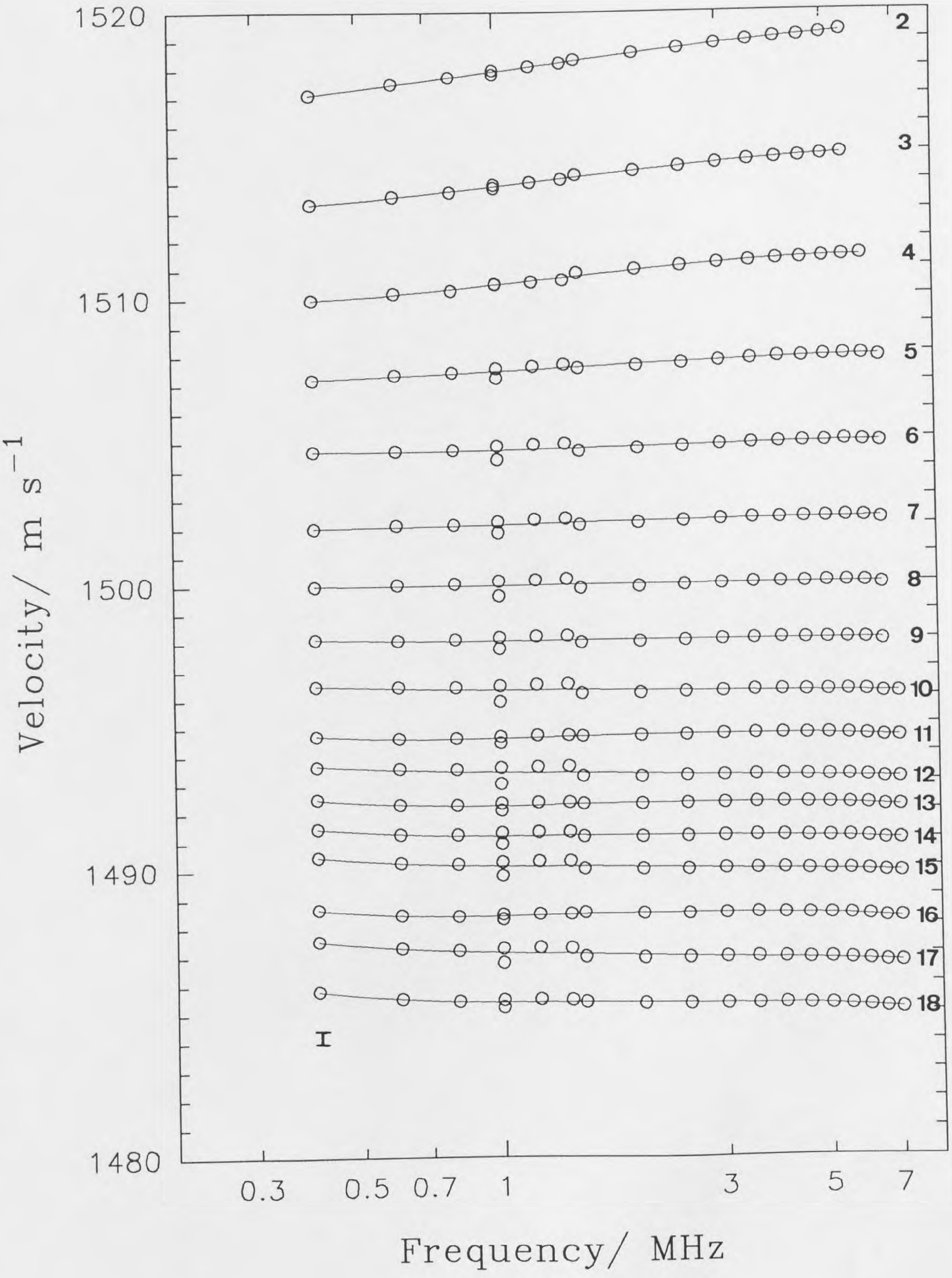

Figure 4.28 The measured ultrasonic velocity in aerated sample five as a function of frequency. Regression lines are drawn through the data which are labelled with the appropriate dilution number. The bar indicates the estimated accuracy of the measurement, when applied to standard liquids under controlled conditions.

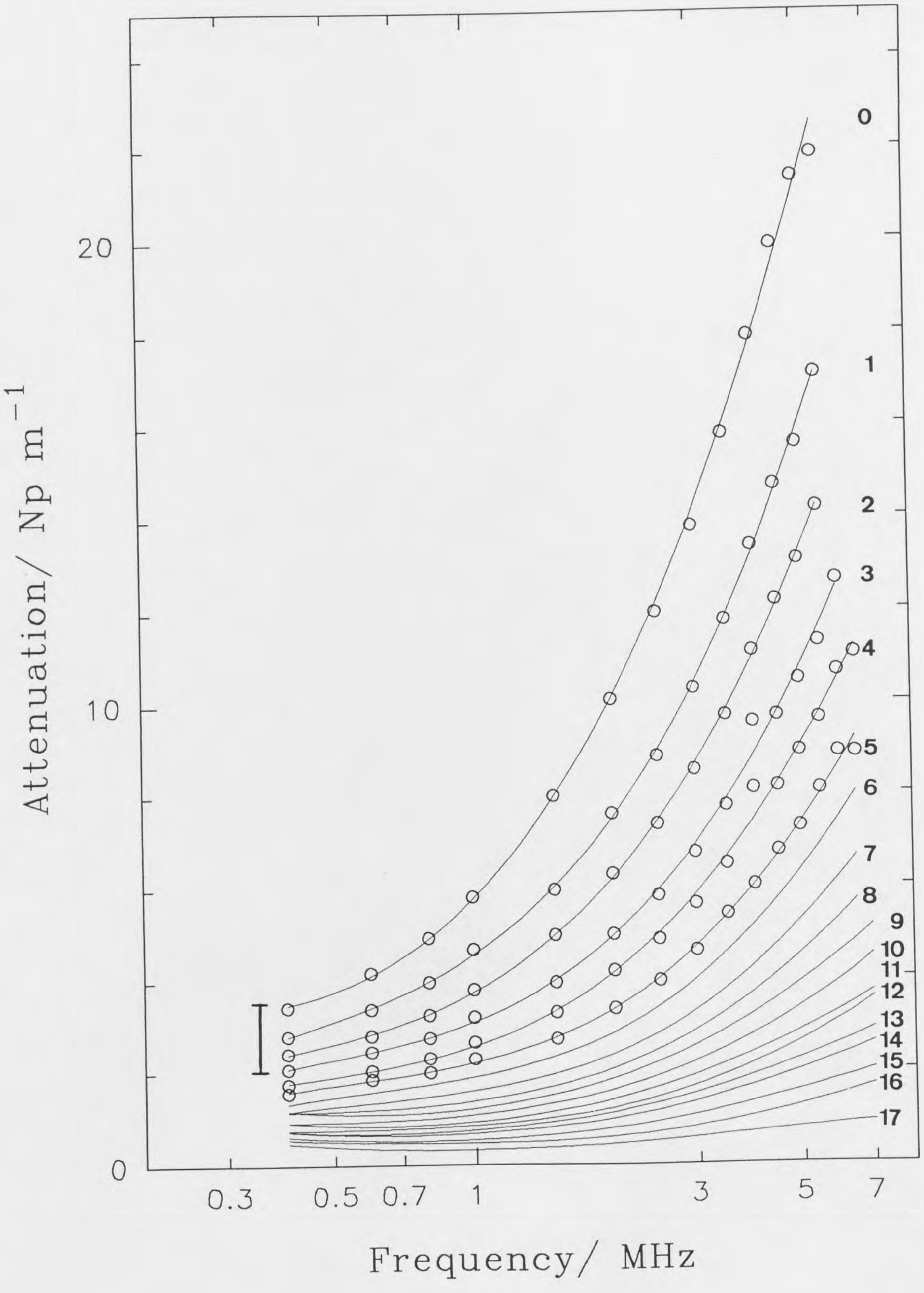

Figure 4.29 The measured attenuation coefficient in aerated sample five as a function of frequency. Regression lines are drawn through the data, which are labelled with the appropriate dilution number. Data points for higher numbered dilutions are omitted for clarity. The bar indicates the estimated accuracy of the measurement, when applied to standard liquids under controlled conditions.

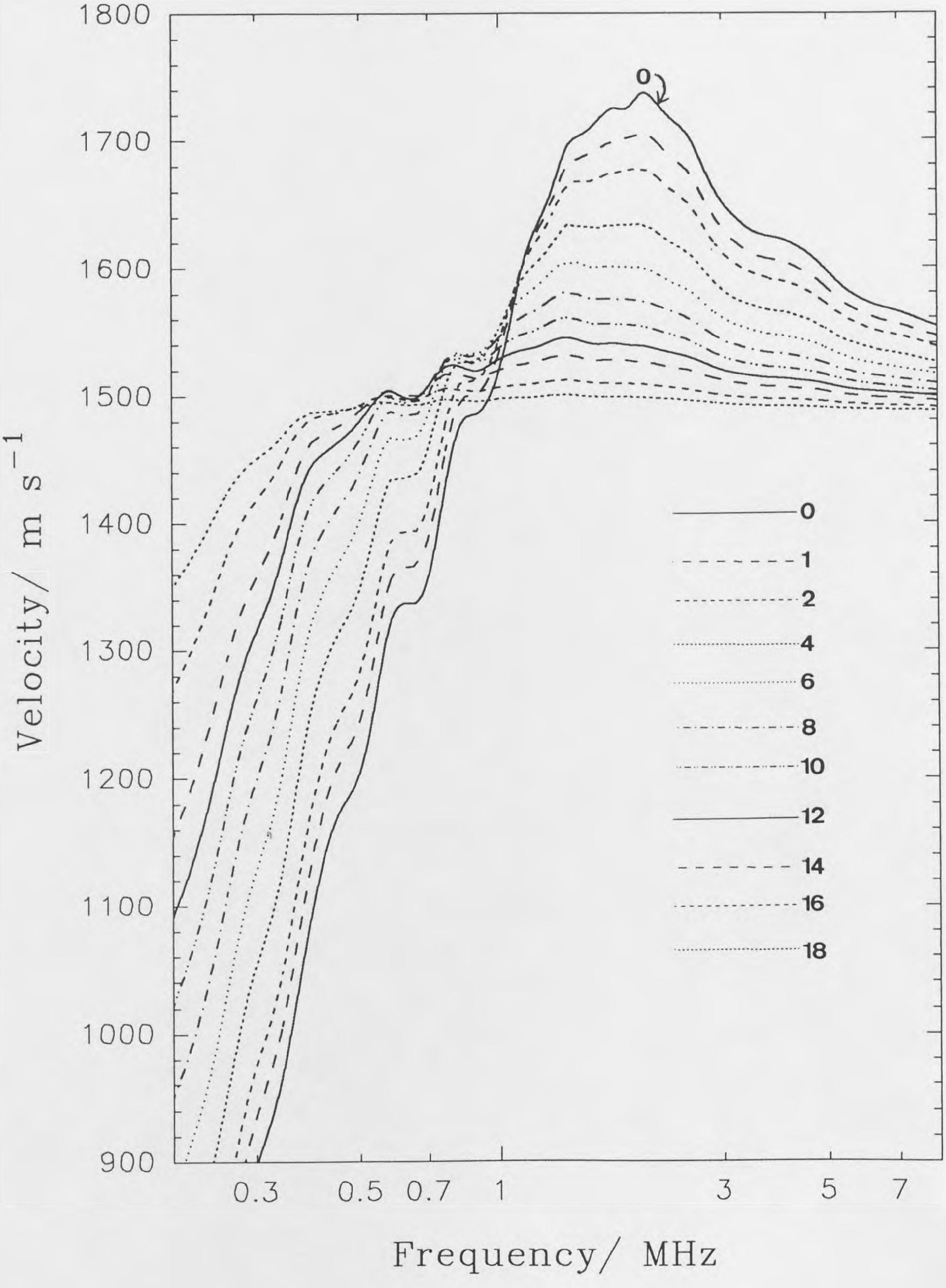

Figure 4.30 The predicted ultrasonic velocity in aerated sample five as a function of frequency. The curves are labelled with the appropriate dilution number.

tions for aerated samples two and three. The predicted ultrasonic velocity for the highest numbered dilution is actually reasonably close to the observed value. Of course, the predictions for lower numbered dilutions are very different from the observed velocities. This can be attributed to the unexpectedly low volume fraction in the liquid in the FSUPER. The predicted attenuation coefficient (*Fig. 4.31*) bears very little resemblance to the measured values of the attenuation coefficient.

The reflection coefficient of aerated sample five is shown in *Fig. 4.32*. The scatter in the measurements at low frequencies which was seen in the measurements for sample four was also seen here. In fact the scatter was rather more marked, especially in the measurements on the higher numbered dilutions. The form of the predicted reflection coefficient (*Fig. 4.33*) is similar in some respects to the form of the measured reflection coefficient. The reliability of the reflection measurements is however too questionable to allow any conclusions to be drawn from this similarity. It is most likely that the resemblance arises from fortuitous scatter in the measured values of the reflection coefficient.

Finally, consider the difference in the inverse squares of the velocity at 4 MHz in aerated and air-free sample five (*Fig. 4.34*). It will be recalled that the relationship between this figure and the total dilution of the sample can be used to obtain the volume fraction (*Equation 4.10*). Notice that the polynomial does not fit the data well at low relative volume fraction. The difference between the velocities at 4 MHz in the aerated and air-free versions was very small, and any scatter in the velocity measurements was made more pronounced by the squaring of the velocity. The coefficient d in *Equation 4.10* was given here by 4.0×10^{-9}, which indicated a volume fraction of air of 5.7×10^{-7}. This was very close to the value of the volume fraction in sample two.

4.2.8 Ultrasound as a probe of the dilute model bubbly liquid

The experimental measurements of velocity and attenuation do not agree with the predictions from theory. The theory relies upon measurements of volume fraction and bubble size from conventional techniques. The presence of bubbles with radius of 20 μm at a volume fraction of 10^{-4} *in the FSUPER* can be ruled out categorically by this disagreement. The absence of resonant behaviour at frequencies

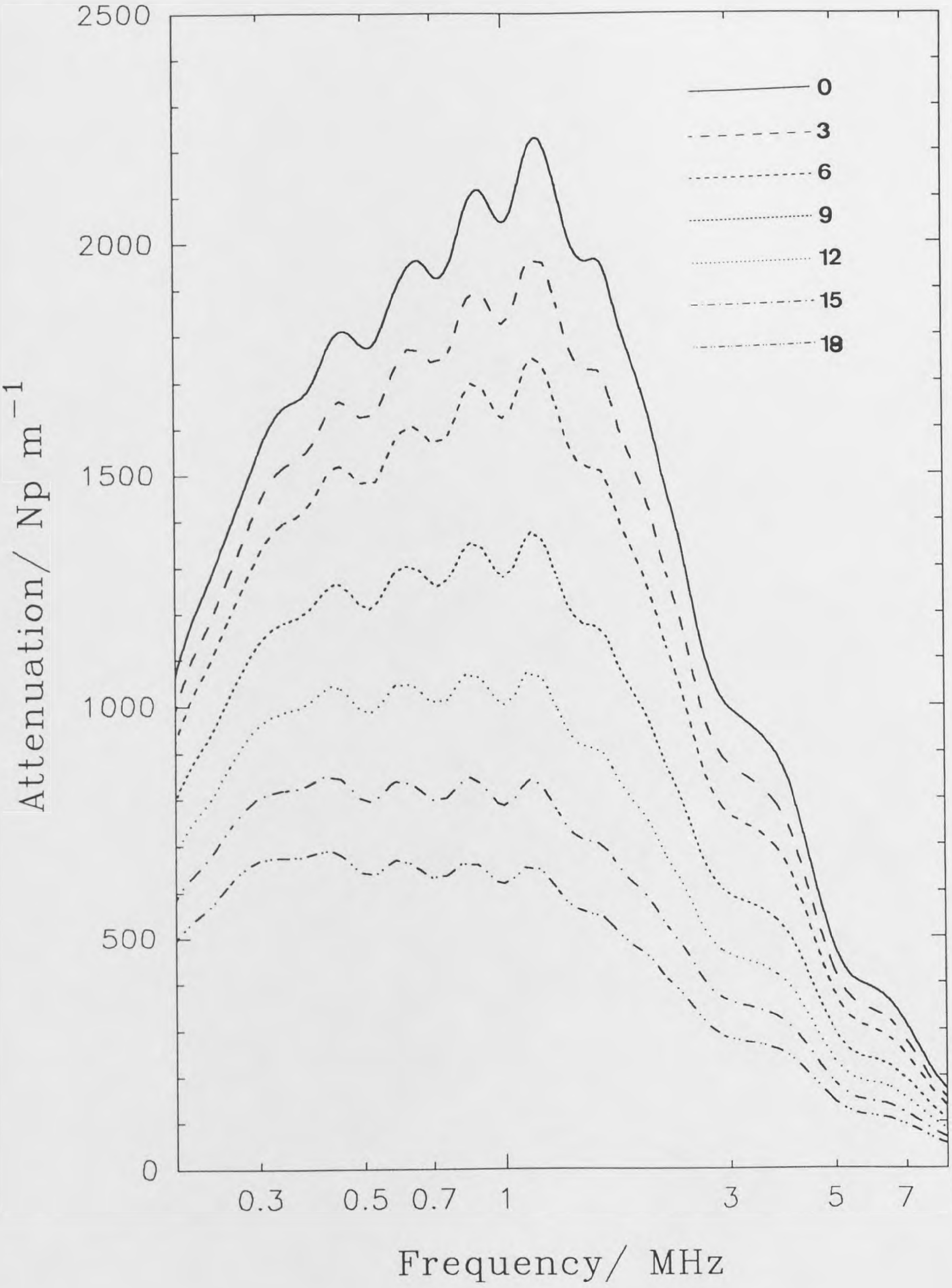

Figure 4.31 The predicted attenuation coefficient in aerated sample five as a function of frequency. The curves are labelled with the appropriate dilution number.

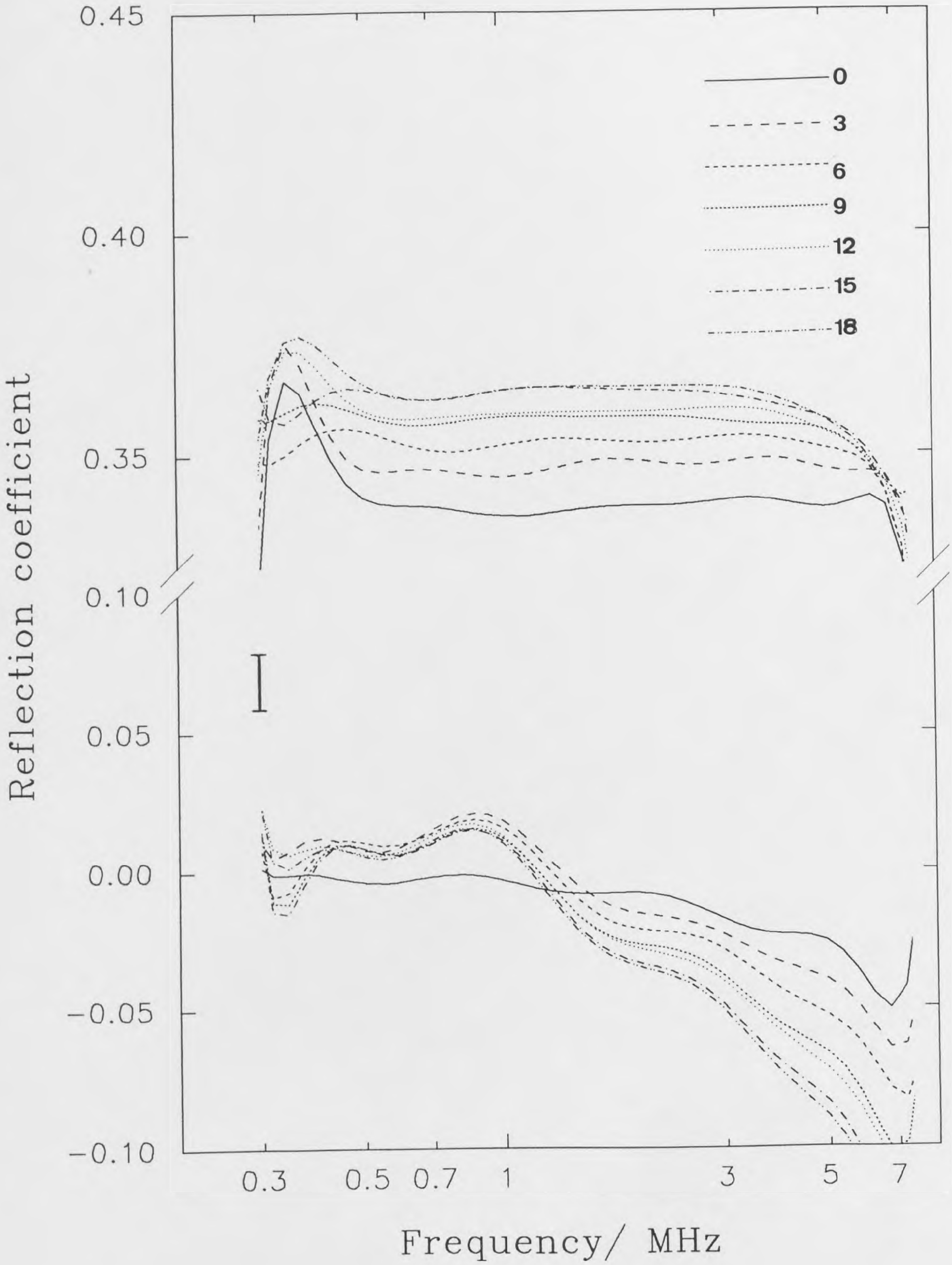

Figure 4.32 The measured real part (upper curves) and imaginary part (lower curves) of the reflection coefficient of aerated sample five as a function of frequency. Regression lines are drawn through the data which are labelled with the appropriate dilution number. The data points have been omitted for clarity. The bar indicates the estimated accuracy of the measurement, when applied to standard liquids under controlled conditions.

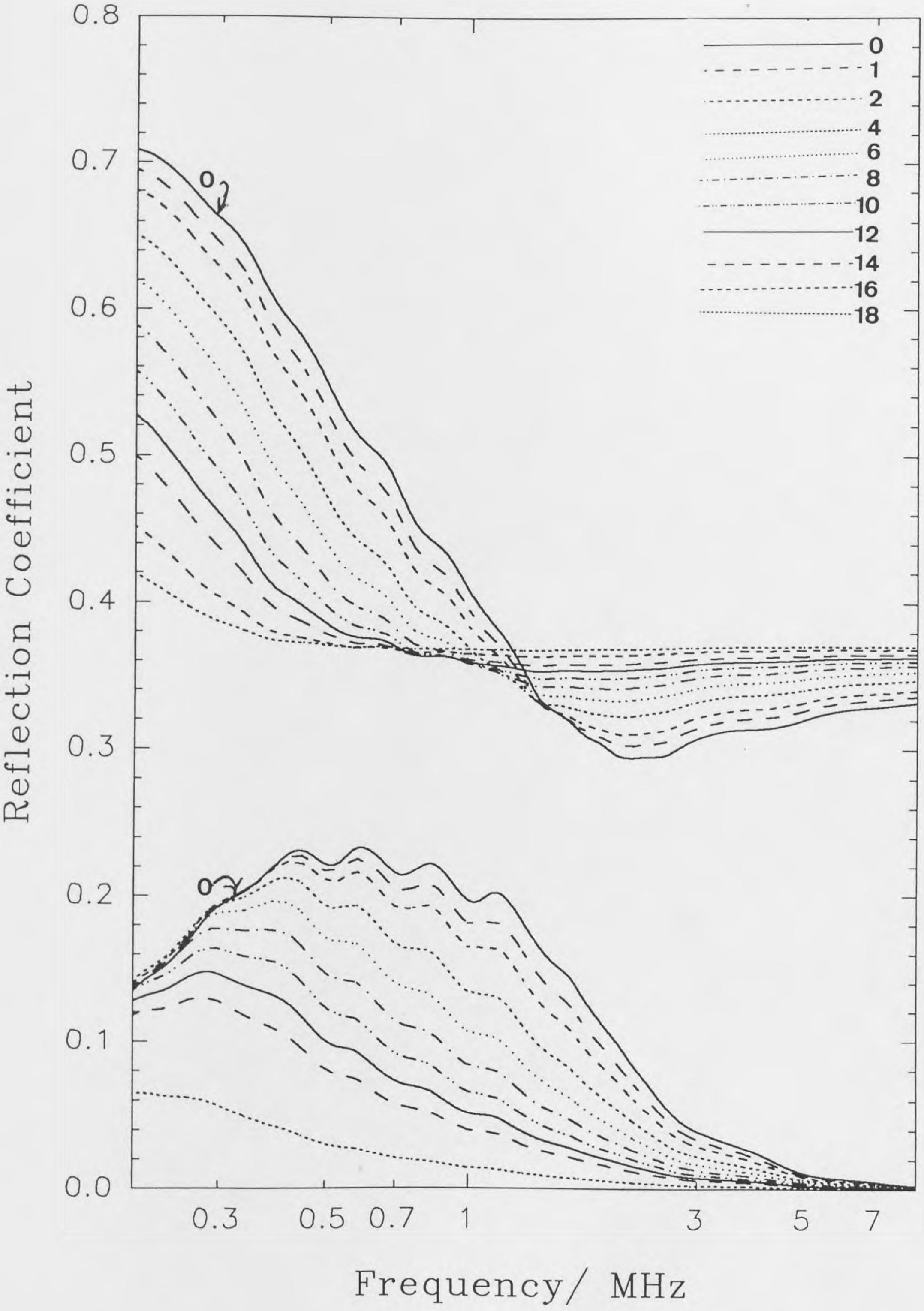

Figure 4.33 The predicted real part (upper curves) and imaginary part (lower curves) of the reflection coefficient of aerated sample five as a function of frequency. The curves are labelled with the appropriate dilution number.

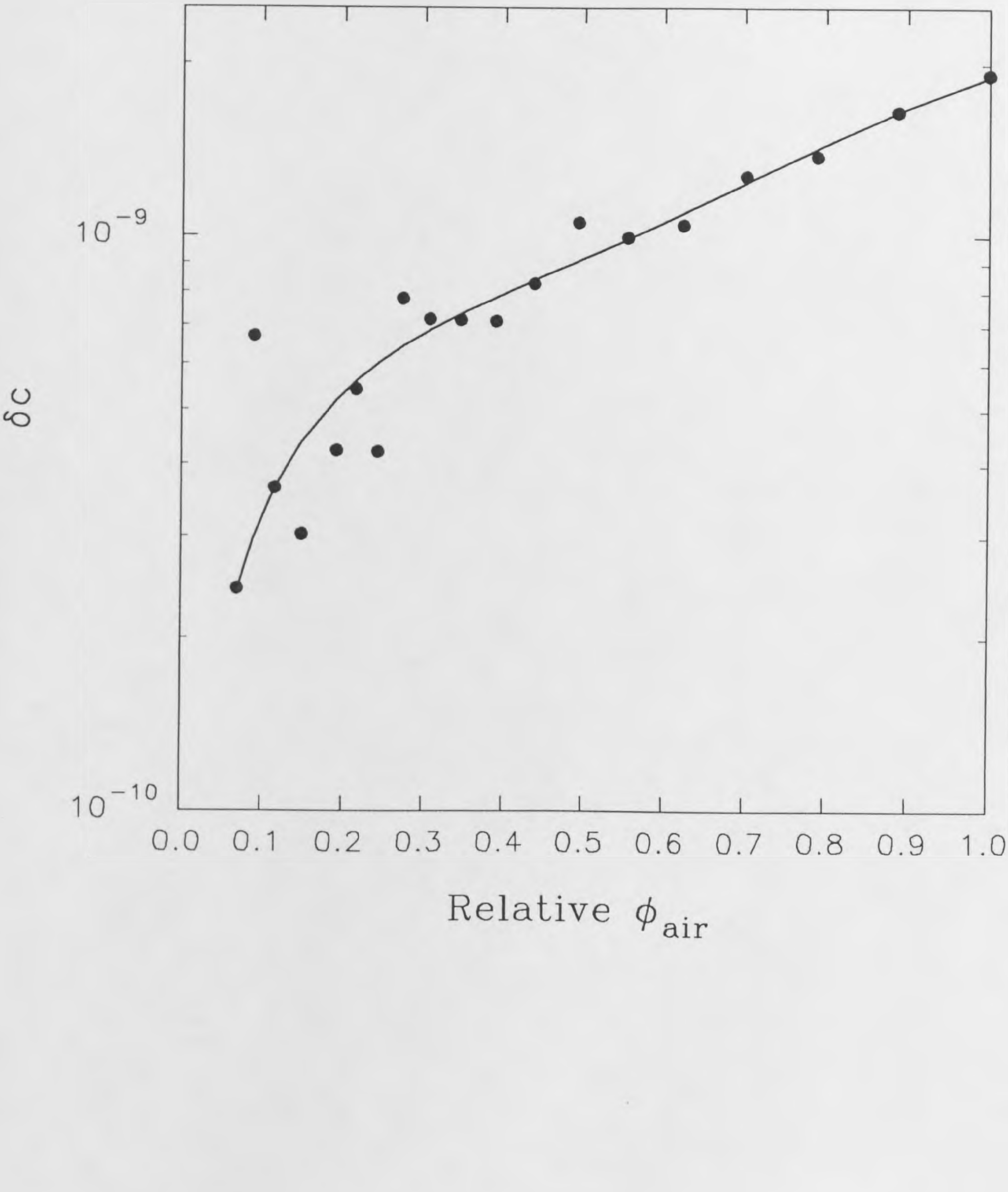

Figure 4.34 The difference in the velocities of aerated and air free versions of sample five (c and c' respectively) are plotted as a function of the relative volume fraction. The quantity δc is given by $1/c^2 - 1/c'^2$. The line is the least squares fit of the polynomial given by *Equation 4.10.*

below 8 MHz indicated that, according to the Minnaert equation, the bubbles had radii which were smaller than 4 μm. The conventional techniques may well have given reasonable values, but these values did not reflect the conditions within the ultrasonic equipment.

Although it was disappointing that the theory could not be shown to agree with measurements, it was at least possible to measure the volume fraction of gas. The serial dilution technique suggests that the volume fraction was of the order of 10^{-7} in two samples, and of the order of 10^{-5} in one sample. The serial dilution method was therefore a very sensitive technique for measuring small volume fractions of dispersed gas. In the absence of equally sensitive conventional techniques it is not possible to assess the accuracy of the ultrasonic technique for characterising the dilute model bubbly liquid.

4.3 Concentrated model bubbly liquid

The volume fraction of gas in real aerated foods of interest is much higher than the volume fraction in the dilute model. Thus from a practical point of view the limited success of the measurements on the dilute model are not terribly significant. The measurements on the concentrated model are the ones which would be expected to be crucial in establishing if it is possible to relate ultrasonic measurements to the volume fraction or the bubble size in real foods. The concentrated bubbly liquid was much too attenuating to allow transmission measurements, so only the reflection coefficient (or the acoustic impedance) of the concentrated samples was determined.

4.3.1 Measurements in the UPER

Concentrated model bubbly liquids were prepared using P1670 at concentrations of 0.5 and 1 wt%, resulting in volume fractions of air of 50-55 ± 1 %. Various amounts of these liquids were mixed with 70 wt% Sweetose to give dilute samples with volume fractions as low as 1.3 ± 0.1 %. The acoustic impedance of the concentrated and dilute liquids was measured in the UPER at 20 °*C*. The results for the systems prepared using 0.5wt% P1670 and 1.0 wt% P1670 are shown in *Fig. 4.35*. As the volume fraction of air increased, the acoustic impedance of the aerated syrup became lower and lower. Unfortunately, the dilute systems were not very

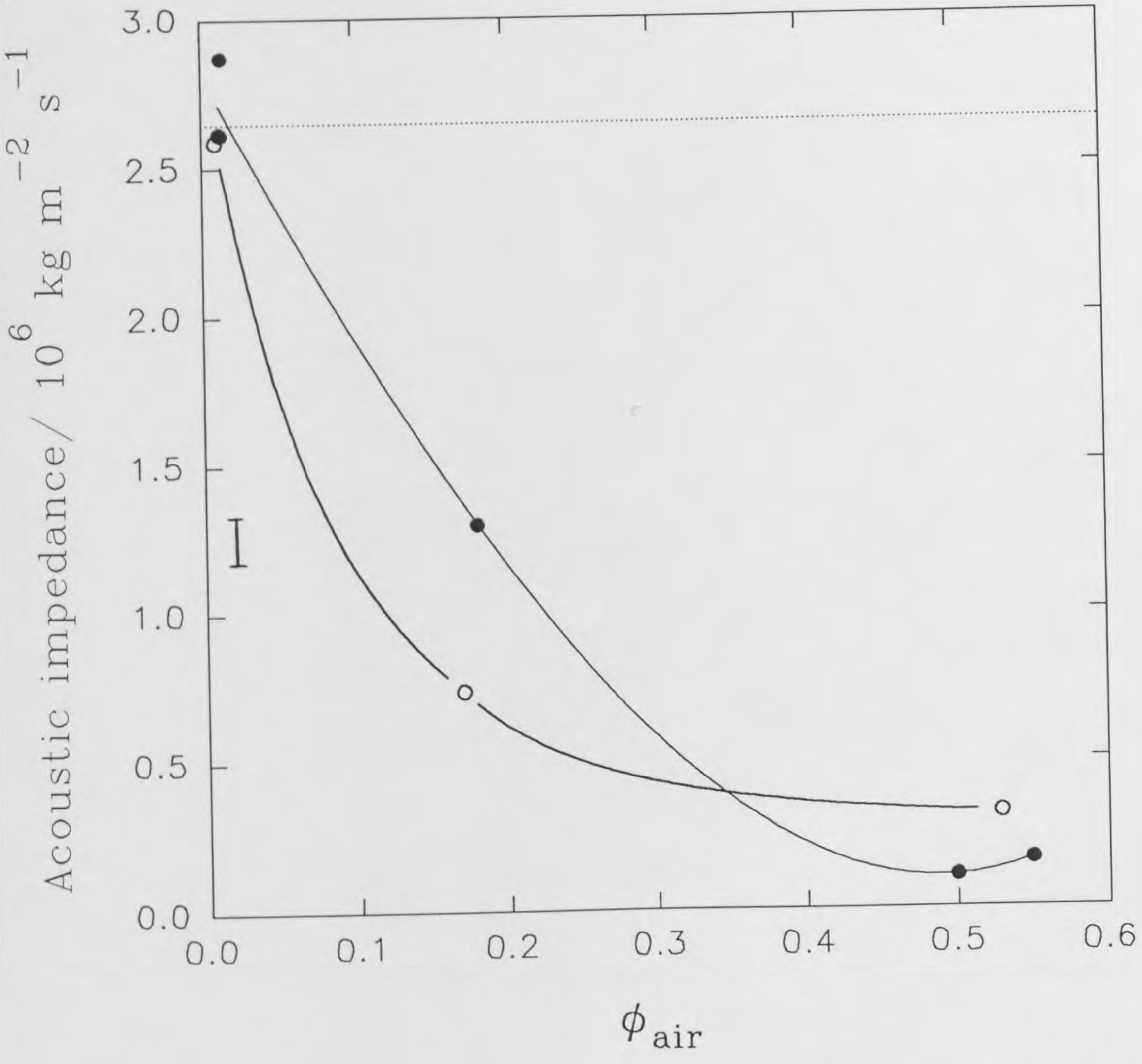

Figure 4.35 The measured acoustic impedance of aerated Sweetose as a function of the volume fraction of air. The dispersions were stabilised by P1670 at concentrations of 0.5 wt% (●) and 1 wt% (○) in the stock bubbly liquid. A regression is drawn through the data points, and the dotted line shows the characteristic impedance of air-free 70 wt% Sweetose. The bar indicates the estimated accuracy of the measurement, when applied to standard liquids under controlled conditions.

Table 4.4 *Measured properties of the concentrated model bubbly liquid*

Sample	*Surfactant*	ϕ_{air}/%	r_{32}/ μm †
1	P1670	56 ± 1	--
2	P1670	58 ± 1	--
3	P1670	53 ± 1	--
4	P1670	45 ± 1	--
5	P1670	49 ± 1	--
6	P1670	56 ± 1	--
7	P1670	55 ± 1	--
8	P1670	46 ± 1	17.2 ± 1.8
9	P1670	53 ± 1	11.2 ± 1.0
10	P1670	44 ± 1	20.4 ± 2.8
11	P1670	55 ± 1	11.6 ± 2.6
12	P1670	56 ± 1	12.5 ± 1.5
average		52 ± 5	14.8 ± 4.3
1	Hyfoama	66 ± 1	--
2	Hyfoama	64 ± 1	--
3	Hyfoama	64 ± 1	--
4	Hyfoama	55 ± 1	--
5	Hyfoama	53 ± 1	--
6	Hyfoama	60 ± 1	--
7	Hyfoama	64 ± 1	48.5 ± 7.3
8	Hyfoama	62 ± 1	46.3 ± 5.9
9	Hyfoama	52 ± 1	38.3 ± 0.8
10	Hyfoama	66 ± 1	48.4 ± 3.7
average		61 ± 5	45.2 ± 6.2

†: average of 3 or 4 measurements for each sample

stable to creaming, despite the high viscosity of the syrup. This approach was therefore dropped, and the remaining measurements on the model bubbly liquid were performed on the unadulterated concentrated form of the bubbly liquid.

4.3.2 Measurements in the FSUPER

Samples of concentrated bubbly liquid were prepared using the surfactants P1670 and Hyfoama at a concentration of 1 wt% in the pre-mix. *Table 4.4* lists the volume fraction of air (ϕ_{air}) and, for selected samples, the Sauter mean radius (r_{32}), determined by the Mastersizer, of the bubbles in each sample. Notice that there was a clear difference in the distributions found in the bubbly liquids stabilised with the different surfactants. The bubbly liquid stabilised by Hyfoama had much larger bubbles, and the volume fraction was rather higher. The bubble sizes were measured by dispersing small amounts of the concentrated bubbly liquid in Sweetose syrup (see Section 3.2.6.1). The r_{32} values were in good agreement with the bubble sizes measured in the dilute model bubbly liquid. There was a fair degree of variability in the bubble size and the volume fraction of air in the concentrated bubbly liquid.

4.3.2.1 Ultrasonic measurements on systems prepared using P1670

Inter sample variation, clearly seen in the volume fraction and particle size, was also observed in the ultrasonic measurement. The measurements have been grouped in order to create clearer graphs and facilitate interpretation of the results. The grouping is thus somewhat arbitrary, and undue importance should not be attached to it.

Samples one and two The results for these samples appeared to be unreliable and hence are not shown. Poor acoustic coupling between the transducers and the buffer rod was probably to blame.

Samples three & six and samples four & five The ultrasonic measurements for these samples are shown in *Figs. 4.36* and *4.37* respectively. The form of the curves through the real and imaginary parts of the reflection coefficient was similar to that of the curves which are predicted by theory (Section 3.2.4.3), which indicated that resonant behaviour was being observed in these samples. However, the theoretical curves to which the measurements are most similar in form are those predicted for systems which have a very much lower volume fraction of air.

The samples have been grouped according to the volume fraction of air in the sample. The volume fraction of air in samples four and five was about 15 per cent lower than in samples three and six, which is well within the variability expected in bubbly systems (Calvert & Nezhati, 1987). The difference in the reflection behaviour of the two pairs of samples was clear. Samples four and five appeared to contain bubbles which were larger than those in samples three and six, because the resonance in the imaginary part of the reflection coefficient occurred at a lower frequency. It is not clear whether or not the possible difference in bubble size was related to the difference in volume fraction between the two samples.

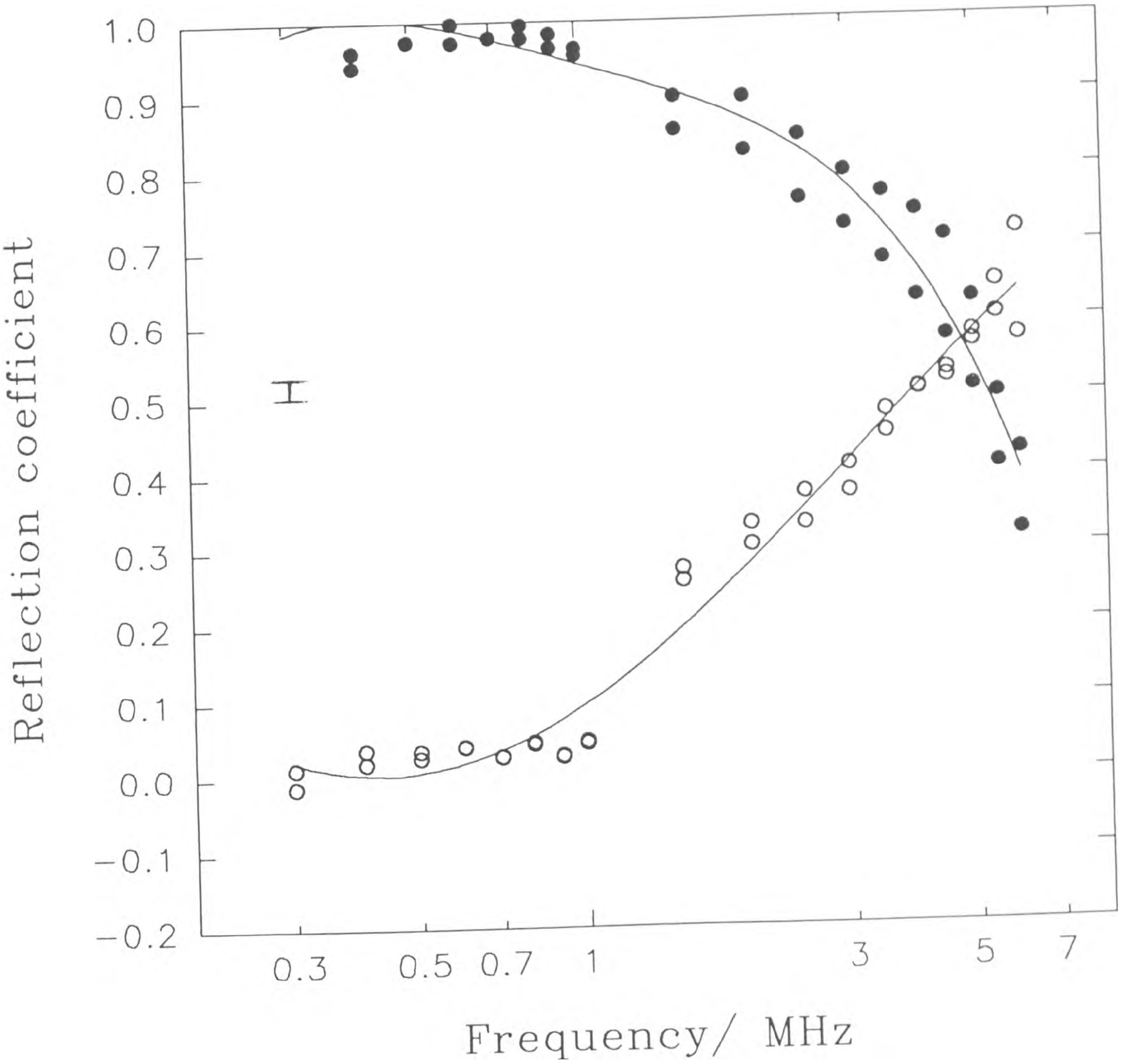

Figure 4.36 The measured real part (●) and imaginary part (○) of the reflection coefficient of concentrated bubbly liquid samples three and six, stabilised with P1670. The lines represent the average of the measurements for the two samples. The bar indicates the estimated accuracy of the measurement, when applied to standard liquids under controlled conditions.

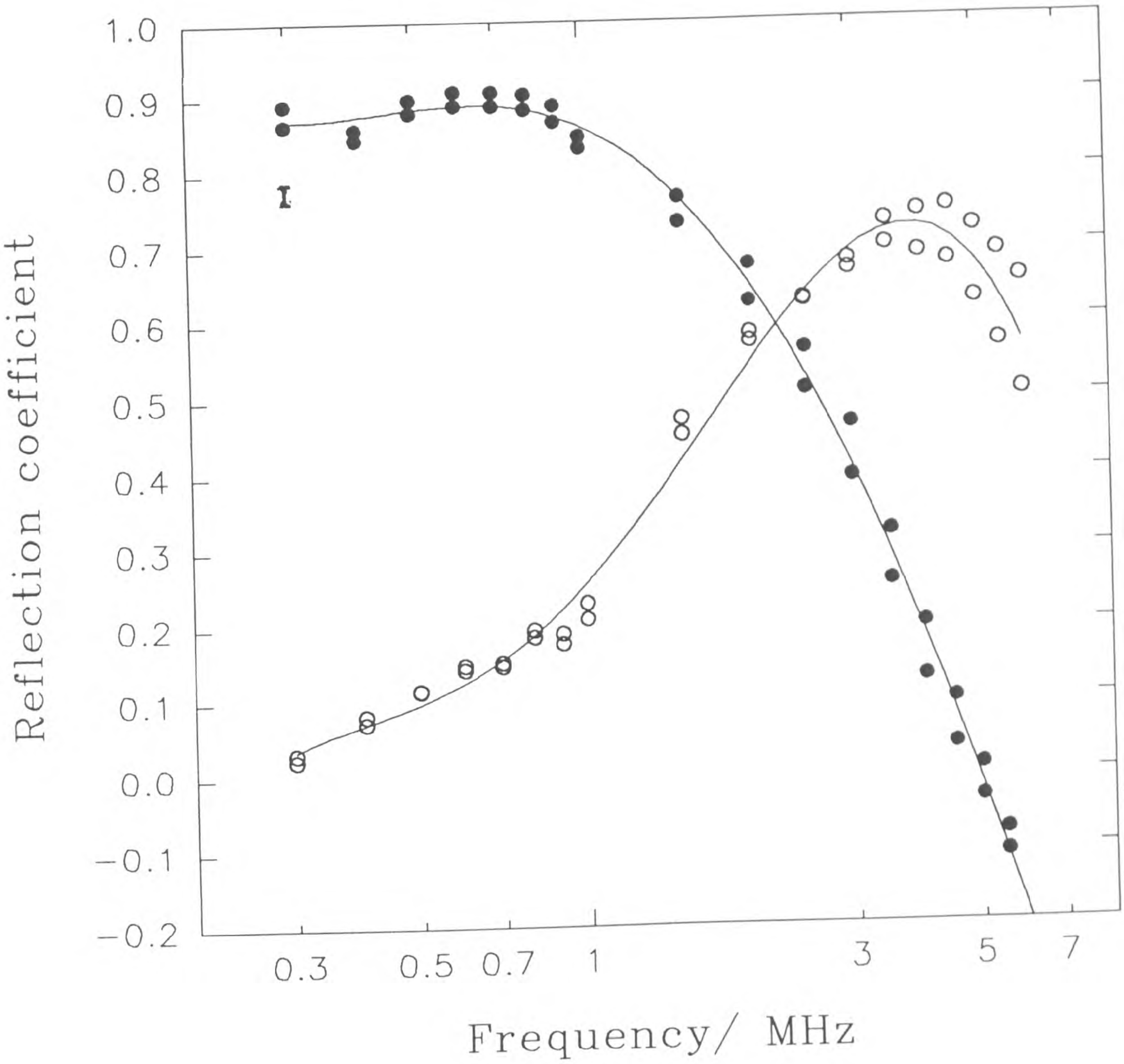

Figure 4.37 The measured real part (●) and imaginary part (○) of the reflection coefficient of concentrated bubbly liquid samples four and five, stabilised with P1670. The lines represent the average of the measurements for the two samples. The bar indicates the estimated accuracy of the measurement, when applied to standard liquids under controlled conditions.

Table 4.5 *The thermophysical properties of 70 wt% Sweetose at 20 °C, as required for calculations of effective medium theory*

Property	*70 wt% Sweetose*
Velocity of sound/ m s^{-1} (measured in FSUPER)	1942.3 ± 0.5
Density/ kg m^{-3} (measured in Paar densitometer)	1361.5 ± 0.1
Dynamic (shear) viscosity/ Pa s (taken from Hodges, 1990)	1.0 ± 0.1
Bulk modulus/ Pa	5.136×10^9
All other properties taken as those of water (see *Table 2.1*)	

Samples seven, eight and nine The ultrasonic measurements for these three samples are shown in *Fig. 4.38*. Note that the ordinate scale runs from -1.0 to +1.0. The resonant behaviour of these samples was rather different from that of samples three to six. The curves through the real and imaginary parts of the reflection crossed each other as expected, but the crossing point occurred at a much lower frequency. The remaining high frequency part of the curves deviated from the behaviour predicted theoretically, because both the real and imaginary parts of the reflection coefficient took on firstly large negative values and then large positive values. There was a suggestion of this behaviour in *Fig. 4.37*, wherein the real part of the reflection coefficient appears to be dropping towards negative values at high frequencies. Note that there was relatively little inter sample variation in the ultrasonic measurements for this group, despite the variation in the volume fraction of air.

Samples ten, eleven and twelve The ultrasonic measurements for these samples are shown in *Fig. 4.39*. The results for these samples were more like the results for samples three to six, and were similar in form to the theoretical curves for systems with a low volume fraction of air. There was a fairly marked inter sample variation in the ultrasonic measurements. The reflection coefficient in each of these samples was predicted using effective medium theory (EMT). The input parameters for the computer model of the EMT were the thermophysical properties of the Sweetose and air (see *Table 4.5*), the volume fraction of air, and the bubble size distribution

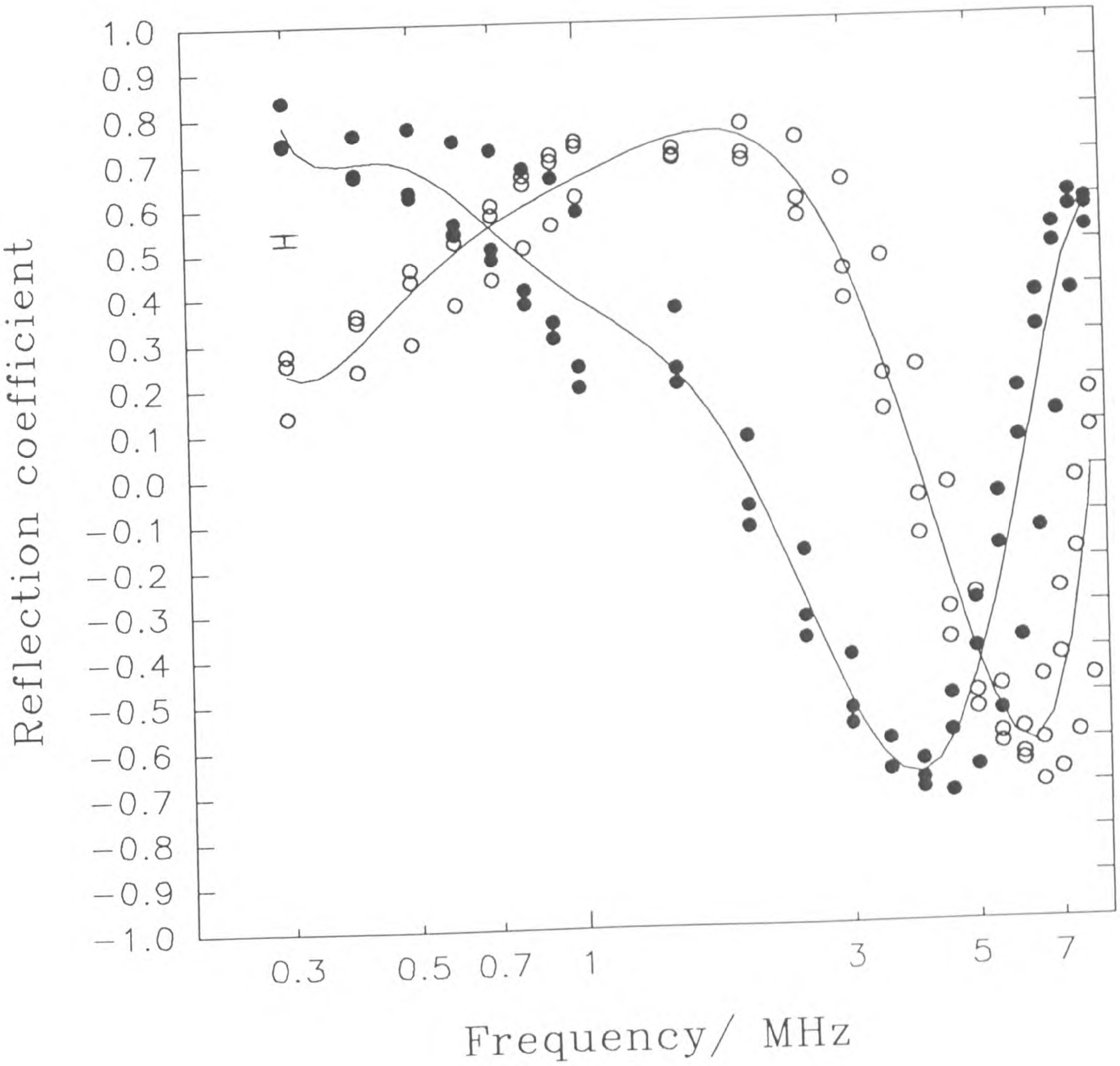

Figure 4.38 The measured real part (●) and imaginary part (○) of the reflection coefficient of concentrated bubbly liquid samples seven, eight and nine, stabilised with P1670. The lines represent the average of the measurements for the three samples. The bar indicates the estimated accuracy of the measurement, when applied to standard liquids under controlled conditions. Note that real and imaginary parts of the reflection coefficient both achieve very large negative values.

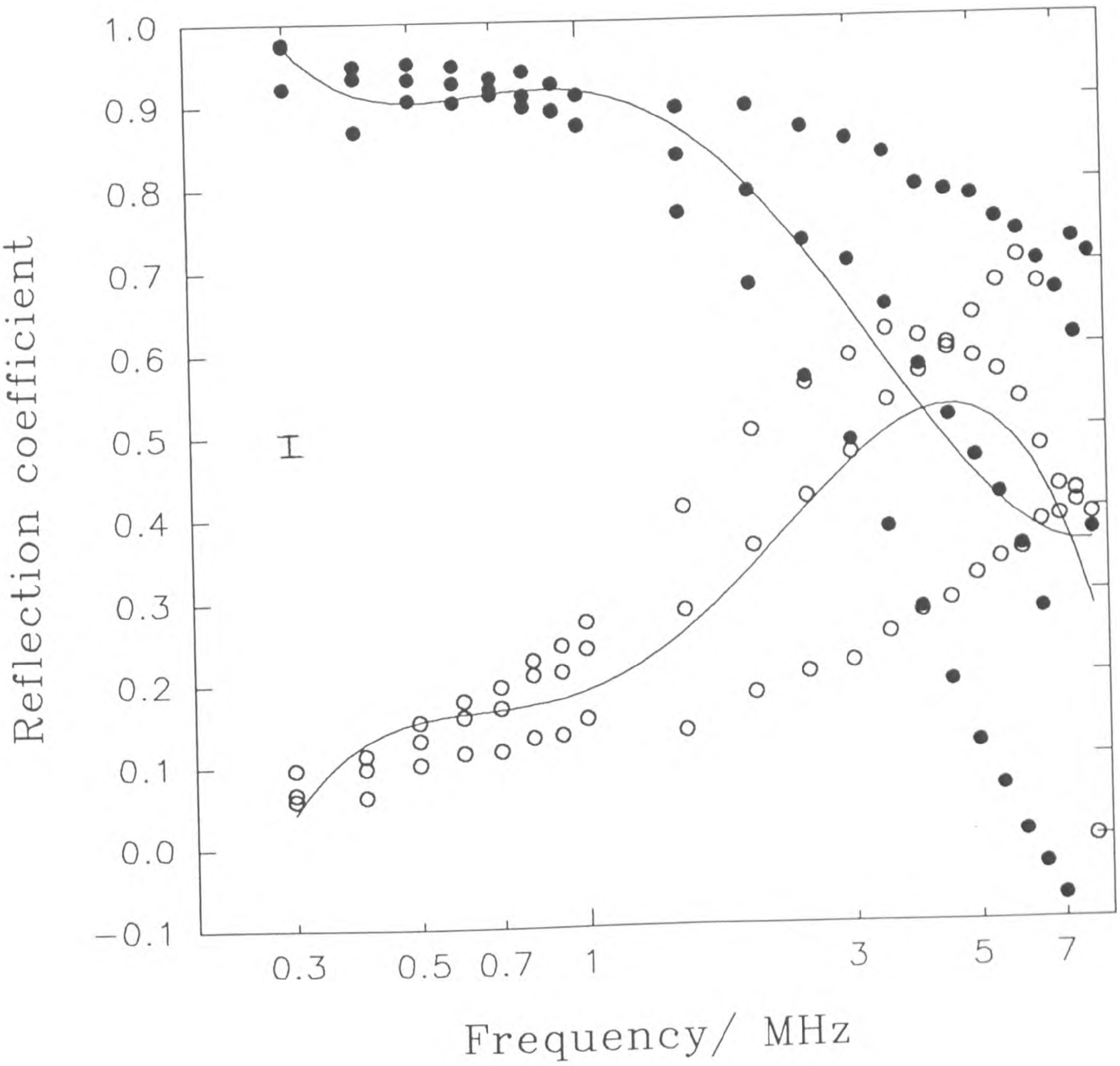

Figure 4.39 The measured real part (●) and imaginary part (○) of the reflection coefficient of concentrated bubbly liquid samples ten, eleven and twelve, stabilised with P1670. The lines represent the average of the measurements for the three samples. The bar indicates the estimated accuracy of the measurement, when applied to standard liquids under controlled conditions.

for each sample (see *Fig. 4.40*). The measured and predicted values of the reflection coefficient are compared for samples 10, 11 and 12 in *Figs. 4.41, 4.42* and *4.43* respectively. There was reasonably good qualitative agreement between the measured and predicted values, but very poor quantitative agreement. There are two main aspects to the discrepancy between the measured and predicted values of the reflection coefficient: the frequency at which the imaginary part of the reflection coefficient is maximal, and the magnitude of the predicted values.

The position of the maximum in the imaginary part of the reflection coefficient The theory[†] predicted that this maximum occurred at a higher frequency than was actually observed. The frequency at which the maximum occurs (the peak frequency) is related to the resonant frequency and is thus inversely proportional to the bubble size. There are five main reasons why the maxima in the measured and predicted curves do not coincide: use of inappropriate thermophysical properties in the theoretical model, the effects of surfactant, errors in bubble sizing, sampling discrepancies and collective effects.

The theoretical model requires values for several thermophysical properties of Sweetose and air. In the case of the Sweetose syrup, not all of these properties were known, and hence were assumed to be equal to those of water. The properties which most affect the resonant frequency are the density and, to a much lesser extent, the surface tension. The density of the syrup was known accurately, and test calculations showed that the value for the surface tension could be reduced to zero without significantly affecting the results. Therefore the use of assumed values is not expected to have a large effect on the position of the peak frequency.

Some discrepancy between the measured and predicted values of the peak frequency would be expected due to the presence of surfactant at the interface. The surfactant is expected to increase the peak frequency, and this is not accounted for in the theory. However, the measured peak frequencies were *lower* than predicted by the theory, so the effect of surfactant must have been relatively small compared to the other factors listed here.

---

†: *ie* Effective Medium Theory, see Section 2.2.4

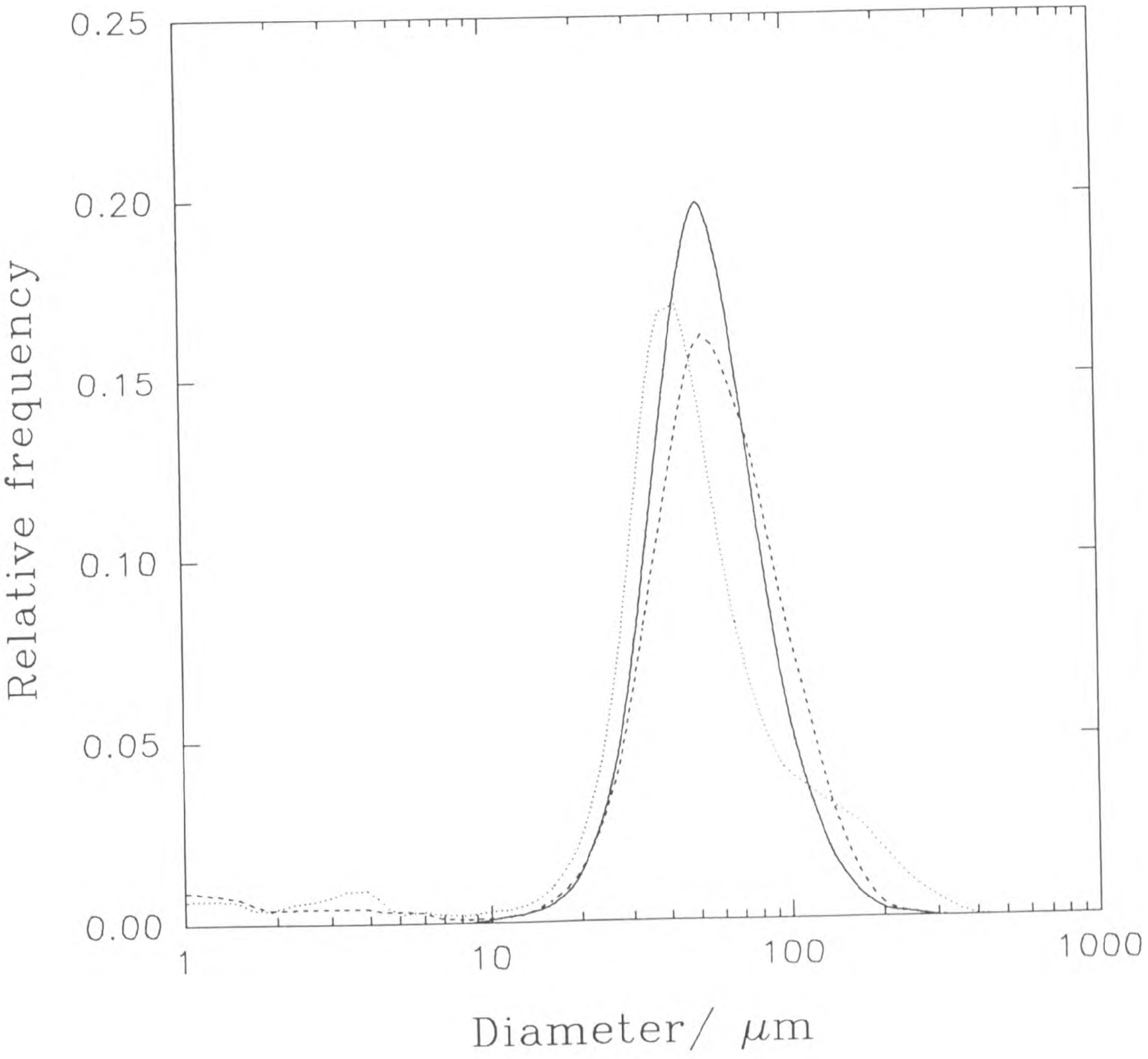

Figure 4.40 The size distribution from the Mastersizer of concentrated bubbly liquid stabilised with P1670. The solid line is the distribution in sample ten, the dashed line is for sample eleven and the dotted line is for sample twelve.

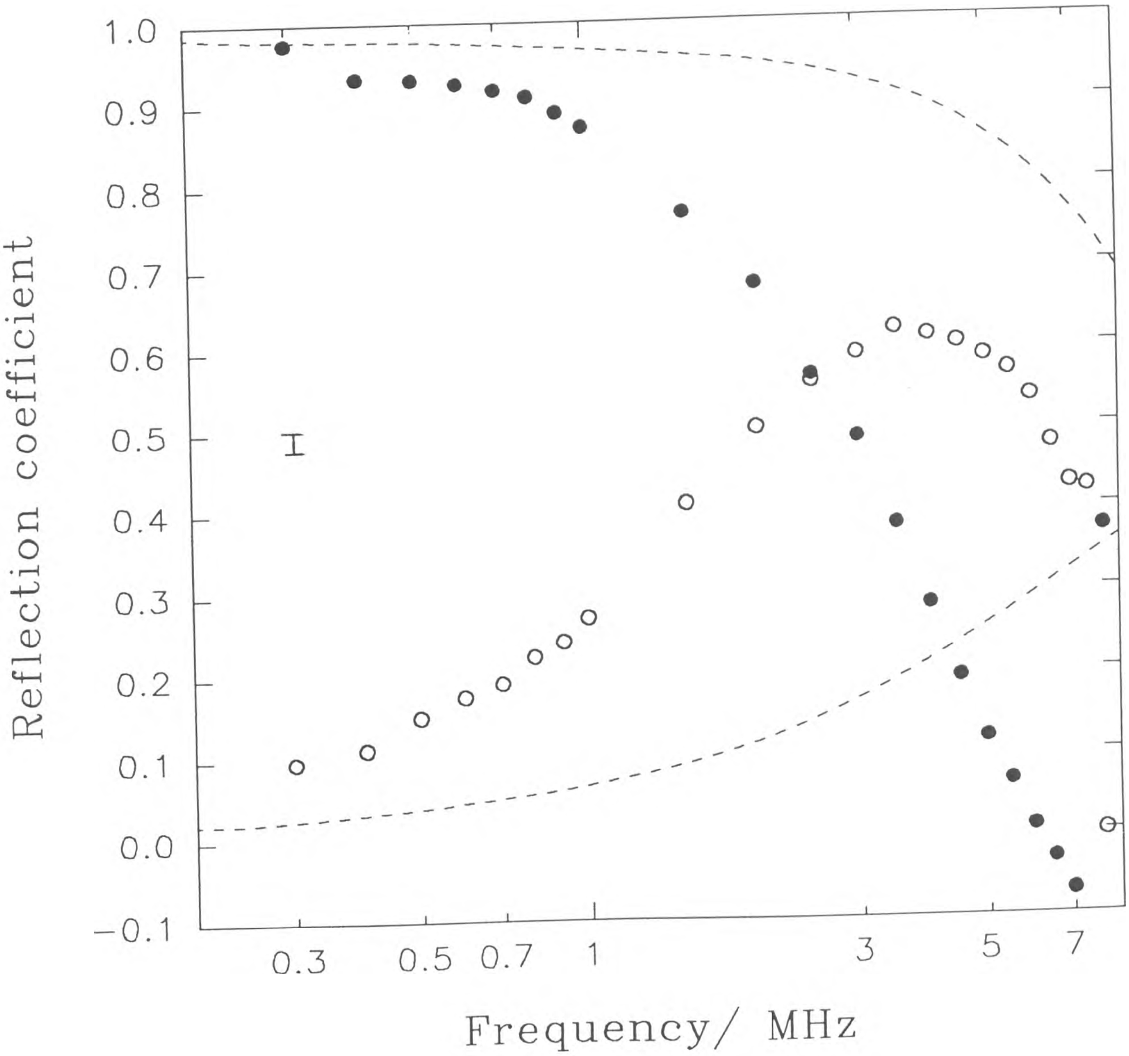

Figure 4.41 The measured real part (●) and imaginary part (○) of the reflection coefficient of concentrated bubbly liquid sample ten, stabilised with P1670. The dashed lines are the values predicted by effective medium theory. The bar indicates the accuracy of the measurement, when applied to standard liquids under controlled conditions.

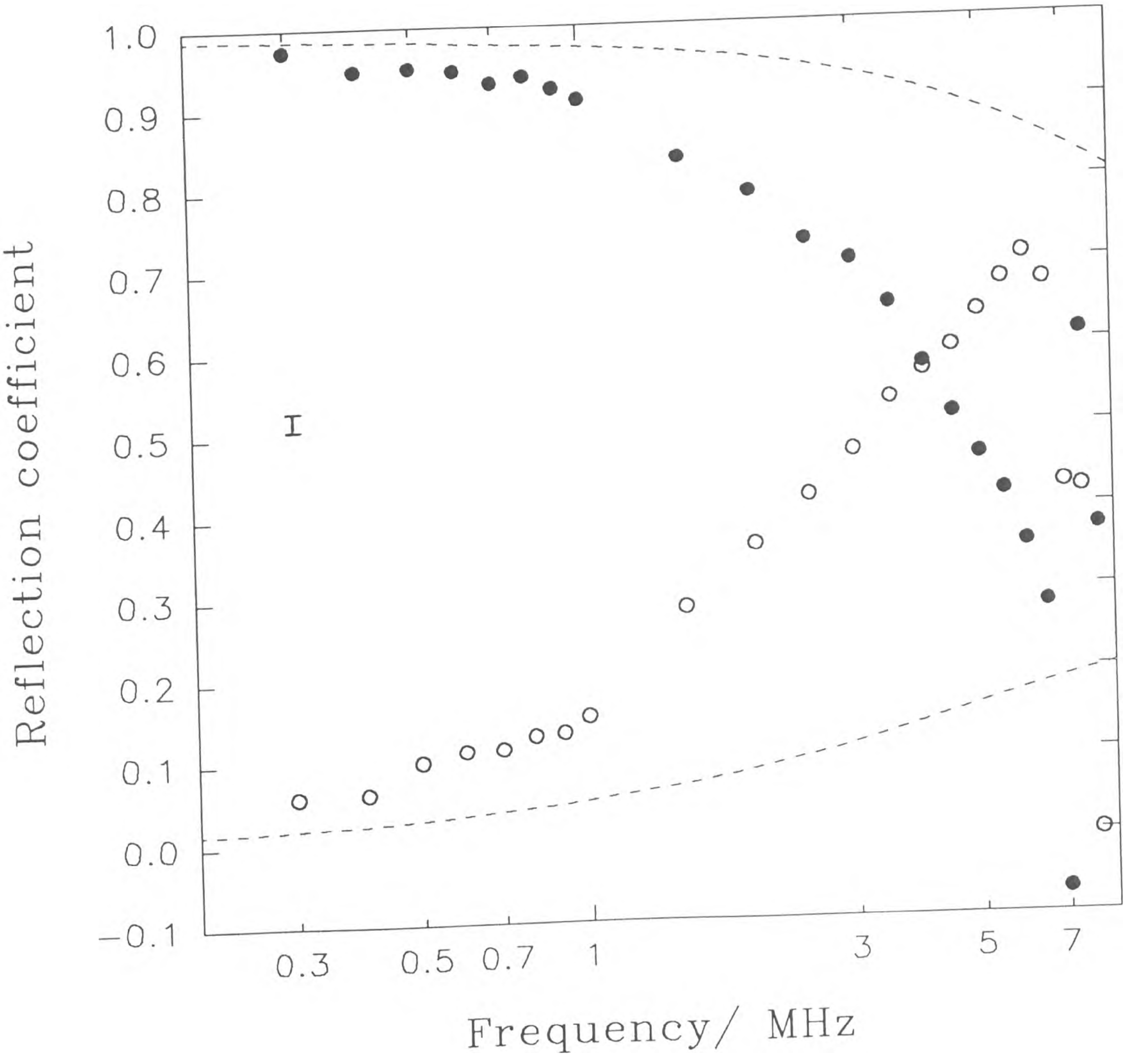

Figure 4.42 The measured real part (●) and imaginary part (○) of the reflection coefficient of concentrated bubbly liquid sample eleven, stabilised with P1670. The dashed lines are the values predicted by effective medium theory. The bar indicates the accuracy of the measurement, when applied to standard liquids under controlled conditions.

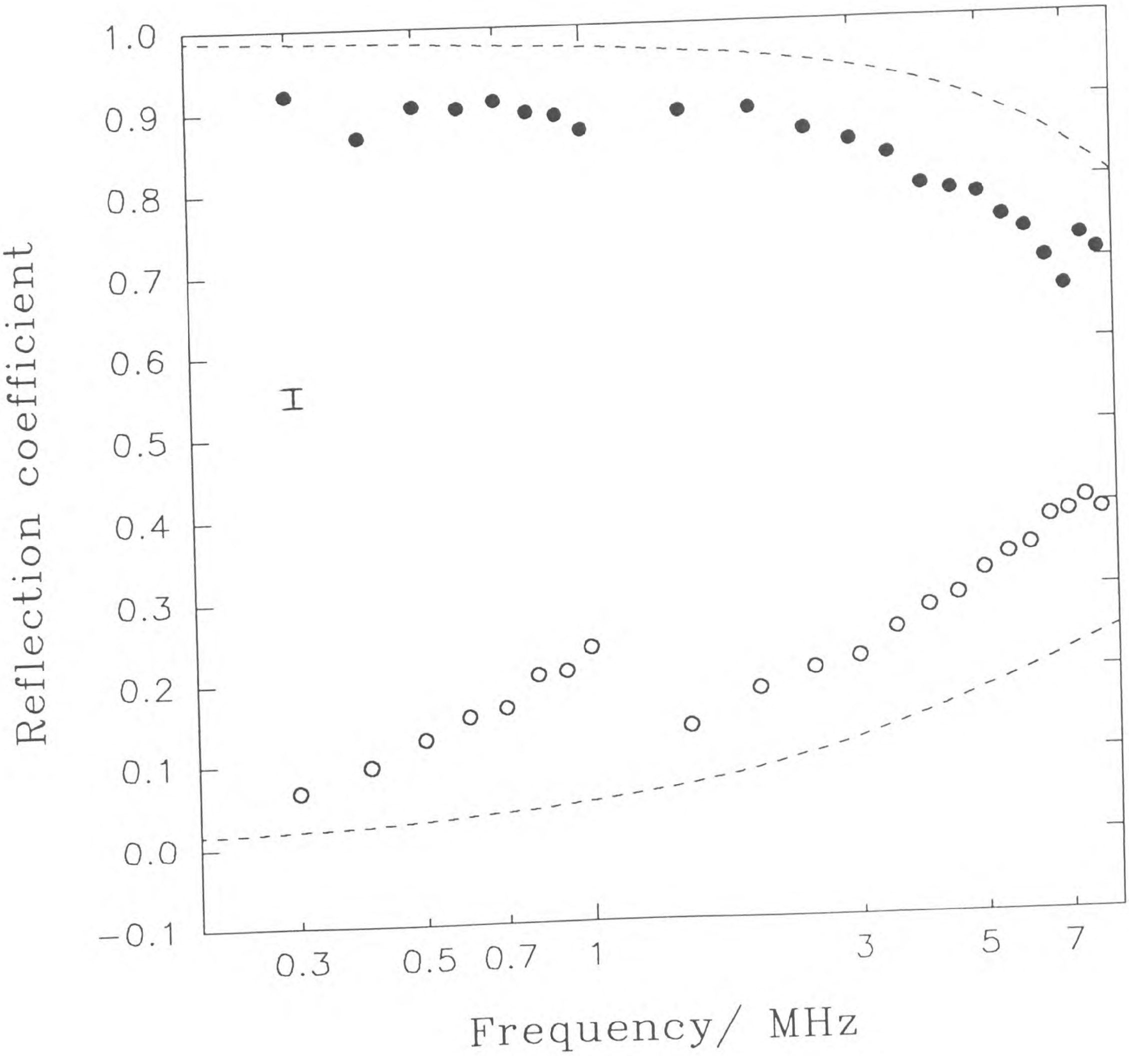

Figure 4.43 The measured real part (●) and imaginary part (○) of the reflection coefficient of concentrated bubbly liquid sample twelve, stabilised with P1670. The dashed lines are the values predicted by effective medium theory. The bar indicates the accuracy of the measurement, when applied to standard liquids under controlled conditions.

It is possible that the bubble size distribution measured in the Mastersizer did not accurately reflect the bubble size distribution present in the FSUPER. This could be due to sampling errors, dilution effects, or the use of the wrong presentation code . Sampling errors are possible because the total amount of material which was removed for characterisation in the Mastersizer was very small. This small amount of material was greatly diluted, affording larger bubbles the opportunity to cream out of the measurement volume. The presentation code used in the calculation of the size distribution was the one which closest to that calculated from the properties of the bubbly liquid/50 wt% Sweetose system, but it is possible that using this code introduced a small error into the size distribution. Of these three possibilities, it seems most likely that it was the dilution step which had the most profound effect on the apparent bubble size distribution. If more large bubbles were to be added to the apparent bubble size distribution, the theoretical curves would be shifted towards lower frequencies and would thus model the experimental measurements more closely.

The discrepancy in the position of the measured and predicted peak frequencies could also be due to the way the FSUPER sampled the bubbly liquid. The precise nature of this sampling is not known. The interrogating ultrasonic pulse was reflected at the buffer rod/sample interface, and was probably only sensitive to the properties of a thin layer of the bubbly liquid near to this interface (because the bubbly liquid was very strongly attenuating). It is possible that the bubble size distribution near the buffer/rod sample interface was not representative of the bubble size distribution in the bulk liquid, which is the quantity that the Mastersizer attempts to measure.

Finally, there is the possibility that collective effects, of the kind described in Chapter Two, had an influence on the resonant frequencies of the bubbles in the concentrated bubbly liquid. At a volume fraction of 50 %, with a bubble radius of 20 μm, there are about 10^{13} bubbles per cubic metre, or about 10^{9} bubbles in the FSUPER itself. The spacing between the bubbles was therefore of the order of micrometres, and the possibility of collective effects is strongly suggested. The exact nature of these collective effects is hard to predict.

Of these five possible reasons for the discrepancy between the measured and predicted peak frequencies, the latter three are the most strongly suspected.

The magnitude of the predicted values The theory overpredicts the value of the real part of the reflection coefficient, and underpredicts the imaginary part. The disparity may be due in part to the values taken for the thermophysical properties of Sweetose. In order to assess the impact of this assumption, the calculations were repeated several times using different values for the unknown properties, such as the thermal conductivity and the specific heat capacity. It was found that the values of some of the properties could be changed considerably without altering the predictions significantly. The key properties were the density, velocity and viscosity, which were all known. The use of the properties of water was not, therefore, a major source of error in the calculations. The poor quantitative prediction of the reflection coefficient is due mainly to shortcomings in the theoretical model. The collective effects mentioned above will have an effect on the ultrasonic properties which is hard to quantify.

Furthermore the factors described in Section 2.2.6 apply very strongly here. The volume fraction of air was well above the limit in which even the mathematically rigorous multiple scattering theories are valid. Furthermore, the assumptions made in the derivation of the single scattering coefficients (which are used in effective medium theory) are violated in concentrated systems: the thermal and viscous skin depths for some bubbles will be less than the bubble separation in this system.

The overprediction of the real part of the reflection coefficient indicates that the velocity in the bubbly liquid was not as low as predicted by the theory. The underestimation of the imaginary part of the reflection coefficient indicates that the attenuation in the bubbly liquid was lower than predicted by theory. Taking into account all the various factors which may be responsible for the difference between the measured and the predicted values of the reflection coefficient, the biggest factor is shortcomings in the theory.

4.3.2.2 Ultrasonic measurements on systems prepared using Hyfoama

Sample one The measurements on this sample, like those for P1670 samples one and two, were rejected as unreliable.

Samples two, three, four and five The results for these samples are shown in *Fig. 4.44*. The inter sample consistency seemed to be better for these samples, and the form of the curves through the real and imaginary parts of the reflection coefficient was very similar to that observed for the samples prepared using P1670.

Sample six The results for this sample (*Fig. 4.45*) seemed to show the same unexpected form which was observed for the P1670 samples seven, eight and nine (see *Fig. 4.38*).

Samples seven, eight, nine and ten The measured bubble size distributions for these samples are shown in *Fig. 4.46*. The measured size distributions were used, along with the thermophysical properties of 70 wt% Sweetose and air, and the measured volume fraction, in order to predict the reflection coefficient using EMT. The measured and predicted values of the reflection coefficient for samples seven to ten are shown in *Figs. 4.47* to *4.50* respectively. There was quite a lot of inter sample variation, and the ultrasonic measurements did not seem to be correlated with the measured volume fraction or bubble size. The Mastersizer indicated that the bubbles in the system prepared with Hyfoama were three times larger than those in the system prepared with P1670. This difference was not very clear in the ultrasonic measurements. The theoretical predictions again agree only qualitatively with the experimental measurements. The use of a larger bubble size in the theoretical calculations has resulted in a better agreement in the frequency at which the imaginary part of the reflection coefficient reaches a maximum value. However, the value of the imaginary part of the reflection coefficient is again drastically underestimated, and the value of the real part is overestimated. It is clear that the curves for the predicted real and imaginary parts of the reflection coefficient do not intersect, whereas in all cases the measured curves crossed each other.

4.3.2.3 Ultrasound as a probe of concentrated model bubbly liquid

Ultrasonic measurements showed limited promise in the concentrated model bubbly liquid. Even though the model itself was not perfect, the primary cause of

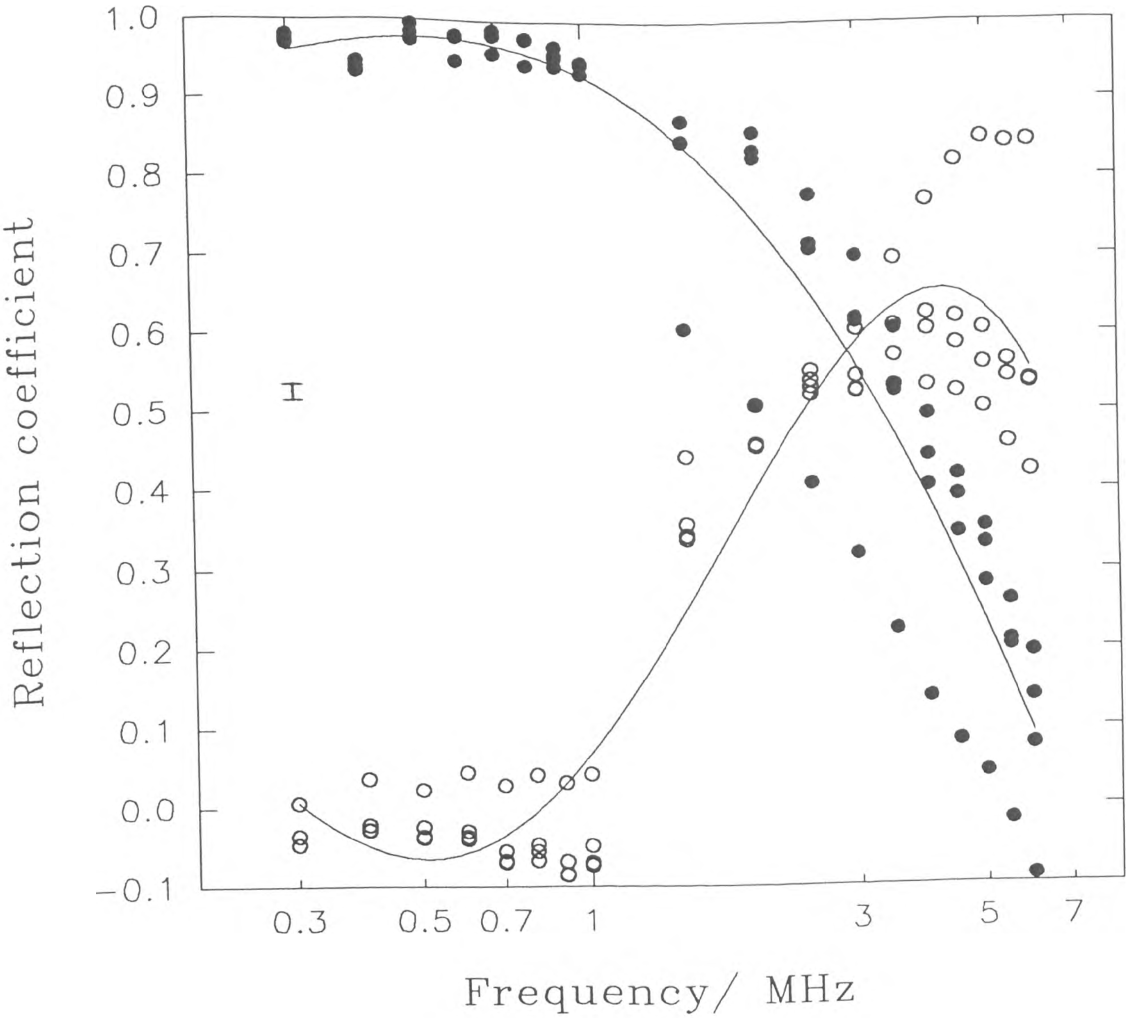

Figure 4.44 The measured real part (●) and imaginary part (○) of the reflection coefficient of concentrated bubbly liquid samples two, three, four and five, stabilised with Hyfoama. The lines represent the average of the measurements for the four samples. The bar indicates the estimated accuracy of the measurement, when applied to standard liquids under controlled conditions.

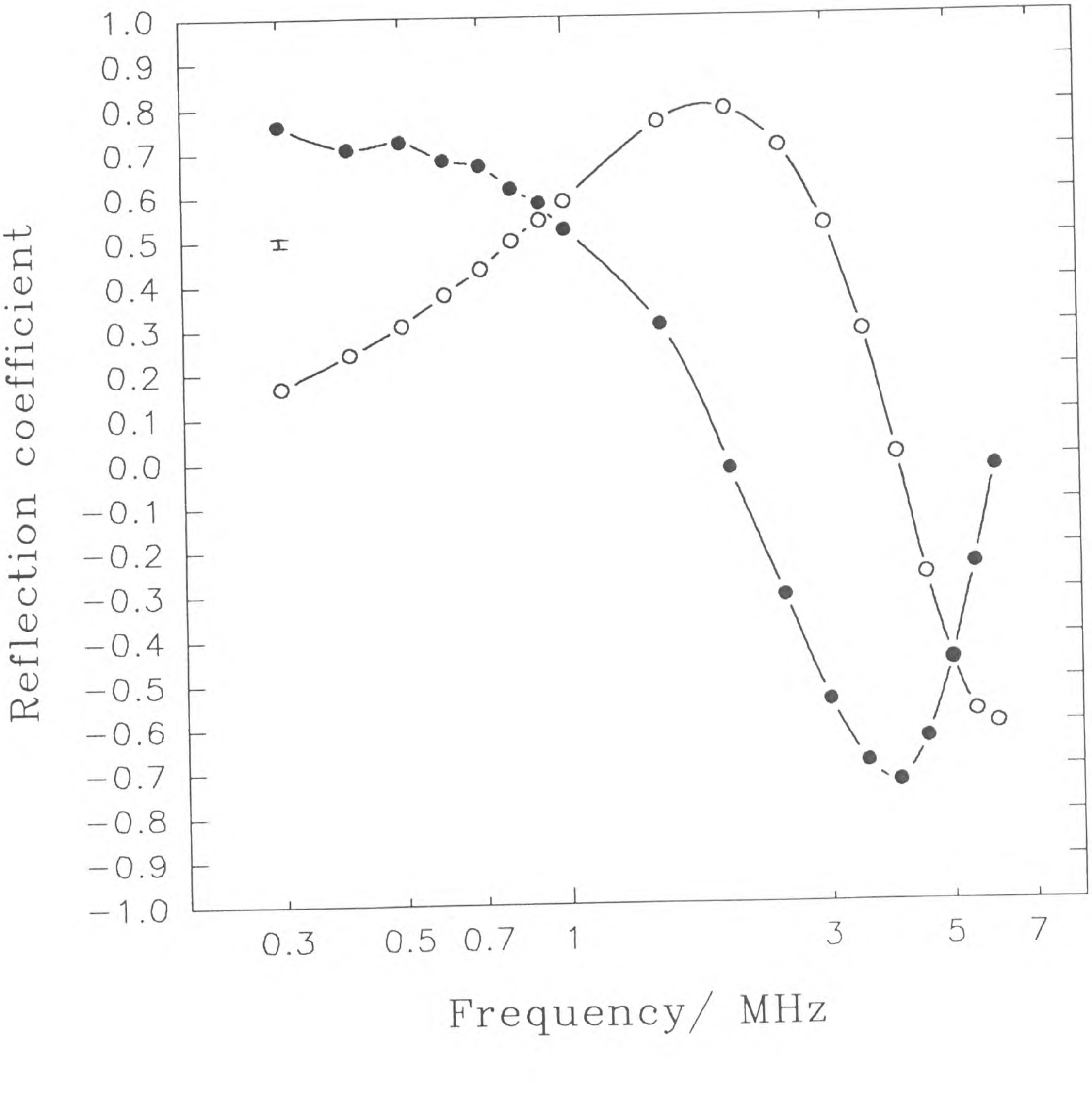

Figure 4.45 The measured real part (●) and imaginary part (o) of the reflection coefficient of concentrated bubbly liquid sample six, stabilised with Hyfoama. Regression lines are drawn through the data points. The bar indicates the estimated accuracy of the measurement, when applied to standard liquids under controlled conditions. Note that the ordinate scale runs from -1 to +1.

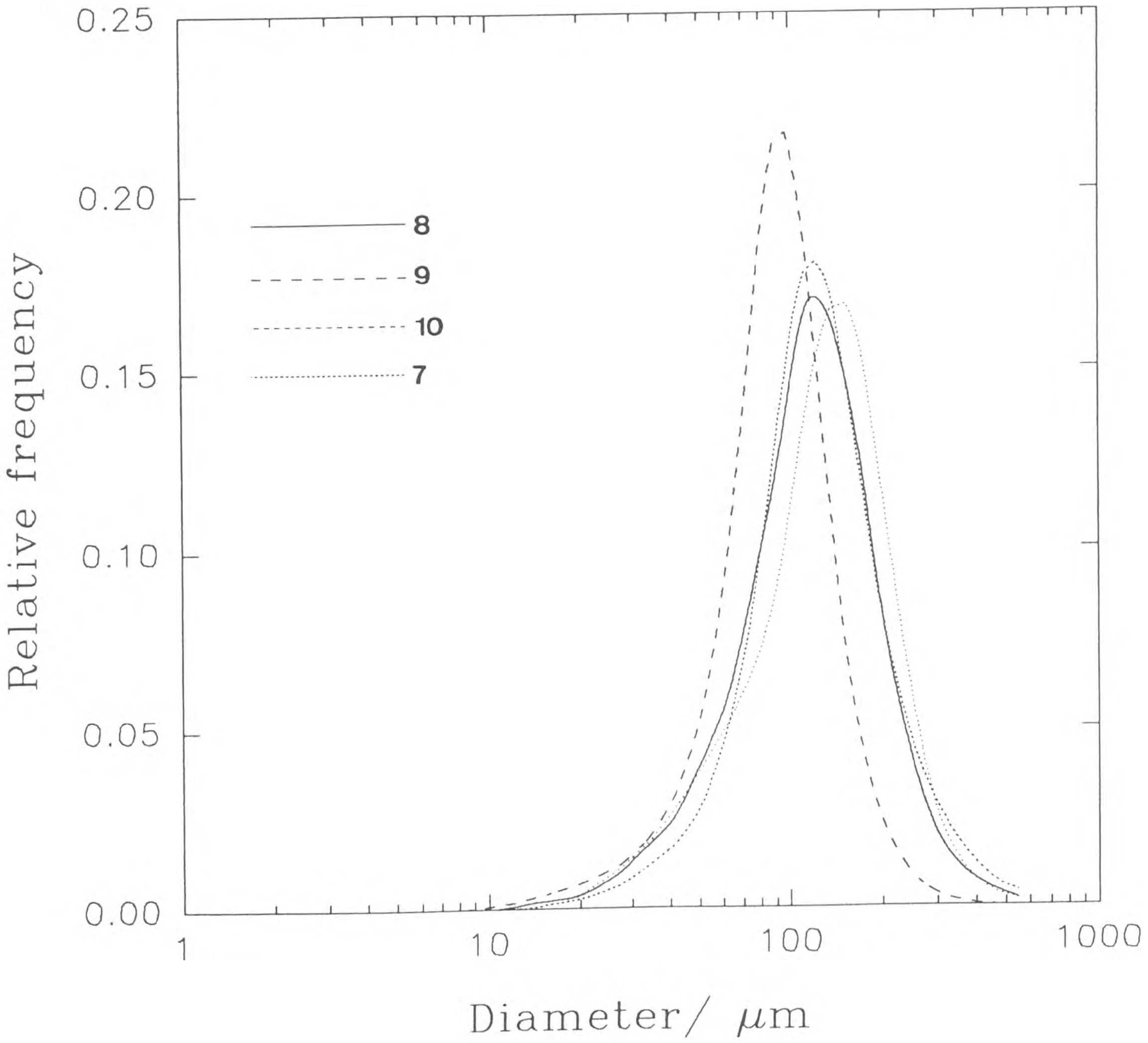

Figure 4.46 The bubble size distribution measured by the Mastersizer in concentrated bubbly liquid samples seven, eight, nine and ten, stabilised with Hyfoama. The lines are labelled with the number of the corresponding sample.

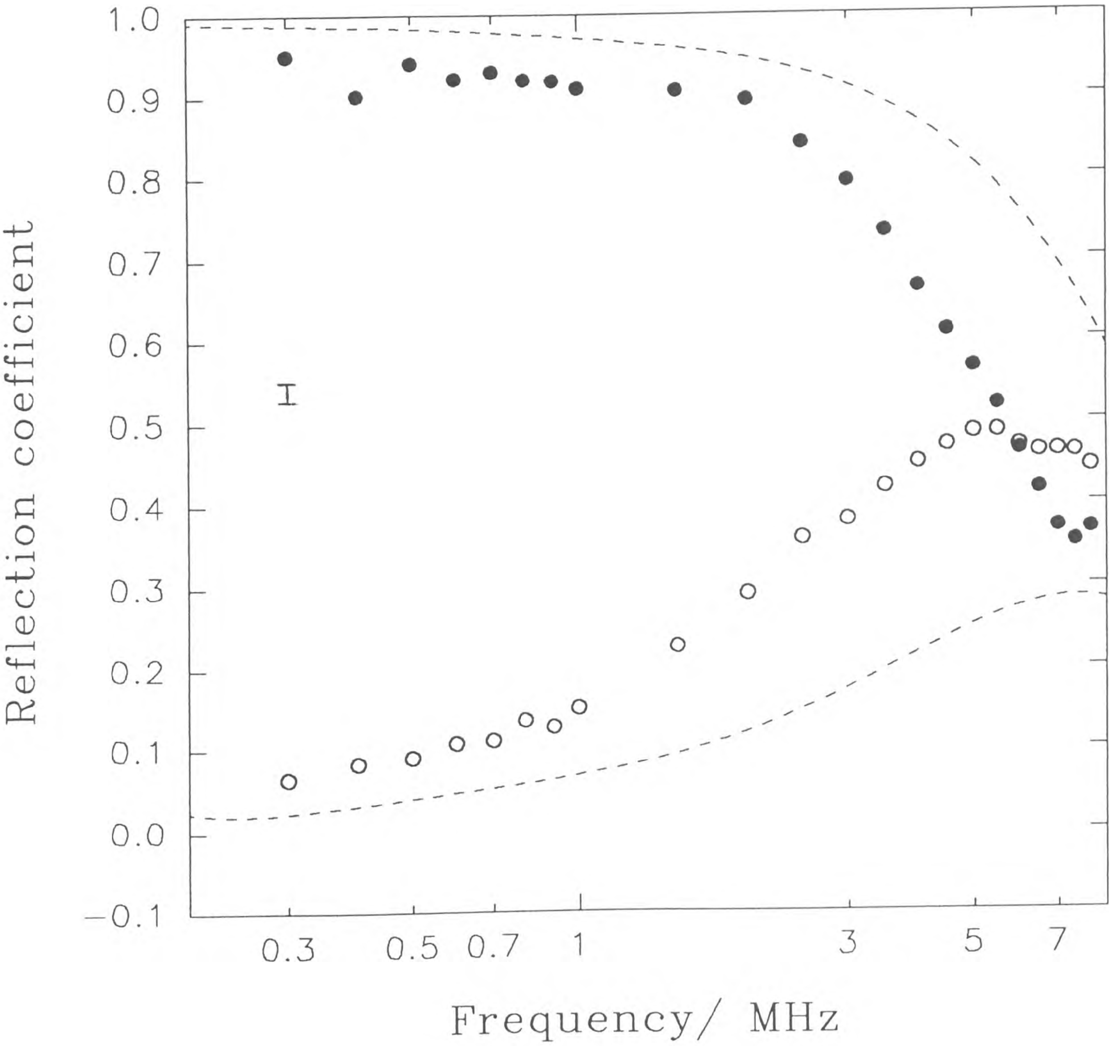

Figure 4.47 The measured real part (●) and imaginary part (○) of the reflection coefficient of concentrated bubbly liquid sample seven, stabilised with Hyfoama. The dashed lines are the predicted values from effective medium theory. The bar indicates the estimated accuracy of the measurement, when applied to standard liquids under controlled conditions.

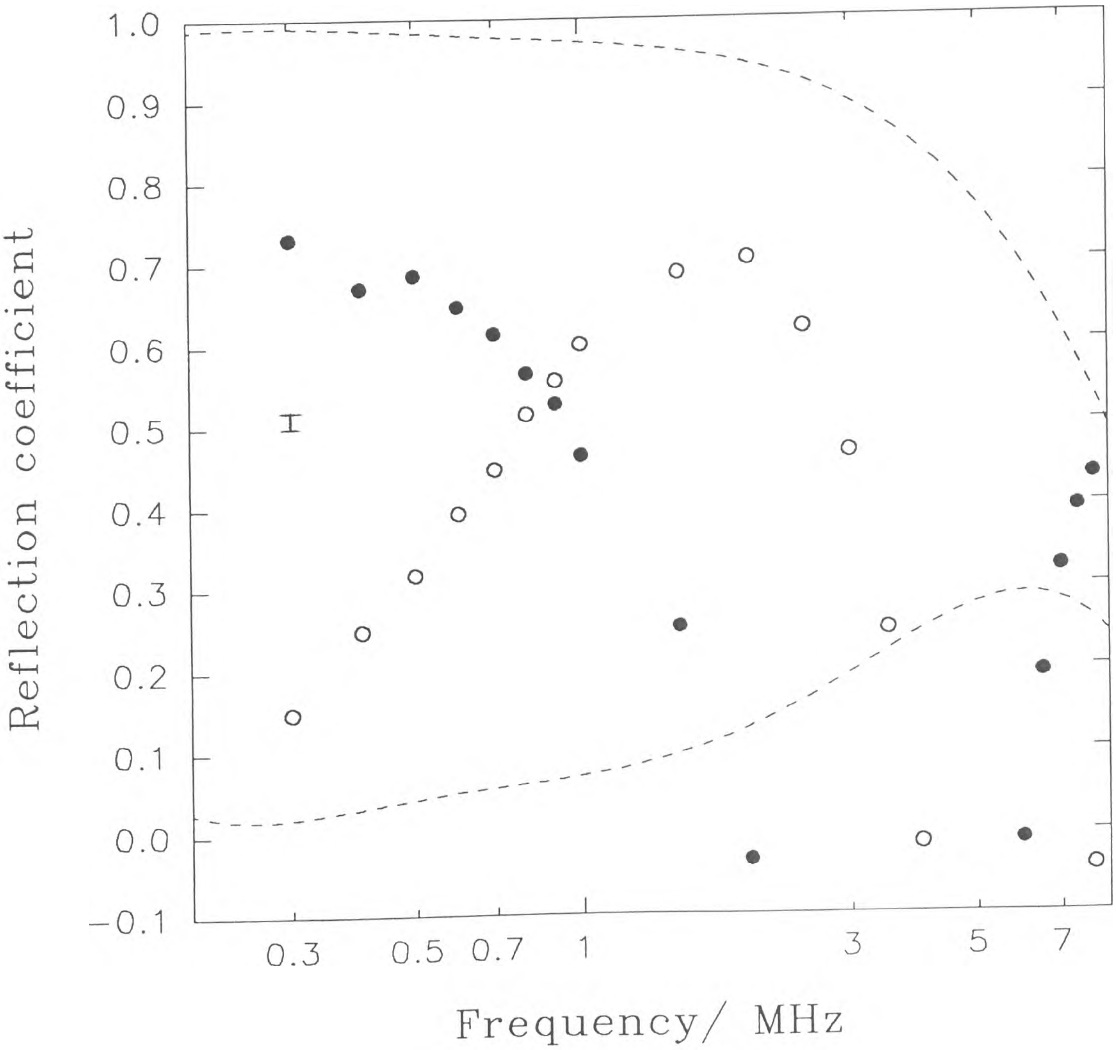

Figure 4.48 The measured real part (●) and imaginary part (○) of the reflection coefficient of concentrated bubbly liquid sample eight, stabilised with Hyfoama. The dashed lines are the predicted values from effective medium theory. The bar indicates the estimated accuracy of the measurement, when applied to standard liquids under controlled conditions.

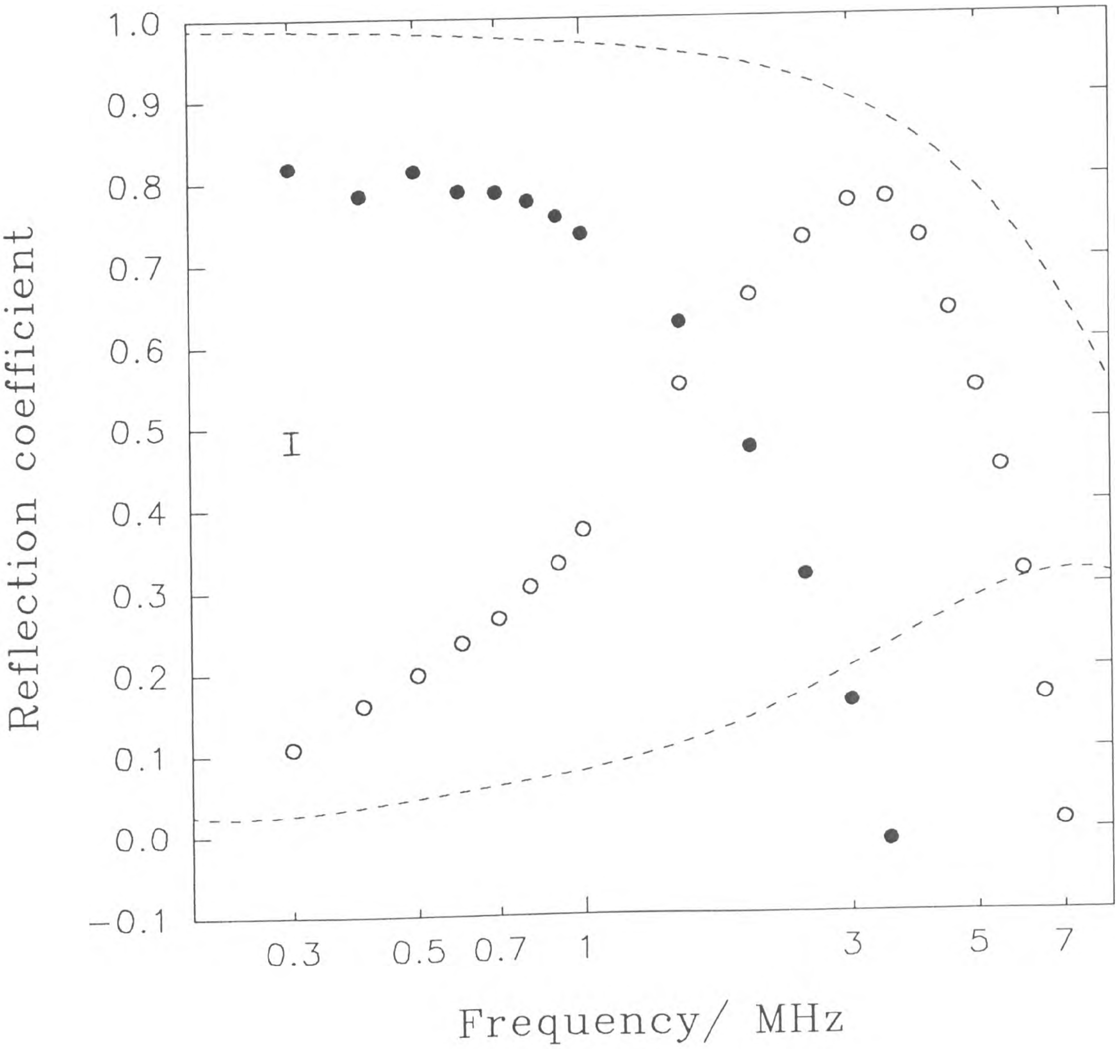

Figure 4.49 The measured real part (●) and imaginary part (○) of the reflection coefficient of concentrated bubbly liquid sample nine, stabilised with Hyfoama. The dashed lines are the predicted values from effective medium theory. The bar indicates the estimated accuracy of the measurement, when applied to standard liquids under controlled conditions.

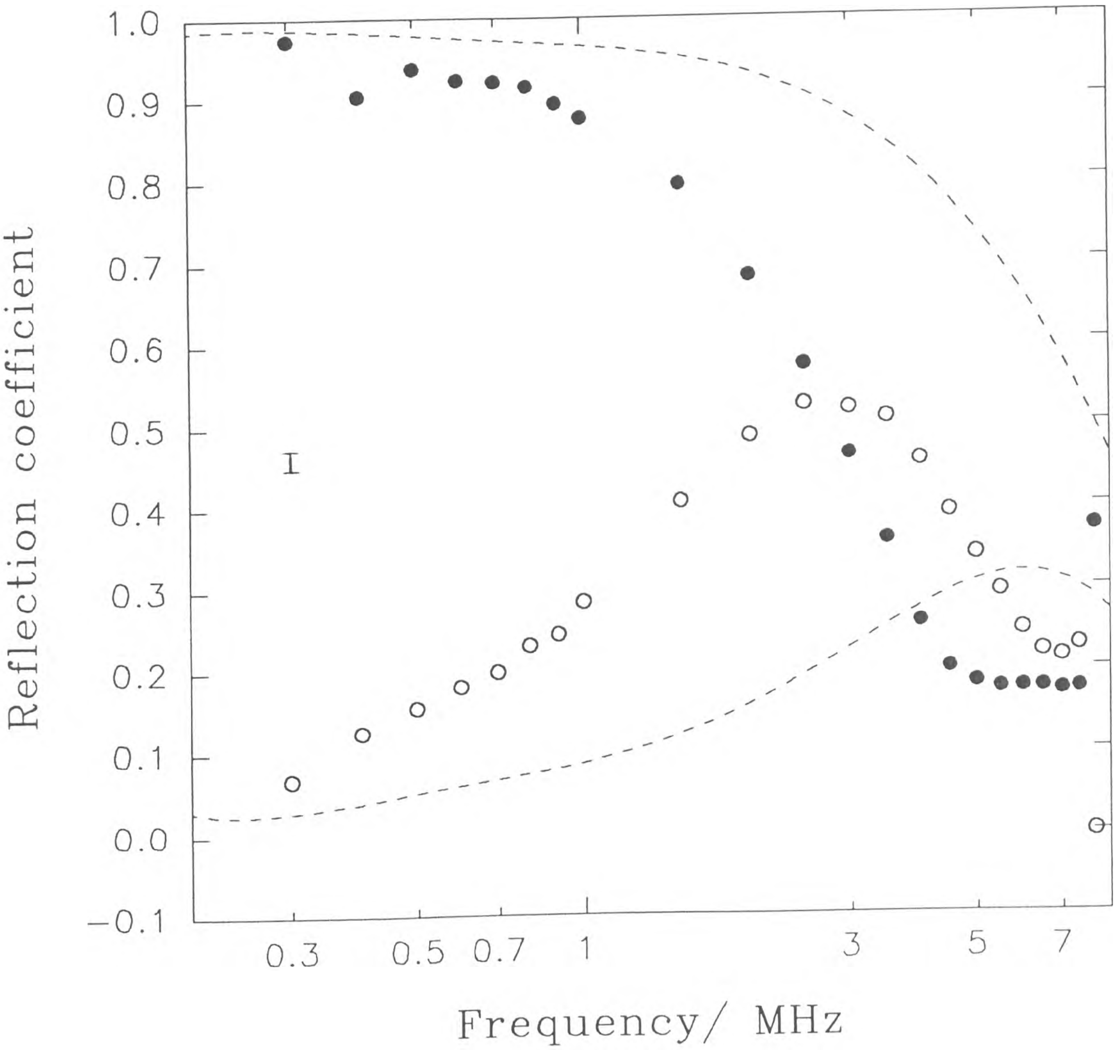

Figure 4.50 The measured real part (●) and imaginary part (o) of the reflection coefficient of concentrated bubbly liquid sample ten, stabilised with Hyfoama. The dashed lines are the predicted values from effective medium theory. The bar indicates the estimated accuracy of the measurement, when applied to standard liquids under controlled conditions.

the marked disagreement between theory and experiment is shortcomings in the theory. The discussion in Chapter Two explains why the theory cannot be expected to work at high volume fractions.

It would not be possible to measure the volume fraction in the concentrated bubbly liquid. The measurements did not discriminate very well between the bubbles in model liquid stabilised with Hyfoama, and liquid stabilised with P1670, despite the very marked difference in volume fraction and bubble size between the two liquids. Nevertheless, the results did indicate that resonant behaviour was occurring in a highly concentrated bubbly system. To the best of the author's knowledge, there are no similar reported ultrasonic measurements on concentrated bubbly liquids.

4.4 Bubbled gel

The results for bubbled gel were rather poor, and are included here mainly for the sake of completeness. They do not add much to the understanding of propagation in bubbly liquids. They do however illustrate some of the pitfalls which are encountered in ultrasonic measurements.

A mixture of 50 wt% Sweetose, 2.50 wt% agar and 0.5 wt% P1670 was used to prepare various air free gels. The mixture was also used to dilute the concentrated model bubbly liquid (prepared using 0.5 wt% P1670), yielding a gel containing air at a volume fraction of 0.020 ± 0.005. The ultrasonic velocity was determined in the gel rig, at various pathlengths (*Fig. 4.51*). The velocity appeared to be strongly dependent on the pathlength of the gel, indicating that large phase shifts were occurring due to diffraction and wearplate effects. The apparently greatly elevated velocity in the aerated gel can be attributed principally to these effects. However, diffraction corrections alone were not sufficient to make the measurements coincide (see *Fig. 4.51*). The temperature in the gel samples ranged between 15.4 and 25.1 °*C*, and was not controlled during the measurements. Such variations in temperature would be expected to alter the measured value by no more than 40 to 50 m s^{-1}. Nevertheless, the effect of the variation in temperature seems to have been quite dramatic. The bubbled gel model was not pursued further because the results were so unreliable.

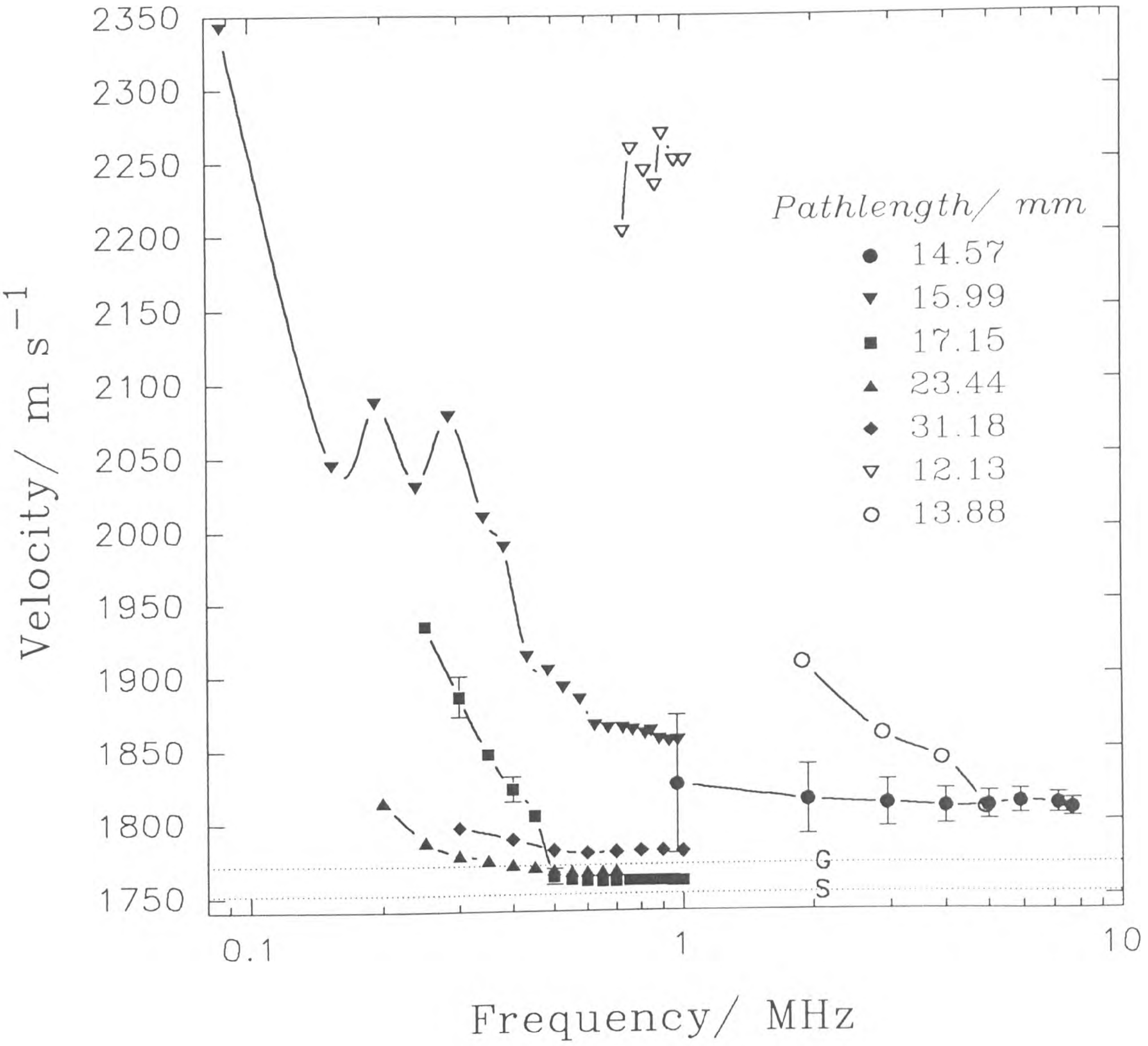

Figure 4.51 The ultrasonic velocity of 50 wt% Sweetose gelled with agar, as measured in the specially constructed rig (see Chapter Three). The solid data points are measurements on air-free gel, and the hollow data points are measurements on gel containing air at a volume fraction of 2%. The legend indicates the separation of the transducers for the relevant set of data points. The bars indicate the magnitude of the diffraction corrections given by the equations set out in Appendix I. The lines labelled G and S are the velocities in the air-free gel and in air-free 50 wt% Sweetose, as measured in the UPER.

4.5 Yogurt

The remainder of this chapter is given over to the measurements on real foods. These were generally simpler than the measurements on the model systems, and in some respects easier to interpret. Despite the relatively disappointing behaviour of the model system, the measurements on real foods were surprisingly instructive.

The measured group velocity and density of the unwhipped yogurts, and the volume fraction of the whipped yogurts are given in *Table 4.6*. No measurements on yogurt were found in the literature.

4.5.1 Unwhipped yogurt

The measured reflection coefficient of the unwhipped low fat yogurt and full fat set yogurt is shown in *Figs. 4.52* and *4.53* respectively. The yogurts were not dispersive in the frequency range examined, and there was very good agreement between the measured reflection coefficient and the values predicted using the measured values of the density and group velocity.

4.5.2 Whipped yogurt

The measured size distributions in the whipped yogurts are shown in *Fig. 4.54*. The measurements for whipped low fat yogurt are shown in *Fig. 4.55*. There was reasonable inter sample consistency in the measurements, and the form of the curves through the real and imaginary parts of the reflection coefficient clearly demonstrates resonant behaviour. The measurements for whipped full fat set yogurt are shown in *Fig. 4.56*. There was excellent inter sample consistency, and the measured bubble size distribution and volume fraction have been used in order to calculate the reflection coefficient according to effective medium theory. Where appropriate, the thermophysical properties of water were used in the calculations, because some of the properties of yogurt were not known. The theoretical prediction agrees very well in terms of the position of the maximum in the imaginary part of the reflection coefficient. The reasons for the slight discrepancy are the same as those discussed previously: differences in the way in which the FSUPER and the light microscope sampled the liquid, deficiencies in the bubble sizing procedure and the presence of surfactant at the interface. The sizing procedure was known to have a slight bias, which favoured larger bubbles with accordingly lower resonant

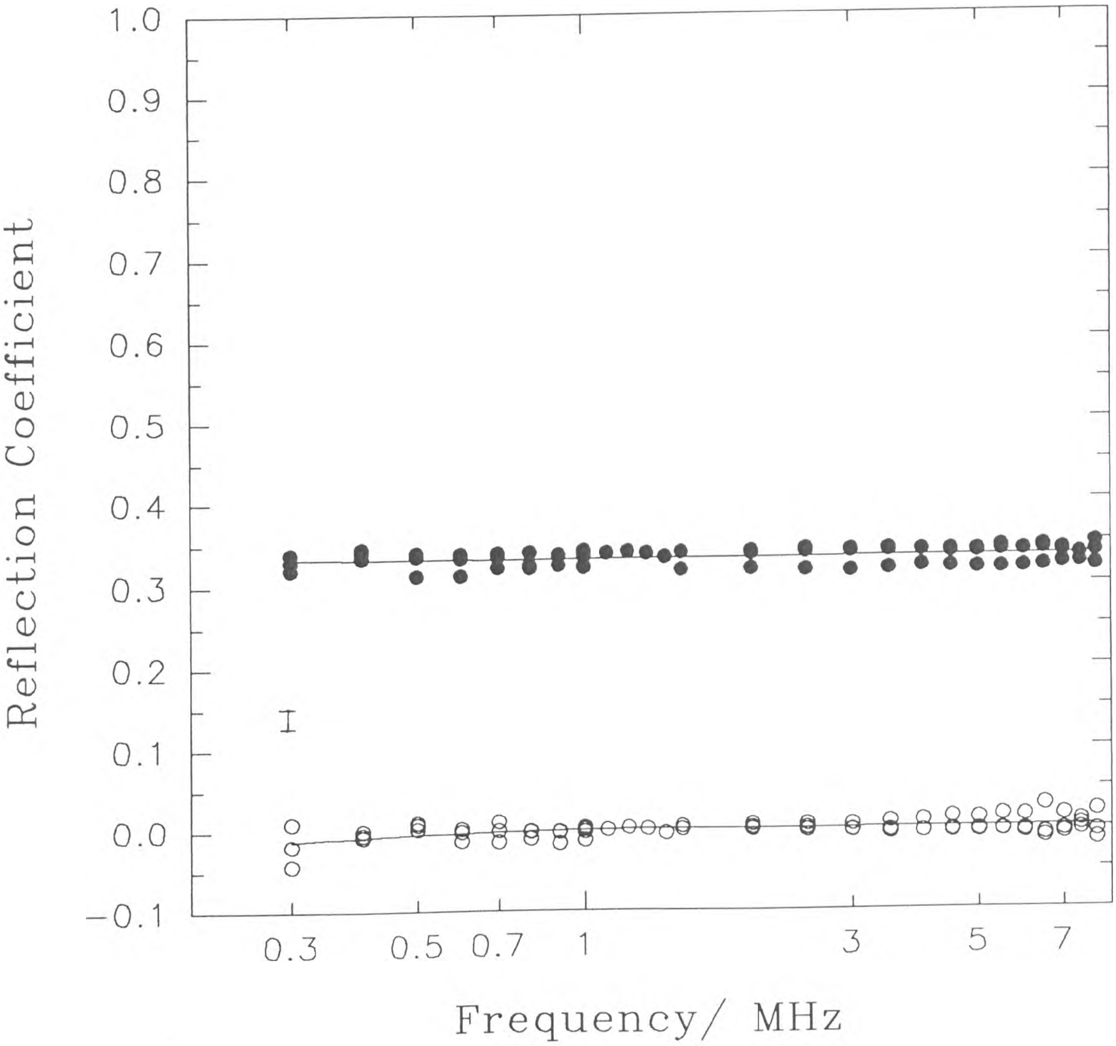

Figure 4.52 The measured real part (●) and imaginary part (○) of the reflection coefficient of air-free low fat natural yogurt. Regression lines are plotted through the data. The bar indicates the estimated accuracy of the measurement, when applied to standard liquids under controlled conditions.

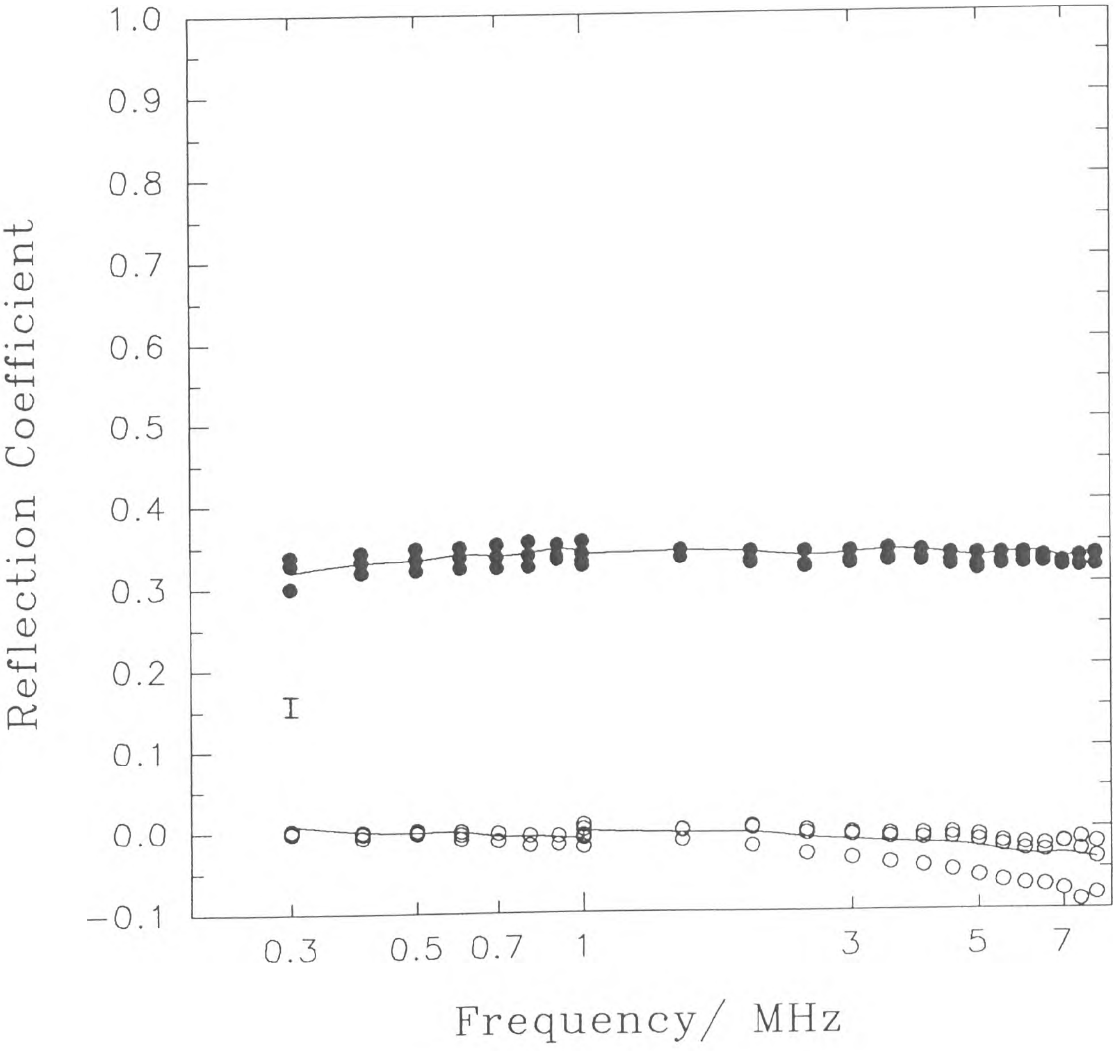

Figure 4.53 The measured real part (●) and imaginary part (○) of the reflection coefficient of air-free full fat set yogurt. Regression lines are plotted through the data. The bar indicates the estimated accuracy of the measurement, when applied to standard liquids under controlled conditions.

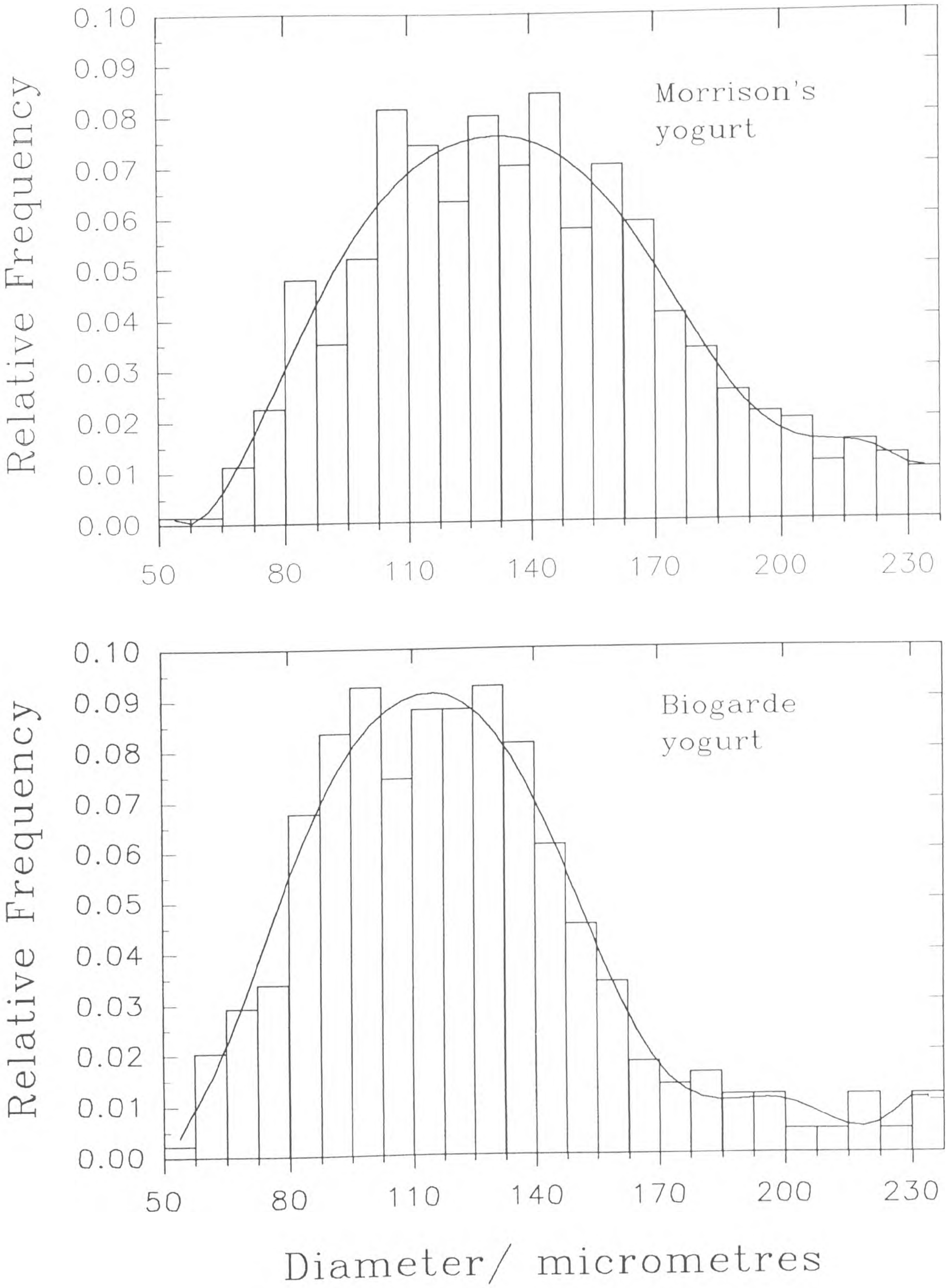

Figure 4.54 The bubble size distribution measured using light microscopy in whipped low fat natural yogurt (top) and full fat set yogurt (bottom).

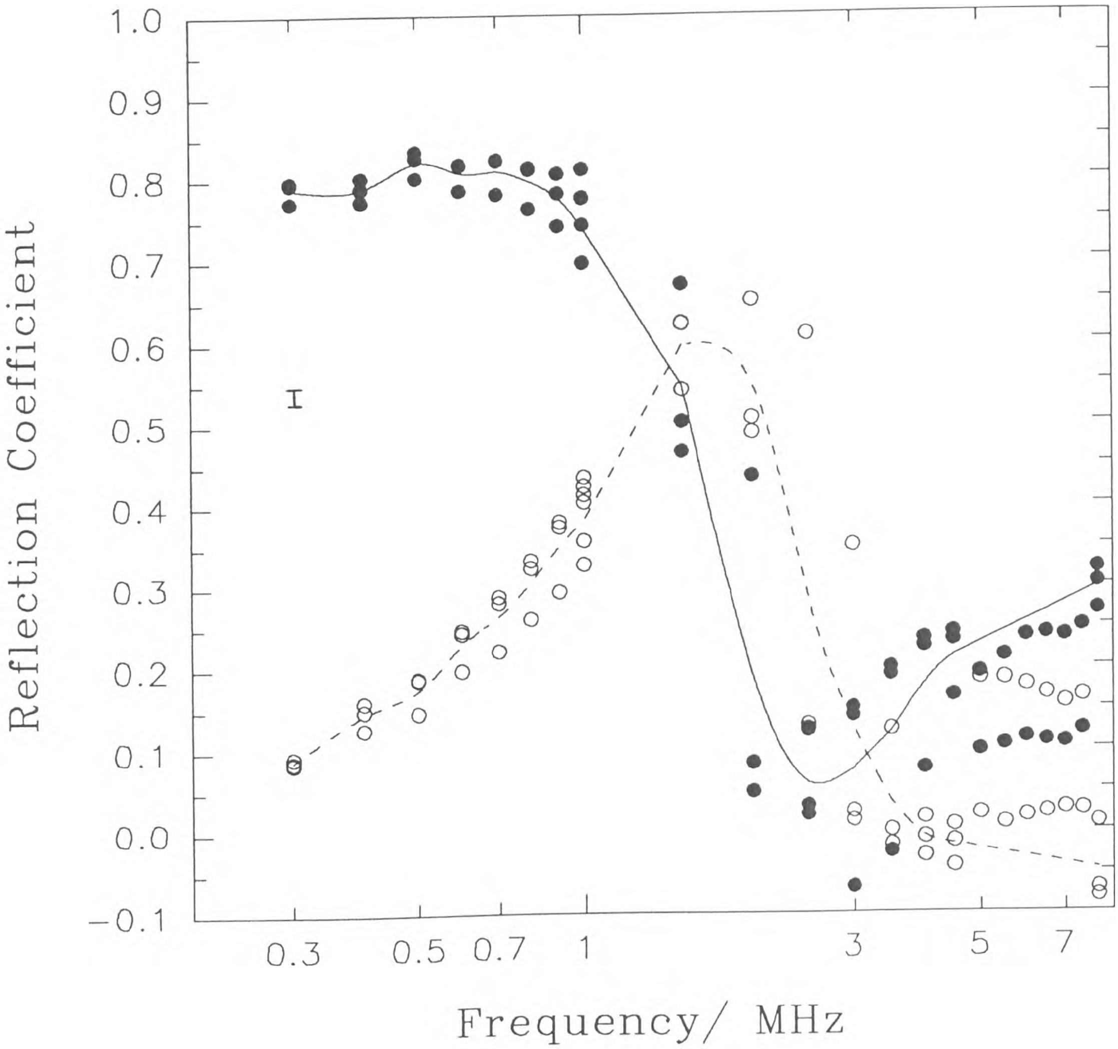

Figure 4.55 The measured real part (●) and imaginary part (○) of the reflection coefficient of whipped low fat natural yogurt. Regression lines are plotted through the average of the data. The bar indicates the estimated accuracy of the measurement, when applied to standard liquids under controlled conditions.

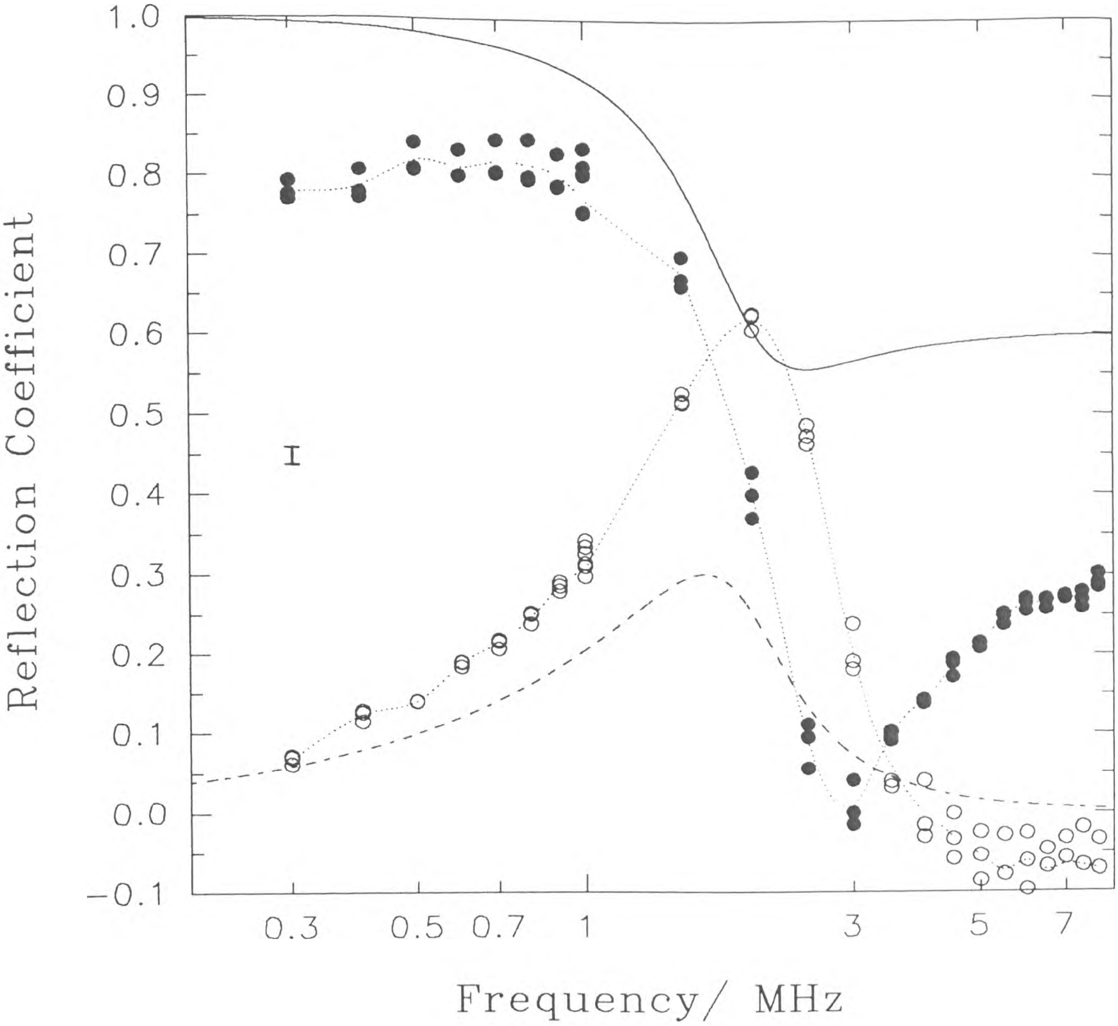

Figure 4.56 The measured real part (●) and imaginary part (○) of the reflection coefficient of whipped full fat set yogurt. Regression lines (dotted) are plotted through the average of the data. The solid line is the predicted value from effective medium theory of the real part of the reflection coefficient, and the dashed line is the predicted value of the imaginary part. The bar indicates the accuracy of the measurement, when applied to standard liquids under controlled conditions.

Table 4.6 *The measured physical properties of yogurt*

Property	Low fat natural yogurt *Morrison's*	Full fat set yogurt *Biogarde*
Density/ kg m^{-3}	1066 ± 3	1040 ± 3
Group velocity/ m s^{-1}	1509 ± 2	1465 ± 3
Reflection coefficient*	0.34	0.36
Volume fraction of air	38 ± 8 %	47 ± 5 %
r_{32}/ μm	79 ± 6	71 ± 6

*: calculated using the characteristic acoustic impedance ($= \rho c$).

frequencies. The presence of surfactant at the interface is expected to have increased the resonant frequency of the bubbles slightly.

4.5.3 Ultrasound as a probe of whipped yogurt

If ultrasound were to be used as a non-destructive technique for the examination of whipped yogurt, then it would be of only limited use. The existing theory has been shown to fail at high volume fractions of air. The value of the imaginary part of the reflection coefficient is grossly underestimated, and the value of the real part is overestimated. At frequencies around the resonant frequency of the bubbles, the reflection coefficient cannot be related to the volume fraction of air. It should be possible to measure the volume fraction by employing frequencies well above resonance. Manetou *et al* (1991) have had some success at measuring the volume fraction of air in marshmallow and frappé using a buffer rod at high frequencies, using an empirical technique.

The ultrasonic technique does show promise as a technique for bubble sizing in yogurt, because the position of the peak in the imaginary part of the reflection coefficient can be related to the bubble size. The discussion in Chapter Three showed that the effects of polydispersity on the shape of the curves through the real and imaginary parts of the reflection coefficient is quite subtle (see *Fig. 3.17*). It would be difficult then to determine the bubble size distribution unequivocally from the ultrasonic measurements, because of the experimental scatter and the

Table 4.7 *The measured physical properties of cream*

Property	Whipping cream	Double cream
Density/ kg m^{-3}	1014 ± 3	1006 ± 3
Group velocity/ m s^{-1}	1526 ± 3	1531 ± 2
Reflection coefficient*	0.35	0.36
Volume fraction of air	53 ± 4	51 ± 3

*: calculated using the characteristic acoustic impedance (= ρc).

quantitative errors in the theoretical predictions. Nevertheless, it is possible that by normalising the ultrasonic measurements and the predictions, the bubble size could be measured ultrasonically. The process by which the bubble size would be determined is similar to the process by which the Mastersizer calculates the particle size distribution. An initial guess is made for the bubble size (or size distribution). The expected properties of a system with such a size are calculated, and compared with the measured properties. On the basis of the comparison, the assumed bubble size is adjusted, the predicted properties recalculated and the new predictions are compared to measurement. This process is iterated until the disagreement between prediction and measurement is minimised.

4.6 Cream

The velocity and density of unwhipped whipping cream and double cream are listed in *Table 4.7*. Reported measurements of attenuation at 20 °*C* exist for native single cream with a fat content of 18 wt% (Miles *et al*, 1990). The attenuation varies linearly from about 4 Np m^{-1} at 1.5 MHz, to about 15 Np m^{-1} at 7 MHz.

4.6.1 Unwhipped cream

The measured reflection coefficient of native whipping cream and double cream is shown in *Figs. 4.57* and *4.58* respectively. The results were very similar to the results for yogurt (*Figs. 4.52* and *4.53*). The creams were not dispersive in the frequency range examined, and the reflection coefficient can be accurately predicted using the characteristic acoustic impedance. This is compatible with the relatively

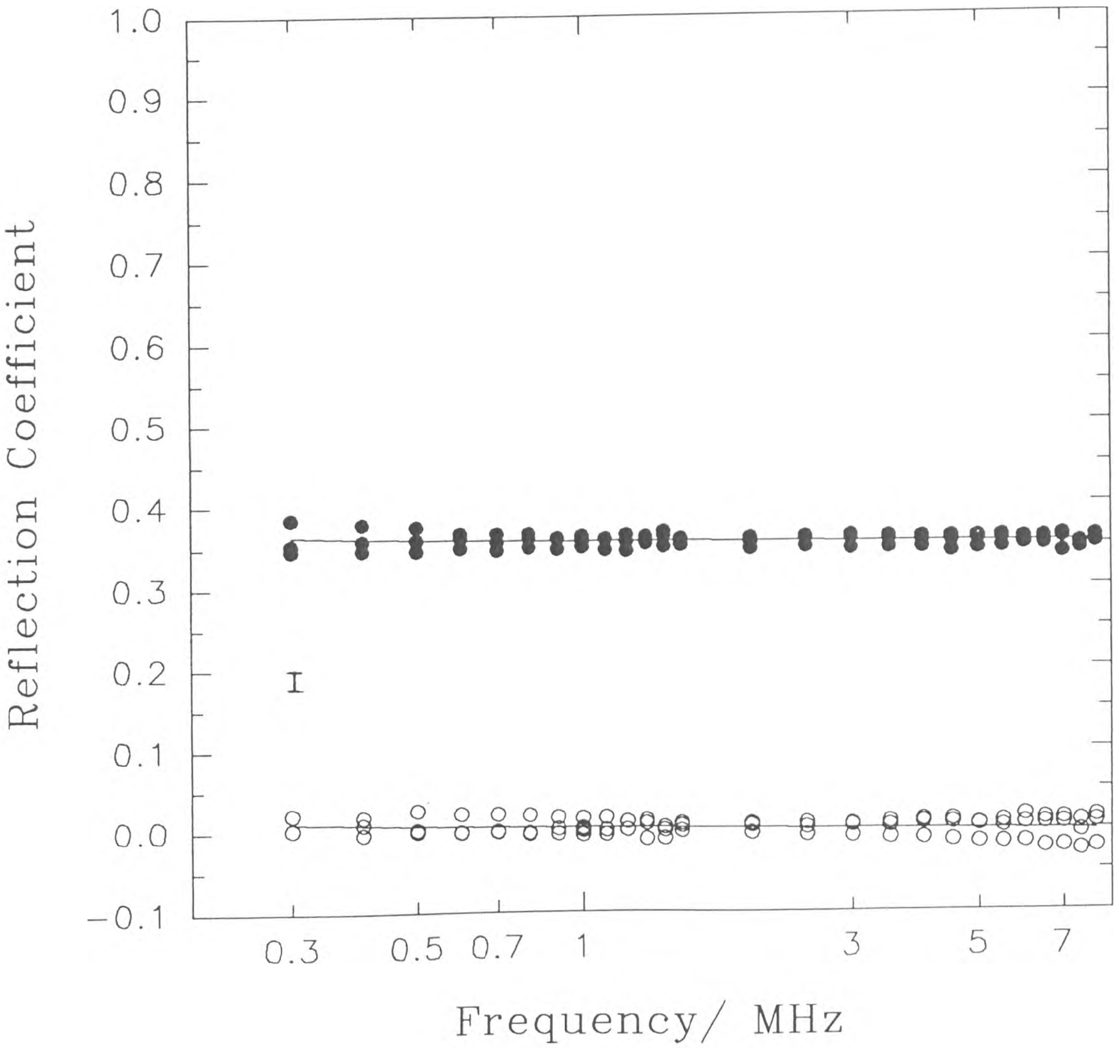

Figure 4.57 The measured real part (●) and imaginary part (○) of the reflection coefficient of air-free whipping cream. Regression lines are drawn through the data. The bar indicates the estimated accuracy of the measurement, when applied to standard liquids under controlled conditions.

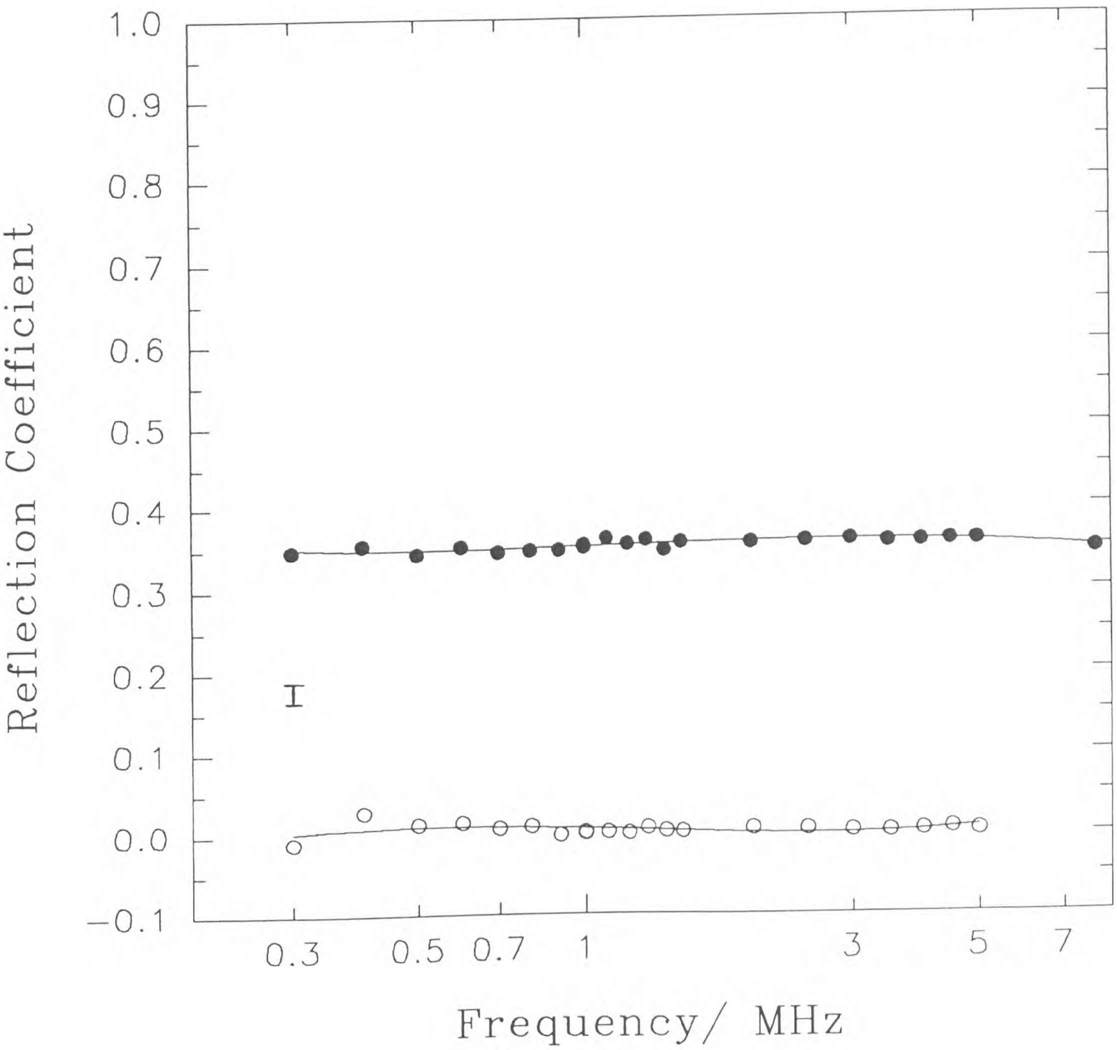

Figure 4.58 The measured real part (●) and imaginary part (○) of the reflection coefficient of air-free double cream. Regression lines are drawn through the data. The bar indicates the estimated accuracy of the measurement, when applied to standard liquids under controlled conditions.

low attenuation measured by Miles *et al* (1990).

4.6.2 Whipped cream

The measured reflection coefficient of whipped whipping cream and double cream is shown in *Figs. 4.59* and *4.60* respectively. There was a fair degree of scatter in the results, but the measurements indicated that the bubbles in the whipped cream resonated at frequencies higher than the ones used here. If whipped cream were treated as simply native cream containing bubbles with radii in the region 5 to 10 μm (cf Anderson & Brooker, 1988) then resonant behaviour would be expected in the frequency range which was examined. This could be due to the presence of much smaller bubbles than those seen by Anderson & Brooker, or due to non-sphericity of some of the bubbles, or it could be an effect of the fat globule network (see Chapter Three).

4.6.3 Ultrasound as a probe of conventional whipped cream

In the absence of accurate bubble size information for the whipped creams examined here it is not possible to be certain that there were no very small bubbles in the cream, but considering the relatively short whipping time and the low shear involved, the formation of very small bubbles does not seem very likely. Some of the bubbles were however almost certainly non-spherical, because of the presence of so many fat globules at the interface. The effects of non-sphericity would not be expected to shift the resonant frequency by a very large amount. The principal effect of the fat globule network is to dramatically increase the effective stiffness of the bubble wall. This certainly would be expected to cause a very large increase in the resonant frequency.

Without knowing the true bubble size distribution or the effects of the fat globule network, it is not possible to predict the reflection coefficient in the whipped creams. In theory, at frequencies well below resonance the velocity in bubbly liquids is described by the Wood equation (see Chapter Two). The Wood velocity in whipped cream is around 20-30 m s^{-1}, leading to a reflection coefficient of very nearly one. The observed real part of the reflection coefficient was rather lower than this, although the imaginary part was very close to zero at frequencies below 1 MHz. It would not be possible therefore to estimate the bubble size or the volume

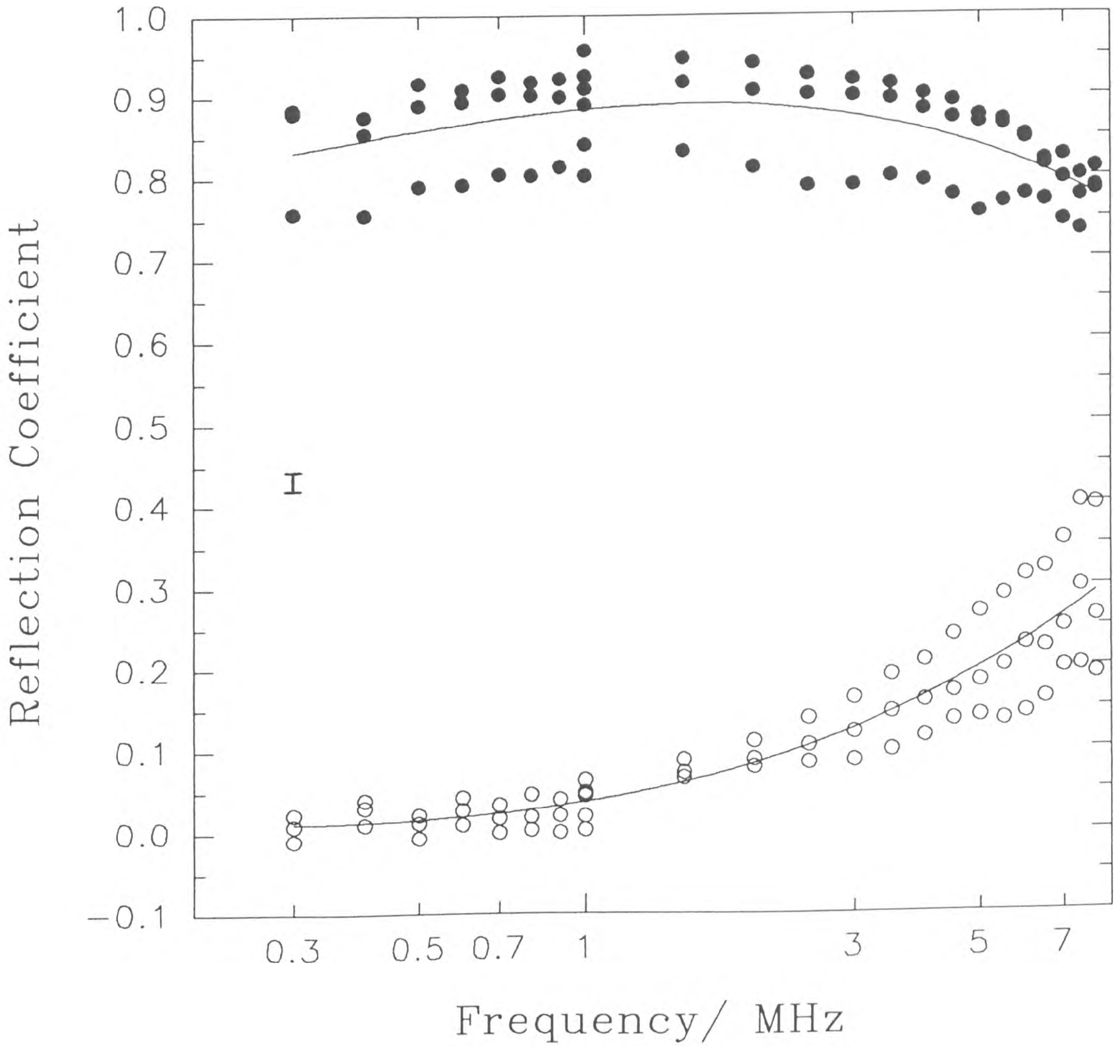

Figure 4.59 The measured real part (●) and imaginary part (○) of the reflection coefficient of whipped whipping cream. Regression lines are drawn through the average of the data. The bar indicates the estimated accuracy of the measurement, when applied to standard liquids under controlled conditions.

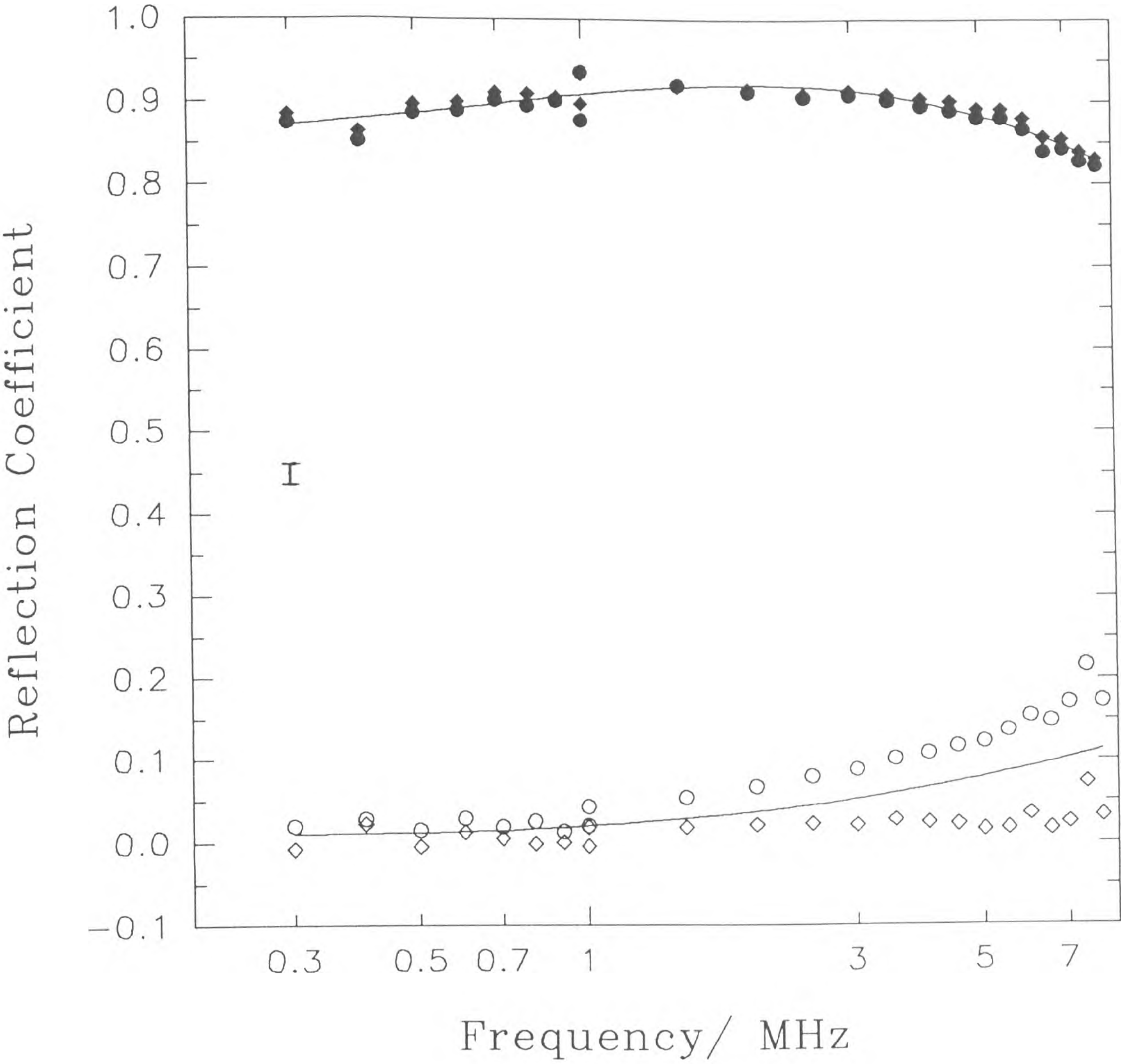

Figure 4.60 The measured real part (●) and imaginary part (○) of the reflection coefficient of whipped double cream. Regression lines are drawn through the average of the data. The bar indicates the estimated accuracy of the measurement, when applied to standard liquids under controlled conditions.

fraction of air in whipped cream from ultrasonic measurements in the frequency range used here.

4.6.4 An unconventional whipped cream: Anchor spray cream

The whipped whipping cream and double cream were stable for several days at 5 °*C*. The measured real part of the reflection coefficient changed relatively little over the course of 24 hours. The behaviour of the imaginary part was less consistent: in most samples it tended to level off to zero as time progressed, while in other samples it stayed the same or increased at higher frequencies. The behaviour of Anchor spray cream was markedly different. The volume fraction of gas in the cream was very high just after it was dispensed. The process of transferring the cream to the FSUPER reduced the volume fraction to roughly 0.75, and there was a lot of inter sample variation. The measured reflection coefficient of Anchor spray cream is shown in *Fig. 4.61*. Surprisingly, resonant behaviour was clearly observed. This may be due in part to the fact that the lamellae between the bubbles are thinner than in conventional whipped cream (see Section 3.1.6.3), or it could be due to the presence of larger bubbles than the electron micrograph shown here would suggest. Although the Anchor cream is stabilised by fat globules, it was not nearly as stable as conventional whipped cream[†]. The change in resonant frequency, and hence bubble size, with time is clearly seen in *Fig. 4.62*, which shows the reflection coefficient of Anchor cream as a function of time over two hours. The ultrasonic technique may be useful therefore for characterising dynamic systems such as spray cream, where the bubble size is changing rapidly, and where the sample would be adversely affected by the use of an invasive or destructive technique.

4.6.5 Ultrasound as a probe of spray cream

Ultrasonic measurements on spray cream in the FSUPER seem to be more useful than measurements on conventional cream. A rough idea of the bubble size can be gained by assuming that the frequency at which the curves through the real and imaginary parts of the reflection coefficient cross is ten times higher than the

[†]: Anchor cream contains hydrocolloid stabilisers which increase the viscosity of the continuous phase in order to enhance the stability. The presence of these stabilisers made it impossible to obtain a satisfactory gas-free sample for ultrasonic analysis.

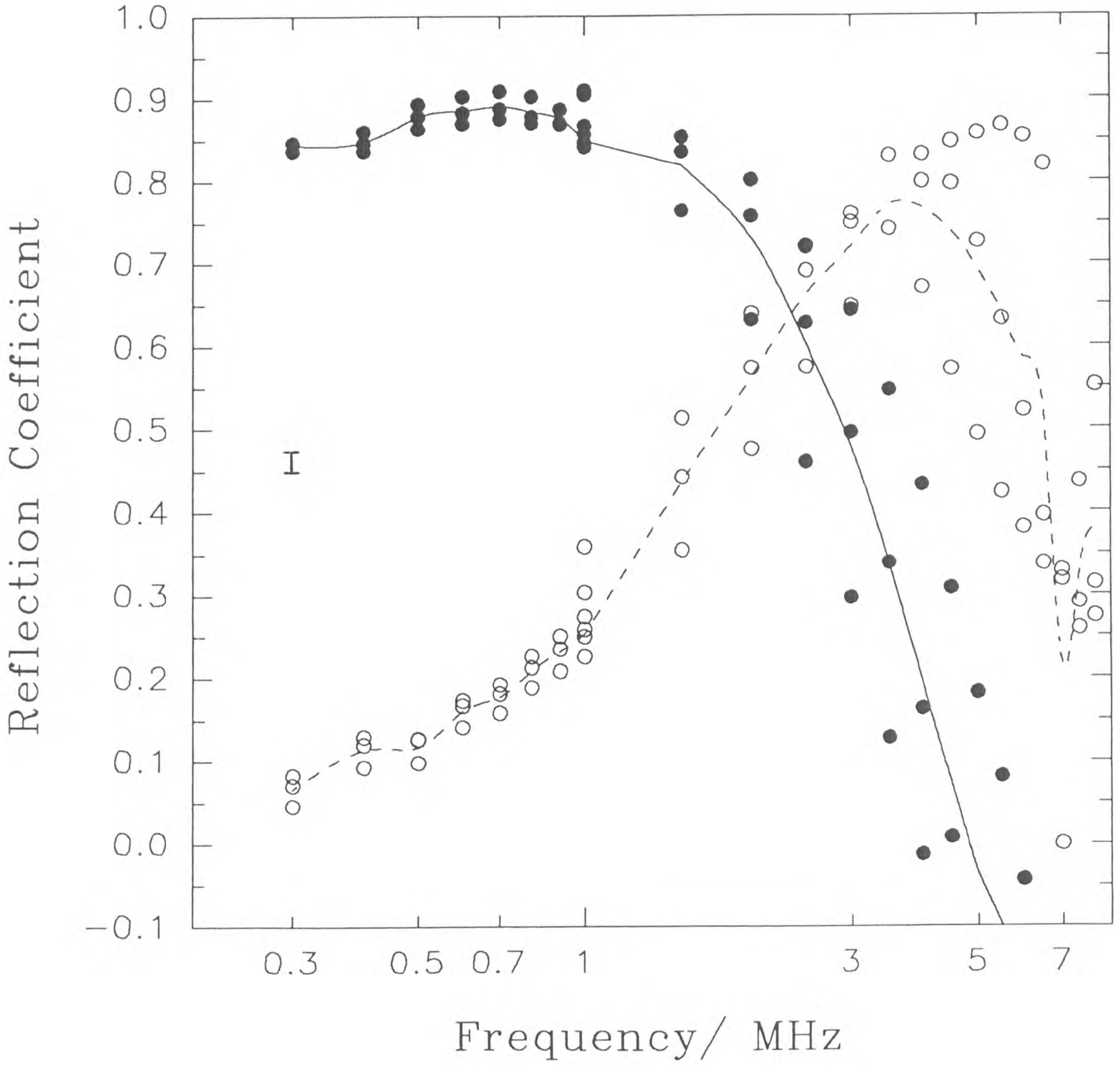

Figure 4.61 The measured real part (●) and imaginary part (○) of the reflection coefficient of Anchor spray cream. Regression lines are drawn through the average of the data. The bar indicates the estimated accuracy of the measurement, when applied to standard liquids under controlled conditions. The kink in the curve through the imaginary part is due to scatter in the data.

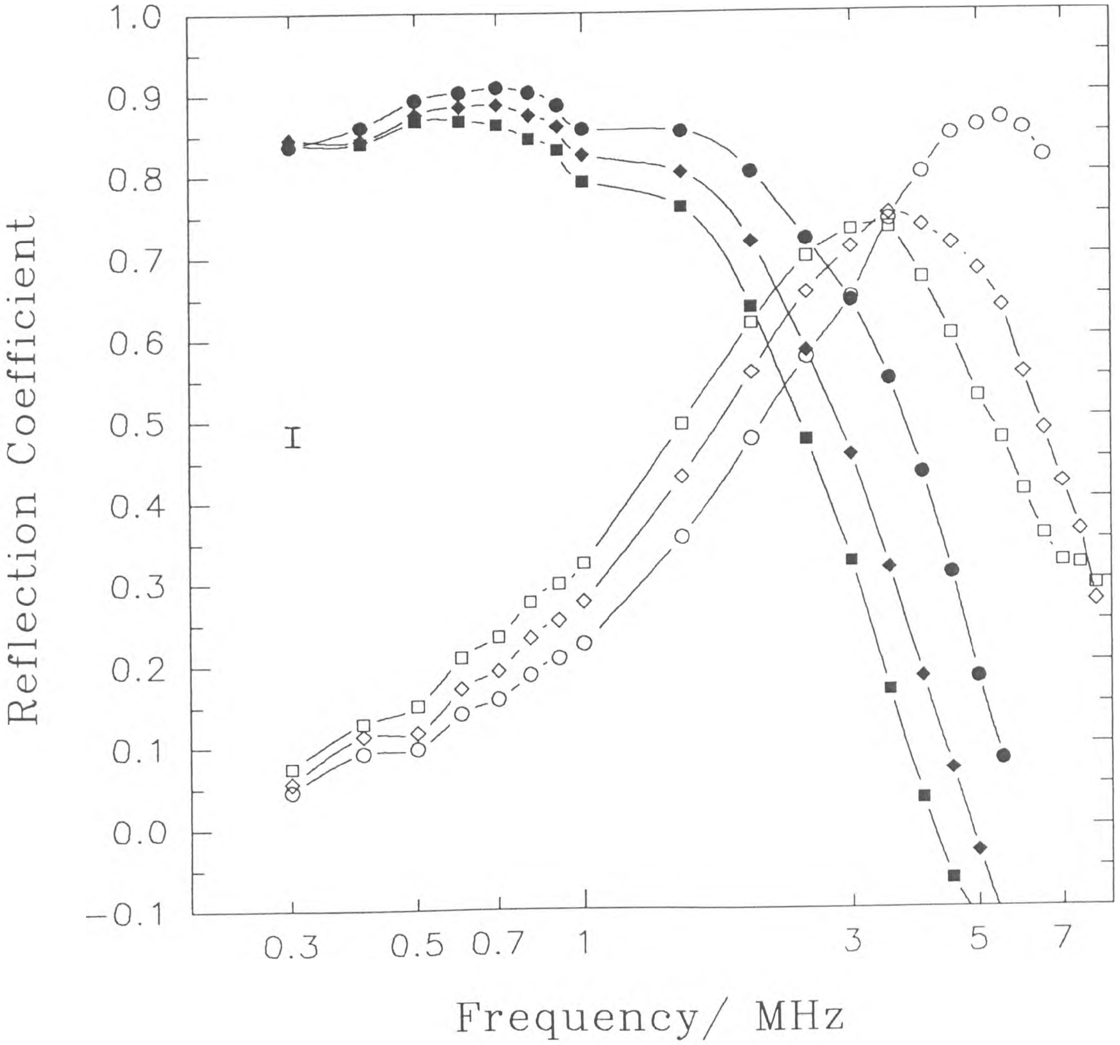

Figure 4.62 The measured real part (solid symbols) and imaginary part (hollow symbols) of the reflection coefficient of Anchor spray cream as a function of time. Regression lines are drawn through the average of the data. The bar indicates the estimated accuracy of the measurement, when applied to standard liquids under controlled conditions. ●: $t = 0$ (cream reaches 5 °C), ◆: $t = 1$ hour, ■: $t = 2$ hours.

resonant frequency. Taking the density of the air-free Anchor cream as 1000 kg m^{-3}, and the apparent resonant frequency as approximately 0.3 MHz, the Minnaert equation gives an approximate bubble radius of 10 μm. This is in keeping with the expected bubble size. The Minnaert equation underpredicts the bubble size because the effect of material at the interface is not accounted for.

4.7 Bread dough

4.7.1 Unyeasted dough

The viscous and cohesive nature of bread dough made it very difficult to measure its density accurately. An approximate figure for the unyeasted dough was 1300 kg m^{-3}. The volume fraction of air in the unyeasted dough was very small, and the inaccuracy in the density determinations made it impossible to measure. A reasonable estimate would be in the range 1-3 %. The reflection coefficient of the unyeasted dough is shown in *Fig. 4.63*. Once again, resonant behaviour was clearly observed, and the real part of the reflection coefficient reached a stable value of about 0.25. This is concomitant with the behaviour expected in systems containing small amounts of air. The velocity above resonance should in theory be equal to the velocity in the air-free medium. If this is so, then the impedance of the medium becomes completely real, and the reflection coefficient can be related to the density of the dough and its velocity. Taking the density as 1300 kg m^{-3}, and the reflection coefficient as 0.25, this would indicate a velocity in the dough of about 1500 m s^{-1}. This is about 20 m s^{-1} higher than the velocity of water at 20 °*C*, and seems to be a reasonable figure.

Moorjani (1984) measured the velocity in unyeasted dough as 114 m s^{-1}, the bulk modulus as 16×10^6 Pa, and the density as 1240 kg m^{-3} at a temperature of 20 °*C* and a frequency of 0.5MHz. At 0.5 MHz, the measurements made in this work show that resonance was occurring and the velocity was therefore elevated. If the reflection coefficient at 0.5 MHz is taken as $(0.8 + 0.35i)$ and the density of air-free unyeasted dough is taken as 1300 kg m^{-3}, the specific acoustic impedance and effective density (*Equation 2.112*) of the dough can be calculated. The velocity, c, and attenuation, α, in the dough are then given by the basic relationships

$$Z = \omega c / k \qquad [4.1]$$

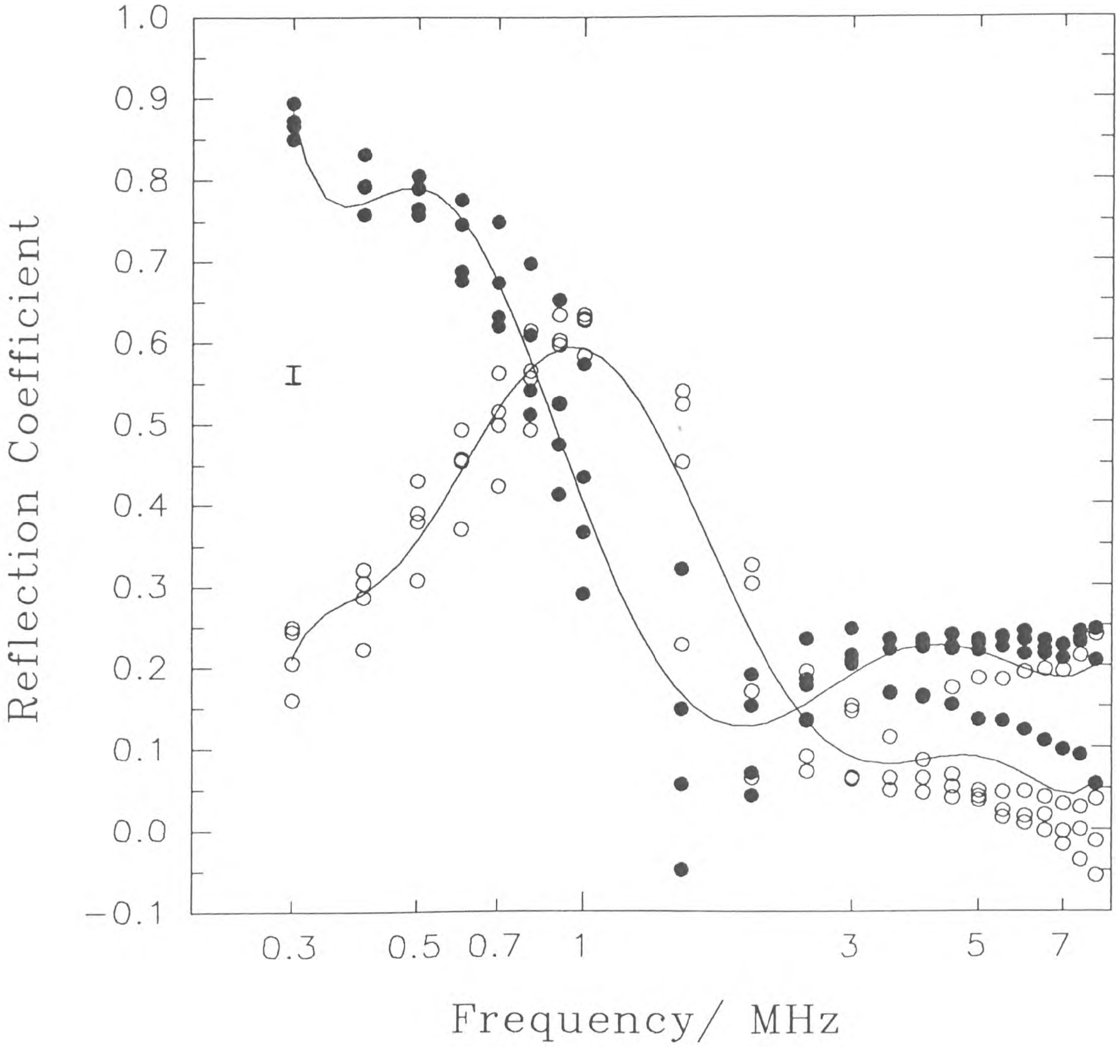

Figure 4.63 The measured real part (●) and imaginary part (○) of the reflection coefficient of unyeasted bread dough. Regression lines are drawn through the average of the data. The bar indicates the estimated accuracy of the measurement, when applied to standard liquids under controlled conditions.

$$k = \omega / c + i\alpha \qquad [4.2]$$

where Z is the specific acoustic impedance, ω is the angular frequency and k is the propagation coefficient. The calculated velocity and attenuation are around 1760 m s^{-1} and 5200 Np m^{-1} if the volume fraction is taken as 1 %. These values change to 1865 m s^{-1} and 5000 Np m^{-1} if the volume fraction is taken as 3 %. The calculated velocity and attenuation should be treated with some caution however. Strictly speaking, they only apply to that portion of the bread dough which was sampled by the FSUPER (which was probably a relatively small proportion of the total dough). Also, the choice of expression for the effective density has a big effect on the calculated velocity and attenuation.

The very low velocity measured by Moorjani suggests that the measurements were made at sub-resonant frequencies. In systems containing small amounts of air, the velocity below resonance is accurately predicted by the Wood equation (*Equation 2.109*). If the density of the air-free unyeasted dough is approximated by the density of the native unyeasted dough, then the Wood equation gives a volume fraction of air of about 0.8 %.

The radius of the bubbles in the unyeasted dough can also be estimated. Taking the resonant frequency as 0.08 MHz, the Minnaert equation yields a radius of roughly 35 μm. This is consistent with the radii of the stable bubbles observed by Shimiya & Yano (1987,1988) and Kumagai *et al* (1991).

4.7.2 Yeasted dough

The ultrasonic measurements on the yeasted dough were not consistent. The results for two different samples are shown in *Figs. 4.64*. The unusual character of the results is genuine (the measurements were made on different occasions, and other samples were satisfactorily characterised in the FSUPER in the interval). The dough did expand greatly over the course of fermentation, so that the volume fraction in the fermented dough was of the order of 60-70 %. The bubbles in the were several millimetres across, and the dough matrix itself was full of smaller bubbles of a range of sizes. It is suggested that the ultrasonic behaviour of this matrix was not straightforward. Ultrasonic measurements were made on the dough

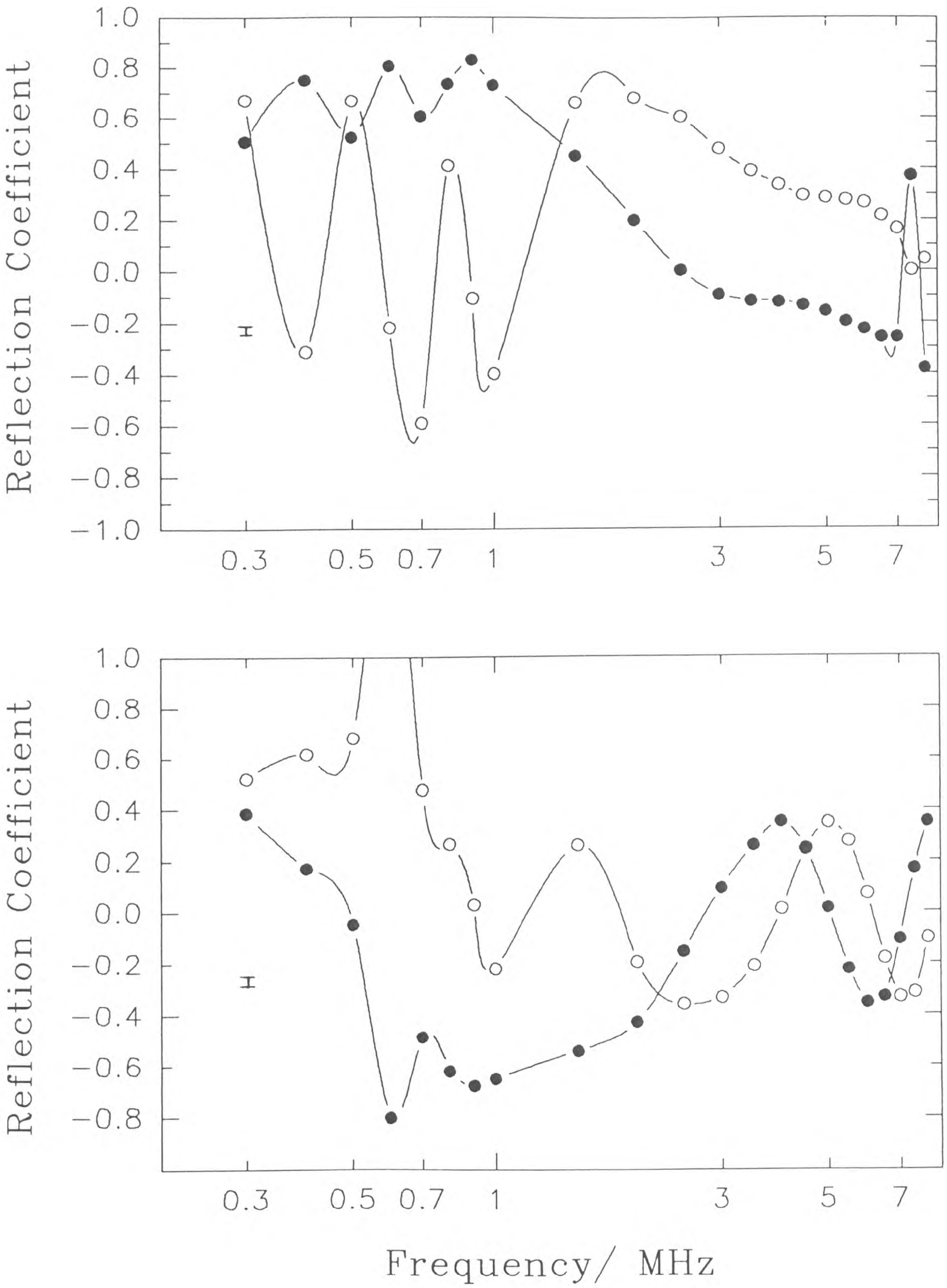

Figure 4.64 The measured real part (●) and imaginary part (○) of the reflection coefficient of fermented bread dough after 24 hours. Regression lines are drawn through the average of the data. The bar indicates the estimated accuracy of the measurement, when applied to standard liquids under controlled conditions. Data are shown for two different samples, plotted separately to enhance clarity.

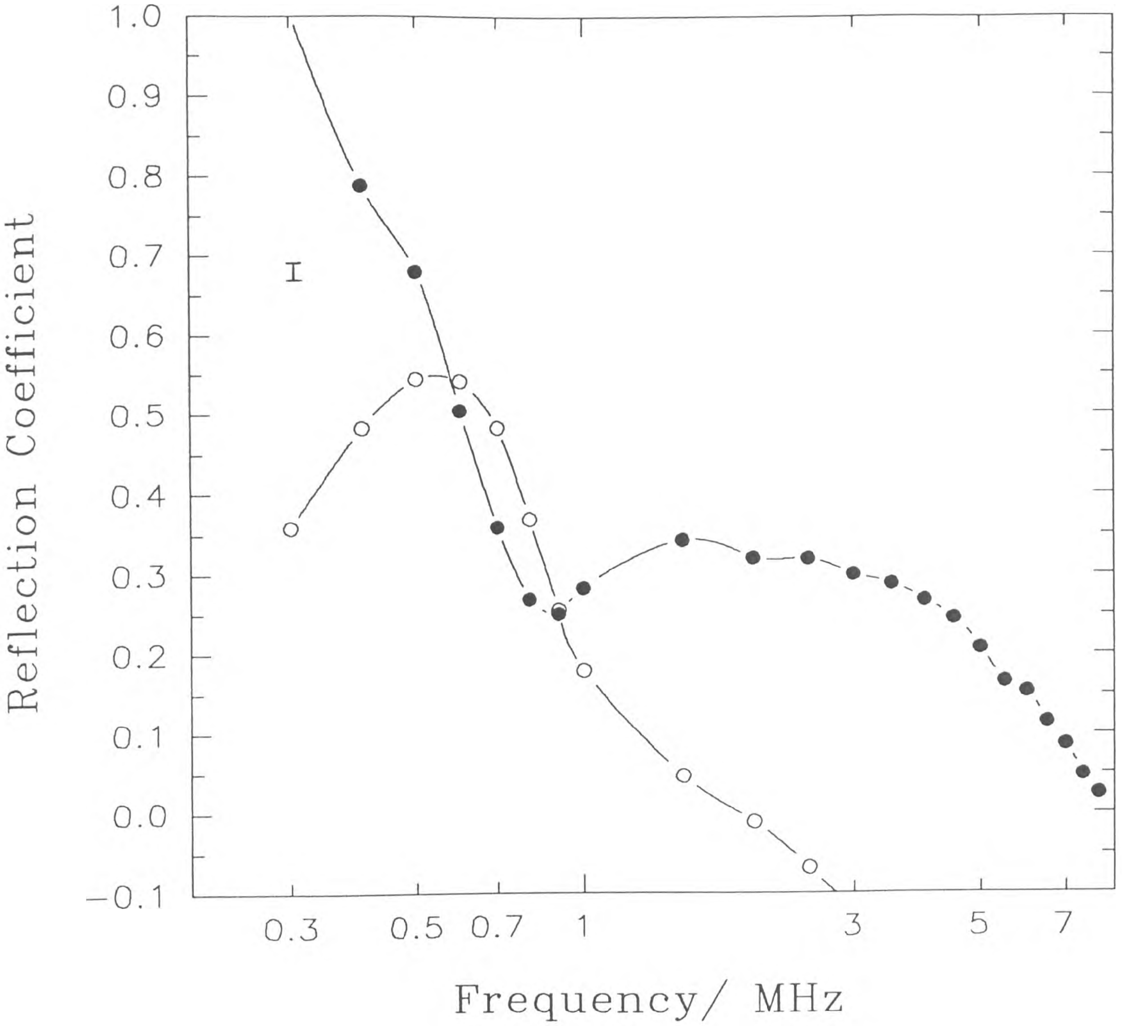

Figure 4.65 The measured real part (●) and imaginary part (○) of the reflection coefficient of fermented dough after 48 hours. Regression lines are drawn through the average of the data. The bar indicates the estimated accuracy of the measurement, when applied to standard liquids under controlled conditions.

after a further 24 hours (see *Fig. 4.65*). The measurements had a form much more like that in the unyeasted dough. A possible explanation is that, once the supply of gas from the yeast had ceased, the normal disproportionation process resumed and the large bubbles shrank. The strange results could also be explained by way in which the FSUPER sampled the dough: the bubbles which were directly adjacent to the buffer rod surface might not have grown in the same way as the bubbles in the bulk dough. Similarly the shrinkage and collapse of these bubbles may have been unrepresentative.

4.7.3 Ultrasound as a probe of bread dough

Clearly a great deal more experimentation would be required in order to establish the full usefulness of ultrasound as a technique for measuring the breadmaking potential of different flours, but the measurements indicate that the technique is sensitive to the tiny bubbles present in the worked, unfermented dough. It may well be possible to establish a correlation between the bubble size in a dough and the breadmaking potential of the flour used to prepare the dough.

The ultrasound technique is of little use for characterising the fermented dough. Ultrasound would be of use in the early stages of fermentation, when sensible results can be obtained. Useful information might be gained by using a wider range of frequencies. The way in which the FSUPER samples the dough would need to addressed, in order to gain meaningful results.

4.8 Beer foam

The measurements on beer foam can be conveniently split between the low frequency and high frequency transducers. This is because the transducers were located at different heights within the FSUPER. The low frequency transducer was nearest to the bottom of the FSUPER, and therefore primarily sampled the bulk beer. The high frequency transducer was located near the top of the instrument, and thus primarily sampled the beer foam.

4.8.1 Low frequency measurements on frothy beer

The measured reflection coefficient of Swan Light, Michelob and Smithwick's beer are shown in *Figs. 4.66* to *4.68* respectively. The measurements on John Smith's

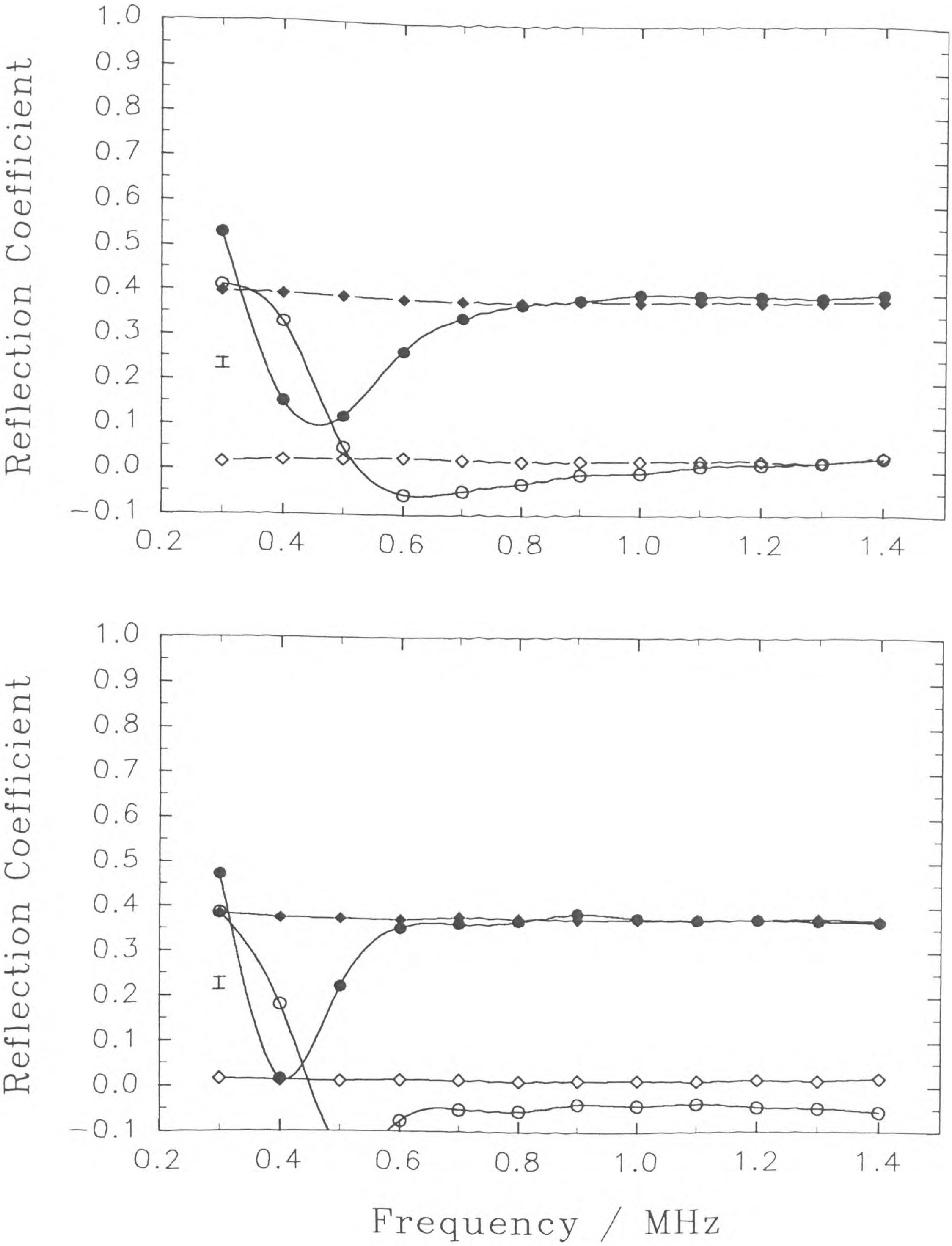

Figure 4.66 The measured real part (solid symbols) and imaginary part (hollow symbols) of the reflection coefficient of frothy Swan light beer. The samples are shown separately for improved clarity. Regression lines are drawn through the data. The bar indicates the estimated accuracy of the measurement, when applied to standard liquids under controlled conditions. ●: $t = 0$ (immediately after pouring into FSUPER), ◆: $t = 30$ seconds.

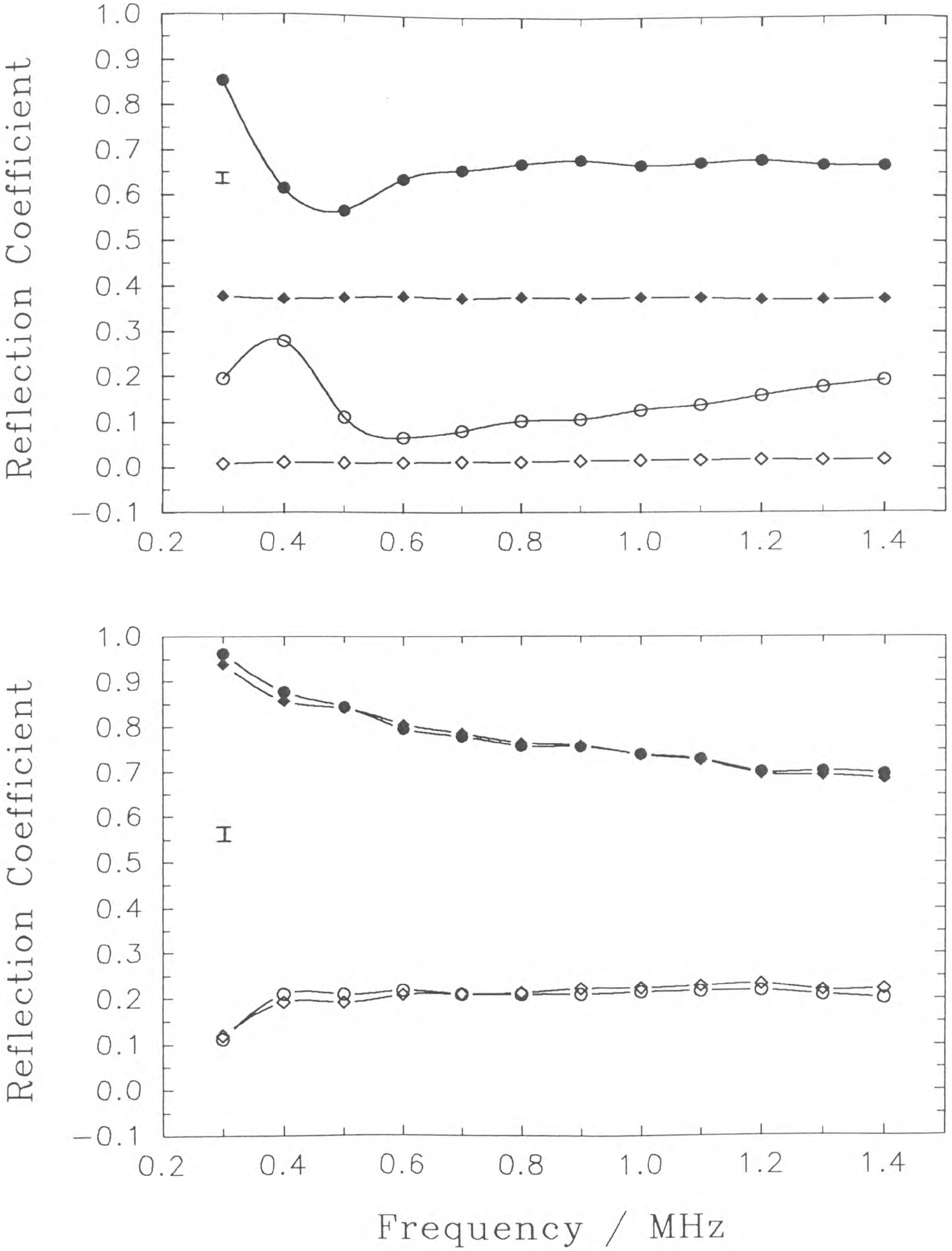

Figure 4.67 The measured real part (solid symbols) and imaginary part (hollow symbols) of the reflection coefficient of frothy Michelob beer. The samples are shown separately for improved clarity. Regression lines are drawn through the data. The bar indicates the estimated accuracy of the measurement, when applied to standard liquids under controlled conditions. ●: t = 0 (immediately after pouring into FSUPER), ◆: t = 30 seconds.

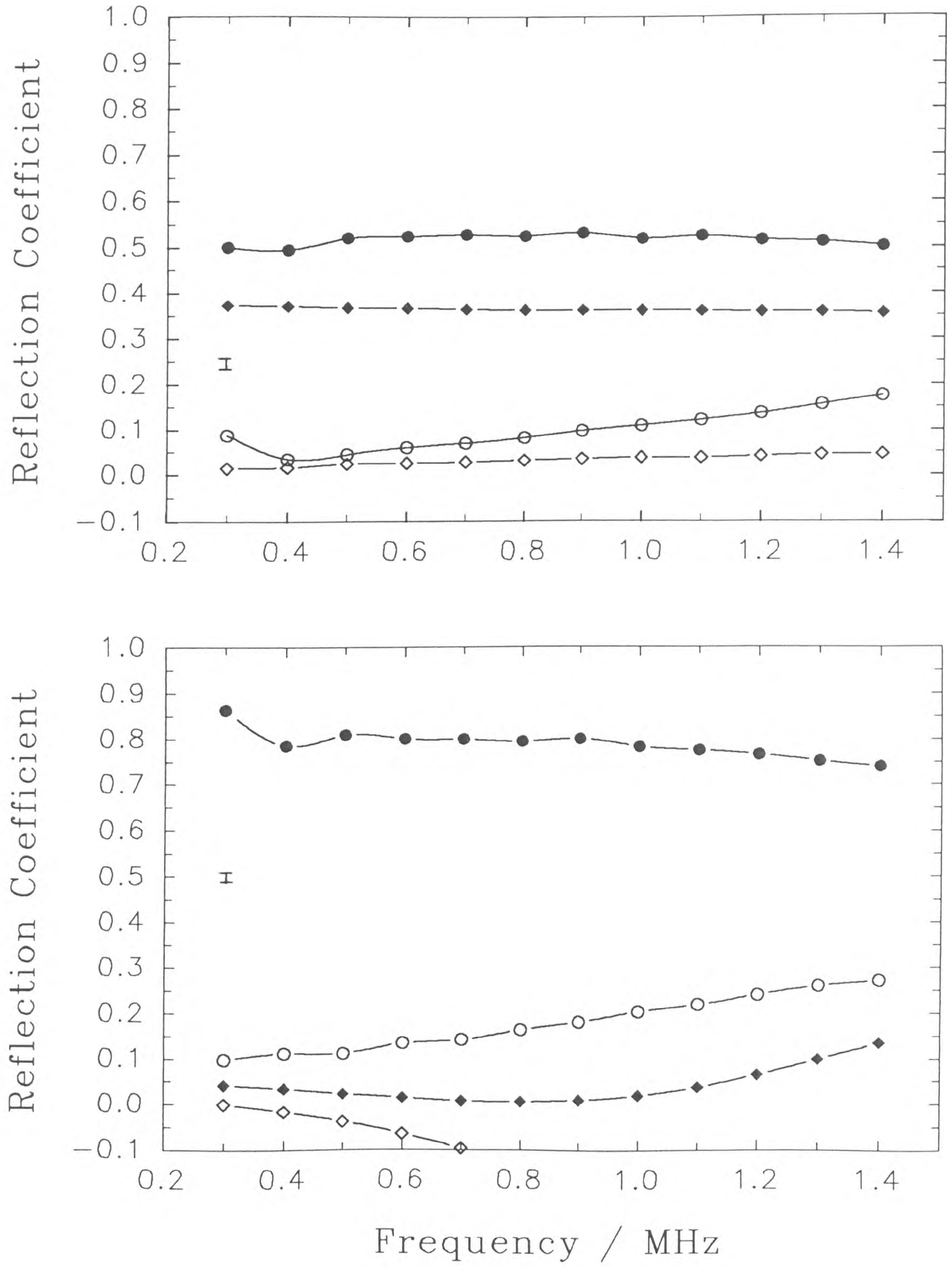

Figure 4.68 The measured real part (solid symbols) and imaginary part (hollow symbols) of the reflection coefficient of frothy Smithwick's beer. The samples are shown separately for improved clarity. Regression lines are drawn through the data. The bar indicates the estimated accuracy of the measurement, when applied to standard liquids under controlled conditions. ●: $t = 0$ (immediately after pouring into FSUPER), ◆: $t =$ 30 seconds.

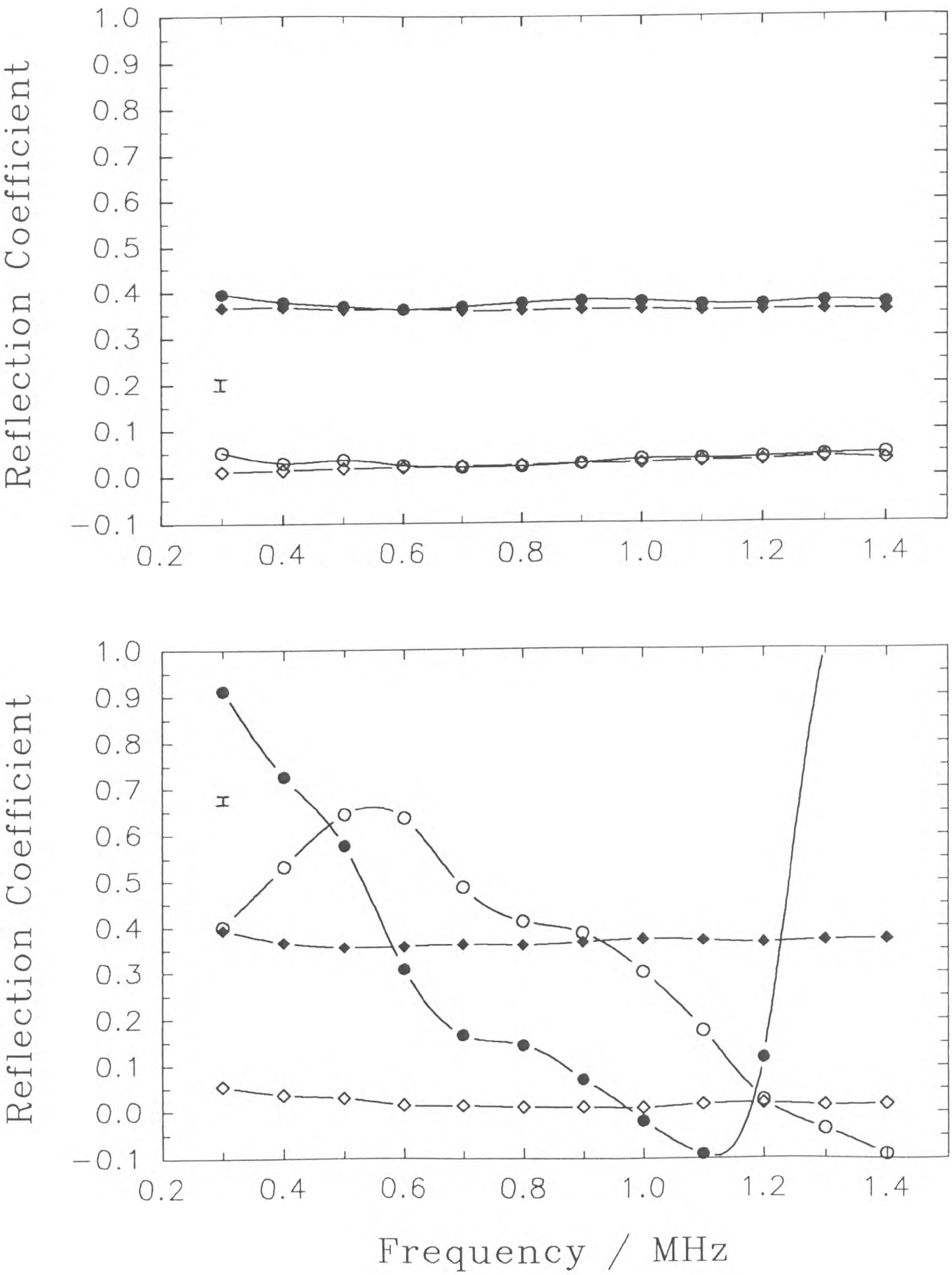

Figure 4.69 The measured real part (solid symbols) and imaginary part (hollow symbols) of the reflection coefficient of frothy John Smith's (top) and Bodington's (bottom) beer. The samples are shown separately for improved clarity. Regression lines are drawn through the data. The bar indicates the estimated accuracy of the measurement, when applied to standard liquids under controlled conditions. ●: $t = 0$ (immediately after pouring into FSUPER), ◆: $t = 30$ seconds.

and Bodington's beer are shown together on *Fig. 4.69*. Unsurprisingly, there was a great deal of variation between the samples. The results for Swan Light (*Fig. 4.66*) were the most consistent, and will be discussed in a little detail.

Initial measurements There was evidence for the presence of large bubbles in the beer when it was first examined. Taking the density of the gas free beer as approximately 1000 kg m^{-3}, and the resonant frequency as approximately 0.03 MHz, then the calculated bubble radius is around 0.1 mm, which seems a reasonable figure. Very large bubbles were observed visually present in the freshly poured beer, but these do not seem to have affected the results. According to Stokes' equation (*Equation 1.1*), a bubble with a radius of 1 mm will have a rise velocity of approximately 1.1 m s^{-1}. The low frequency transducer sampled a cross section of the beer with a diameter of roughly five centimetres, and a bubble with a radius of 1 mm would cream through this distance in about 0.05 seconds. The ultrasonic data was collected over a period of about 10 seconds, so there was ample time for the big bubbles to cream, even though their motion was retarded somewhat by the presence of the many neighbouring bubbles. A bubble with a radius of 0.1 mm would be expected to have a rise velocity of about 0.02 m s^{-1}, so it would stay in the area probed by the transducer for at least 2.5 seconds.

Measurements after 30 seconds After the beer had settled somewhat, nearly all the large bubbles had risen out of the volume which was probed by the low frequency transducer. The beer appeared to be non-dispersive in the frequency range examined, and the reflection coefficient was completely real and approximately equal to 0.4. At 5 °C, the ultrasonic velocity in water is about 1426 m s^{-1} (del Grosso & Mader, 1972), and the reflection coefficient is therefore approximately 0.39. The ultrasonic velocity of gas-free beer was not measured, but in this low alcohol beer, it would be expected to be slightly higher than the velocity of water, as would the density. This would lead to a reflection coefficient which is less than 0.39. The slight elevation in the reflection coefficient was probably due to the presence of small amounts of gas in the beer, which depressed the velocity.

Low frequency measurements on the other beers The results for the other beers varied quite a lot from sample to sample and from beer to beer. The initial results were the most varied. The measurements on Bodington's (*Fig. 4.69*) were noticeably different. The presence of rather smaller bubbles was indicated, which is in keeping with the finely textured foam which was observed as a result of the presence of the nitrogen insert. After 30 seconds, the results for all beers tended towards those seen in the Swan Light, with a reflection coefficient in the range 0.38 to 0.40.

4.8.2 High frequency measurements on frothy beer

The high frequency transducer primarily sampled the foam which formed on the top of the beer. The measurements on Swan Light, Michelob and Smithwick's beer are shown in *Figs. 4.70* to *4.72* respectively. The measurements on John Smith's and Bodington's are shown in *Fig. 4.73*. The high frequency results were much more consistent. Interestingly, these were the only measurements in which the curves through the real and imaginary parts of the reflection coefficient did not cross, despite the evidently resonant behaviour. This was presumably an effect of the very high volume fraction of gas in the foam. The results for John Smith's and Bodington's (*Fig. 4.73*) were rather different, and were much more like the results at low frequencies. The reasons for this behaviour are not clear. The results did not change a great deal after 30 seconds, which belies the aging of the foam, which was easily observed. This was probably a sampling effect, because foam which is adjacent to a solid surface ages differently to bulk foam. This effect is clearly observed when beer is drunk: foam persists on the sides of the glass long after the bulk foam has collapsed.

4.8.3 Ultrasound as a probe of beer and beer foam

On the basis of these measurements, ultrasound does not appear to be very useful for the characterisation of beer and beer foam. There was poor inter sample consistency, and no clear difference was observed between beers, except for Bodington's. The FSUPER did not sample the beer foam satisfactorily, and the results were difficult to interpret. The presence of alcohol is known to have a marked effect on the ultrasonic velocity (Winder *et al*, 1970, Zacharias & Parnell, 1972), yet there was little difference between the results for the low alcohol Swan Light and Smithwick's and the other normal beers. The poor quality of the results was partly due to the way in which the foams were prepared. A much more repeatable

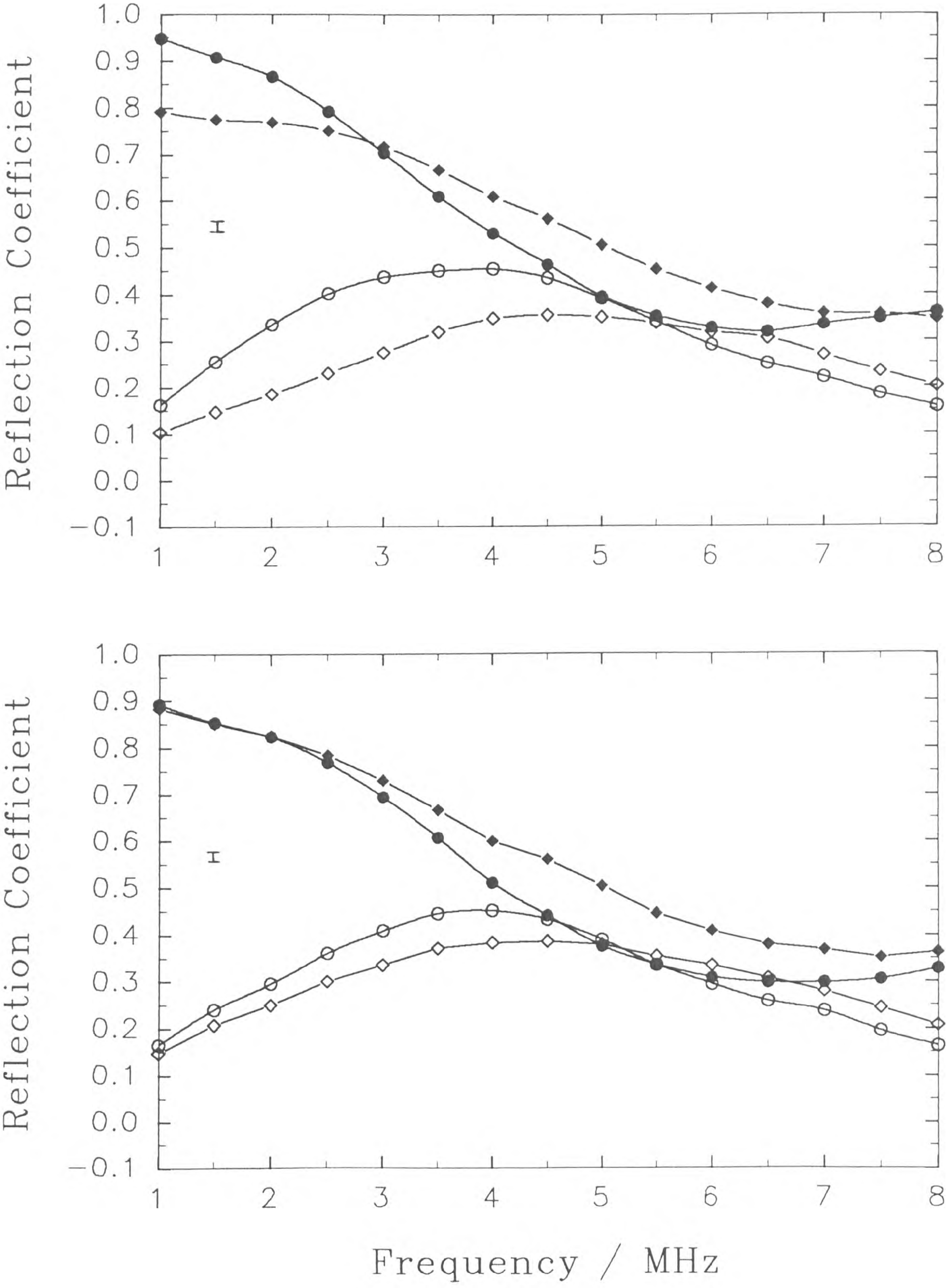

Figure 4.70 The measured real part (solid symbols) and imaginary part (hollow symbols) of the reflection coefficient of frothy Swan light beer. The samples are shown separately for improved clarity. Regression lines are drawn through the data. The bar indicates the estimated accuracy of the measurement, when applied to standard liquids under controlled conditions. ● : $t = 0$ (immediately after pouring into FSUPER), ◆ : $t =$ 30 seconds.

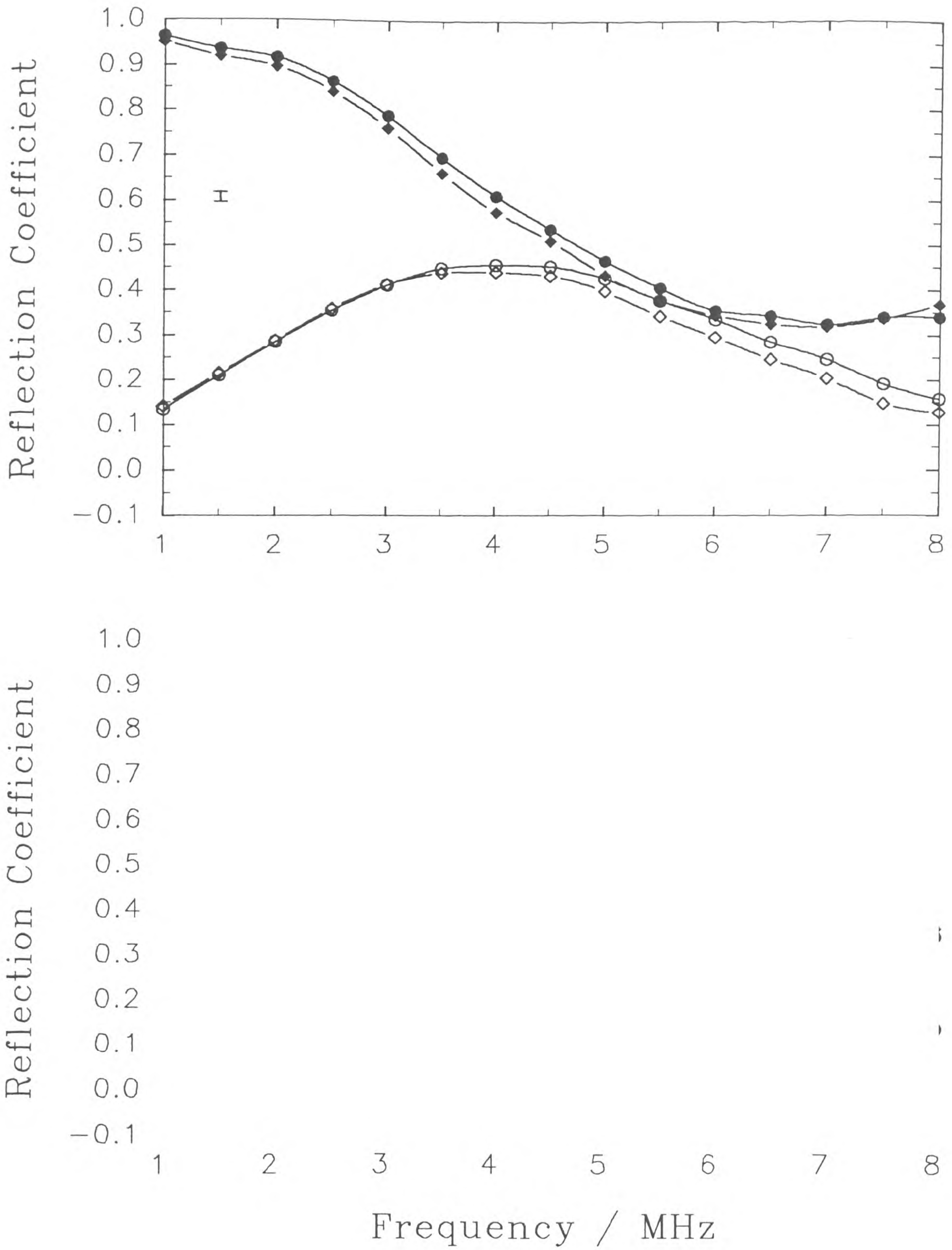

Figure 4.71 The measured real part (solid symbols) and imaginary part (hollow symbols) of the reflection coefficient of frothy Michelob beer. The samples are shown separately for improved clarity. Regression lines are drawn through the data. The bar indicates the estimated accuracy of the measurement, when applied to standard liquids under controlled conditions. ●: $t = 0$ (immediately after pouring into FSUPER), ◆: $t =$ 30 seconds.

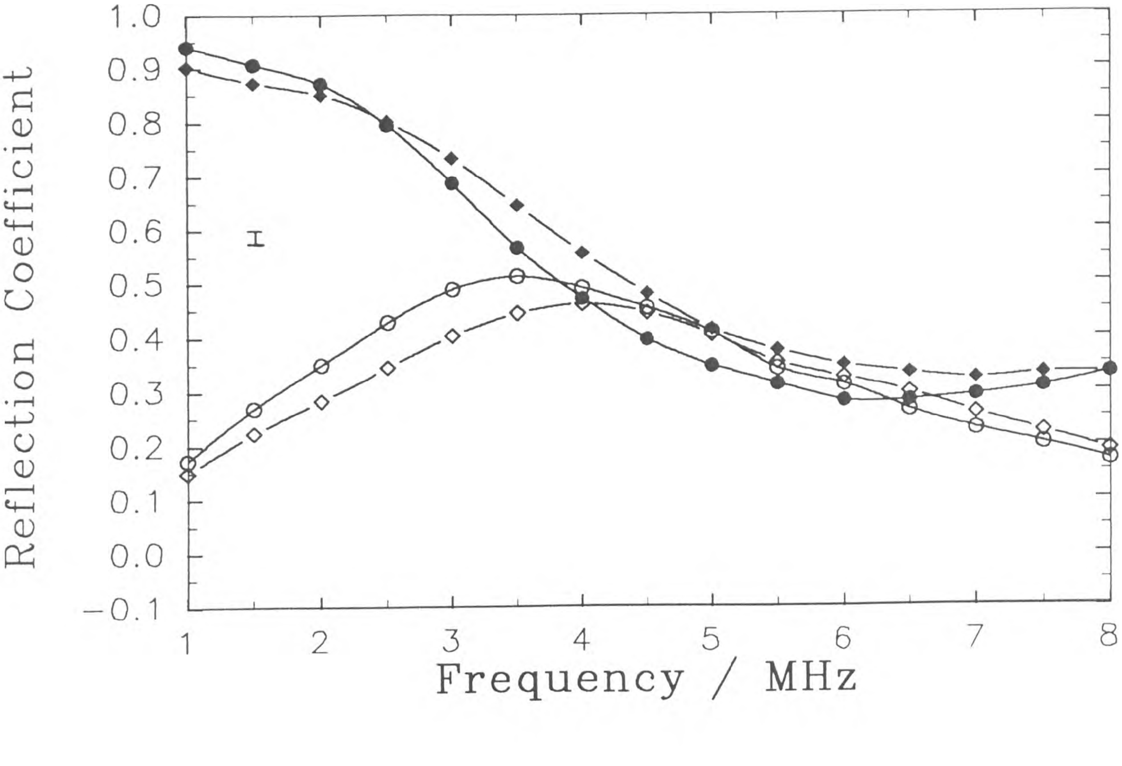

Figure 4.72 The measured real part (solid symbols) and imaginary part (hollow symbols) of the reflection coefficient of frothy Smithwick's beer. The samples are shown separately for improved clarity. Regression lines are drawn through the data. The bar indicates the estimated accuracy of the measurement, when applied to standard liquids under controlled conditions. ●: t = 0 (immediately after pouring into FSUPER), ◆: t = 30 seconds.

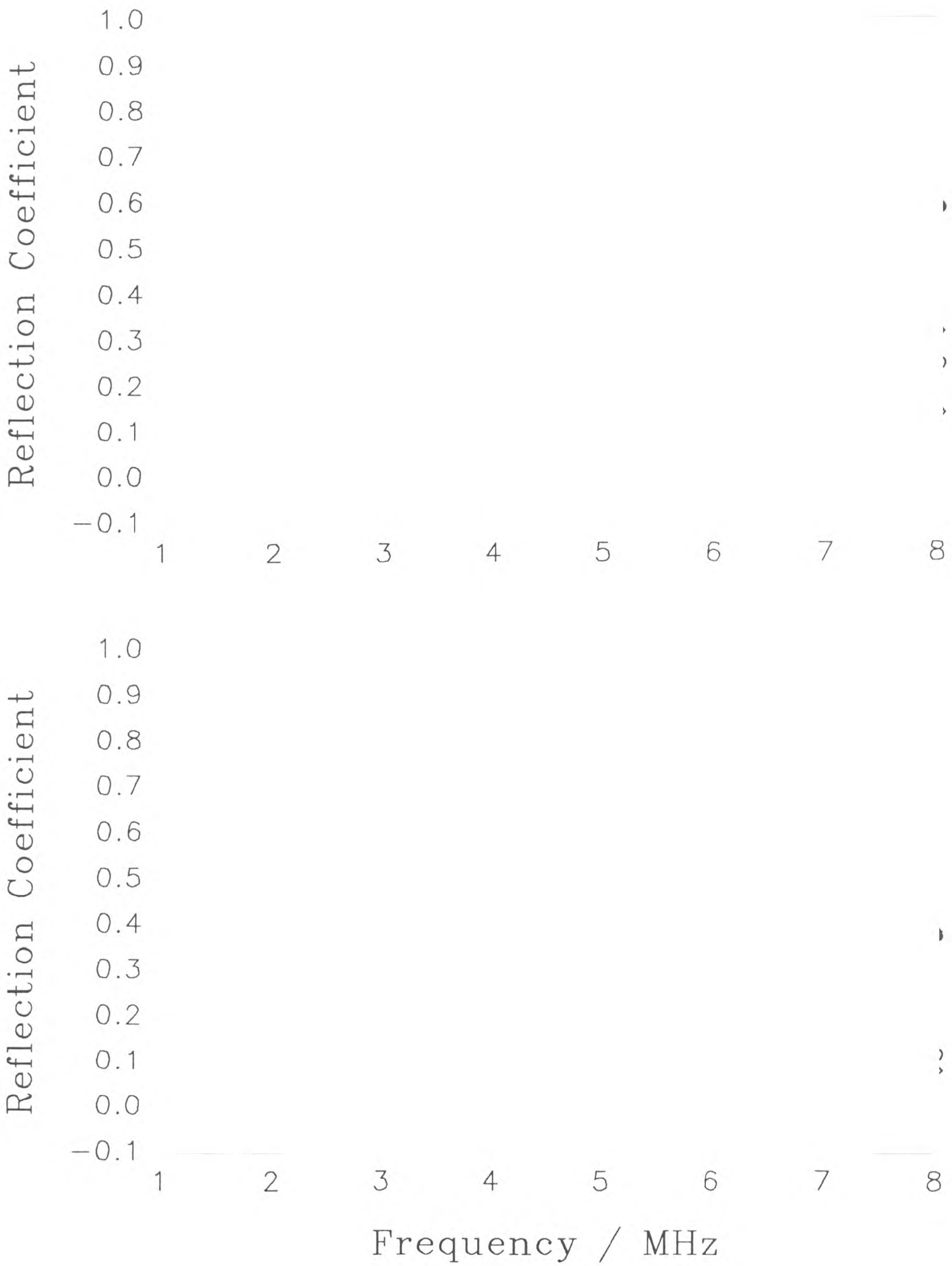

Figure 4.73 The measured real part (solid symbols) and imaginary part (hollow symbols) of the reflection coefficient of frothy John Smith's (top) and Bodington's (bottom) beer. The samples are shown separately for improved clarity. Regression lines are drawn through the data. The bar indicates the estimated accuracy of the measurement, when applied to standard liquids under controlled conditions. ●: $t = 0$ (immediately after pouring into FSUPER), ◆: $t = 30$ seconds.

method of dispensing the beer is required, such as sparging with a known volume of gas. Many more samples would need to be examined in order to draw firm conclusions about the usefulness of ultrasound in the testing of beers. As with the fermented dough, the use of a wider range of frequencies may be useful, and the way in which the FSUPER samples the foam would need to be addressed.

4.9 Summary

Characterisation of the dilute model bubbly system by conventional techniques did not agree very well with the ultrasonic measurements. The ultrasonic measurements indicated the stable existence of very small bubbles at a very low volume fraction. Ultrasound was a rather poor probe of the concentrated model bubbly liquid, because the theory of ultrasonic propagation was seen to fail at high volume fractions of air. Measurements on yogurt were rather more encouraging, and indicated that ultrasound could be used to measure the bubble size but not the volume fraction of air. The resonant frequency of the bubbles in conventional whipped cream was rather higher than expected, and the FSUPER was not able to characterise the system. Useful measurements were obtained on spray cream, which may reflect a difference in the nature of the fat globules in this system. The presence of stable small bubbles in unfermented dough was revealed by the ultrasonic technique. Ultrasound was a poor probe of fermented bread dough, and of beer foam.

CHAPTER FIVE

Conclusions

5.1 Introduction

In contrast to the preceding chapter, this chapter is very brief. The summaries which run throughout the thesis provide a distillation of the key points of the theory and the experimental results, and it seems pointless to recapitulate them here. Instead, the two main findings of this work are outlined.

5.2 The model bubbly liquid

The model bubbly liquid stabilised with P1670 sucrose ester has been shown to be a very interesting system. Sucrose ester has been shown to promote bubbles which are very small and very stable. The formation of an unusual structured surfactant mesophase at the interface has been demonstrated. The properties of the mesophase are largely unknown, and more investigation is called for. The long term stabilisation of bubbles by *structured* surfactant layers is thought to be novel.

5.3 Ultrasound as a probe of aerated foods

This thesis started with the implied question "Can ultrasound be used to characterise aerated foods?". The answer to this question is a highly qualified "yes". The measurements on yogurt, on spray cream and on dough all showed a great deal of promise. However the measurements on the concentrated model, whipped cream and beer foam illustrated several drawbacks to the ultrasonic technique.

Two of these drawbacks are practical ones which could be fairly easily overcome. The frequency range measured by the FSUPER was not wide enough to characterise whipped cream, and no doubt there are many other systems which would be poorly characterised in the FSUPER. However, a revised FSUPER could easily be constructed with a wider operating frequency range. The FSUPER did not always sample a representative cross-section of the liquid of interest. This could be rectified by circulating the sample more effectively, or by periodically cleaning the face of the buffer rod.

The biggest drawback with the ultrasonic technique was the failure of the theory to properly describe propagation in concentrated systems. Given the complex behaviour of bubbly liquids, it is unlikely that the existing theoretical approaches will ever be able to describe propagation in concentrated bubbly liquids. This means that the comparatively accurate ultrasonic characterisation which is possible for emulsions is not likely to be possible for their gaseous counterparts.

5.4 Future work

Two possibilities for future work are proposed: a fuller investigation of dilute model bubbly liquid and an empirical investigation of bubbly foods.

By diluting large amounts of concentrated bubbly liquid it should be possible to obtain a solution containing stable bubbles with sub-micrometre radius at a volume fraction which is high enough to enable reliable characterisation by conventional techniques. By employing measurements over a wide frequency range it should be possible to establish the influence of the surfactant layer at the interface on the ultrasonic properties. By preparing very dilute solutions it should be possible to measure the ultrasonic properties over the entire resonant frequency range. By increasing the volume fraction it should be possible to determine the concentration at which multiple scattering effects start to become important. By further increasing the volume fraction it should be possible to establish the concentration at which multiple scattering theory starts to break down.

Having established that the theory is of limited use, the experimenter has no option but to fall back on empirical techniques. By adjusting the measurement frequency, it should be possible to establish correlations between the ultrasonic properties and conventional measurements of the volume fraction of gas and/or bubble size. This approach is likely to be fruitful in aerated solid foods as well as in bubbly liquids. Ultrasonic measurements may yet prove useful in process control in the manufacture of aerated foods.

APPENDIX I

Diffraction effects

I.1 Introduction

In theories of the propagation of ultrasound, the incident wave is assumed to be perfectly plane and of infinite extent. However, the transducers used to produce ultrasound are of finite size, and this has important consequences for the geometry of the ultrasonic beam which they produce. Consider a transducer (which, for convenience, is assumed to act as a perfect piston) situated in an infinite baffle. The ultrasonic beam produced by such a transducer can be treated as if it had been produced by a myriad of point sources located on the face of the transducer. Each of the point sources produces a spherically symmetric wavelet. These wavelets add together according to Huygens' principle (Blitz, 1963), to produce a wavefront whose nature depends on the diameter of the transducer. This phenomenon is termed *diffraction*. When the diameter of the transducer is small compared to the wavelength of the ultrasound it produces, the effects of diffraction on the ultrasonic beam are quite pronounced. The nature of diffraction effects (sometimes referred to as beam spreading) has been expounded by Papadakis (1975), and the following discussion summarises his treatment.

The ultrasonic beam can be divided into two areas, the near field or Fresnel zone, and the far field or Fraunhofer zone (*Figure I.1*). In the near field there are zeros of pressure along the central axis of the transducer, and there are local minima and maxima of pressure and phase across the beam. In the far field the ultrasonic beam is divided into a primary central lobe, and symmetrically positioned higher order lobes. In practical measurements, when the same transducer is used to generate and receive the ultrasound, diffraction effects add a non-monotonic loss to the amplitude of the received signal. The effect on the phase of the received signal is to add a monotonic but nonlinear increment to the phase as the distance from the transducer increases.

It is possible to make corrections for the effects of diffraction on the amplitude and phase of the received signal (Seki *et al*, 1956, Papadakis, 1967, Benson & Kiyohara, 1974). Indeed, if it desired to make accurate measurements of velocity

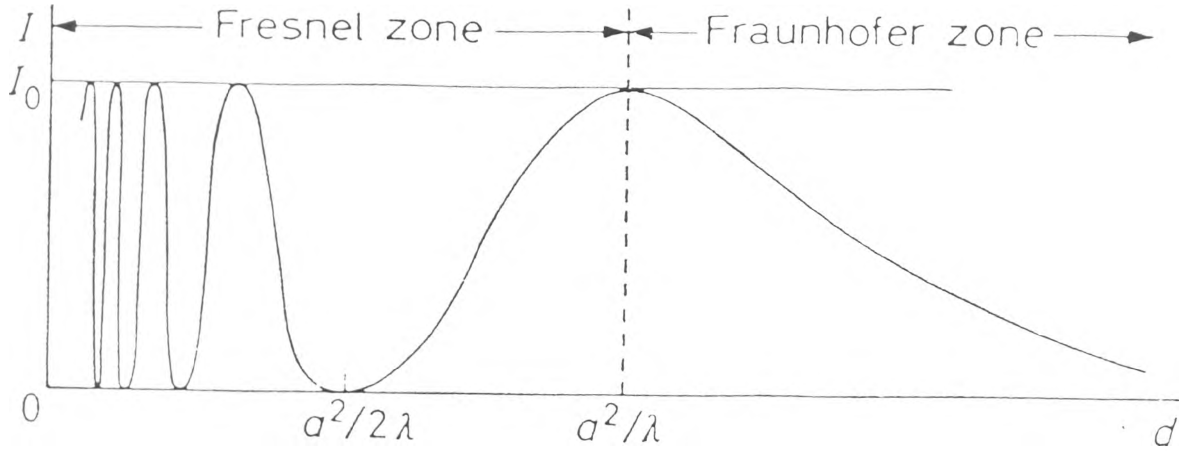

Figure I.1 The sound pressure as a function of distance along the central axis of a transducer, illustrating the near and far fields. *From Blitz, 1963.*

and attenuation, then diffraction corrections must be applied. In this work, the approach of Khimunin (1972, 1975) has been adopted.

I.2 Assumptions made in the calculation of the diffraction corrections

It is assumed that, as a source of ultrasound, the transducer acts as a perfect piston in an infinite baffle. As a detector of ultrasound, the transducer is assumed to be acoustically transparent, and uniformly sensitive across the face of the transducer. These assumptions are necessary in order to achieve tractable equations. Real transducers will deviate from this ideal behaviour to some unknown extent, and the calculated diffraction corrections will therefore be in error by an unknown amount. Nevertheless, the success of the method in practice would suggest that the assumptions are not too restrictive.

The calculation of diffraction corrections is something of a circular process, because the full expressions require values for the velocity and the attenuation coefficient of the sample, the very quantities whose true values are sought. Since these are unknown, the following approximations are made: the attenuation coefficient of the sample is small and can be ignored, and the value of c_s used in the calculations can be taken as the group velocity. It is not expected that the diffraction corrections calculated in this way will be perfect, especially if the sample is particularly attenuating or dispersive.

I.3 Expressions for the diffraction corrections

Consider a circular transducer of radius a, arranged coaxially with a receiver transducer with the same radius, in an infinite uniform isotropic liquid with no intrinsic absorption. The average pressure on the receiver transducer, P, is given by

$$P = \rho_1 c_1 v_0 e^{-ikz} - 4\rho_1 c_1 v_0 / \pi \times \int_0^{\pi/2} \exp\left[-ik\,(z^2 + 4a^2\cos^2\Theta)^{1/2}\right] \sin^2\Theta \, d\Theta \qquad [I.1]$$

where ρ, c and k have their usual meanings, z is the distance between the transducers and v_0 is a constant given by the normal velocity on the surface of a piston source oscillating harmonically in an infinite baffle. P^*, is defined as the pressure which would be experienced by the receiver if the source transducer produced a perfect plane wave. P^* can be extracted from *Equation I.1*

$$P^* = \rho_1 c_1 v_0 \exp(\, i\omega t - ikz) \qquad [I.2]$$

The modulus of the ratio of the two pressures is given by

$$|\,P / P^*\,| = (A^2 + B^2)^{1/2} \qquad [I.3]$$

where $A = 1 - 4 / \pi\,(C \cos kz + D \sin kz)$ [I.4]

$$B = 4 / \pi\,(D \cos kz - C \sin kz) \qquad [I.5]$$

$$C = \int_0^{\pi/2} \cos\left[k\,(z^2 + 4a^2\cos^2\Theta)^{1/2}\right] \sin^2\Theta \, d\Theta \qquad [I.6]$$

$$D = \int_0^{\pi/2} \sin\left[k\,(z^2 + 4a^2\cos^2\Theta)^{1/2}\right] \sin^2\Theta \, d\Theta \qquad [I.7]$$

The difference in phase angle, ϕ, caused by diffraction is given by

$$\phi = \tan^{-1}(B / A) \qquad [I.8]$$

I.4 Diffraction corrections in the UPER and FSUPER

In the UPER and FSUPER, the separation of the transducers is replaced by the pathlength of the signal, because the same transducer acts as both source and receiver. It is necessary to calculate the diffraction corrections, $|P / P^{*}|$ and ϕ, at two different pathlengths, z_0 and z_1, corresponding to Echo 1 and Echo 2. The kz terms in *Equations I.4 and I.5* are replaced by $(kz)^{*}_{n}$, and in *Equations I.6 and I.7*, the k term is replaced by $(kz)^{*}_{n} / z_n$. The term $(kz)^{*}_{n}$ is given by

$$(kz)^{*}_{n} = \omega\,[z_0 / c_P + (z_n - z_0) / c_s] \qquad [I.9]$$

$$z_0 = 2\,d_P \qquad [I.10]$$

$$z_1 = z_0 + 2\,d_s \qquad [I.11]$$

where d_P is the length of the Perspex buffer rod, d_s is the length of the sample liquid, c_P is the ultrasonic velocity in Perspex, c_s is the velocity in the sample and n = 0 for Echo 1, n = 1 for Echo 1. This leads to two values for the pressure ratio, $|P / P^{*}|_0$ and $|P / P^{*}|_1$. Similarly, two values are calculated for the phase angle, ϕ_0 and ϕ_1.

I.4.1 Applying the corrections: the UPER

In the UPER, the calculation is performed for a frequency of 2.1 MHz, and the corrections are applied as follows: In *Equation 3.7*, the ratio $A_{1,s} / A_{2,s}$ is multiplied by M, where

$$M = [\,|P / P^{*}|_0] / |P / P^{*}|_1 \qquad [I.12]$$

In *Equation 3.8*, the time δ_s is reduced by an amount Δt, where

$$\Delta t = (\phi_1 - \phi_0) / \omega \qquad [I.13]$$

I.4.2 Applying the corrections: the FSUPER

In the FSUPER, the diffraction corrections are calculated over a range of frequencies appropriate to the transducer being considered. At each frequency, the corrections are applied in the same way. In *Equation 3.15*, the ratio $M_{1,s} / M_{2,s}$ is multiplied by M, where M is defined as before. In *Equation 3.17*, the value of $\delta\phi$ is given by $(\phi_1 - \phi_0)$.

I.5 Summary

Accurate measurements of ultrasonic velocity and attenuation require a consideration of the diffraction effects associated with the transducer(s) used for the measurement. A scheme for the approximate correction of diffraction effects has been outlined. The deviation between the unknown true diffraction correction and the present approximate value is not known, but measurements on liquids of known velocity suggest that the deviation is acceptably small.

APPENDIX II

Spreadsheet for the FSUPER

II.1 Introduction

When measurements were made in the Frequency Scanning Pulse Echo Reflectometer (FSUPER), the results for each sample were stored in data files. In order to obtain the velocity and attenuation as a function of frequency it was necessary to analyse the results according to the equations which were set out in Chapter Three. The analysis was carried out using a spreadsheet package†, Lotus Symphony, on a personal computer. A copy of the spreadsheet, which was developed by Dr Julian McClements and the author, is provided separately. The spreadsheet can be split into various sections, according to the function performed by each section (*Figure II.1*). Note that where a matrix element contains a formula, only the result of the calculation is displayed on the spreadsheet (ie the formula itself does not appear). All the required formulae are available in Chapter Three and Appendix One. The functions performed by each of the various sections are explained in more detail below.

II.2 Analysis of the spreadsheet by section

II.2.1 Section t *(times)*

The oscilloscope measures the time elapsed from the trigger event (which in this case is the electronic spike which initially excites the transducer) for each of the echoes returning from the interfaces in the FSUPER. These times are recorded by the computer, and by subtracting the delay for the first echo from the delay for the second echo, the time taken by the pulse to travel across the cell and back again can be calculated. This section calculates the transit time for the pulse, for each transducer, for both calibrant (water) and sample.

---

†: A spreadsheet package is a program which is intended to facilitate calculations on large groups of numbers. The user is presented with a computerised version of a large two dimensional matrix. Using a simple programming language, it is possible to enter data into appropriate elements of the matrix and perform calculations on the data, the results of which are available in other elements of the matrix. The computer automatically re-evaluates all the calculations when any matrix element is changed, and the results of calculations can be exported into data files for storage. For more information about spreadsheets, see for example the Lotus Symphony reference manual (1987).

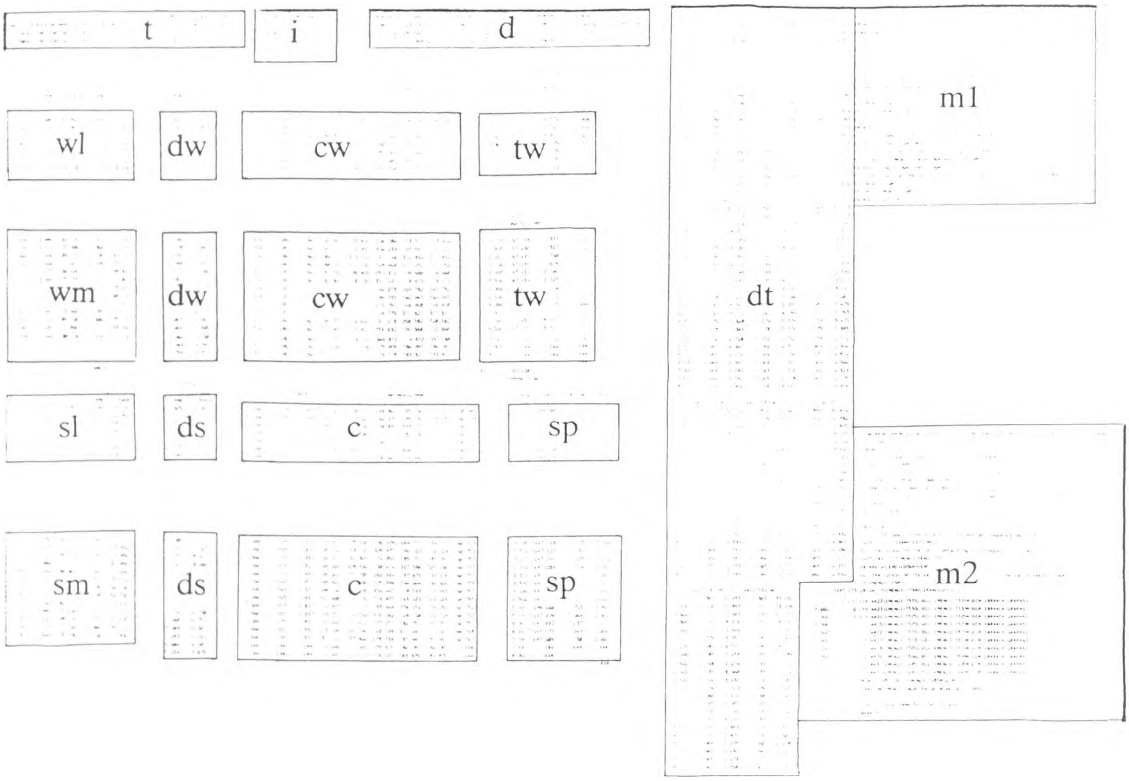

Figure A3.1 The spreadsheet used to analyse the measurements obtained using the FSUPER.

II.2.2 Section i *(impedances)*

In this section, the characteristic acoustic impedances of the calibrant and the backplate are recorded. The impedance value for the calibrant is calculated from the velocity and density of the calibrant (using $Z = \rho c$).

II.2.3 Section d *(densities)*

The readings from the Paar densitometer, for water, air and sample, are entered in this section, and the density of the sample is calculated from the readings according to *Equations 3.19-21*

II.2.4 Sections wl *and* wm *(water low and water medium)*

These sections contain the Fourier transforms of echoes one and two for water, for both the low frequency and the medium frequency transducers. The results are tabulated as columns containing, respectively, the frequency, the magnitude and phase of the transform of echo one, and the magnitude and phase of the transform of echo two.

II.2.5 Section dw *(diffraction, water)*

This section contains the corrections to account for diffraction effects, as a function of frequency for each transducer.

II.2.6 Section cw *(calculations, water)*

The reflection coefficients at the interface between the buffer rod and the water, and at the interface between the water and the aluminium, are calculated using the known properties of Perspex, water and aluminium. The rest of the section calculates the true phase difference between the transforms of the echoes, taking into account the phase difference due simply to the delay between the echoes, the diffraction correction, and the 180° phase shift. The value of the phase shift is converted to a value in the range 0 to 360°, by adding 360° if necessary.

II.2.7 Section tw *(times, water)*

In this section, the transit time of the pulse is calculated as a function of frequency, and the average is calculated, excluding the values for the extremes of frequency. The pathlength of the cell is calculated from the average transit time and the known velocity of ultrasound in water. The pathlength for each transducer is slightly different because the buffer rod for one transducer was not completely flush with the wall of the FSUPER cell. The apparent attenuation is also calculated as a function of frequency. The transducers do not behave ideally, so the diffraction corrections are not completely successful. The apparent attenuation is thus somewhat higher than expected in water.

II.2.8 Sections sl *and* sm *(sample, low and sample, medium)*

The Fourier transforms of echoes one and two for the sample are entered in this section, in the same format as the measurements for water.

II.2.9 Section ds *(diffraction, sample)*

The corrections to be applied to the measurements on the sample in order to account for diffraction are entered in this section. These corrections depend on the velocity of the sample, and are obtained from a look-up table which contains corrections appropriate to a variety of velocities.

II.2.10 Section c *(calculations)*

In this section, the reflection coefficients at the buffer rod/sample and sample/reflector plate interfaces are calculated, using the velocity in the sample and the known densities of the sample. The true phase difference between the transforms of the echoes for the sample is calculated as a function of frequency, and these values are used to calculate the apparent time of flight of the pulse as a function of frequency. In dispersive samples it may be necessary to add or subtract an amount of time equivalent to one period at the appropriate frequency. This is necessary when the group velocity is significantly different to the phase velocity at the frequency in question.

II.2.11 Section sp *(sample properties)*

The properties of the sample (ie the velocity and attenuation) are calculated in this section. The velocity is calculated using the apparent transit time of the pulse at each frequency, the equivalent transit time for water, and the known velocity of water. The attenuation is calculated using the formula given in Chapter Three, with correction for diffraction effects. The apparent attenuation in water is subtracted from the attenuation, in order to account to some extent for the imperfections in the diffraction corrections.

II.2.12 Section dt *(diffraction, table)*

This sections contains a look-up table for the diffraction corrections which should be applied at various values of ultrasonic velocity.

II.2.13 Section m1 *(macro 1)*

A macro is an area of the spreadsheet which contains a simple control language. The macro m1 is used to copy the data files which contain the FSUPER measurements for water, into an area of the spreadsheet set aside for this purpose (not shown on diagram). Since the data files usually contain some unwanted information, the macro copies only the relevant values into the sections wl and wm, whereupon the computer automatically updates the values in sections cw and tw.

II.2.14 Section m2 *(macro 2)*

This macro copies the data files containing the FSUPER measurements for the sample into the area of the spreadsheet mentioned above. Again the appropriate part of the data is copied into the areas sl and sm. The sections ds and dm are then updated with appropriate diffraction corrections obtained from the table dt. The calculations in sections c and sp are automatically updated, and graphs of velocity and attenuation as a function of frequency can be reviewed. The properties of the sample can be stored in an output file if required.

APPENDIX III

Presentations and Publications

III.1 Oral Presentations

Various elements of this work have been presented as papers at the following conferences:

Review of Progress in Physical Acoustics and Ultrasonics, September 1989, University of Bath, United Kingdom.

Review of Progress in Physical Acoustics and Ultrasonics, September 1990, University College London, United Kingdom.

First British Colloid and Surface Science Student Meeting, March 1991, University of Nottingham, United Kingdom.

Acoustics '91, April 1991, University of Keele, United Kingdom, published as:

Fairley P, McClements DJ and Povey MJW (1991) Ultrasonic characterisation of some aerated foodstuffs *Proceedings of the Institute of Acoustics* **13(2)** 63-70.

Ultrasonics '91, July 1991, Le Touquet, France, published as:

Fairley P, McClements DJ and Povey MJW (1991) Ultrasonic characterisation of aerated foodstuffs *Proceedings of Ultrasonics International '91* Butterworth-Heinemann, Oxford, United Kingdom 79-82.

III.2 Poster Presentations

Posters describing various aspects of this work have been shown at the following conferences:

Procter Department of Food Science Centenary Meeting, September 1991, University of Leeds, United Kingdom.

Review of Progress in Physical Acoustics and Ultrasonics, September 1991, University of Leeds, United Kingdom, to be published in *Developments in Acoustics and Ultrasonics* Institute of Physics Publishing, Bristol, U.K.

III.3 Publications

The following papers have resulted partly or wholly from the work in this thesis:

McClements DJ, Fairley P and Povey MJW (1990) Comparison of the effective medium and multiple-scattering theories of predicting the ultrasonic properties of dispersions *Journal of the Acoustical Society of America* **87**(5) 2244-2246.

McClements DJ and Fairley P (1991) Ultrasonic pulse echo reflectometer *Ultrasonics* **29** 58-62.

Contreras NI, Fairley P, McClements DJ and Povey MJW Analysis of the sugar content of fruit juices and drinks using ultrasonic velocity measurements, to appear in *International Journal of Food Science and Technology*, October 1992.

Fairley P, McClements DJ, Bee RD and Povey MJW An ultrasonic study of two aerated liquid foods, submitted to *Ultrasonics*.

McClements DJ and Fairley P Frequency scanning ultrasonic pulse echo reflectometer, to appear in *Ultrasonics*.

APPENDIX IV

Glossary

Absorption cross-section The absorption coefficient, σ_a, of an inhomogeneity is defined as the ratio of the power absorbed by an inhomogeneity to the total intensity. Thus for a beam of cross-sectional area S and power W, the power absorbed by the scatterer is given by $\sigma_a W/S$ (Bamber, 1986).

Attenuation coefficient In the far field, the amplitude of an ultrasonic wave, A, decreases exponentially with distance, x, according to $A = A_0 \exp(-\alpha x)$, where A_0 is the amplitude at $x = 0$. The factor α is defined as the attenuation coefficient, and has units Neper (Np) m^{-1}.

B/A When the amplitude of the incident acoustic wave is small, the propagation medium usually responds linearly to the stresses associated with the passage of the wave. Depending on the amplitude of the incident wave and the nature of the propagation medium, the response may be non-linear, such that the pressure fluctuations, p, and corresponding density fluctuations, ρ, are related by

$$p = c^2 [\rho + (B/2A)(\rho^2/\rho_0)]$$

where c is the ultrasonic velocity, ρ_0 is the density in the undisturbed medium and the ratio B/A is known as the non-linearity parameter. A completely linear medium has a B/A value of -2. The higher the value of B/A, the more the ultrasonic velocity depends on acoustic pressure amplitude (Bamber, 1986).

Back fat thickness The thickness of the subcutaneous fat layer on the back of food animals such as pigs can be correlated with the total fat content of the carcass. Measurements of the back fat thickness are therefore a convenient means of classifying carcasses.

Bandwidth A transducer converts most of the applied electrical energy into ultrasonic energy at a characteristic resonant frequency, known as the centre frequency. A proportion of the electrical energy is transformed in ultrasonic energy at frequencies which are slightly lower and higher than the centre frequency. The spread of energy around the centre frequency is termed the bandwidth. The more heavily damped the transducer, the greater the bandwidth.

Capacitive transducer Consider a capacitor made up of two parallel plates, one of which is fixed and the other of which is free to vibrate. A high d.c. voltage can be applied (in series with a very high resistance) across the plates, and they will become charged. If the free plate is caused to oscillate, the capacitance of the system is changed, and this results in an alternating current with the same frequency as the oscillations of the plate.

Cleaning-in-place In food processing, the equipment must be sanitised thoroughly. Complex equipment cannot easily be dismantled for cleaning, so cleaning solution is circulated through the equipment. This operation is referred to as cleaning-in-place.

Colloidal dimensions A dispersed phase is described as colloidal if its characteristic dimension is in the range 1 nm to 1 μm (Dickinson, 1992). In practice the upper limit of this definition is rather loosely interpreted. The fat globules in cream could reasonably be described as colloidal, despite having a typical diameter of 3-4 μm.

Disulphide bond The covalent bond which is formed between sulphur atoms in the amino acids found in protein molecules and polypeptides is often referred to as a disulphide bond. Disulphide bonds occur both within and between molecules, and are responsible for the structure of some proteins. The addition of ‘improvers’ to bread dough is chiefly aimed at breaking down the existing intramolecular disulphide bonds in gluten, and promoting the formation of new intermolecular disulphide bonds.

Dispersion 1. In ultrasonics, dispersion is said to occur when the velocity is a function of frequency. Dispersion is always associated with a large frequency dependent attenuation. A bubbly liquid is highly dispersive around the resonant frequency of the bubbles within it. 2. In colloid science, a dispersion is an inhomogeneous system consisting of a dispersed phase (droplets, bubbles or particles) and a continuous phase (typically a liquid). The two phases are immiscible, so dispersions are usually unstable. A bubbly liquid is a gas-in-liquid dispersion.

Echocardiography, Echocardiology By means of the addition of a contrast agent to the blood (such as tiny gas bubbles) the heart and its blood vessels can be imaged using ultrasound. This imaging is known as echocardiography or echocardiology.

Fourier Transform Any arbitrary waveform can be regarded as being composed of the summation of an infinite series of sine waves of different amplitudes and frequencies. The Fourier transform performs this decomposition, and converts the information contained in the waveform from the time domain to the frequency domain.

Gibbs-Marangoni effect When a film between two gas cells is draining into the Plateau borders, the flow of liquid can sweep surfactant molecules along the interface. This produces a surface tension gradient which in turn opposes the movement of the surfactant molecules. The system therefore acts to keep the surface tension constant over the entire interface, and resists local thinning of the film. This phenomenon is called the Gibbs-Marangoni effect (Dickinson, 1992), and is an important mechanism by which low molecular weight surfactants stabilise lamellae against rupture.

Hamaker's constant A constant used in the calculation of the van der Waals forces between bubbles (see *Van der Waals Forces*, below). It accounts for the chemical nature of the gas in the bubbles and the liquid in between them.

HLB number The Hydrophile-Lipophile balance (HLB) number is an indicator of the type of emulsion promoted by a particular emulsifier. Emulsifiers with low HLB numbers (4-6) promote water-in-oil emulsions (such as margarine), and those with high HLB (8-18) numbers promote oil-in-water emulsions (such as salad cream) (Dickinson, 1992).

Lithotrypsy The use of high power ultrasound to shatter kidney stones, resulting in particles which can be excreted normally, is known as lithotrypsy. The ultrasonic beam is focussed to minimise damage to the surrounding tissues.

Micelles Molecules of low molecular weight surfactant can self associate to form spherical bodies, where the molecules are aligned so that the part of the molecule with the greatest affinity for the continuous phase is on the outside of the sphere. Micelles are usually of nanometre dimensions, and form spontaneously when the surfactant concentration exceeds a critical value, which is rather low. The P1670 used here would be found in the form of micelles (and other structures which result from self-association) at concentrations above about 0.1 wt%.

Palmitic acid A straight chain saturated hydrocarbon molecule, containing 16 carbon atoms, terminating in a carboxyl (COOH) group.

Polypeptide A molecule made up of a number of amino acids, which through their various hydrophobicities confer amphiphilic properties on the molecule. Protein molecules are giant polypeptides.

Propagation Coefficient The propagation coefficient, k, is given by $\omega/c + i\alpha$, where ω is the angular frequency ($2\pi f$), c is the speed of sound and α is the attenuation coefficient.

***Q* factor** The Quality (Q) factor of a vibrating system indicates the degree of resonance. It is defined as the ratio of the energy supplied per cycle to the energy dissipated per cycle. Broadband highly damped transducers have low Q factors, freely resonating quartz crystals have high Q factors (Blitz, 1963).

Reynolds number The flow of a liquid of density ρ and viscosity η is described by the Reynolds number, which is a dimensionless group given by $\rho va/\eta$, where v is the velocity of the liquid and a is a characteristic dimension such as the diameter of a tube (CRC Handbook, 1987). In this work, a is taken as the diameter of a bubble moving with velocity v through stationary liquid. At low values of the Reynolds number the flow of liquid over the bubble is laminar (streamline).

Scattering cross-section The scattering cross-section, σ_s, of an inhomogeneity is defined as the ratio of the power scattered out of the beam to the incident intensity. The power scattered by one inhomogeneity out of a beam of total power W and cross-sectional area S is thus $\sigma_s W/S$ (Bamber, 1986).

Solid fat content (SFC) At any particular temperature, a certain proportion of the fat in a food is crystalline (solid) and a certain proportion is disordered (liquid). The proportion of the total fat which is solid is known as the solid fat content, and is an important functional parameter of the fat. For example, the SFC of margarine governs the texture and spreadability.

Sonochemistry High power ultrasound produces transient temperatures and pressures of the order of thousands of degrees Centigrade and hundreds of atmospheres respectively. When cavitation occurs there is also greatly enhanced mixing due to the shock waves associated with bubble collapse. In sonochemistry, these conditions are exploited to enhance the rate of many reactions.

Stearic acid A straight chain saturated hydrocarbon molecule, containing 18 carbon atoms, terminating in a carboxyl (COOH) group.

Surfactant A surfactant is any molecule which displays surface activity *ie* an ability to lower interfacial tension or surface tension. Surfactants can be broadly classed as low or high molecular weight, and they are amphiphilic molecules which adsorb strongly at the interface in dispersions. Low molecular weight surfactants typically consist of a hydrophilic head group and a (larger) hydrophobic tail group. They may also be charged. High molecular weight surfactants typically consist of a mixture of hydrophobic and hydrophilic regions. In the context of bubbly liquids, surfactants are often referred to as foaming agents.

Syneresis The process whereby the matrix of a gel shrinks, and forces some liquid out of the bulk of the gel. Syneresis is commonly observed on the top of set yogurt.

Transducer A transducer is a device which converts energy from one form to another. Ultrasonic transducers convert electrical energy into mechanical energy (sound or ultrasound) and vice versa. The transducers used here employ the piezoelectric effect: when a voltage is applied to the active element of the transducer, it produces a stress which makes the element expand or contract. When a stress is applied to the active element a corresponding voltage is produced.

Van der Waals Forces In this thesis, the term van der Waals forces has been used in a rather loose sense, to describe the weak, long-range attractive force which acts between bubbles. Hamaker's approach states that this attractive force arises from the summation of the true van der Waals forces acting between all the pairs of molecules within each of the bubbles. For gas molecules these are the so-called dispersion (London) forces, which arise as a result of transient dipole/induced dipole interactions (Tabor, 1991).

REFERENCES

Adler L, Rose JH and Mobley C (1986) Ultrasonic method to determine gas porosity in aluminium alloy castings: theory and experiment *J. Appl. Phys.* 59(2) 336-347.

Ahuja AS (1972) Effect of particle viscosity on propagation of sound in suspensions and emulsions *J. Acoust. Soc. Am.* 51 182-191.

Allegra JR and Hawley SA (1972) Attenuation of sound in suspensions and emulsions: Theory and experiments *J. Acoust. Soc. Am.* 51(5) 1545-1564.

Anderson AL and Hampton LD (1980) Acoustics of gas-bearing sediments I. Background *J. Acoust. Soc. Am.* 67(6) 1865-1889.

Anderson M and Brooker BE (1988) Dairy Foams in: *Advances in Food Emulsions and Foams* (Eds Dickinson, E and Stainsby, G), Elsevier Applied Science, London, UK.

Anson LW and Chivers RC (1989a) Ultrasonic propagation in mammalian cell suspensions based on a shell model *Physics in Medicine and Biology* 34 1153-1167.

Anson LW and Chivers RC (1989b) Ultrasonic propagation in suspensions - a comparison of a multiple scattering and an effective medium approach *J. Acoust. Soc. Am.* 85(2) 535-540.

Bamber JC (1986) Attenuation and absorption, in *Physical principles of medical ultrasonics* Ed Hill CR, John Wiley and Sons, Chichester, UK.

Barigou M and Greaves M (1991) A capillary probe for bubble size measurement *Measurement Science and Technology* 2 318-326.

Barker JA and Henderson D (1971) Monte Carlo values for the radial distribution function of a system of fluid hard spheres *Molecular Physics* 21(1) 187-191.

Bee RD, Clement A and Prins A (1987) Behaviour of an aerated food model in: *Food Emulsions and Foams* (Ed Dickinson E) Royal Society of Chemistry, London, UK 128-143.

Belyayev AY (1988) Compression waves in a fluid with gas bubbles *PMM J. Appl. Maths.* 52(3) 344-348.

Benson GC and Kiyohara O (1974) Tabulation of some integral functions describing diffraction effects in the ultrasonic field of a circular piston source *J. Acoust. Soc. Am.* 55(1) 184-185.

Berryman JG (1980(a)) Long wavelength propagation in composite elastic media I. Spherical inclusions *J. Acoust. Soc. Am.* 68(6) 1809-1819.

Berryman JG (1980(b)) Long wavelength propagation in composite elastic mediaII. Ellipsoidal inclusions *J. Acoust. Soc. Am.* 68(6) 1820-1831.

Biot MA (1962) Generalised theory of acoustic propagation in porous dissipative media *J. Acoust. Soc. Am.* 34(9) 1254-1264.

Biro T, Kelemen A and Pavlicsek I (1990) Acoustic detection of neutrons by bubble detectors *Int. J. Radiat. Appl. Instrum. Part D* 17(4) 587-589.

Bjϕrnϕ L (1991) Ultrasound in the food industry *Proceedings of Ultrasonics International '91* Butterworth-Heinemann, Oxford, UK, 23-29.

Bleeker HJ, Shung KK and Barnhart JL (1990) Ultrasonic characterisation of Albunex, a new contrast agent *J. Acoust. Soc. Am.* 87(4) 1792-1797.

Blitz J (1963) Fundamentals of ultrasonics, Butterworths, London, UK.

Blitz J (1971) Ultrasonics: methods and applications, Butterworths, London, UK.

Brauner N and Beltzer AI (1985) The Kramers-Kronig relations method and wave propagation in porous elastic media *Int. J. Engng. Sci.* 23(11) 1151-1162.

Breitz N and Medwin H (1989) Instrumentation for in situ acoustical measurement of bubble spectra under breaking waves *J. Acoust. Soc. Am.* 86(2) 739-743.

Brill D, Gaunaurd GD and Uberall H (1980) Resonance theory of elastic shear wave scattering from spherical fluid obstacles in solids *J. Acoust. Soc. Am.* 67(2) 414-424.

Brooke Benjamin T (1989) Note on shape oscillations of gas bubbles *J. Fluid Mech.* 203 419-424.

Brylyakov YE and Gorlovskii SI (1988) Effects of inorganic compounds on stability of air bubbles *Colloid Journal of the USSR* 50(4) 701-702.

Bugmann G and von Stockar U (1989a) Mesure du diamètre moyen de bulles de gaz par la méthode de l'écart-type *Helvetica Physica Acta* 62 314-317.

Bugmann G and von Stockar U (1989b) Characterising bubbles in bioreactors by ultrasound *Trends in Biotechnology* 7(7) 166-169.

Bugmann G, Lister JB and von Stockar U (1991) Characterising bubbles in bioreactors using light or ultrasound probes: data analysis by classical means and by neural networks *Canadian Journal of Chemical Engineering* 69 474-480.

Cable M and Frade JR (1988) The influence of surface tension on the diffusion-controlled growth or dissolution of spherical gas bubbles *Proc. Roy. Soc. Lond.* A420 247-265.

Caflisch RE, Miksis MJ, Papanicolaou GC and Ting L (1985) Effective equations for wave propagation in bubbly liquids *J. Fluid Mech.* 153 259-273.

Calvert JR and Nezhati K (1987) Bubble size effects in foams *Int. J. Heat & Fluid Flow* 8(2) 102-106.

Carstensen EL and Foldy LL (1947) Propagation of sound through a liquid containing bubbles *J. Acoust. Soc. Am.* 19(3) 481-501.

Chapelon JY, Shankar PM and Newhouse VL (1985) Ultrasonic measurement of bubble cloud size profiles *J. Acoust. Soc. Am.* 78(1) 196-201.

Chapelon JY, Newhouse VL, Cathignol D and Shankar PM (1988) Bubble detection and sizing with a double frequency Doppler system *Ultrasonics* 26 148-154.

Cheng LY, Drew DA and Lahey RT (1985) An analysis of wave propagation in bubbly two-component, two-phase flows *Journal of Heat Transfer* 107 402-408.

Choi KH and Lee WK (1990) Comparison of probe methods for measurement of bubble properties *Chem. Eng. Comm.* 91 35-47.

Chow JCF (1964) Attenuation of acoustic waves in dilute emulsions and suspensions *J. Acoust. Soc. Am.* 36 2395-2401.

Church CC (1988a) Prediction of rectified diffusion during nonlinear bubble pulsations at biomedical frequencies *J. Acoust. Soc. Am.* 83(6) 2210-2217.

Church CC (1988b) A method to account for acoustic microstreaming when predicting bubble growth rates produced by rectified diffusion *J. Acoust. Soc. Am.* 84(5) 1758-1764.

Commander KW and Moritz E (1989) Off-resonance contributions to acoustical bubble spectra *J. Acoust. Soc. Am.* 85(6) 2665-2669.

Commander KW and Prosperetti A (1989) Linear pressure waves in bubbly liquids: Comparison between theory and experiments *J. Acoust. Soc. Am.* 85(2) 732-746.

Coste C, Laroche C and Fauve S (1990) Sound propagation in a liquid with vapour bubbles *Europhysics Letters* 11(4) 343-347.

Cracknell AP (1980) Ultrasonics, Wykeham Publications Ltd, London, UK.

CRC Handbook of chemistry and physics (1987) Eds Weast RC, Astle MJ and Beyer WH, CRC Press Inc, Boca Raton, Florida, USA.

Crespo A (1969) Sound and shock waves in liquids containing bubbles *Phys. Fluids* 12(11) 2274-2282.

Crum LA (1980) Measurements of the growth of air bubbles by rectified diffusion *J. Acoust. Soc. Am.* 68(1) 203-211.

Crum LA (1982) Nucleation and stabilisation of microbubbles in liquids *Applied Scientific Research* 38 101-115.

Crum LA (1983) The polytropic exponent of gas contained within air bubbles pulsating in a liquid *J. Acoust. Soc. Am.* 73(1) 116-120.

Crum LA and Prosperetti A. (1983) Nonlinear oscillations of gas bubbles in liquids: an interpretation of some experimental results *J. Acoust. Soc. Am.* 73(1) 121-127.

Czuchajowska Z and Pomeranz Y (1990) Quest for a universal test of commercial gluten quality for breadmaking *Cereal Foods World* 35(5) 458-469.

d'Agostino L and Brennen CE (1988) Acoustical absorption and scattering cross-sections of spherical bubble clouds *J. Acoust. Soc. Am.* 84(6) 2126-2134.

d'Agostino L and Brennen CE (1989) Linearised dynamics of spherical bubble clouds *J. Fluid Mech.* 199 155-176.

de Jong N, Tencate FJ, Lancee CT, Roelandt JRTC and Bom N (1991) Principles and recent developments in ultrasound contrast agents *Ultrasonics* 29 324-330.

de Jong N, Hoff L, Skotland T and Bom N (1992) Absorption and scatter of encapsulated gas filled microspheres: theoretical considerations and some measurements *Ultrasonics* 30(2) 95-103.

De S (1987) On the oscillations of bubbles in body fluids *J. Acoust. Soc. Am.* 81(2) 566-567.

Del Grosso VA and Mader CW (1972) Speed of sound in pure water *J. Acoust. Soc. Am.* 54(2) 1442-1446.

Detsch RM (1990) Dissolution of 100 to 1000μm diameter air bubbles in reagent grade water and seawater *J. Geophys. Res.* 95(C6) 9765-9773.

Detsch RM (1991) Small air bubbles in reagent grade water and seawater 1. Rise velocities of 20- to 1000-μm-diameter bubbles *J. Geophys. Res.* 96(C5) 8901-8906.

Devin C (1959) Survey of thermal, radiation and viscous damping of air bubbles in water *J. Acoust. Soc. Am.* 31(12) 1654-1667.

Dickinson E (1992) An introduction to food colloids, Oxford University Press, Oxford, UK.

Doinikov AA and Zavtrak ST (1988) Allowance for compressibility of the liquid in the problem of the interaction of gas bubbles in a sound field *Sov. Phys. Acoust.* 34(2) 144-147.

Doinikov AA and Zavtrak ST (1989) Relative motion of two gas bubbles in a compressible liquid *Sov. Phys. Acoust.* 35(2) 154-156.

Doinikov AA and Zavtrak ST (1990) Radiation effects of the interaction of two gas bubbles in a compressible non-ideal liquid *Sov. Phys. Acoust.* 36(3) 238-40.

Dontsov VE, Kuznetsov VV, Markov PG and Nakoryakov VE (1989) Propagation of pressure waves in a liquid containing gas bubbles of different sizes *Sov. Phys. Acoust.* 35(1) 95-96.

Drumheller DS and Bedford A (1979) A theory of bubbly liquids *J. Acoust. Soc. Am.* 66(1) 197-208.

Du G and Wu J (1990) Comparison between two approaches for solving nonlinear radiations from a bubble in a liquid *J. Acoust. Soc. Am.* 87(5) 1965-1967.

Eatock BC, Nishi RY and Johnston GW (1985) Numerical studies of the spectrum of low-intensity ultrasound scattered by bubbles *J. Acoust. Soc. Am.* 77(5) 1692-1701.

Epstein PS and Carhart RR (1953) The absorption of sound in emulsions and suspensions I. Water fog in air *J. Acoust. Soc. Am.* 25(3) 553-565.

Epstein PS and Plesset M (1950) On the stability of gas bubbles in liquid-gas solutions *J. Chem. Phys.* 18(11) 1505-1509.

Floyd ER (1981) Thermodynamic corrections to the velocity of propagation in a bubbly medium *J. Acoust. Soc. Am.* 70 1748-1751.

Flynn HG and Church CC (1988) Transient pulsations of small gas bubbles in water *J. Acoust. Soc. Am.* 84(5) 1863-1876.

Foldy LL (1945) The multiple scattering of waves. I: General theory of isotropic scattering by randomly distributed scatterers *Physical Review* 67 107-119.

Fox FE, Curley SR and Larson GS (1955) Phase velocity and absorption measurements in water containing air bubbles *J. Acoust. Soc. Am.* 27(3) 534-539.

Fox FE and Herzfeld KF (1954) Gas bubbles with organic skin as cavitation nuclei *J. Acoust. Soc. Am.* 26(6) 984-989.

Francescutto A and Nabergoj R (1983) Steady-state oscillations of gas bubbles in liquids: explicit formulas for frequency response curves *J. Acoust. Soc. Am.* 73(2) 457-460.

Friberg SE and Fang JH (1987) Foams from aqueous systems of polymerizable surfactants *J. Coll. Interf. Sci.* 118(2) 543-552.

Gaunaurd GC and Barlow J (1984) Matrix viscosity and cavity-size distribution effects on the dynamic effective properties of perforated elastomers *J. Acoust. Soc. Am.* 75(1) 23-34.

Gaunaurd GC and Uberall H (1981) Resonance theory of bubbly liquids *J. Acoust. Soc. Am.* 69(2) 362-370.

Gaunaurd GC and Uberall H (1982) Resonance theory of the effective properties of perforated solids *J. Acoust. Soc. Am.* 71(2) 282-295.

Gaunaurd GC and Uberall H (1983(a)) Resonance theory of the effective properties of perforated solids: Erratum *J. Acoust. Soc. Am.* 73(1) 372.

Gaunaurd GC and Uberall H (1983(b)) Resonance effects and the ultrasonic properties of particulate composites *J. Acoust. Soc. Am.* 74 305-313.

Gaunaurd GC and Wertman WH (1988) Resonance scattering of elastic waves by an elastic inclusion in an elastic matrix: numerical calculations *IEEE Transactions on ultrasonics, ferroelectrics and frequency control* 35(5) 628-636.

Geary NW and Rice RG (1991) Bubble size prediction for rigid and flexible spargers *A.I.Ch.E. Journal* 37(2) 161-168.

Gibson FW (1970) Measurement of the effect of air bubbles on the speed of sound in water *J. Acoust. Soc. Am.* 48(5) 1195-1197.

Glazman RE (1983) Effects of adsorbed films on gas bubble radial oscillations *J. Acoust. Soc. Am.* 74(3) 980-986.

Glazman RE (1984) Damping of bubble oscillations induced by transport of surfactants between the adsorbed film and the bulk solution *J. Acoust. Soc. Am.* 76(3) 890-896.

Gorskii SM, Zinov'ev AY and Chichagov PK (1989) Normal vibrational modes of a "pinned" gas bubble in a liquid *Sov. Phys. Acoust.* 34(6) 587-589.

Graf KF (1981) A history of ultrasonics. In *Physical Acoustics* XV, Eds Mason WP and Thurston RN, Academic Press, New York, USA, 2-90.

Gryzhina EV and Trapeznikov AA (1988) Stability of foams and bilateral films of human serum albumin and secondary alcohol sulfates, with and without added alcohols *Colloid Journal of the USSR* 50(2) 198-203.

Gurikov YV (1989) Pulsation regimes of cavitation bubbles *Sov. Phys. Acoust.* 35(5) 477-479.

Hafsteinsson H, Chivers RC and Rizvi (1992) Ultrasonics and food engineering: review paper (private communication).

Hall MV (1989) A comprehensive model of wind-generated bubbles in the ocean and predictions of the effects on sound propagation at frequencies up to 40 kHz *J. Acoust. Soc. Am.* 86(3) 1103-1117.

Hansen GM (1985) Mie scattering as a technique for the sizing of air bubbles *Applied Optics* 24(19) 3214-3220.

Harker AH and Ogilvy JA (1991) Coherent wave propagation in inhomogeneous materials: a comparison of theoretical models *Ultrasonics* **29** 235-244.

Harker AH and Temple JAG (1988) Velocity and attenuation of ultrasound in suspensions of particles in fluids *J. Phys. D: Appl. Phys.* **21** 1576-1588.

Harris IA and Detsch RM (1991) Small air bubbles in reagent grade water and seawater 2. Dissolution of 20- to 500-μm-diameter bubbles at atmospheric pressure *J. Geophys. Res.* **96(C5)** 8907-8910.

Hodges A (1990) The effect of S1670 in Sweetose *unpublished student project report*, Unilever Research Limited, Bedford, UK.

Hudales JBM and Stein HN (1990) The influence of solid particles on foam and film drainage *J. Coll. Interf. Sci.* **140(2)** 307-313.

Ishimaru A and Kuga A (1982) Attenuation constant of a coherent field in a dense distribution of particles *J. Opt. Soc. Am.* **72(10)** 1317-1320.

Jackson I, Niesler H and Weidner DJ (1981) Explicit corrections of ultrasonically determined elastic wave velocities for transducer-bond phase shifts *Journal of Geophysical Research* **86** 3736-3748.

Javanaud C (1988) Applications of ultrasound to food systems *Ultrasonics* **26** 117-123.

Javanaud C and Thomas A (1988) Multiple scattering using the Foldy-Twersky integral equation *Ultrasonics* **26** 341-343.

Jones DS (1986) Acoustic and electromagnetic waves, Oxford University Press, Oxford, UK.

Karras M, Pietikainen T, Kortelainen H and Tornberg J (1988) Ultrasonic measurement of gaseous air in pulp suspensions *Tappi Journal* **71(1)** 65-69.

Kawakami M, Tomimoto N, Kitazawa Y and Ito K (1988) Estimation of size distribution of bubbles in iron melt from the chord length distribution *Transactions of the Iron and Steel Institute of Japan* **28(4)** 271-277.

Kaye GWC and Laby TH (1986) Tables of physical and chemical constants, Longman, London, UK.

Keller JB and Miksis M (1980) Bubble oscillations of large amplitude *J. Acoust. Soc. Am.* **68(2)** 628-633.

Kerr FH (1992(a)) The scattering of a plane elastic wave by spherical elastic inclusions *Int. J. Engng. Sci.* **30(2)** 169-186.

Kerr FH (1992(b)) An effective medium approach to the study of plane wave propagation in an elastic matrix with spherical elastic inclusions *Int. J. Engng. Sci.* 30(2) 187-198.

Khimunin AS (1972) Numerical calculation of the diffraction corrections for the precise measurement of ultrasound absorption *Acustica* 27 173-181.

Khimunin AS (1975) Numerical calculation of the diffraction corrections for the precise measurement of ultrasound phase velocity *Acustica* 32 192-200.

Kim JW and Lee WK (1988) Coalescence behaviour of two bubbles growing side-by-side *J. Coll. Interf. Sci.* 123(1) 303-305.

Kobelev YA, Ostrovskii LA and Sutin AM (1980) Self-illumination effect for acoustic waves in a liquid with gas bubbles *JETP Letters* 30(7) 395-398.

Kobelev YA and Ostrovskii LA (1989) Nonlinear acoustic phenomena due to bubble drift in a gas-liquid mixture *J. Acoust. Soc. Am.* 85(2) 621-629.

Kolbe WF, Turko BT and Leskovar B (1986) Fast ultrasonic imaging in a liquid filled pipe *IEEE Transactions on Nuclear Science* 33(1) 715-722.

Kol'tsova IS and Mikhailov IG (1976) Attenuation and scattering of ultrasonic waves in suspensions *Sov. Phys. Acoust.* 21(4) 351-355.

Kol'tsova IS, Krynskii LO, Mikhailov IG and Pokrovskaya IE (1979) Attenuation of ultrasonic waves in low-viscosity liquids containing gas bubbles *Sov. Phys. Acoust.* 25(5) 409-413.

Kozhevnikova IN and Bjorno L (1992) Experimental study of acoustical emission from bubble cloud excitation *Ultrasonics* 30(1) 21-25.

Kumagai H, Lee BH, Kumagai H and Yano T (1991) Critical radius and time course of expansion of an isolated bubble in wheat flour dough under temperature rise *Agric Biol Chem* 55(4) 1081-1087.

Kuster GT and Toksöz MN (1974) Velocity and attenuation of seismic waves in two-phase media: Part I. Theoretical formulation; Part II. Experimental results *Geophysics* 39 587-618.

Lachaise J, Graciaa A, Marion G and Salager JL (1990) A new reflectometry method to measure a liquid foam stability *Journal of Dispersion Science and Technology* 11(4) 409-430.

Laird DT and Kendig PM (1952) Attenuation of sound in water containing air bubbles *J. Acoust. Soc. Am.* 24(1) 29-32.

Lauterborn W and Koch A (1987) Holographic observation of period-doubled and chaotic bubble oscillations in acoustic cavitation *Phys. Rev. A* 35(4) 1974-1976.

Lefebvre J, Frohly J, Torguet R, Bruneel C and Rouvaen JM (1980) Experimental and theoretical study of the multiple scattering of acoustical waves in inhomogeneous media *Ultrasonics* 18 170-174.

Leighton TG (1989) Transient excitation of insonated bubbles *Ultrasonics* 27 50-53.

Leighton TG, Lingard RJ, Walton AJ and Field JC (1991) Acoustic bubble sizing by combination of subharmonic emissions with imaging frequency *Ultrasonics* 29 319-323.

Liu KC (1991(a)) Wave scattering in discrete random media by the discontinuous stochastic field method. I: Basic method and general theory *J. Sound Vib.* 147(2) 301-311.

Liu KC (1991(b)) Wave scattering in discrete random media by the discontinuous stochastic field method. II: Contribution of the second order moment of the β-field *J. Sound Vib.* 147(2) 313-321.

Lloyd P and Berry MV (1967) Wave propagation through an assembly of spheres IV. Relations between different multiple scattering theories *Proc Phys Soc* 91 678-688.

Longuet-Higgins MS (1989a) Monopole emission of sound by asymmetric bubble oscillations Part 1. Normal modes *J. Fluid Mech.* 201 525-541.

Longuet-Higgins MS (1989b) Monopole emission of sound by asymmetric bubble oscillations Part 2. An initial value problem *J. Fluid Mech.* 201 543-565.

Longuet-Higgins MS (1989c) Some integral theorems relating to the oscillations of bubbles *J. Fluid Mech.* 204 159-166.

Longuet-Higgins MS (1990) Bubble noise spectra *J. Acoust. Soc. Am.* 87(2) 652-661.

Longuet-Higgins MS (1991) Bubble noise *IMA J. Appl. Maths.* 46 67-70.

Longuet-Higgins MS (1992) Non-linear damping of bubble oscillations by resonant interaction *J. Acoust. Soc. Am.* 91(3) 1414-1422.

Lotus Symphony Reference Manual (1987) Lotus Development Corporation, Cambridge, MA, USA.

Lubetkin SD (1989) Measurement of bubble nucleation rates by an acoustic method *Journal of Applied Electrochemistry* 19 668-676.

Ma Y, Varadan VV and Varadan VK (1984(a)) Multiple scattering theory for wave propagation in discrete random media *Int. J. Engng. Sci.* 22 1139-1148.

Ma Y, Varadan VK and Varadan VV (1984(b)) Application of Twersky's multiple scattering formalism to a dense suspension of elastic particles in water *J. Acoust. Soc. Am.* 75(2) 335-339.

Ma Y, Varadan VV and Varadan VK (1987) Acoustic response of sedimentary particles in the near field of high-frequency transducers *IEEE Transactions on ultrasonics, ferroelectrics and frequency control* UFFC-34 3-7.

Ma Y, Varadan VK and Varadan VV (1990) Comments on ultrasonic propagation in suspensions *J. Acoust. Soc. Am.* 87(6) 2779-2782.

MacPherson JD (1957) The effect of gas bubbles on sound propagation in water *Proc. Phys. Soc. Lond.* B70 85-92.

Malhotra AK and Wasan DT (1987) Effect of film size on drainage of foams and emulsion films *A.I.Ch.E. Journal* 33(9) 1533-1541.

Malvern Mastersizer User Manual (1989) Malvern Instruments Ltd, Malvern, United Kingdom.

Mandel F, Bearman RJ and Bearman MY (1970) Numerical solutions of the Percus-Yevick equation for the Lennard-Jones (6-12) and hard-sphere potentials *Journal of Chemical Physics* 52(7) 3315-3323.

Manetou A (1990) Development of an ultrasonic sensor for monitoring air content *Research Report Number 667* Leatherhead Food Research Association, Leatherhead, UK.

Matsumoto Y and Watanabe M (1989) Nonlinear oscillation of gas bubble with internal phenomena *JSME International Journal Series II* 32(2) 157-162.

McCann JD (1986) A review of ultrasonic techniques and applications, with particular reference to low frequency systems and their use in the food processing industry *Report AERE R 11271* United Kingdom Atomic Energy Authority, Harwell, UK.

McClements DJ (1991) Ultrasonic characterisation of emulsions and suspensions *Advances in Colloid and Interface Science* 37 33-72.

McClements DJ (1992) Comparison of multiple scattering theories with experimental measurements in emulsions *J. Acoust. Soc. Am.* 91(2) 849-853.

McClements DJ and Fairley P (1991) Ultrasonic Pulse Echo Reflectometer *Ultrasonics* 29(1) 58-62.

McClements DJ and Fairley P (1992) Frequency Scanning Ultrasonic Pulse Echo Reflectometer *Ultrasonics*, to appear.

McClements DJ, Fairley P and Povey MJW (1990) Comparison of effective medium and multiple scattering theories of predicting the ultrasonic properties of dispersions *J. Acoust. Soc. Am.* 87(5) 2244-2246.

McClements DJ and Povey MJW (1989) Scattering of ultrasound by emulsions *J. Phys. D: Appl. Phys.* 22 38-47.

Medwin H (1974) Acoustic fluctuations due to microbubbles in the near-surface ocean *J. Acoust. Soc. Am.* 56(4) 1100-1104.

Medwin H and Breitz ND (1989) Ambient and transient bubble spectral densities in quiescent seas and under spilling breakers *J. Geophys. Res.* 94(C9) 12751-12759.

Medwin H and Daniel AC (1990) Acoustical measurements of bubble production by spilling breakers *J. Acoust. Soc. Am.* 88(1) 408-412.

Medwin H (1991) Reply to comment on *Ambient and transient bubble spectral densities in quiescent seas and under spilling breakers J. Geophys. Res.* 96(C1) 867-868.

Mehta CH (1983) Scattering theory of wave propagation in a two-phase medium *Geophysics* 48 1359-1370.

Meyer E and Skudrzyk E (1953) Uber die akustischen eigenschaften von gasblasenschleiern in wasser *Acustica* 3 434-440.

Miksis MJ and Ting L (1984) Nonlinear radial oscillations of a gas bubble including thermal effects *J. Acoust. Soc. Am.* 76(3) 897-905.

Miksis MJ and Ting L (1987) Viscous effects on wave propagation in a bubbly liquid *Phys. Fluids* 30(6) 1683-1689.

Miles CA, Shore D and Langley KR (1990) Attenuation of ultrasound in milks and creams *Ultrasonics* 28 394-400.

Miller DL (1979) A cylindrical-bubble model for the response of plant-tissue gas bodies to ultrasound *J. Acoust. Soc. Am.* 65(5) 1313-1321.

Minnaert M (1933) On musical air bubbles and the sounds of running water *Philos. Mag.* 16 235-248.

Mond M (1987) Kinetic theory of waves in bubbly liquids *Phys. Lett. A* 122(4) 153-156.

Moorjani R (1984) An investigation into the acoustics of bread doughs, unpublished MSc thesis, University of Leeds.

Morse PM & Ingard KU (1968) Theoretical Acoustics, McGraw Hill, New York, USA.

Nair SM, Hsu DK and Rose JH (1989) Porosity estimation using the frequency dependence of the ultrasonic attenuation *Journal of Nondestructive Evaluation* 8(1) 13-26.

Nigmatulin RI, Shagapov VS and Vakhitova NK (1989) Effect of the compressibility of the carrier phase in wave propagation in a bubble medium *Sov. Phys. Acoust.* 34(2) 98-100.

Nishi RY (1975) The scattering and absorption of sound waves by a gas bubble in a viscous liquid *Acustica* 33 65-74.

Omta R (1987) Oscillations of a cloud of bubbles of small and not so small amplitude *J. Acoust. Soc. Am.* 82(3) 1018-1033.

Oosterwegel GG and de Groot HJ (1980) On the possibility to measure volumes of small gas bubbles and the bubble producing gas flow rates acoustically *Review of Scientific Instruments* 51(2) 201-205.

Paar DMA 45 Digital Density Meter Instruction Manual by Kratky O, Leopold H and Stabinger H, Anton Paar, Graz, Austria.

Papadakis E (1967) Ultrasonic phase velocity by the pulse echo overlap method incorporating diffraction phase corrections *J. Acoust. Soc. Am.* 42(5) 1045-1051.

Papadakis E (1975) Ultrasonic diffraction from single apertures with application to pulse measurements and crystal physics, in *Physical Acoustics* XI, Edited by Mason WP and Thurston RN, Academic Press, New York, USA, 151-212.

Percus JK and Yevick GJ (1958) Analysis of classical statistical mechanics by means of collective coordinates *Phys. Rev.* 110 1-13.

Peterson B and Strom S (1974) Matrix formulation of acoustic scattering from an arbitrary number of scatterers *J. Acoust. Soc. Am.* 56(3) 771-780.

Phillips LG, Haque Z and Kinsella JE (1987) A method for the measurement of foam formation and stability *J. Food Sci.* 52(4) 1074-1077.

Piefke F (1976) Estimation of linear properties of spherical bodies in thin films from their projections *Proceedings of the 4th International Congress for Stereology*, Eds Underwood E, de Wit R and Moore GA, National Bureau of Standards Special Publication 431, Washington, USA.

Povey MJW (1989) Ultrasonics in food engineering. Part II: Applications *Journal of Food Engineering* 9 1-20.

Povey MJW and McClements DJ (1988) Ultrasonics in food engineering. Part I: Introduction and experimental methods *Journal of Food Engineering* 8 217-245.

Pradhan MS, Sita Ram Sarma DSH and Khilar KC (1990) Stability of aqueous foams with polymer additives *J. Coll. Interf. Sci.* 139(2) 519-526.

Prins A (1988) Principles of foam stability, in: *Advances in Food Emulsions and Foams* (Eds Dickinson E and Stainsby S) Elsevier Applied Science, London, UK. 128-143.

Prosperetti A (1977) Thermal effects and damping mechanisms in the forced radial oscillations of gas bubbles in liquids *J. Acoust. Soc. Am.* 61(1) 17-27.

Prosperetti A (1984) Bubble phenomena in sound fields: part two *Ultrasonics* 22 115-124.

Prosperetti A (1987) The equation of bubble dynamics in a compressible liquid *Phys. Fluids* 30(11) 3626-3628.

Prosperetti A (1991) The thermal behaviour of oscillating gas bubbles *J. Fluid Mech.* 222 587-616.

Prosperetti A, Crum LA and Commander KW (1988) Nonlinear bubble dynamics *J. Acoust. Soc. Am.* 83(2) 502-514.

Pyler EJ (1973) Baking science and technology, Siebel Publishing Company, Chicago, USA.

Randall EW, Goodall CM, Fairlamb PM, Dold PL and O'Connor CT (1989) A method for measuring the sizes of bubbles in 2- and 3-phase systems *J. Phys. E: Sci. Instrum.* 22 827-833.

Randall N, Wilkinson VM and Roberts RT (1987) Possible applications for an ultrasonic impedance probe *Research Report Number 588* Leatherhead Food Research Association, Leatherhead, UK.

Reynolds O (1886) On the theory of lubrication and its applications to Mr Beauchamp Tower's experiments, including an experimental determination of viscosity of olive oil *Phil. Trans. Roy. Soc. Lond.* A177 157.

Rieser LA and Lemlich R (1988) Permeability to interbubble gas diffusion in liquid foams *J. Coll. Interf. Sci.* 123(1) 299-302.

Rubinstein J (1985) Bubble interaction effects on waves in bubbly liquids *J. Acoust. Soc. Am.* 77(6) 2061-2066.

Ruffa AA (1992) Acoustic wave propagation through periodic bubbly liquids *J. Acoust. Soc. Am.* 91(1) 1-11.

Ryoto Sugar Ester Technical Information (1987) Mitsubishi-Kasei Food Corporation, Tokyo, Japan.

Sahi SS (1992) Formation and stabilisation of gas cell walls in bread doughs, Unpublished report, Flour Milling and Baking Research Association, Chorleywood, Herts, UK.

Samek L (1987) A multiscale analysis of nonlinear oscillations of gas bubbles in liquids *J. Acoust. Soc. Am.* 81(3) 632-637.

Samek L (1989) A multiscale analysis of non-linear oscillations of gas bubbles in compressible liquids *Czech. J. Phys.* B39 1354-1365.

Saxena AC, Rao NS and Saxena SC (1990) Bubble size distribution in bubble columns *Can. J. Chem. Eng.* 68 159-161.

Sayers CM (1981) Ultrasonic velocity dispersion in porous materials *J. Phys. D: Appl. Phys.* **14** 413-20.

Sayers CM and Smith RL (1982) The propagation of ultrasound in porous media *Ultrasonics* **20** 201-205.

Scharnhorst KP (1987) Comments on the applicability of the Kuster-Toksoz method to the derivation of the dynamic material parameters of inhomogeneous media *J. Acoust. Soc. Am.* **82(2)** 692-695.

Schmitt-von Schubert R (1991) Sound waves in an elastic tube containing a gas-droplet or a liquid-bubble mixture *Acta Mechanica* **87** 81-92.

Schneider M, Bussat P, Barrau M-B, Arditi M, Yan F and Hybl E (1992) Polymeric microballoons as ultrasound contrast agents: Physical and ultrasonic properties compared with sonicated albumin *Investigative Radiology* **27(2)** 134-139.

Schott H (1988) Foaming of nonionic surfactant solutions: effect of surfactant concentration and temperature *J. A. O. C. S.* **65(5)** 816-819.

Schwarz WH and Margulies TS (1991) Sound wave propagation through emulsions, colloids and suspensions using a generalised Fick's law *J. Acoust. Soc. Am.* **90(6)** 3209-3217.

Seki H, Granato A and Truell R (1956) Diffraction effects in the ultrasonic field of a piston source and their importance in the accurate measurement of attenuation *J. Acoust. Soc. Am.* **28(2)** 230-238.

Sharma A and Ruckenstein E (1987) Critical thickness and lifetimes of foams and emulsions: role of surface wave-induced thinning *J. Coll. Interf. Sci.* **119(1)** 14-29.

Sharma A and Ruckenstein E (1989) Effects of surfactants on wave-induced drainage of foam and emulsion films *Colloid and Polymer Science* **266** 60-69.

Shima A, Rajvanshi SC and Tsujino T (1985) Study of nonlinear oscillations of bubbles in Powell-Eyring fluids *J. Acoust. Soc. Am.* **77(5)** 1702-1709.

Shimiya Y and Yano T (1987) Diffusion-controlled shrinkage and growth of an air bubble entrained in water and in wheat flour particles *Agric. Biol. Chem.* **51(7)** 1935-1940.

Shimiya Y and Yano T (1988) Rates of shrinkage and growth of air bubbles entrained in wheat flour dough *Agric. Biol. Chem.* **52(11)** 2879-2883.

Shukla KN (1987) A generalisation of the Rayleigh-Plesset equation of bubble dynamics *Z. angew. Math. Mech.* **67(9)** 470-471.

Silberman E (1957) Sound velocity and attenuation in bubbly mixtures measured in standing wave tubes *J. Acoust. Soc. Am.* **29(8)** 925-933.

Sirotyuk MG (1970) Stabilization of gas bubbles in water *Sov. Phys. Acoust.* 16(2) 237-240.

Sita Ram Sarma DSH and Khilar KC (1988) Effects of initial gas volume fraction on stability of aqueous gas foams *Ind. Eng. Chem. Res.* 27(2) 892-894.

Smereka P, Birnir B and Banerjee S (1987) Regular and chaotic bubble oscillations in periodically driven pressure fields *Physics of Fluids* 30(11) 3342-3350.

Smereka P and Banerjee S (1988) The dynamics of periodically driven bubble clouds *Physics of Fluids* 31(12) 3519-3531.

Snyder HA and Mord AJ (1990) Co-operative oscillations of bubbles *Cryogenics* 30 187-192.

Stravs AA and von Stockar U (1985) Measurement of interfacial areas in gas-liquid dispersions by ultrasonic pulse transmission *Chemical Engineering Science* 40(7) 1169-1175.

Stravs AA, Wahl J, von Stockar U and Reilly PR (1987) Development of an ultrasonic pulse reflection method for measuring relative size distributions of air bubbles in aqueous solutions *Chemical Engineering Science* 42(7) 1677-1688.

Tabor D (1991) Gases, liquids and solids and other states of matter, Cambridge University Press, Cambridge, UK.

Temkin S (1990) Attenuation and dispersion of sound in bubbly fluids via the Kramers-Kronig relations *J. Fluid Mech.* 211 61-72.

Teunissen JAM (1982) Mechanics of a fluid-gas mixture in a porous medium *Mechanics of Materials* 1 229-237.

Thiele E (1963) Equation of state for hard spheres *Journal of Chemical Physics* 39(2) 474-479.

Throop GJ and Bearman RJ (1965) Numerical solutions of the Percus-Yevick equation for the hard-sphere potential *Journal of Chemical Physics* 42(7) 2408-2411.

Tobocman W (1985) Comparison of the *T*-matrix and Helmholtz integral equation methods for wave scattering calculations *J. Acoust. Soc. Am.* 77(2) 369-374.

Tolstoy I (1986) Superresonant systems of scatterers I *J. Acoust. Soc. Am.* 80(1) 282-294.

Tsang L and Kong JA (1981) Multiple scattering of acoustic waves by random distributions of discrete scatterers with the use of quasicrystalline-coherent potential approximation *J. Appl. Phys.* 52(9) 5448-5458.

Tsang L, Kong JA and Habashy T (1982) Multiple scattering of acoustic waves by random distribution of discrete spherical scatterers with the quasicrystalline and Percus-Yevick approximation *J. Acoust. Soc. Am.* 71(3) 552-558.

Tsujino T, Shima A and Oikawa Y (1988) Effect of polymer additives on the generation of subharmonic and harmonic bubble oscillations in an ultrasonically irradiated liquid *J. Sound Vib.* 123(1) 171-184.

Turko BT, Kolbe WF and Leskovar B (1986) Ultrasonic system for imaging of vapor bubbles in a liquid filled pipe *IEEE Transactions on Nuclear Science* 33(4) 1115-1122.

Turner WR (1961) Microbubble persistence in fresh water *J. Acoust. Soc. Am.* 33(9) 1223-1233.

Twersky V (1962) Multiple scattering of waves and optical phenomena *J. Opt. Soc. Am.* 52(2) 145-171.

Twersky V (1964) Acoustic bulk parameters of random volume distributions of small scatterers *J. Acoust. Soc. Am.* 36(7) 1314-1329.

Twersky V (1977) Coherent scalar field in pair-correlated random distributions of aligned scatterers *J. Math. Phys.* 18(12) 2468-2486.

Twersky V (1978) Acoustic bulk parameters in distributions of pair-correlated scatterers *J. Acoust. Soc. Am.* 64(6) 1710-1719.

Van Wijngaarden L (1972) One-dimensional flow of liquids containing small gas bubbles *Ann. Rev. Fluid Mech.* 4 369-396.

Varadan VK (1979) Scattering of elastic waves by randomly distributed and oriented scatterers *J. Acoust. Soc. Am.* 65(3) 655-657.

Varadan VK, Bringi VN and Varadan VV (1979) Coherent electromagnetic wave propagation through randomly distributed dielectric scatterers *Phys. Rev. D* 19 2480-2489.

Varadan VK, Bringi VN, Varadan VV and Ma Y (1983) Coherent attenuation of acoustic waves by pair-correlated random distribution of scatterers with uniform and Gaussian size distributions *J. Acoust. Soc. Am.* 73(6) 1941-1947.

Varadan VK, Ma Y and Varadan VV (1985(a)) A multiple scattering theory for elastic wave propagation in discrete random media *J. Acoust. Soc. Am.* 77(2) 375-385.

Varadan VK, Varadan VV and Ma Y (1985(b)) A propagator model for scattering of acoustic waves by bubbles in water *J. Acoust. Soc. Am.* 78(5) 1879-1881.

Varadan VV and Varadan VK (1979) Low frequency expansions for acoustic wave scattering using Waterman's *T-matrix* method *J. Acoust. Soc. Am.* 66(2) 586-589.

Varadan VV, Ma Y and Varadan VK (1985) Propagator model including multipole fields for discrete random media *J. Opt. Soc. Am. A* 2(12) 2195-2201.

Varadan VV, Lakhtakia A and Varadan VK (1988) Comments on recent criticism of the *T*-matrix method *J. Acoust. Soc. Am.* **84(6)** 2280-2284.

Varatharajulu VV and Pao YH (1976) Scattering matrix for elastic waves: I. Theory *J. Acoust. Soc. Am.* **60(3)** 556-566.

Verlet L and Weis J-J (1972) Equilibrium theory of simple liquids *Physical Review A* 5(2) 939-952.

Vincent A (1987) Influence of wearplate and coupling layer thickness on ultrasonic velocity measurement *Ultrasonics* **25** 237-243.

Visscher WM (1980) A new way to calculate scattering of acoustic and elastic waves I) Theory illustrated for scalar waves *J. Appl. Phys.* **51(2)** 825-845.

Vokurka K (1987) A simple model of a vapor bubble *J. Acoust. Soc. Am.* **81(1)** 58-61.

Vokurka K (1989) Free oscillations of a cavitation bubble *J. Sound Vib.* **135(3)** 399-410.

Walsh AL and Mulhearn PJ (1987) Photographic measurements of bubble populations from breaking wind waves at sea *J. Geophys. Res. - Oceans* **92(C13)** 14553-14565.

Waterman PC (1969) New formulation of acoustic scattering *J. Acoust. Soc. Am.* **45(6)** 1417-1430.

Waterman PC (1976) Matrix theory of elastic wave scattering *J. Acoust. Soc. Am.* **60(3)** 567-580.

Waterman PC and Truell R (1961) Multiple scattering of waves *Journal of Mathematical Physics* 2(4) 512-537.

Weinberg MC, Kondos PA and Subramanian RS (1990) The shrinkage of a rising gas bubble containing a diffusing and a nondiffusing gas *Glass Technology* **31(2)** 72-76.

Wertheim MS (1963) Exact solution of the Percus-Yevick integral equation for hard spheres *Physical Review Letters* **10(8)** 321-323.

Winder WC, Aulick DJ and Rice AC (1970) An ultrasonic method for direct and simultaneous determination of alcohol and extract content of wines *American Journal of Enology and Viticulture* 21(1) 1-11.

Wolf J (1988) Investigation of bubbly flow by ultrasonic tomography *Particle and Particulate Systems Characterisation* 5(4) 170-173.

Wood AB (1964) A textbook of sound, 3rd edition, Bell & Sons Ltd, London, UK.

Wu J and Hwang PA (1991) Comment on *Ambient and transient bubble spectral densities in quiescent seas and under spilling breakers* by H Medwin and ND Breitz *J. Geophys. Res.* **96(C1)** 865-866.

Wu J and Zhu Z (1991) Measurements of the effective nonlinearity parameter B/A of water containing trapped cylindrical bubbles *J. Acoust. Soc. Am.* 89(6) 2634-2639.

Yianatos JB, Finch JA, Dobby GS and Manqiu X (1988) Bubble size estimation in a bubble swarm *J. Coll. Interf. Sci.* 126(1) 37-44.

Yildiz A (1988) Attenuation of sound waves due to scattering from bubbles and liquid drops *J. Sound Vib.* 121(1) 127-133.

Yoon SW, Crum LA, Prosperetti A and Lu NQ (1991) An investigation of the collective oscillations of a bubble cloud *J. Acoust. Soc. Am.* 89(2) 700-706.

Yount DE (1979) Skins of varying permeability: a stabilization mechanism for gas cavitation nuclei *J. Acoust. Soc. Am.* 65(6) 1429-1439.

Yount DE and Strauss RH (1976) Bubble formation in gelatin: a model for decompression sickness *Journal of Applied Physics* 47(11) 5081-5089.

Yu PYW and Varty RL (1988) Laser doppler measurement of the velocity and diameter of bubbles using the triple-peak technique *Int. J. Multiphase Flow* 14(6) 765-776.

Yung CN, de Witt KJ, Brockwell JL, McQuillen JB and Chai AT (1989) A numerical study of parameters affecting gas bubble dissolution *J. Coll. Interf. Sci* 135 442-452.

Zacharias EM and Parnell RA (1972) Measuring the solids content of foods by sound velocimetry *Food Technology* April 160-6.

Zavtrak ST (1988) Scattering of a sound wave by a swarm of gas bubbles *Sov. Phys. Acoust.* 34(1) 42-43.

Zeqiri B (1989) Reference liquid for ultrasonic attenuation *Ultrasonics* 27 314-315.

```
                                                  Water             Sample
                                               Low      Mid      Low      Mid         ACOUSTIC IMPEDANCES          PROPERTIES OF WATER        PROPERTIES OF SAMPLE          PROPERTIE S OF AIR
Time difference between succesive echoes =   67.180   67.435   66.510   66.765                                     Time        43.734         Time       43.734             Time        33.043 A       823.289
Left hand time reading for pulse A =         10.000    4.235   10.000    4.235        Aluminium  17.000            Velocity 1482.340          Velocity 1497.077                                B      1090.856
Left hand time reading for pulse B =         77.180   71.670   76.510   71.000                                     Density     0.998 g cm-3   Density   998.200 kg m-3   Density      0.001 g cm-3
                                                                                      Water       1.480
```

```
                                                                                                                                        Distilled water results  20C
                                            Diffraction
freq.       Echo 1             Echo 2       Corrections        R12    Z(water)  R32       Phase difference between echoes              freq.   Time     Atten
          Amp.    Phase      Amp.   Phase    Amp.   Phase

 0.200    1.680 -165.800    1.440   37.400   1.817  32.304     0.374   1.480   0.840  203.200  156.960 -193.936  166.064  166.064    0.200  67.306   2.174   0.998
 0.400   11.720  101.900   16.770  -61.900   1.092  21.801     0.374   1.480   0.840  196.200  313.920  -40.479  319.521  319.521    0.400  67.219   2.141   1.000
 0.600   19.060   -9.600   31.700  177.200   1.073  12.080     0.374   1.480   0.840  186.800  110.880 -243.840  116.160  116.160    0.600  67.204   0.807   1.000
 0.800   18.980  -77.500   31.220  105.400   1.155   8.283     0.374   1.480   0.840  182.900  267.840  -86.777  273.223  273.223    0.800  67.199   0.179   1.000
 1.000   21.300 -141.800   35.740   40.100   1.121   9.440     0.374   1.480   0.840  181.900   64.800 -287.660   72.340   72.340    1.000  67.201   0.279   1.000
 1.200   19.430  143.600   33.670  -36.600   1.073   8.357     0.374   1.480   0.840  179.800  221.760 -129.683  230.317  230.317    1.200  67.200   0.395   1.000
 1.400   12.130   74.100   21.260 -108.300   1.091   6.242     0.374   1.480   0.840  177.600   18.720 -332.638   27.362   27.362    1.400  67.197   0.114   1.000

                                                                                                                                     AVG.      67.200
                                                                                                                                     2d =    99613.6 mm

 1.000    8.060  -63.500   12.670  131.400   1.190  12.214     0.374   1.480   0.840  194.900  156.600 -206.086  153.914  153.914    1.000  67.428   0.333   1.000
 1.500   10.010 -172.000   15.800   19.200   1.128  11.867     0.374   1.480   0.840  191.200   54.900 -304.433   55.567   55.567    1.500  67.436   0.327   1.000
 2.000   10.000   89.500   15.780  -81.500   1.135   8.654     0.374   1.480   0.840  189.000  313.200  -47.146  312.854  312.854    2.000  67.435   0.768   1.000
 2.500    9.600   -1.600   14.390 -173.200   1.099   7.952     0.374   1.480   0.840  188.400  211.500 -148.948  211.052  211.052    2.500  67.435   1.505   1.000
 3.000    9.070  -88.400   12.730   98.800   1.107   7.088     0.374   1.480   0.840  187.200  109.800 -250.312  109.688  109.688    3.000  67.435   2.190   1.000
 3.500    8.300 -175.000   10.810   10.800   1.087   6.203     0.374   1.480   0.840  185.800    8.100 -351.497    8.503    8.503    3.500  67.435   3.120   1.000
 4.000    7.400   95.300    8.850  -78.000   1.088   6.082     0.374   1.480   0.840  186.700  266.400  -94.218  265.782  265.782    4.000  67.435   3.964   1.000
 4.500    6.340    2.500    6.860 -168.500   1.080   5.265     0.374   1.480   0.840  189.000  164.700 -199.035  160.965  160.965    4.500  67.433   5.040   1.000
 5.000    5.000    0.000    4.810  101.400   1.076   5.308     0.374   1.480   0.840  101.400   63.000 -213.092  146.908  146.908    5.000  67.482   6.253   0.999
 5.500    3.540  179.300    3.090   13.500   1.074   4.721     0.374   1.480   0.840  194.200  321.300  -48.179  311.821  311.821    5.500  67.430   7.244   1.000
 6.000    2.310   89.100    1.880  -75.200   1.067   4.682     0.374   1.480   0.840  195.700  219.600 -151.418  208.582  208.582    6.000  67.430   8.010   1.000
 6.500    1.520   -0.900    1.150 -159.000   1.069   4.368     0.374   1.480   0.840  201.900  117.900 -259.632  100.368  100.368    6.500  67.428   8.721   1.000
 7.000    1.040  -88.100    0.690  122.100   1.062   4.188     0.374   1.480   0.840  210.200   16.200 -369.812   -9.812  350.188    7.000  67.425  10.100   1.000
                                             1.063   4.091     0.374   1.480   0.840    0.000    0.000 -175.909  184.091  184.091    7.500    ERR     ERR     ERR
                                             1.059   3.822     0.374   1.480   0.840    0.000    0.000 -176.178  183.822  183.822    8.000    ERR     ERR     ERR
                                                                                                                                                             ERR
                         Sample
                                                                                                                                     AVG.      67.438
                                                                                                                                     2d =    99966.7 mm
                                            Diffraction
freq.                          B            Corrections        R12     Z      R23                  Time measurements                           FREQ     VEL.     ATTEN.   a.v/f
                             Amp.   Phase    Amp.   Phase
 0.200    1.410 -161.900    1.260   39.500   1.829  32.840     0.366   1.507   0.837  201.400  108.720 -239.840  120.160  120.160  66.669    0.200 1498.881  -0.240   0.002
 0.400    9.660  104.600   14.250  -60.900   1.096  22.090     0.366   1.505   0.837  194.500  217.440 -134.970  225.030  225.030  66.563    0.400 1497.369  -0.110  -0.000
 0.600   15.830   -6.700   27.250  178.600   1.073  12.310     0.366   1.505   0.837  185.300  326.160  -26.830  333.170  333.170  66.542    0.600 1497.181   0.114   0.000
 0.800   15.920  -74.700   27.130  106.200   1.154   8.300     0.366   1.505   0.837  180.900   74.880 -277.720   82.280   82.280  66.536    0.800 1497.077  -0.116   0.000
 1.000   18.120 -139.000   31.240   40.700   1.123   9.470     0.366   1.505   0.837  179.700  183.600 -166.630  193.370  193.370  66.537    1.000 1497.145  -0.059  -0.000
 1.200   16.600  146.500   29.590  -36.700   1.075   8.510     0.366   1.505   0.837  176.800  292.320  -55.970  304.030  304.030  66.537    1.200 1497.095  -0.072  -0.000
 1.400   10.460   77.300   18.690 -108.700   1.090   6.320     0.366   1.505   0.837  174.000   41.040 -306.640   53.360   53.360  66.534    1.400 1497.036   0.046   0.000


 1.000    6.780  -62.900   11.040  135.000   1.188  12.271     0.366   1.505   0.837  197.900  275.400  -90.229  269.771  269.771  66.749    1.000 1497.158  -0.105  -0.000
 1.500    8.430 -171.200   13.630   23.900   1.131  12.023     0.366   1.505   0.837  195.100   53.100 -309.977   50.023   50.023  66.759    1.500 1497.322  -0.035  -0.000
 2.000    8.250   90.700   13.290  -74.900   1.135   8.650     0.366   1.505   0.837  194.400  190.800 -174.950  185.050  185.050  66.757    2.000 1497.297   0.025   0.000
 2.500    7.860    1.100   11.910 -163.900   1.100   8.086     0.366   1.505   0.837  195.000  328.500  -38.414  321.586  321.586  66.757    2.500 1497.289   0.114   0.000
 3.000    7.440  -84.600   10.440  111.000   1.108   7.076     0.366   1.505   0.837  195.600  106.200 -262.324   97.676   97.676  66.757    3.000 1497.311   0.225   0.000
 3.500    6.900 -170.500    8.870   25.100   1.087   6.304     0.366   1.505   0.837  195.600  243.900 -125.396  234.604  234.604  66.758    3.500 1497.319   0.363   0.000
 4.000    6.120   99.800    7.180  -62.100   1.090   6.093     0.366   1.505   0.837  198.100   21.600 -350.407    9.593    9.593  66.757    4.000 1497.307   0.406   0.000
 4.500    5.170    7.700    5.390 -150.700   1.079   5.323     0.366   1.505   0.837  201.600  159.300 -216.977  143.023  143.023  66.755    4.500 1497.262   0.613   0.000
 5.000    4.040  -83.500    3.710  122.400   1.077   5.352     0.366   1.507   0.837  205.900  297.000  -83.548  276.452  276.452  66.754    5.000 1499.466   0.703   0.000
 5.500    2.890 -172.200    2.320   37.500   1.074   4.738     0.366   1.505   0.837  209.700   74.700 -310.262   49.738   49.738  66.752    5.500 1497.209   1.069   0.000
 6.000    1.930   98.100    1.420  -47.500   1.068   4.750     0.366   1.505   0.837  214.400  212.400 -177.250  182.750  182.750  66.751    6.000 1497.220   1.232   0.000
 6.500    1.270    7.500    0.860 -129.500   1.069   4.361     0.366   1.505   0.837  223.000  350.100  -48.539  311.461  311.461  66.748    6.500 1497.177   1.341   0.000
 7.000    0.830  -79.200    0.500  150.900   1.063   4.261     0.366   1.505   0.837  230.100  127.800 -278.039   81.961   81.961  66.747    7.000 1497.089   1.188   0.000
                                             1.064   4.085       ERR     ERR     ERR    0.000    0.000 -175.915  184.085  184.085    ERR    7.500    ERR      ERR      ERR
                                             1.059   3.879       ERR     ERR     ERR    0.000    0.000 -176.121  183.879  183.879    ERR    8.000    ERR
                                                                                                                                                                     ERR
```

```
Vel=1485 ms-1               Vel=1490 ms-1      Vel=1495 ms-1      (MENU)EWM-(MENU)ESL-(MENU)ESM-
  0.200    1.820   32.343    1.824   32.416    1.829   32.840 (GOTO)Q-
  0.400    1.093   21.864    1.094   21.981    1.096   22.090 (MENU)EA-
  0.600    1.073   12.130    1.073   12.221    1.073   12.310 (PANELON)
  0.800    1.155    8.286    1.154    8.293    1.154    8.300 Change the directory to the one containing your data files-(BEEP)
  1.000    1.121    9.448    1.122    9.463    1.123    9.470 (SERVICES)FD(?)-
  1.200    1.073    8.391    1.074    8.456    1.075    8.510 Enter the name of the file containing the low frequency water data-(BEEP)
  1.400    1.091    6.258    1.091    6.289    1.090    6.320 (SERVICES)FISDISTWAT.LO2(?)-
  1.000    1.189   12.226    1.189   12.248    1.188   12.271 Put the cursor on the cell containing the frequency 0.2-(BEEP)
  1.500    1.129   11.901    1.130   11.962    1.131   12.023 (GOTO)A91-(?)(MENU)-(DOWN 6)(RIGHT 4)-WL-
  2.000    1.135    8.653    1.135    8.651    1.135    8.650 (BLANK Q)(END)(DOWN)(END)(DOWN)(UP 1)
  2.500    1.099    7.980    1.100    8.033    1.100    8.086 Put the cursor on the cell containing the lower time value-(BEEP)(DOWN 1)
  3.000    1.107    7.086    1.107    7.081    1.108    7.076 (?)(MENU)--TWL1-
  3.500    1.087    6.224    1.087    6.264    1.087    6.304 (RIGHT 1)(MENU)--TWL2-
  4.000    1.088    6.085    1.089    6.090    1.090    6.093 (GOTO)Q-
  4.500    1.079    5.277    1.079    5.299    1.079    5.323 (MENU)EA-
  5.000    1.076    5.319    1.076    5.336    1.077    5.352 Enter the name of the file containing the medium frequency water data-(BE
  5.500    1.074    4.724    1.074    4.730    1.074    4.738 (SERVICES)FISDISTWAT.ME2(?)-
  6.000    1.068    4.697    1.068    4.724    1.068    4.750 Put the cursor on the cell containing the frequency 1.0-(BEEP)
  6.500    1.069    4.366    1.069    4.363    1.069    4.361 (GOTO)A92-(?)(MENU)-(END)(DOWN)(RIGHT 4)-WM-
  7.000    1.062    4.203    1.063    4.232    1.063    4.261 (BLANK Q)(END)(DOWN)(END)(DOWN)(UP 1)
  7.500    1.064    4.091    1.064    4.088    1.064    4.085 Put the cursor on the cell containing the lower time value-(BEEP)(DOWN 1)
  8.000    1.059    3.833    1.059    3.855    1.059    3.879 (?)(MENU)--TWM1-
                                                              (RIGHT 1)(MENU)--TWM2-
       Vel=1500 ms-1       Vel=1505 ms-1      Vel=1510 ms-1   (BLANK Q)(GOTO)R15-
  0.200    1.833   32.561    1.838   32.632    1.843   32.703
  0.400    1.097   22.213    1.099   22.328    1.100   22.443
  0.600    1.072   12.406    1.072   12.498    1.072   12.590
  0.800    1.154    8.310    1.154    8.319    1.153    8.329
  1.000    1.124    9.489    1.125    9.500    1.126    9.511
  1.200    1.075    8.582    1.076    8.645    1.076    8.707
  1.400    1.090    6.353    1.090    6.387    1.090    6.422
  1.000    1.188   12.295    1.188   12.319    1.187   12.345
  1.500    1.132   12.083    1.133   12.141    1.134   12.199
  2.000    1.135    8.650    1.135    8.650    1.135    8.652
  2.500    1.101    8.138    1.101    8.189    1.102    8.240
  3.000    1.108    7.071    1.108    7.066    1.109    7.061
  3.500    1.087    6.345    1.087    6.387    1.087    6.429
  4.000    1.090    6.094    1.091    6.094    1.010    6.093
  4.500    1.079    5.348    1.079    5.376    1.079    5.405
  5.000    1.078    5.365    1.078    5.376    1.079    5.385
  5.500    1.074    4.748    1.074    4.760    1.073    4.774
  6.500    1.069    4.361    1.069    4.361    1.069    4.364
  6.000    1.069    4.774    1.069    4.796    1.070    4.814
  6.500    1.069    4.361    1.069    4.361    1.069    4.364
  7.000    1.063    4.289    1.063    4.316    1.064    4.343
  7.500    1.064    4.082    1.065    4.078    1.065    4.075
  8.000    1.059    3.904    1.059    3.930    1.059    3.956

       Vel=1515 ms-1       Vel=1520 ms-1      Vel=1525ms-1
  0.200    1.847   32.774    1.852   32.844    1.856   32.914
  0.400    1.101   22.557    1.103   22.671    1.104   22.784
  0.600    1.072   12.684    1.072   12.777    1.072   12.870
  0.800    1.153    8.340    1.153    8.351    1.153    8.363     (ONERROR ERROR,Q)(GOTO)D-Enter the time reading from the densitometer for your sample-
  1.000    1.128    9.521    1.129    9.530    1.130    9.539     (GOTO)Q-
  1.200    1.077    8.769    1.078    8.830    1.078    8.890     (MENU)EA-
  1.400    1.089    6.458    1.089    6.495    1.089    6.533     Enter the name of the file with the low frequency data-(BEEP)
  1.000    1.187   12.372    1.186   12.400    1.186   12.429     (SERVICES)FISSAMPLE(?).LO2(?)-
  1.500    1.135   12.256    1.136   12.311    1.137   12.366     Put the cursor on the cell containing the frequency 0.2-(BEEP)
  2.000    1.135    8.654    1.135    8.658    1.135    8.662     (GOTO)A91-(?)(MENU)-(DOWN 6)(RIGHT 4)-SL-
  2.500    1.102    8.290    1.103    8.340    1.103    8.388     (BLANK Q)(END)(DOWN)(END)(DOWN)(UP 1)
  3.000    1.109    7.056    1.109    7.051    1.109    7.047     Put the cursor on the cell containing the lower time value-(BEEP)(DOWN 1)
  3.500    1.087    6.472    1.087    6.515    1.088    6.558     (?)(MENU)--TSL1-
  4.000    1.092    6.092    1.092    6.089    1.092    6.085     (RIGHT 1)(MENU)--TSL2-
  4.500    1.079    5.435    1.079    5.467    1.079    5.500     (GOTO)Q-
  5.000    1.079    5.393    1.080    5.398    1.080    5.401     (MENU)EA-
  5.500    1.073    4.791    1.073    4.810    1.073    4.830     Enter the name of the file with the medium frequency data-(BEEP)
  6.000    1.070    4.833    1.071    4.848    1.071    4.861     (SERVICES)FISSAMPLE(?).ME2(?)-
  6.500    1.069    4.369    1.069    4.375    1.069    4.384     Put the cursor on the cell containing the frequency 1.0-(BEEP)
  7.000    1.064    4.367    1.064    4.390    1.065    4.411     (GOTO)A92-(?)(MENU)-(END)(DOWN)(RIGHT 4)-SM-
  7.500    1.065    4.073    1.065    4.071    1.065    4.071     (BLANK Q)(END)(DOWN)(END)(DOWN)(UP 1)
  8.000    1.060    3.983    1.060    4.009    1.060    4.034     Put the cursor on the cell containing the lower time value-(BEEP)(DOWN 1)
                                                                  (?)(MENU)--TSM1-
       Vel=1530 ms-1       Vel=1535 ms-1                 1497.273 (RIGHT 1)(MENU)--TSM2-(PANELOFF)
  0.200    1.861   32.983    1.865   33.052                   0.000 (IF AR22)(MENU)-1535L-DCL-(MENU)-1535M-DCM-(BRANCH GRAPHS)
  0.400    1.106   22.897    1.107   23.009       1.000           0 (IF AR23)(MENU)-1530L-DCL-(MENU)-1530M-DCM-(BRANCH GRAPHS)
  0.600    1.072   12.963    1.072   12.057       1.000           0 (IF AR24)(MENU)-1525L-DCL-(MENU)-1525M-DCM-(BRANCH GRAPHS)
  0.800    1.152    8.376    1.152    8.390       1.000           0 (IF AR25)(MENU)-1520L-DCL-(MENU)-1520M-DCM-(BRANCH GRAPHS)
  1.000    1.131    9.546    1.131    9.553       1.000           0 (IF AR26)(MENU)-1515L-DCL-(MENU)-1515M-DCM-(BRANCH GRAPHS)
  1.200    1.079    8.950    1.080    9.009       1.000           0 (IF AR27)(MENU)-1510L-DCL-(MENU)-1510M-DCM-(BRANCH GRAPHS)
  1.400    1.089    6.571    1.088    6.611       1.000           0 (IF AR28)(MENU)-1505L-DCL-(MENU)-1505M-DCM-(BRANCH GRAPHS)
  1.000    1.185   12.458    1.185   12.489       1.000           0 (IF AR29)(MENU)-1500L-DCL-(MENU)-1500M-DCM-(BRANCH GRAPHS)
  1.500    1.138   12.419    1.139   12.472       1.000           1 (IF AR30)(MENU)-1495L-DCL-(MENU)-1495M-DCM-(BRANCH GRAPHS)
  2.000    1.135    8.668    1.135    8.674       0.000           0 (IF AR31)(MENU)-1490L-DCL-(MENU)-1490M-DCM-(BRANCH GRAPHS)
  2.500    1.104    8.436    1.104    8.483                         (MENU)-1485L-DCL-(MENU)-1485M-DCM-
  3.000    1.109    7.043    1.109    7.040                         (PANELON)(MENU)G1NUATTEN-QP1NUVELOCITY-QPQ
  3.500    1.088    6.600    1.088    6.643                         (GOTO)Z-(?)
  4.000    1.093    6.081    1.093    6.077                         (SERVICES)PSDFSAMPLE(?).PR2(?)-QGQ
  4.500    1.079    5.534    1.079    5.569                         (BRANCH S)
  5.000    1.081    5.403    1.081    5.404
  5.500    1.073    4.853    1.073    4.877
  6.000    1.072    4.871    1.073    4.880
  6.500    1.069    4.395    1.068    4.408
  7.000    1.065    4.430    1.066    4.447
  7.500    1.065    4.073    1.065    4.077
  8.000    1.060    4.058    1.061    4.081
```